FROM THE BEGINNING TO THE END: THE STORY OF THE MITOCHONDRIAL DISEASE ASSOCIATED WITH THE ADCK2 GENE, GOING THROUGH COQ10 SUPPLEMENTATION AND CALORIC RESTRICTION.

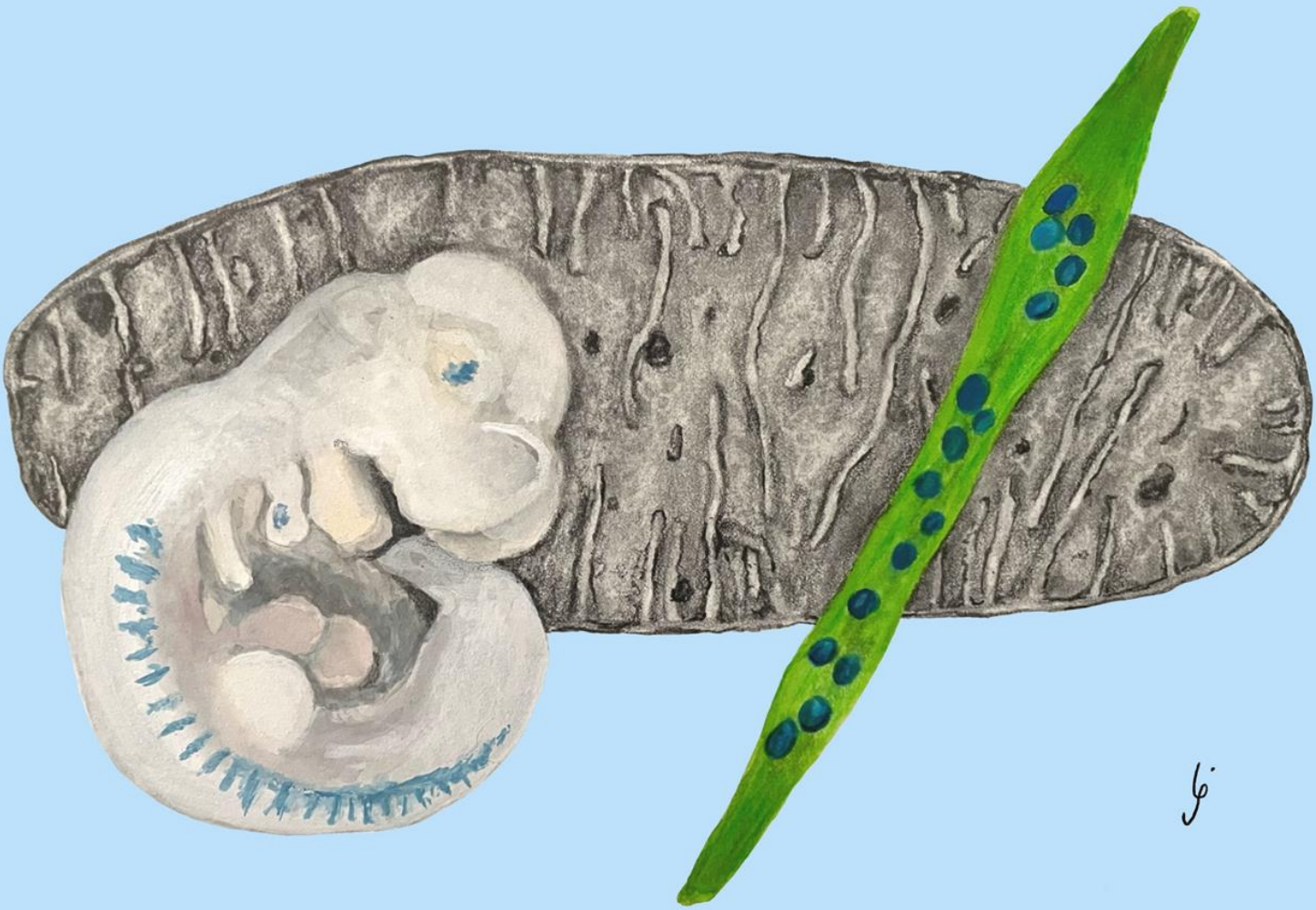

Juan Diego Hernández Camacho

TESIS DOCTORAL. Sevilla, 2022

UNIVERSIDAD PABLO DE OLAVIDE SEVILLA

TESIS DOCTORAL

From the beginning to the end: the story of the mitochondrial disease associated with the ADCK2 gene, going through CoQ_{10} supplementation and caloric restriction.

Juan Diego Hernández Camacho

Sevilla, 2022

From the beginning to the end: the story of the mitochondrial disease associated with the ADCK2 gene, going through CoQ10 supplementation and caloric restriction.

TESIS DOCTORAL

Universidad Pablo de Olavide

Dpto. Fisiología, Anatomía y Biología Celular

Área de Biología Celular

Memoria presentada por

Juan Diego Hernández Camacho

para optar al título de

Doctor en Biotecnología, Ingeniería y Tecnología Química

Programa de Doctorado en Biotecnología, Ingeniería y Tecnología Química

(RD: 99/2011)

Sevilla, 2022

El director de la tesis

Dr. Daniel J. Moreno Fernández Ayala
Profesor titular
Dpto. Fisiología, Anatomía y Biología Celular.
Área de Biología Celular
Universidad Pablo de Olavide.

El director de tesis

Dr. Jaime J. Carvajal García-Valdecasas
Científico titular
Grupo de investigación de embriología molecular
Centro Andaluz de Biología del Desarrollo. CSIC,
UPO y JA

D. Daniel José Moreno Fernández-Ayala, Doctor en Análisis Experimental en Biología por la Universidad Pablo de Olavide y Profesor Titular del Área de Biología Celular en el Departamento de Fisiología, Anatomía y Biología Celular de la Universidad Pablo de Olavide de Sevilla.

INFORMA

Que D. JUAN DIEGO HERNÁNDEZ CAMACHO, ha realizado bajo su dirección la tesis doctoral titulada "FROM THE BEGINNING TO THE END: THE STORY OF THE MITOCHONDRIAL DESEASE ASSOCIATED WITH THE *ADCK2* GENE, GOING THROUGH COQ_{10} SUPPLEMENTATION AND CALORIC RESTRICTION", y que a su juicio reúne los méritos suficientes para superar el programa de Doctorado en Biotecnología, Ingeniería y Tecnología Química.

Y para que conste, firmo el presente en Sevilla, 2022

Fdo.: Daniel J. Moreno Fernández-Ayala

D. Jaime J. Carvajal García-Valdecasas, Doctor en Bioquímica y Genética Molecular por el Imperial College de Londres y Científico titular del CSIC en el Centro Andaluz de Biología del Desarrollo de la Universidad Pablo de Olavide de Sevilla.

INFORMA

Que D. JUAN DIEGO HERNÁNDEZ CAMACHO, ha realizado bajo su dirección la tesis doctoral titulada "FROM THE BEGINNING TO THE END: THE STORY OF THE MITOCHONDRIAL DESEASE ASSOCIATED WITH THE *ADCK2* GENE, GOING THROUGH COQ_{10} SUPPLEMENTATION AND CALORIC RESTRICTION", y que a su juicio reúne los méritos suficientes para superar el programa de Doctorado en Biotecnología, Ingeniería y Tecnología Química.

Y para que conste, firmo el presente en Sevilla, 2022

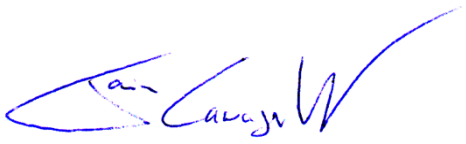

Fdo.: Jaime J. Carvajal García-Valdecasas

Dipartimento Universitario
Scienze della Vita e Sanità Pubblica
Sezione di Biologia

Daniela Palacios, PhD

Department of Life Sciences and Public Health

Università Cattolica del Sacro Cuore

Largo Francesco Vito, 1

00168 Rome

e-mail: daniela.palacios@unicatt.it

Rome, February 28th 2022

Report for the PhD thesis entitled: "From the beginning to the end: the story of the mitochondrial disease associated with the *ADCK2* gene, going through CoQ_{10} supplementation and caloric restriction", presented by Juan Diego Hernandez Camacho

The thesis presented by Juan Diego Hernandez Camacho investigates the role of ADCK2 -a protein involved in CoQ_{10} biosynthesis- in regulating mitochondria function and skeletal myogenesis, revealing its role as a metabolic modulator during aging. To this end he uses a vast array of techniques ranging from microarray analysis of gene expression, genetic manipulations, cell cultures and *in vivo* analysis of embryonic and adult skeletal muscle formation. The methodology is adequate and very complete, and the results obtained are original and shed light into the mechanisms by which ADCK2 regulates mitochondrial function, metabolism and skeletal muscle aging. The major findings obtained in this PhD work show that:

- Damages in transgenic *ADCK2* knockout mice start during embryonic development and involve the activation and repression of specific genes and pathways.
- *ADCK2* mutant mice present a skeletal muscle decline associated with ageing resulting in impaired satellite cells activity, change in the myofiber size and composition and exacerbated loss of muscle functionality through the ageing process.
- CoQ_{10} administration could recover some defects associated with the *ADCK2* gene.
- Mutant mice present a defective *in vivo* mitochondrial respiration that is recovered upon CoQ_{10} administration.
- Caloric restriction (CR) interventions in mutant mice improves mitochondrial physiology, reducing CoQ decrease and ameliorating mitochondrial respiration

Overall, this thesis contributes significantly to our knowledge in the skeletal muscle, aging and mitochondria fields. The design, analysis, and interpretation of the results are clear and rigorous. In addition, the PhD candidate shows a good knowledge of relevant literature and he critically discusses both the state-of-the-art in the field and current open questions.

DANIELA PALACIOS GARCIA, PhD by the Universidad Autonoma de Madrid, and Professor of Cellular and Molecular Biology at Università Cattolica del Sacro Cuore, Rome, Italy, consider that the scientific quality of this thesis is worthy of obtaining the International Doctor Mention

Informo favorablemente que la calidad científica de esta tesis doctoral es merecedora de obtener la mención Doctor Internacional.

Daniela Palacios, PhD
Department of Life Sciences and Public Health, Biology section.
Universitá Cattolica del Sacro Cuore
Largo Francesco Vito, 1
00168 Rome

Professor Peter S. Zammit

Faculty of Life Sciences and Medicine
Randall Centre for Cell and Molecular Biophysics
New Hunt's House
King's College London
London SE1 1UL, UK

11th March 2022

Thesis: **From the beginning to the end: the story of the mitochondrial disease associated with the *ADCK2* gene, going through CoQ_{10} supplementation and caloric restriction.**

PhD Student: **Juan Diego Hernández Camacho**

University: **Universidad Pablo de Olavide**, Centro Andaluz de Biología del Desarrollo CABD,Carretera de Utrera km1, 41013 Sevilla, Spain

The thesis of Juan Diego Hernández Camacho is well presented and written in a clear and accessible manner, being well-supported with appropriate figures, tables and diagrams. Juan Diego Hernández Camacho presents a comprehensive and informative thesis describing the phenotype of *Adck2*$^{+/-}$ and *Adck2*-null mice during development and aging, with a focus on skeletal muscle function and myogenesis. Importantly, dietary supplementation of CoQ_{10} generally improved muscle function in older mutant mice. Calorific restriction was also examined in *Adck2*$^{+/-}$ and revealed general improvements in muscle function and metabolism.

The Introduction generally covers the relevant background information in sufficient detail and with reference to appropriate papers to set the context of the experimental work and aid interpretation of the data. The Material and Methods is comprehensive and detailed enough to allow experiments to be reproduced.

Results presented in Chapter 1 describe transcriptomic analysis on *Adck2*$^{+/-}$ mice and effects of CoQ_{10}, highlighting affected processes/pathways. Examination of early muscle development reveals perturbation in myotome formation in certain somites, which can be ameliorated by prenatal CoQ_{10} administration

In Chapter 2, regenerative myogenesis in *Adck2*$^{+/-}$ mice and the effects of CoQ_{10} was investigated, reporting that satellite cell numbers differ, and examining proliferation and myogenic differentiation, with smaller/less branched myotubes derived from mutant *Adck2*$^{+/-}$ satellite cells. Again, exogenous CoQ_{10} improves myotube formation/differentiation in mutant cells. Aging was found associated with a more severe phenotype in older *Adck2*$^{+/-}$ mice.

Chapter 3 reports that mutant *Adck2*$^{+/-}$ mice have a decline in skeletal muscle function with age, resulting in less force generation, accompanied by changes in muscle fibre type and size. Levels of $CoQ_{9/10}$ were also described. Administration of CoQ_{10} to mutant mice delayed skeletal muscle changes associated with ageing. Detailed and sophisticated analysis of mitochondria and respiration (e.g. Seahorse technology) revealed that mutant mice have defective mitochondrial respiration, which was again ameliorated by CoQ_{10}.

Finally in Chapter 4, the effects of caloric restriction on the phenotype of *Adck2*$^{+/-}$ mice was explored *in vivo* and *in vitro* and was found to improve mitochondrial physiology in mutant mice, ameliorating CoQ_{10} decrease and *in vivo* mitochondrial respiration. Caloric restriction was also found to have tissue-specific effects in mutant mice, and cause a shift to more oxidative profile in muscle in both genotypes, with an increase in the proportion of oxidative type IIA, and fewer glycolytic type IIB, myofibres. Using mouse serum to culture satellite cells *ex vivo* demonstrated that myotubes differentiated from mutant *Adck2*$^{+/-}$ satellite cells cultured in serum from mutant mice on *ad libitum* weresmaller and less branched, which was less severe when serum from mutant caloric restricted mice was used.

Each experimental chapter contains a scholarly discussion in which the data is discussed and interpreted, with reference to the literature, allowing it to be placed in the context of the wider field. Novel findings are explained, as is where the current work supports or differs from published work. Bullet points for the conclusion section are a useful and accessible way to summarise such a large bodyof work. In summary, the candidate Juan Diego Hernández Camacho is to be congratulated on conducting such a thorough investigation on many aspects of the phenotype of *Adck2*$^{+/-}$ mice by performing many different types of experiments encompassing a diverse range of techniques, to produce such a high-quality thesis. There is potential for several high-impact publications from thisextensive and interesting project.

I inform that the scientific quality of this thesis is worthy of obtaining the international Doctor mention.

Your Sincerely

Professor Peter S. Zammit

Acknowlegements/Agradecimientos

Tras cuatro años y medio ha llegado el momento de finalizar esta etapa de mi vida. En la que ha habido momentos buenos y malos, en la que he vivido buenas y malas experiencias, en la que algunas cosas han salido bien y otras mal, pero lo más importante es que he aprendido mucho tanto de ciencia como en lo personal, y que todo lo vivido suma y es un entrenamiento más para lo que está por venir. Por todo ello, me gustaría agradecer a todas las personas que me han ayudado a lo largo de este camino y que han contribuido en este proyecto y a mi evolución como persona.

En primer lugar, a Daniel por su dedicación en el día a día, por haber estado siempre disponible cuando tenía una duda, de poder tener la oportunidad de poder discutir ideas o resultados de los experimentos para ver como avanzábamos en el proyecto y por la libertad que me has dado para intentar hacer cosas nuevas o ideas y poder aprender de los errores. También gracias por haberte preocupado por mí más allá de los resultados y experimentos, por haberte cuidado de mi persona durante cuatro años y por la oportunidad de ser tu primer doctorando. A Jaime, por la oportunidad de poder trabajar contigo, que hayas sido mi codirector me ha permitido poder trabajar en tu laboratorio junto a personas magníficas, poder haber aprendido técnicas nuevas, poder aprender sobre una nueva área de conocimiento como el músculo esquelético y poder haber ido de estancia al laboratorio de Peter Zammit.

A Plácido por estar ahí siempre para responder mis dudas y discutir ideas o experimentos, respondiendo emails a las 07:00 de la mañana y por confiar en mí para este proyecto. Por intentar echar una mano, implicando a tus colaborares en mi trabajo. Por haber podido aprender de tu experiencia y de todo el camino que has recorrido en ciencia, por aportar siempre tu punto de vista sobre las diferentes situaciones a las que nos hemos enfrentado en este proyecto.

A Cristina por ser la persona que más me ha enseñado, de la que más he aprendido y con la que más he disfrutado haciendo experimentos. Por enseñarme la importancia de hacer las cosas de forma planeada y organizada y por mostrarme tu forma de ver la ciencia. Te mereces todo lo bueno que te pase y más.

A María por ser mi compañera de laboratorio durante muchos años, por estar siempre ahí cuando hacía falta, por compartir tantos momentos en el laboratorio fuera la hora que fuera, por tantos almuerzos en el CABD a las 17:00 y por tantas ideas compartidas. Por todos estos congresos y por todas las experiencias vividas.

A Guillermo por ser la persona que me dio la oportunidad de empezar en el laboratorio en su día y por estar siempre ahí para discutir una idea o experimento. A Mariví por estar en mi día a día durante todos estos años para ayudar en lo que hiciera falta, por mostrarme tu forma de ver las cosas y darme su punto de vista más sincero. A Anita por estar cada día en el laboratorio preocupándose de todos y haberme ayudado en todo lo que hiciera falta. A Gloria por escuchar todo lo que hiciera falta, compartir tu opinión y haberme ayudado científicamente y en lo personal, por enseñarme otra forma de ver la ciencia y por tu forma de ser. A Carlos por aportar siempre su opinión desde su experiencia y ver los problemas como un reto. A Ana Q por enseñarme a medir CoQ y por su visión sincera de todo. A Manu y Antonio Arroyo por aportar consejos sobre los experimentos.

A Peter Zammit por la oportunidad de irme de estancia durante tres meses a su laboratorio, por acogerme y tratarme como un miembro más desde el primer hasta el último día para que mi estancia fuera lo más agradable y productiva. Por mantener el contacto años después de la estancia y por resolver mi numerosas dudas y preguntas durante este tiempo. A Johanna, Phipps, Isabella y Massimo por ayudarme en mi día a día durante mi tiempo en el Zammit lab tanto en el laboratorio como fuera de él. A Jeff, Tapan, Reuben, Mike, Sarah, Adam, Ainara y Ailbhe por todos los buenos ratos que compartimos durante mi tiempo en el King's College. Y todos los miembros del King's con lo que compartí los "footy Fridays".

A todos y cada una de las personas con los que he coincidido durante estos años en el laboratorio de Biología Celular. A Daniel Jesús García y Cathe por ser mis compañeros de "Westerns" durante mi primer año en el laboratorio. A Andrés, Simone y Verónica por el tiempo que compartimos en el laboratorio. A Aída por compartir años como doctorandos y por tu ayuda con los ratones cuando estaba de congreso o fuera. A Ana Belén por el tiempo que compartimos durante tu TFG. A Pablo Jiménez, y Manu Torralba por todos los almuerzos, por las bromas y por tener la oportunidad de otro punto de vista de las cosas. A Valentina y Alessandra por la oportunidad de poder enseñar y aprender de ustedes al mismo tiempo. A Carmine por haberse convertido en otro compañero de batallas, por la oportunidad de enseñarle el camino, como María me lo enseño a mí y por ver cómo vas creciendo. A Lorena por tener la oportunidad de poder empezar un proyecto nuevo y aprender a hacer BlueNative y de ver que las cosas no son tan difíciles cuando se quiere. A Laura y María del Mar por el tiempo que hemos compartido, por su experiencia desde su posición de postdoc y por ayudarme con todo lo que ha hecho falta. A Iván por los memes y por su actitud. A Ana por ser la última persona con la que tengo la oportunidad de enseñar, aprender y compartir su proyecto. A todos los estudiantes que han

pasado por el laboratorio y me han preguntado alguna cosa, yo también he aprendido en esas situaciones.

A todos y cada uno de los miembros del CABD con los que estos años he tenido la oportunidad de compartir algún momento, experiencia o experimento. A Laura Tomás, Alejandro y María por ayudarme con los westerns, las blue natives y los secretos del pHmetro. A Macarena por tus consejos y por compartir tu opinión sobre las dificultades que he ido encontrando y por tu forma de ser. A Marta por tus consejos, por tu ayuda y por todo lo que significas. A Kathy, Corín y Alejandro por toda vuestra ayuda y dedicación por formarme en microscopía, ayudarme con los problemas que he encontrado en el uso de los microscopios y con el análisis de imagen. A Ana Franco, Candy Mateos, Alejandro y Paula de animalario por ayudarme con el manejo y la organización de la colonia de los ratones. A todos los miembros que CABD y externos con los que he compartido los martes de fútbol, aunque a última hora la rodilla me esté dando problemas, porque una tesis con fútbol es más llevadera. Muchas gracias a todos los miembros del CABD que velan por que todo funcione en el centro como el personal de limpieza, el personal de cocina y los conserjes, a los miembros del CABD que siempre están dispuestos a preguntar ¿cómo va todo? como Ana Neto, Ana Miñán, Machupi, a todos los grupos de investigaciones que siempre están dispuestos a ayudar o prestar algún reactivo. A todas esas personas que seguro me han ayudado y he olvidado mencionar.

A mis amigos de toda la vida que siempre han estado ahí durante este tiempo para ayudarme a desconectar y pasar un buen rato ya fuera en el Betis, echando un partido de fútbol, en el pádel, saliendo a cenar o a tomar algo.

Por último, me gustaría agradecer su apoyo durante todos estos años a mi familia, especialmente a mis padres, que desde chico me han enseñado el significado del trabajo duro y del esfuerzo, gracias por estar siempre ahí.

Funding

I am grateful to all institutions and people that have made possible this PhD project. Most of the research has been carried out in the Centro Andaluz de Biología del Desarrollo (CABD-CSIC-UPO-JA), in the Department of Physiology, Anatomy and Cell Biology at Pablo de Olavide University. I have been working in Professor Plácido Navas Lloret`s laboratory and Professor Jaime Carvajal's laboratory.

This PhD project has been funded by the "Ayudas para la formación de profesorado Universitario" FPU grant (FPU16/03264) from the Spanish Government (Ministerio de Educación, Culture y Deporte), from 2017 to 2022. I was also awarded with the grant "Ayudas CIBERER para el inicio de tesis doctorales en Enfermedades Raras" from Centro de Investigaciones Biomédicas en Red de Enfermedades Raras (CIBERER). I was also awarded with the grant "Ayudas a la movilidad para estancias breves y traslados temporales FPU" (EST18/00298) from the Spanish Government (Ministerio de Educación, Culture y Deporte) to work for three months (from May 2019 until July 2019) in Professor Peter Zammit's laboratory at King's College London, Randall Centre of Cell and Molecular Biophysics, London, UK.

I have presented some data from my PhD project in several international and national meeting thanks to several grants: "Ayudas destinadas a cubrir gastos para la mejora cualitativa en el desarrollo de sus tesis doctorales" from Pablo de Olavide University, "Registration Award" from Wellcome Genome Campus Scientific Conferences and "EMBO Travel Grant" from EMBO (2017 National Congress for Young Researchers in Biomedicine. Hospital Universitari l Politécnic La Fe, Valencia, Spain. 2018 Mitochondrial Medicine Congress, Wellcome Genome Campus, Hinxton, Cambridge, UK. 2019 Mitochondrial Medicine Congress, Wellcome Genome Campus, Hinxton, Cambridge, UK. 2021 EMBO Workshop Mitochondrial homeostasis and human disease. Girona, Spain).

The work of my PhD project has been partially funded by the project "Diagnóstico molecular y patogénesis de las enfermedades mitocondriales con deficiencia de coenzima Q10" awarded by the Instituto de Salud Carlos III (Ministerio de Salud, Spanish Government) in 2018 (Reference FIS PI17-01286) to Professor Plácido Navas Lloret.

ABSTRACT

From the beginning to the end: the story of the mitochondrial disease associated with the *ADCK2* gene, going through CoQ_{10} supplementation and caloric restriction.

Mitochondria are enclosed membrane organelles that burn nutrient molecules to produce adenosine triphosphate (ATP) by oxidative phosphorylation (OXPHOS) and are present in cells of animals, plants and fungi. Mitochondria also carry out other important processes such as urea cycle, fatty acids β-oxidation and the Krebs cycle. A crucial element in mitochondrial function is Coenzyme Q_{10} (CoQ_{10}) is a unique lipid endogenously produced, a crucial element in the mitochondrial electron transport chain (ETC) and antioxidant found in all cell membranes. The main function of CoQ is to send electrons that receive from complex I and complex II to complex III at the ETC resulting in ATP production. But, CoQ_{10} could be also reduced by different hydrogenases, showing the high number of pathways where CoQ_{10} participates.

CoQ is composed of a benzoquinone ring and a polyisoprenoid chain which inserts CoQ into the phospholipid bilayer. CoQ is produced at mitochondria by a nuclear-encoded CoQ proteins cluster. The biosynthetic pathway is not clear yet and it is carried by at least 13 proteins. The *ADCK2* gene has been recently associated with CoQ pool regulation and fatty acids metabolism. *ADCK2* haploinsufficiency in humans is related to mitochondrial myopathy, muscle wasting, reduction of CoQ levels and impairment of fatty acids β-oxidation. We developed a heterozygous *Adck2* knockout mouse that reproduces the mutation. The four chapters of the thesis are focused on this mutant mouse model to better understand the mitochondrial syndrome associated with the *ADCK2* gene.

Firstly, we present a detailed study of the embryonic development of mutant mice to elucidate if damages could start during this stage. We analysed the transcriptomic profile during early and late development, finding a clear tissue-specific deregulation during late embryonic development. Heterozygous *Adck2* knockout mouse embryos presented an abnormal somatogenesis analysed with two different Myogenic Regulatory Factors. We examined a prenatal CoQ_{10} administration obtaining that mutant embryos under CoQ_{10} supplementation showed a reversion to wild type profile in the transcriptomic profile and skeletal muscle formation. From this part of the project, we propose that mutant mice suffer damages since embryonic development, while CoQ_{10} supplementation could reduce these alterations.

Secondly, we decided to focus on postnatal myogenesis based on the results from the first chapter. For that purpose, adult muscle stem cells (satellite cells) were isolated from wild type and mutant mice under standard conditions and under CoQ_{10} administration and differentiated.

Mutant cells presented a defect in differentiation that leads to smaller myotubes and delayed differentiation that was associated with a reduction in oxygen consumption and fatty acids β-oxidation. Mutant cells isolated from mutant mice supplemented with CoQ_{10} showed an improvement in differentiation and also on mitochondrial respiration. An *in vivo* analysis of satellite cells was performed to support our *in vitro* data inducing muscle damage and examining skeletal muscle regeneration. Mutant mice presented an impaired skeletal muscle regeneration and were more susceptible to muscle damage, CoQ_{10} administration improved skeletal muscle regeneration. We performed the experiments in cells from young and old mice, the differences were bigger in cells from old mice suggesting that ageing could act as a modulator in the phenotype of mutant mice. As summary of this chapter, mutant mice suffer a defect in postnatal myogenesis, particularly during myogenic differentiation.

We decided to study the decline associated with the ageing process in our mutant mice in the third chapter. Old mutant mice presented a decrease in myofiber size and a different myofiber composition while old mutant mice longitudinally supplemented with CoQ_{10} exhibited a myofiber size and composition more similar to wild type mice. Skeletal muscle performance was assessed through ageing, mutant mice presented a more severe decline in physical capacity compared to wild type mice. CoQ_{10} administration ameliorated skeletal muscle function decline in mutant mice. We developed a method to examine respiration in isolated mitochondria from skeletal muscle. Mitochondria from skeletal muscle of mutant mice presented a reduction in oxygen consumption while isolated mitochondria from mutant mice on CoQ_{10} administration showed an increase in respiration with both glucose and fatty acids substrates. Heterozygous *Adck2* knockout mice suffer a more severe decline through ageing and CoQ_{10} administration could improve the phenotype of mutant mice.

Finally, we studied the metabolic modulation of the phenotype of mutant mice by caloric restriction (CR). CR restored glucose and insulin homeostasis in mutant mice to wild type levels. CR modulated skeletal muscle metabolic profile, resulting in a more oxidative myofiber composition and increased oxygen consumption using glucose and fatty acids substrates in isolated mitochondria. To further explore the effect of CR on muscle stem cells, satellite cells were cultured with serum obtained from mice on ab libitum and on CR. Mutant cells cultivated with CR serum showed an increase in differentiation and oxygen consumption. As summary, we propose that CR intervention improved age-associated decline and defects in mutant mice.

The four chapters of the project are focus on the study of *Adck2* mutant mice but under different conditions and methods including CoQ_{10} administration or under CR condition, resulting in a

completed phenotype analysis of the model studied to show the development, progression and affectation and affectation of this mitochondrial dysfunction.

Desde el principio al final: la historia de la enfermedad mitocondrial asociada con el gen *ADCK2*, pasando por la suplementación con CoQ_{10} y la restricción calórica.

Las mitocondrias son orgánulos membranosos que a partir de los nutrientes que ingerimos producen adenosín trifosfato (ATP) a través de la fosforilación oxidativa, y están presentes en todas las células de animales, plantas y hongos. También llevan a cabo una sería de procesos de vital importancia como el ciclo de la urea, la β-oxidación de ácidos grasos y el ciclo de Krebs. Un elemento crucial de la función mitocondrial es el Coenzima Q_{10} (CoQ_{10}) un lípido producido de forma endógena, que es importante en la cadena de transporte de electrones y asimismo actúa como antioxidante en las membranas celulares. La principal función del CoQ es enviar electrones al complejo III que previamente recibe de los complejos I y II, resultando esta transferencia en la producción de ATP. Pero el CoQ_{10} puede ser también reducido por diferentes deshidrogenasas, demostrando el gran número de rutas donde el CoQ_{10} participa.

La estructura del CoQ se compone de un anillo de benzoquinona y de una cadena isoprenoide a través de la cual el CoQ se inserta en la barrera fosfolipidica de las membranas. El CoQ es producido en la mitocondria por un grupo de proteínas nucleares conocidas como proteínas CoQ. La ruta de síntesis no ha sido totalmente descrita aún y se estima que es llevada a cabo por al menos 13 proteínas CoQ. Recientemente, el gen *ADCK2* ha sido asociado con la regulación del pool de CoQ y el metabolismo de los ácidos grasos. La haploinsuficiencia del gen *ADCK2* en humanos está asociada con miopatía mitocondrial, la pérdida de músculo, la reducción de los niveles de CoQ y un defecto en la β-oxidación de ácidos grasos. Hemos desarrollo un modelo de ratón knockout que reproduce la mutación del paciente, los cuatro capítulos del proyecto de tesis están centrados en el estudio de este modelo de ratón para entender mejor el síndrome mitocondrial asociado con el gen *ADCK2*.

Primero, realizamos un estudio detallado del desarrollo embrionario del modelo para averiguar si los daños pudieran incluso comenzar durante esta etapa. Hemos analizado el perfil transcriptómico durante el desarrollo embrionario temprano y tardío, encontrando que la desregulación génica durante el desarrollo embrionario es tejido-específica. Los embriones heterocigotos presentan una somatogénesis anormal, estudiada mediante dos factores de transcripción reguladores de la miogénesis diferentes. También hemos estudiado la administración prenatal de CoQ_{10} en nuestro modelo, observando que una reversión del perfil transcriptómico hacía el perfil de los embriones wild type y una mejora en la formación del músculo esquelético. Como resultado de esta parte del proyecto, podemos proponer que los

ratones mutantes están afectados desde el desarrollo embrionario, y que la administración prenatal de CoQ_{10} mejora el fenotipo de los embriones mutantes.

En segundo lugar, decidimos centrarnos en el estudio de la miogénesis postnatal basándonos en los resultados obtenidos en el primer capítulo. Para ello, se aislaron células madre de músculo (células satélites) de ratones wild type y de ratones mutantes en condiciones estándar y bajo la suplementación con CoQ_{10}, y posteriormente se indujo su diferenciación a células musculares. Las células mutantes presentaban un defecto en la diferenciación que resultaba en miotubos más pequeños y en un retraso en la diferenciación asociado con un menor consumo de oxígeno y un defecto en la β-oxidación de ácidos grasos. Las células mutantes de ratones mutantes suplementados con CoQ_{10} presentaron una mejora en la diferenciación y en la respiración mitocondrial. Adicionalmente, se llevó a cabo un análisis *in vivo* de las células satélites para refutar nuestros resultados *in vitro* mediante la inducción de daño muscular y examinando la regeneración muscular. Los ratones mutantes presentan una regeneración muscular deteriorada y eran más susceptibles al daño muscular, en cambio la administración de CoQ_{10} mejoró la regeneración del músculo esquelético. Realizamos estos experimentos en células procedentes de ratones jóvenes y viejos, las diferencias fueron mayores en células de ratones viejos sugiriendo que el envejecimiento podría actuar como modulador del fenotipo de los ratones mutantes. Como resumen de este capítulo, podríamos resaltar que los ratones mutantes sufren un defecto en la miogénesis postnatal, particularmente durante la diferenciación miogénica.

En el tercer capítulo, estudiamos el decaimiento progresivo del ratón mutante asociado al envejecimiento. Los ratones mutantes viejos presentaban un menor tamaño de la fibra muscular y una diferente composición de las fibras mientras que los ratones mutantes viejos que han sido suplementados longitudinalmente con CoQ_{10} presentan un tamaño y composición de fibras más similar a los wild type. Los ratones mutantes viejos sufrían un descenso más severo de la capacidad física durante el envejecimiento comparado con los ratones wild type. La administración de CoQ_{10} mejora la función del músculo esquelético en los ratones mutantes a lo largo del envejecimiento. Para estudiar la respiración mitocondrial de los músculos de nuestros ratones, desarrollamos un método para el análisis de la respiración en mitocondrias aisladas. Las mitocondrias del musculo de ratones mutantes viejos presentaron un descenso en el consumo de oxígeno mientras que las mitocondrias aisladas de músculo de ratones mutantes suplementados con CoQ_{10} mostraron un incremento de la respiración usando glucosa y ácidos grasos como sustrato. Podemos concluir que los ratones *Adck2* knockout sufren una mayor

afectación asociada a la edad más severa y la administración de CoQ_{10} podría mejorar el fenotipo de los ratones mutantes.

Por último, hemos examinado la modulación metabólica del fenotipo de los ratones mutantes a través de la restricción calórica (CR). La CR restaura la homeostasis de la glucosa y la insulina a niveles de ratones wild type. La CR modula el perfil metabólico del músculo esquelético, resultando en una composición de las fibras más oxidativa y un incremento en el consumo de oxígeno usando glucosa y ácidos grasos como sustratos en mitocondrias aisladas. Para analizar el efecto de la CR sobre el estatus de las células madre del músculo esquelético cultivamos las células con suero de ratones en situación de ratones wild type y mutantes en ad libitum y CR. Las células mutantes cultivadas con suero de ratones en CR mostraron un incremento de la diferenciación y del consumo de oxígeno. Como sumario de este capítulo, la CR mejora los defectos asociados a la mutación en el gen *ADCK2*.

Los cuatro capítulos de la tesis están centrados en el estudio de modelo de ratón *Adck2* knockout pero bajo diferentes condiciones y usando diferentes métodos y aproximaciones como la suplementación con CoQ_{10} o la CR, resultado en un completo análisis fenotípico del modelo estudiado para demostrado el establecimiento, la progresión y la afectación de esta disfunción mitocondrial.

Table of contents

LIST OF FIGURES

LIST OF TABLES

ABBREVIATIONS

- 3-hydroxy-3-methyl-glutaryl-coenzyme A (HMG-CoA)
- 4-hydroxy-benzoate (pHB)
- Acetyl-coenzyme A (acetyl-CoA)
- Adenosine triphosphate (ATP)
- Ammonia (NH_4^+)
- Ascorbic acid (ASC)
- Barium chloride ($BaCl_2$)
- Blue native polyacrylamide gel (BN-PAGE)
- Body weight (BW)
- Bovine serum albumin (BSA)
- Caloric restriction (CR)
- Carbon dioxide (CO_2)
- Carbonyl cyanide-p-trifluoromethoxyphenylhydrazone (FCCP)
- Cell Signaling (CS)
- Central nervous system (CNS)
- Centro Andaluz de Biología del Desarrollo (CABD)
- Chicken embryo extract (CEE)
- Choline dehydrogenase (CHDH)
- Coenzyme Q (CoQ)
- Complementary DNA (cDNA)
- Complex I (CI)
- Complex II (CII)
- Complex III (CIII)
- Complex IV (CIV)
- Complex V (CV)
- Coupling Assay medium (CAM)
- Cytochrome C (Cyt C)
- Days post coitum (DPC)
- Days post injection (dpi)
- Decaprenyl hydroxybenzoic acid (DPHB)
- Decaprenyl-dihydroxybenzoate (DPDHB)
- Decaprenyl-PP (DPP)
- Decaprenyl-vanillic acid (DPVA)
- Demethoxy-coenzyme Q10 (DMQ10)
- Demethoxy-demethyl-coenzyme Q10 (DDMQ10)
- Demethyl-coenzyme Q10 (DMeQ10)
- Developmental Studies Hybridoma Bank (DSHB)
- Dihydroorotate dehydrogenase (DHODH)
- Dithiothreitol (DTT)
- Dynamin-related/-like protein 1 (DRP1)
- Electron transport chain (ETC)
- Electron transport flavoprotein dehydrogenase (ETFDH)
- Electron-transferring flavoprotein dehydrogenase (ETFDH)

- Endoplasmic reticulum (ER)
- Endoplasmic reticulum-mitochondria encounter structure (ERMES)
- Extensor digitorum longus (EDL)
- Extracellular matrix (ECM)
- Facioscapulohumeral muscular dystrophy (FSHD)
- Farnesyl pyrophosphate (FPP)
- Fetal Bovine Serum (FBS)
- Fibroblast Growth Factor (FGF)
- Flavin adenine dinucleotide (FADH2)
- Gas chromatography coupled to mass spectrometry (GC-MS)
- Gene Ontology (GO)
- Geranyl pyrophosphate (GPP)
- Glucose tolerance test (GTT)
- Glycerol-3-phosphate dehydrogenase (G3PDH)
- Guanosine triphosphate (GTP)
- High-performance liquid chromatography (HPLC)
- Homeostatic model assessment (HOMA)
- Horse Serum (HS)
- Horseradish peroxidase (HRP)
- Immunohistochemistry (IHC)
- Inner mitochondrial membrane (IMM)
- Inorganic phosphate (Pi)
- Insulin Tolerance Test (ITT)
- Intermembrane space (IMS)
- Intermyofibrillar mitochondria (IFM)
- Intraperitoneal (IP)
- Intraperitoneal pyruvate tolerance test (IPPTT)
- Isopentenyl pyrophosphate (IPP)
- Jackson Laboratory (JL)
- Lactate dehydrogenase (LDH)
- Lactate dehydrogenase A- subunit (LDHA)
- MicroRNA (miRNA)
- Minor allelic frequency of (MAF)
- Mitochondrial calcium uniporter (MCU)
- Mitochondrial DNA (mtDNA)
- Mitofusin (MFN)
- Muscular dystrophies (MDs)
- Myogenic precursor cells (MPCs)
- Myogenic Regulatory Factors (MRFs)
- Myosin Heavy Chain (MyHC)
- Nicotinamide adenine dinucleotide (NADH)
- Optic atrophy 1 (OPA1),
- Outer mitochondrial membrane (OMM)
- Oxidative phosphorylation (OXPHOS)
- Oxygen consumption rate (OCR)
- Paraformaldehyde (PFA)

- Penicillin-Streptomycin (PS)
- Peroxisome proliferator-activated receptor-gamma coactivator 1-α (PGC1α)
- Phosphate-buffered saline (PBS)
- Polymerase Chain Reaction (PCR)
- Polyunsaturated fatty acids (PUFAs)
- Polyvinylidene difluoride (PVDF)
- Principal Component Analysis (PCA)
- Proline dehydrogenase (PROD)
- Protease inhibitor cocktail (PIC)
- Quantitative real-time PCR (qPCR)
- Respiratory control ratio (RCR)
- Respiratory exchange ratio (RER)
- Resuspension Buffer (RB)
- Room temperature (RT)
- SAFE D40 (Scientific Animal Food and Engineering)
- Santa Cruz (SC)
- Satellite cells (SCs)
- Semi-ubiquinone (CoQH)
- Senescence-accelerate mouse prone 8 (SAMP8)
- SN1 (Supernatant Number 1)
- SN2 (Supernatant Numb 2)
- Subsarcolemmal mitochondria (SSM)
- Sulphide-quinone oxidoreductase (SQR)
- Tibialis anterior (TA)
- Translocase complex of the inner membrane (TIM)
- Translocase complex of the outer membrane (TOM)
- Tris/Glycine/SDS (TGS)
- Tween-Tris-buffered saline (TTBS)
- Ultraviolet (UV)
- Voltage-dependent anion channels (VDAC)
- Western Blot (WB)
- α-tocopherol (α-TOC)
- β-oxidation medium (BOXM)

Introduction

1 INTRODUCTION

1.1 Mitochondria

1.1.1 History and general introduction

Mitochondria are enclosed membrane organelles specialized in energy conversion that burn nutrient molecules to produce adenosine triphosphate (ATP) by oxidative phosphorylation (OXPHOS) and are present in cells of animals, plants and fungi. Bacteria present simpler a version of protein complexes for ATP production. Originally, mitochondria in eukaryotes were prokaryotic cells, specifically anaerobic α-proteobacterium, which were endocytosed during eukaryotic evolution. For this reason, these organelles present their own DNA that encodes still a small group of proteins (1). Mitochondrial DNA (mtDNA) and ribosomes are localized in the mitochondrial matrix, organized into compact structures known as nucleoids, but most of mtDNA has been lost over evolution and nowadays only encodes a reduced group of mitochondrial proteins. However, these organelles are very dependent on proteins encoded by nuclear genes as the eukaryotes' cells have become highly dependent on mitochondria due to ATP production through the OXPHOS that they need for essential bioenergetic processes, as well by other specific reactions and pathways that take part inside of the mitochondria, such as urea cycle, fatty acids β-oxidation and Krebs cycle (2). Mitochondria incorporation was necessary for the evolution of eukaryotes cells because confers the capability to produce their own ATP via respiration, a reaction that produces almost 15 times more ATP than anaerobic glycolysis. This bioenergetic improvement allowed eukaryotic cells to evolve in terms of shape, size and function, leading to complex multicellular organisms. Moreover, mitochondrial aerobic metabolism offered the opportunity to produce large amounts of energy from different organics sources (2).

Mitochondria cover approximately 20-25% of cytoplasmatic space in eukaryotic cells and present a body diameter of 0.5-1 um. They can also fuse and divide, and their size and number are tissue and cell type-specific, although can change in function to different stimuli. Also, the specific function of the cell that contains mitochondria determines their intracellular movement. For instance, mitochondria move long intracellular distances along the microtubular cytoskeleton in neurons whereas they remain fixed at one specific point in skeletal or cardiac muscle. On the other hand, mitochondria present associations with membrane systems in the cell such as the endoplasmic reticulum (ER) to promote lipids exchange between both organelles (2).

1.1.2 Mitochondrial architecture

Mitochondria are composed of two developed membranes, an outer and an inner membrane as can be observed in Figure 1. The presence of both membranes is considered proof of their prokaryotic origin. Both membranes are crucial for energy production and have structural functions, although they present different biochemical properties. The inner mitochondrial membrane (IMM) shows a series of invaginations, the cristae, where are localized the proteins of the electron transport chain (ETC). Particularly, the inner membrane joins, where the membrane of crista creates a narrow membrane, are known as crista junctions. The IMM encloses the mitochondrial matrix and the space between both membranes is known as intermembrane space (IMS) (20-30nm). The outer mitochondrial membrane (OMM) is highly permeable to molecules until 5000 Daltons due to the presence of porins, proteins known as voltage-dependent anion channels (VDAC) that leads to aqueous pores across the membrane (2). The translocase complex of the outer membrane (TOM) is the main way used by most nucleus-encoded mitochondrial precursor proteins to enter into the mitochondria (3). Subsequently, the IMS has the same pH and ionic composition as the cytoplasm, and there is no electrochemical gradient across the OMM (2).

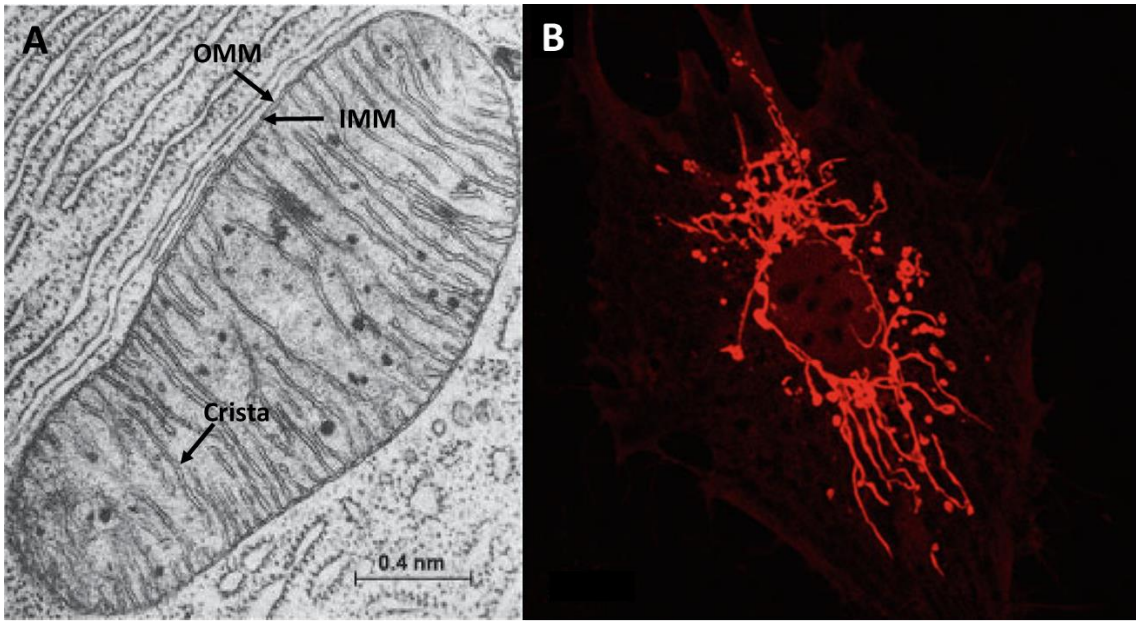

Figure 1. Mitochondria introduction.
(A) Electron micrograph of mitochondria. Outer mitochondria membrane (OMM), inner mitochondrial membrane (IMM) and mitochondrial crista were indicated. Adapted from (4). (B). Mitochondrial network immunostaining was photographed with a fluorescence microscope to observe the mitochondrial fusion/fission process. (Adapted from (5).

In contrast, the IMM constitutes a diffusion barrier characterized by high protein concentration and low permeability that can be only passed by selected ions (protons and phosphates) and

essential metabolites (ATP and ADP). The control of this permeability allows the formation and preservation of an electrochemical gradient over the IMM that is crucial for ATP production (6). IMM is divided into functionally differentiated areas, the boundary region holds the protein's import tools (translocase complex of the inner membrane, TIM) and constructing respiratory-chain complexes whereas more inward is localized the ATP synthase, ETC protein complexes (2). Mitochondria also hold their own mtDNA, which is attached to all the proteins needed for mtDNA processing and maintenance, forming a structure known as nucleoids. The mitochondrial matrix carries groups of proteins and ions that participate in the essential process for the cell such as the Krebs cycle, coenzyme Q (CoQ) biosynthesis or steroids production (7). IMS is also very important because permits the transference of ions, proteins and lipids between the mitochondrial matrix and the cytoplasm, regulates the apoptotic process, the mitochondrial morphogenesis and controls the generation of oxygen species. Cytochrome c, a central element for electron transfer at the ETC, is also localized in IMS (8).

Secondly, mitochondria are continuously on cycles of fusion and fission moving along the microtubules of the cytoskeleton in a process known as mitochondrial dynamics (9). Fusion and fission are highly complex processes due to are necessary to protect the integrity of the different mitochondrial parts by controlling the number and size of the mitochondrial populations specifically in each tissue. These processes depend on GTPases that modulate both the contraction needed for fission and the fusion-specific complex formation, such as optic atrophy 1 (OPA1), Mitofusin (MFN) and Dynamin-related/-like protein 1 (DRP1). Fusion and fission regulate the number and shape of mitochondria populations in the distinct cell types to respond to the needs of the cell and to maintain mitochondria quality and function (2)(9).

1.1.3 Energy production in mitochondria

In the energetic metabolism that occurs in mitochondria, pyruvate derived from glucose, fatty acids from fats and amino acids from proteins are converted into acetyl-CoA in the mitochondrial matrix (10). One molecule of glucose is transformed into two molecules of pyruvates through glycolysis in the cytosol where Nicotinamide adenine dinucleotide (NADH) and ATP are also produced. Regarding β-oxidation, fatty acids (fatty acyl CoA) are imported into the mitochondria and catabolized in a cycle of reactions where they lose two carbons in each reaction from its carboxyl end, producing one molecule of acetyl CoA, a molecule of NADH and a molecule of flavin adenine dinucleotide ($FADH_2$) (2). Acetyl-CoA is completely oxidized to two molecules of CO_2 in the critic acid cycle to produce three NADH, one $FAHD_2$ and one guanosine triphosphate (GTP) (2).

Simultaneously, NADH and $FAHD_2$ produced in these catalytic pathways are used by the complexes in the ETC where electrons go to complex I and II respectively, each complex present a higher affinity for electrons than the previous one, breaking free new NAD^+ and FAD. Finally, electrons bind to an O_2, the molecule that exhibits the higher electron affinity, at complex IV and produces H_2O a low energy molecule. The energy liberated across complex I, complex III, CoQ and complex IV creates an electrochemical proton gradient across the IMM. This process originates a pH and voltage gradient across the IMM that leads to ATP production by the ATP synthase, which successfully transforms the energy from this electrochemical gradient into biological active energy known as ATP from ADP (adenosine diphosphate) and a molecule of inorganic phosphate (Pi). The ATP synthesis through this process is known as OXPHOS (2).

ETC transport electrons from $FADH_2$ produced by acyl-CoA dehydrogenase that transform acyl-CoA to trans- Δ^2-enoyl-CoA in fatty acids β-oxidation pathway. Then, these electrons are given to ETF protein and later to ETFQO protein from where electrons finally reach the CoQ (2). ATP synthase is localized in the membranes of the mitochondrial cristae alongside the large protein complexes of the ETC, that pump electrons to the IMS. Furthermore, two-electron carriers are also in ETC, CoQ (Figure 2) and cytochrome C (Cyt C) that assist in the electron transference between complexes (2).

Complex I (CI) or NADH dehydrogenase complex is the largest complex. CI receives electrons from NADH and transfers the electrons through a flavin mononucleotide and eight iron-sulfur clusters to the ubiquinone electron carrier pumping four protons to the IMS and leading to ubiquinone reduction (2)(11).

Complex II (CII) or succinate dehydrogenase regulates the oxidation of succinate to fumarate and sends electrons directly to the ubiquinone without pumping protons to the IMS. CII is localized in the mitochondrial crista as the rest of the complexes but does not participate in the proton-motive force. Strictly, CII could not be considered part of the mitochondrial respiratory chain but contributed to the ubiquinone reduction transferring electrons that later would pass to the CIII (12) (2). CII is also a component of the TCA cycle (2).

Complex III (CIII), cytochrome c reductase or cytochrome b-c1 works as a dimer where each monomer presents three cytochrome hemes and an iron-sulfur cluster. CIII receives electrons from the ubiquinol and transfers them to another electron carrier, the cytochrome c. Four protons are transferred to the IMS for each cycle of two electrons transported through CIII (2)(13). The redox cycle takes place by two consecutive electron transferences generating a CoQ intermediate during this process known as semi-ubiquinone (CoQH) (13)

Complex IV (CIV) or cytochrome c oxidase complex presents two cytochrome hemes and three copper atoms. This complex receives electrons from the reduced cytochrome c and transfers them to molecular oxygen to finally produce water. CIV also transfer H^+ to the IMS (2).

Complex V or ATP synthase (CV) could be considered a nanomachine constituted by 23 subunits and it has a mass of around 600 kDa. CV uses the protein gradient generated by the rest of the complexes to produce ATP from ADP and Pi. CV could work as a proton drive turbine because its structure is formed by a rotor and a stator. CV is powered by the flow of H^+ into the matrix, spinning at 8.000 revolutions per minute and producing three ATP molecules per round scan to generate 400 molecules of ATP per second. The generated ATP is then transferred to the cytosol via ADP/ATP transporters (2)(14).

Supercomplex formation in the mitochondria crista membrane has been proposed as a structure to facilitate the transference of electrons from the electron carriers the ubiquinone and the cytochrome c. The establishment of the supercomplex is subjected to the mitochondrial lipid cardiolipin which is thought to work as a glue that sustains the complexes side by side (2). However, it has been proposed that supercomplexes could be formed by different subunits III_2V_1, I_1III_2, $I_1III_2V_1$, and $I_2III_2IV_1$-$_2$. The supercomplex that includes $I_1III_2IV_1$ is known as the respirasome and the supercomplex that groups $I_2III_2V_2$ is denominated as the megacomplex (15)(16). It has been suggested that CoQ and cytochrome c could be established in different pools within each supercomplex (17).

1.1.4 Other mitochondrial functions

Apart from ATP generation, mitochondria are also essential for buffering the redox potential in the cytosol. A critical step in glycolysis, transforming glyceraldehyde 3-phosphate to 1,3-bisphosphoglycerate, produces a constant supply of electrons in the cytosol that is countered by NAD^+. This excess of electrons is transferred to small cytosol molecules that can go through the inner mitochondrial membrane up to the matrix and transfer the electrons to NAD^+ creating new NADH that will feed the ETC to generate more ATP (2).

Another function of mitochondria is to carry out two essential steps in the urea cycle. The urea cycle transforms the ammonia (NH_4^+) coming from the breakdown of the nitrogen-containing compounds, into urea for its elimination as urine. Mitochondria also participated in heme groups biosynthesis. Iron-sulfur clusters that are critical for the stability of the nuclear genome are produced in mitochondria. Mitochondrial also is involved in calcium buffers accepting calcium from ER and sarcoplasmic reticulum membrane connections through the mitochondrial calcium uniporter (MCU) (18).

1.1.5 Mitochondrial diseases

Mitochondrial diseases are considered rare syndromes that present heterogenic causes and potentially affect energy production. Clinical symptoms are heterogeneous and often affect tissues that present a very high energetic demand such as the brain, skeletal muscle, kidneys, or heart. This clinical variation could lead to a delay in disorder diagnosis. The clinical manifestation can appear at any age and affect also to different organs. The approximate prevalence is 1 out of 5000 people (19)(20). Particularly, mitochondrial diseases could be associated with mutations in nDNA that includes autosomal and X-linked inheritance or mtDNA, which are inherited through the mother. However, mitochondrial disease can be also originated from de novo mutation in nuclear or mitochondrial DNA (20).

1.2 Coenzyme Q_{10}

1.2.1 Coenzyme Q history, structure, function, and properties

An essential element in mitochondria function is Coenzyme Q (CoQ) or ubiquinone. CoQ was isolated and identified by Festenstein et al. in 1955 (21) and validated by Crane et al. in 1957, who demonstrated its main function in the ETC and its redox properties (22). CoQ is the unique redox-active lipid endogenously produced, a crucial component of the mitochondrial ETC and an antioxidant found in all plasma membranes, endomembranes and lipoproteins (23). CoQ is conserved from proteobacteria to humans and can be found reduced ($CoQH_2$ or ubiquinol), carrying two electrons, completely oxidized (CoQ or ubiquinone), or in a semi-reduced state known as a semi-ubiquinone intermediate (CoQH). Its main function is to shut electrons that receive from complexes I and II to complex III in the mitochondrial ETC which leads to ATP production by the ATP synthase (Figure 2) (24). Reduced CoQ is oxidized by complex III in the ETC. This constant oxidation/reduction cycle confers to CoQ the property to transfer electrons from different biological processes and acts as an antioxidant at membrane location preserving lipids, protein, and nucleic acids from oxidative damage (25)(26) and preventing lipid peroxidation (27)(28). CoQ is also important to preserve vitamin C and α-tocopherol reduced in the plasma membrane (29) (30).

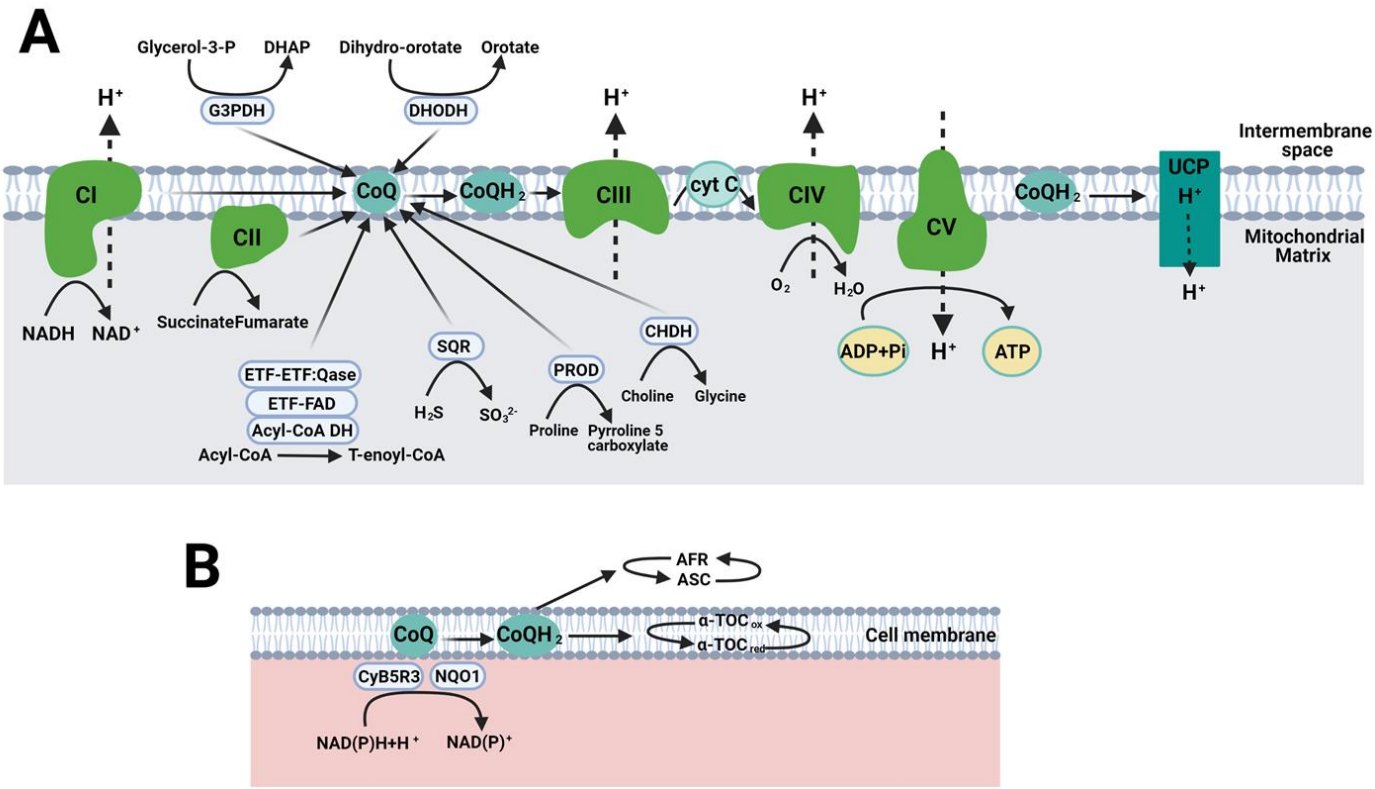

Figure 2. Molecular functions of coenzyme Q.
(A) Coenzyme Q integration into the inner mitochondrial membrane. Coenzyme Q receives electrons from complexes I and II and after the reduction/oxidation cycle sends the electrons to complex III. Coenzyme is also reduced by several hydrogenases showing the importance of Coenzyme Q in different pathways. (B) Coenzyme Q integration in extramitochondrial cell membranes where its functions depend on the reversible oxidation and reduction of its benzoquinone ring. (Image elaborated by the PhD candidate).

Figure 2A shows CoQ at the IMM where is reduced by hydrogenases from different cellular reactions such as mitochondrial glycerol-3-phosphate dehydrogenase (G3PDH) that connect glycolysis, oxidative phosphorylation and fatty acid metabolism; electron transport flavoprotein dehydrogenase (ETFDH) that is an essential enzyme in fatty acids β-oxidation and branched amino acid oxidation; proline dehydrogenase (PROD) that participates in glyoxylate metabolism; sulphide-quinone oxidoreductase (SQR) that participates in sulfide detoxification, (an important gas in many cellular processes). CoQ is also reduced by hydrogenases from choline to glycine conversion, the choline dehydrogenase (CHDH), and dihydroorotate dehydrogenase (DHODH) that convert dihydro-orotate to orotate for pyrimidine nucleotide metabolism, as is depicted in Figure 2. CoQ also participated in energy dissipation in the ETC by the dissemination of the proton gradient as heat due to CoQ association to uncoupling protein localized in the IMM. CoQ is also a structural component of complex I and complex III in the ETC (31) (32) and is involved in complex I stability (33). Outside of the mitochondria, CoQ shows antioxidant protection reducing α-tocopherol (α-TOC) and ascorbic acid (ASC) as part of the plasma membrane redox system (34). CoQ also is involved in the regulation of cytosolic redox intermediates such as NAD(P)H as a component of the response of cells to alterations in the redox environment (35).

Regarding CoQ structure, CoQ is composed of a benzoquinone ring bonded to a polyisoprenoid side chain that preserves the molecule inserted into a lipidic bilayer. The number of isoprene units in the chain is species-specific: human isoform encloses mainly ten isoprene units (CoQ_{10}) but few molecules also present 9 isoprene units (CoQ_9); rodents present nine units (CoQ_9) and ten units (CoQ_{10}); the yeasts Saccharomyces cerevisiae holds six units (CoQ_6), whereas Schizosaccharomyces pombe contains ten units (CoQ_{10}); the fruit fly Drosophila melanogaster present 3 isoforms with 8, 9 and 10 subunits (36) and Escherichia coli contains eights isoprenes (CoQ_8) (37). CoQ has been found in all tissues, cells and isolated lipoprotein fractions in variable amounts. In rodents, about 10-20% of the total CoQ has 10 isoprenes, except for the brain, intestines and spleen where 30-40% of total CoQ has 10 isoprenes. However, CoQ concentration differs between different organs, even between regions or cells population of the same organs suggesting structural and functional specializations such as the number of mitochondria. Regarding the intracellular distribution, the highest amount of CoQ is found in the outer and inner mitochondrial membrane, lysosomes and Golgi vesicles. Particularly, the intramembranous localization of CoQ is the central hydrophobic region, between the double layers of phospholipid fatty acids and the central location to elevate membrane fluidity and permeability. Moreover, CoQ could move to the inner or outer membrane surface depending on cell functional requirements (24).

1.2.2 Coenzyme Q biosynthesis and distribution

Although CoQ could be incorporated through the diet, most CoQ is endogenously produced in mitochondria and after that delivered to the rest of the cell membranes (38). CoQ is formed by a benzoquinone ring and a polyisoprenoid chain which inserts CoQ into the phospholipid bilayer. CoQ is biosynthesized in mitochondria by a nuclear-encoded CoQ proteins cluster, although the initial biosynthesis of the tail and head takes part in the endoplasmic reticulum and the cytosol respectively, Figure 3. Furthermore, the biosynthetic pathway is not clear yet and is carried out by at least 13 genes (39). The polyisoprenoid chain is produced through the mevalonate pathway from which other lipids such as cholesterol or dolichol, heme A and protein prenylation elements are also synthesized in extra-mitochondrial membranes. The initial substrate is acetyl-coenzyme A (acetyl-CoA) so that, three acetyl-CoA molecules are condensed to form 3-hydroxy-3-methyl-glutaryl-coenzyme A (HMG-CoA) due to acetoacetyl-CoA thiolase and HMG-CoA synthase action. Subsequently, mevalonate is produced from HMG-CoA by HMG-CoA reductase. Mevalonate is phosphorylated and decarboxylated to produce isopentenyl pyrophosphate (IPP). Farnesyl pyrophosphate synthase uses IPP to make farnesyl pyrophosphate (FPP), a common precursor for the lipids synthesized through the mevalonate pathway, and intermediary product for

geranyl pyrophosphate (GPP) production. The next enzyme involved in CoQ biosynthesis is the trans-prenyl-transferase that converts FPP into polyprenyl-PP, which is considered the rate-limiting step (24). The transport of FPP to the mitochondria is not totally described yet, but it has been proposed to occur in the ER-mitochondria contact sites through the endoplasmic reticulum-mitochondria encounter structure (ERMES) complex (40) (41). *COQ1* protein (*PDSS1* and *PDSS2*) would assemble the side chain and determine the number of isoprene units in the polyprenyl tail producing decaprenyl-PP (DPP).

The precursor of the quinone head of CoQ is 4-hydroxy-benzoate (pHB), which is synthesized from tyrosine or phenylalanine in the cytosol of mammalian cells. pHB is attached to the polyprenylated tail by *COQ2* protein (42) leading to the production of decaprenyl hydroxybenzoic acid (DPHB) in the mitochondrial matrix (Figure 3). The next set of reactions will occur on the matrix side of the IMM that would consist of sequential changes in the aromatic ring. Initially, DPHB would suffer a C5-hydroxylation by *COQ6* resulting in decaprenyl-dihydroxybenzoate (DPDHB) formation (43). Subsequently, DPDHB would be O-methylated by *COQ3* to form decaprenyl-vanillic acid (DPVA) (44)(45). Later, a C1-hydroxylation and C1-decarboxylation would happen by an unidentified protein to form demethoxy-demethyl-coenzyme Q_{10} ($DDMQ_{10}$). Afterwards, *COQ5* would carry a C2-methylation to form demethoxy-coenzyme Q_{10} (DMQ_{10}) (46). Thereafter, DMQ10 would be C6-hydroxylated by *COQ7* to form demethyl-coenzyme Q_{10} ($DMeQ_{10}$) (47). Finally, *COQ3* would produce CoQ_{10} from $DMeQ_{10}$.

Other *COQ* proteins present regulatory functions such as *COQ8A* (*ADCK3*) and *COQ8B* (*ADCK4*) which show properties of an atypical kinase that phosphorylates *COQ3*, *COQ5,* and *COQ7* (48)(49)(50). *COQ4* function is still not elucidated but some indications show that could modulate the formation and maintenance of the CoQ biosynthetic complex (51). Moreover, *COQ9* is a lipid-binding protein that balances *COQ7* (52)(53). *COQ10A* and *COQ10B* possibly regulate CoQ proper location within the IMM, taking CoQ_{10} to the IMM where displays its functions (54).

During the last times, it has been proposed that all *COQ* proteins would join a membrane-linked complex denominated the CoQ synthome, CoQ biosynthesis complex or Q synthome (Figure 3). This structure would help to secure the CoQ biosynthesis process and prevent the escape of reactive intermediates (55). Related to the role of *COQ4* in CoQ biosynthesis, it has been suggested that *COQ4* could act as a scaffolding component for the CoQ synthome (51).

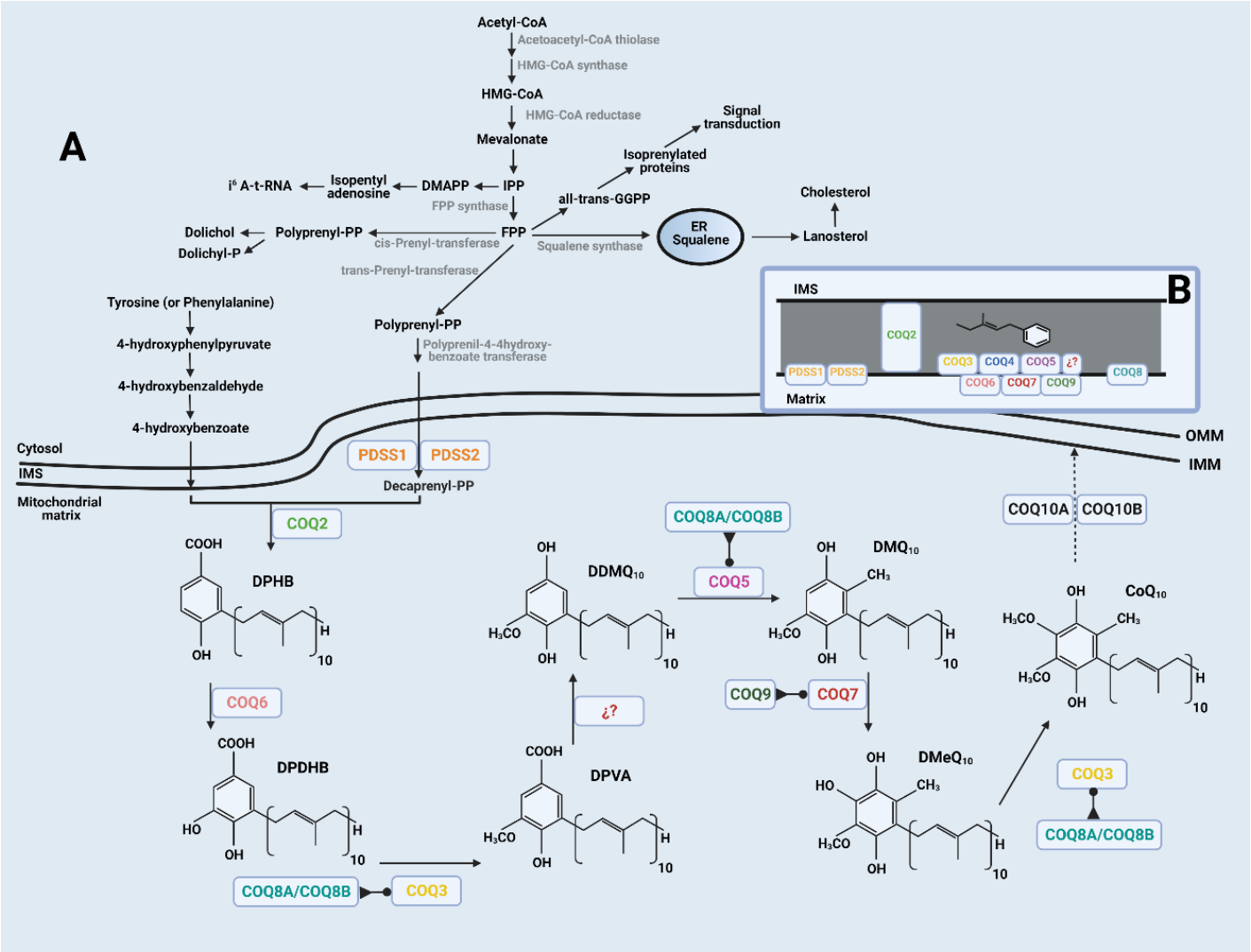

Figure 3. Coenzyme Q biosynthesis in mammals.
(A). CoQ biosynthetic pathway takes part in the cytosol where the benzoquinone ring and the polyisoprenoid chain are produced from acetyl-CoA and tyrosine, then they are transported into the mitochondria where they are fused to form the first CoQ intermediary, the DPHB. Next, several enzymes that form a biosynthetic complex modify the benzoquinone ring to finally produce the CoQ. (B) CoQ biosynthetic complex composed of the different CoQ proteins located in the IMM. Adapted from (56).

Additionally, other lipids synthesized through the mevalonate pathway apart from CoQ are dolichyl-P, cholesterol and dolichol (Figure 3). Concerning its intracellular distribution, dolichol is highly localized in lysosomes and Golgi vesicles. Cholesterol is enriched in rough microsomes, smooth microsomes, lysosomes, Golgi vesicles and plasma membranes. Dolichyl-P and dolichol are found in the central position of the plasma membrane increasing membrane permeability while cholesterol is localized on one side of the membrane reducing fluidity and permeability (24).

1.2.3 Coenzyme Q primary and secondary deficiencies

Regarding the CoQ function at the OXPHOS to produce ATP, CoQ deficiency produced different mitochondrial dysfunctions that course with energy deficiency (Figure 2). Indeed, they are a heterogeneous group of diseases reproducing a highly severe range of clinical manifestations where many different tissues, organs, and systems are damaged (57). CoQ deficiencies are a consequence of hypomorphic mutations or polymorphisms, epigenetics, maternal inheritance, ageing process, compensatory process and environmental factors, and they could be classified as primary and secondary deficiencies depending on the etiology of the syndrome. Primary CoQ deficiencies are a group of extremely rare diseases originated from mutations in any of the genes needed for CoQ biosynthesis at the enzymatic or regulatory level. Secondary CoQ deficiencies present a decrease in CoQ levels caused by defects not directly associated with CoQ biosynthesis (39). The pathogenesis has not been well elucidated yet, it has been proposed two main aspects: the bioenergetic defect and an increase in reactive oxygen species (ROS). However, the undescribed functions of some COQ genes, the heterogenic clinical manifestations and the high number of CoQ functions inside and outside of the mitochondria suggest the idea that other mechanisms could be involved in the pathogenesis of these syndromes (39).

About primary CoQ deficiencies, the clinical phenotype is very heterogenic and includes damages mainly to the central and peripheral nervous system, kidney, skeletal muscle and heart. Even mutations in the same gene can lead to different clinical manifestations (39). The age of onset usually ranges from childhood to adolescence, but it is also adulthood-onset. Primary CoQ deficiencies are normally originated from autosomal recessive mutations, and to date, pathogenic mutations have been found in *PDSS1*, *PDSS2*, *COQ2*, *COQ4*, *COQ5*, *COQ6*, *COQ7*, *COQ8A*, *COQ8B* and *COQ9*. However, it is complicated to establish a possible connection between genotype-phenotype due to the lack of patients (around 275 patients from 180 families have been reported) and the large variety of symptoms associated with the same *COQ* gene mutated (39).

Secondary deficiencies are more common than primary deficiencies possibly due to the diversity of biological processes, functions and pathways in which CoQ participates. All of them are characterized by a decrease in CoQ levels not directly caused by defects in CoQ biosynthesis such as respiratory chain defects, multiple acyl-CoQ dehydrogenase decrease, ataxia and oculomotor apraxia (58)(39). Moreover, secondary deficiencies are increasing day by day because of recently Next-Generation Sequencing (NGS) tools for diagnosis (59), which show additional genes involved in either CoQ maintenance or degradation, resulting in a decrease in CoQ levels which is a common feature in a wide range of diseases (60).

While the main pool of CoQ is localized in the mitochondria, particularly in the ETC, mutations in genes that encode proteins with non-direct mitochondrial functions could also lead to a decrease in CoQ levels, such as the glucose transporter GLUT1 (61) and the calcium-activated chloride channel Anoctamin 10 (62), which raises the question if CoQ decrease could be associated with the CoQ dependent functions that are altered during the mechanism of the disease and interestingly if CoQ supplementation could lead to an improvement (61)(62). Besides, secondary CoQ deficiency could be also associated with mutations in the IMM close to the main pool of CoQ such as ETFDH (63) which present a more clear relation due to a decrease in this enzyme could downregulate CoQ biosynthesis or could lead to a faulty binding to CoQ, increasing CoQ degradation because it is the acceptor molecule of ETFDH (63). Moreover, low CoQ levels are common in patients that suffer mitochondrial diseases, a group of clinically heterogeneous disorders that includes myopathy (64). Particular symptoms in secondary CoQ deficiencies are determined by underlying conditions, despite most of the clinical manifestations are described on skeletal muscle including hypotonia, muscle weakness or exercise intolerance, and in the central nervous system (CNS) counting ataxia and CNS impairment (65) (66). Regarding muscle damage in secondary deficiency, pathogenic mutations in mtDNA in patients that suffer mitochondrial myopathy also present a clear CoQ deficiency (64). However, there is a great range of CoQ deficiency in patients that suffer the same condition, suggesting the idea that genetic factors could be also involved in secondary deficiencies (67).

1.2.4 Coenzyme Q administration in deficiencies

CoQ administration is helpful in CoQ deficiencies (65) (66) and its effects are summarized in Table 1, above where a prompt diagnosis and an early initiation of CoQ_{10} supplementation are crucial for improvement (60) because CoQ_{10} can delay or stop the progression of damages. However, when severe damage was already established, CoQ_{10} supplementation is not able to carry out a total recovery (68). Main CoQ_{10} treatment consists of oral CoQ_{10} administration where doses range from 5 to 30-50 mg/kg/day (69), despite in mice studies (Table 2) doses used tend to be higher than 200 mg/kg/day (70). Regarding CoQ_{10} preparations, they tend to vary in their characteristics and absorption (71), soluble forms, soft-gel or oily formulations would be recommended while tables should be avoided due to their low absorption (72)

Initially, the oxidized form of CoQ (ubiquinone) was the only redox state available to treat these syndromes, but modern pharmacologic methods can maintain CoQ reduced (ubiquinol), making possible a higher bioavailability (58). Several aspects could influence the different results of CoQ administration such as the doses, preparation, formulation, disorder severity, tissues damaged, or even environmental, genetic, or epigenetic elements (73).

As can be observed in Table 1, CoQ administration presented beneficial effects on muscle weakness strength, ataxia, hypotonia and stabilized plasma levels of metabolites. However, CoQ administration was not able to improve deafness or neurodegeneration associated with neuropathy, supporting the importance of a rapid diagnosis and early treatment to avoid the establishment of an irreparable disease.

Table 1 CoQ_{10} administration in Secondary CoQ deficiency in humans

Gene affected	Protein location	Clinical manifestations	Patient(s) reported	CoQ formulation	Effect	Reference
SUCLA2 c.1276C>T (p.Arg407Trp)	Mitochondria (TCA cycle)	Psychomotor delay, deafness, myopathy, ataxia, and chorea.	A 9-year-old Brazilian boy	Escalating doses up to 2000 mg daily	Improvement of muscle weakness.	(74)
SLC2A1 (c.18+2T>G)	Cell membrane	Truncal ataxia, nystagmus, dysarthria and myoclonic epilepsy.	A 15-year-old girl	CoQ supplementation (30 mg/Kg/day)	Improvements in ataxia and nystagmus	(61)
ANO10	Cell membrane	Cerebellar ataxia, epilepsy, learning difficulties. retinal degeneration and cataracts.	A 57-year-old and 52-year-old women.	Dose patient1: 1,000 mg/day. Dose patient 2: 120–180 mg/day.	Beneficial effects fatigue and mobility within 3–4 months. Improvement of the ataxia and gait, in the oculomotor movement score and in the dysarthria	(62)
APTX	Nucleus	Ataxia, wheelchair-bound, with alternating esotropia, severe limb ataxia with the slightest purposeful movement, peripheral neuropathies and scoliosis.	Four affected individuals from the same family	CoQ started at 200 mg and progressively increased to to 600 mg daily.	Improvement in strength and ataxia. Seizures disappeared	(75)
Recessive mutations in ETFDH	Mitochondrial inner membrane	Lipid accumulation, mitochondrial myopathy, exercise intolerance, fatigue, proximal myopathy and high serum CK.	Seven patients from 5 different families (2 adults, 5 teenagers)	500 mg/day plus riboflavin (100mg/day)	Normal CK levels, improvement of muscle strength.	(63)
Pathogenic R257Q BRAF gene mutation	Cell membrane, nucleus, cytoplasm	Cardiofaciocutaneous, psychomotor development was severely impaired, hindered by muscular hypotonia and ataxia.	A 4-year-old girl	Dose not reported	Improvement in ataxia and muscular hypotonia	(76)
ADCK2	Mitochondria	Liver dysfunction and severe mitochondrial myopathy with lipid droplets in skeletal muscle.	A 45-years-old male patient	35-150 mg per day	Stabilization of the plasma levels of lactate, CK, myoglobin, and LDH.	(77)

As can be observed below in Table 2 doses used in mice tend to be higher than doses used in humans, thus it is not clear if the effects obtained on mice would be also experienced in humans. Consequently, it would be crucial to study the dose normally used in humans in mice. CoQ administration leads to improvements in most of the mice models studied including an increase in lifelong, attenuation of ROS and brain atrophy. But most of the studies only examined acute CoQ supplementation and during adulthood, it is not known yet the effect of chronic administration through generations.

Table 2 CoQ_{10} administration in mice models

Syndrome	Phenotype	CoQ dose	Effect	Duration	Reference
Huntington disease	Huntington disease and neuronal death	12-600 mg/day (400-20000 mg/kg/day)	Increase in survival, motor performance and grip strength and reduction in weight loss and brain atrophy.	35 days	(78)
Alzheimer	Deposition of senile plaques with meta-amyloid	40mg/day (1200 mg/kg/day)	Attenuation of A beta overproduction and intracellular A beta deposit, decrease oxidative stress and increase antioxidant capacity	60 days	(79)
Alzheimer	Induce neurotoxicity	40mg/day (1200 mg/kg/day)	Reduction of oxidative damage in the brain	30 days	(80)
Atherosclerosis	Atherosclerosis	37.5 mg/day (1000 mg/kg/day)	No effect on atherosclerosis lesions	6-15 weeks	(81)
Accelerated ageing	Accelerated degeneration	15 mg/day (500 mg/kg/day)	Decelerating effects on degenerative process	6-14 months	(82)
Neurodegeneration	Impairments associated to normal brain aging	2.88-13.71 mg/day (96-457 mg/kg/day)	Improves spatial learning and attenuates oxidative damage	15 weeks	(83)
Diabetes mellitus type 2	Elevated urinary albumin excretion rates and albumin:creatinine ratio	10 mg/day (300 mg/kg/day)	Attenuation of ROS production and mitochondrial membrane potential in kidneys	10 weeks	(84)
Accelerated ageing	Accelerated senescence and severe senile amyloidosis	7.5 mg/day (250 mg/kg/day)	Increased lifelong	1 week	(85)
Primary Q deficiency	Interstitial nephritis and die from end-stage renal disease.	6-7 mg/day (200 mg/kg/day)	Rescue of both proteinuria and interstitial nephritis	-	(70)
Neuropathy in diabetes	Loss of sensation, hypoalgesia and decreases in mechanical hyperalgesia, cold allodynia, and sciatic nerve conduction velocity	4 mg/day (120 mg/kg/day)	Phenotype attenuation	6 months	(86)

1.3 *ADCK2* gene and *Adck2* mouse model

1.3.1 *Adck2* patient and *Adck2* knockout mouse

ADCK2 gene has been included in a quinone family known as ABC1 that also includes *ADCK1*, *ADCK3*, *ADCK4* and *ADCK5*. *ADCK2* is an acronym of aarf domain-containing protein kinase 2. Human *ADCK3* (*COQA*) and *ADCK4* (*COQB*) stabilize CoQ biosynthetic complex (87). Mutations in *ADCK3* lead to autosomal recessive cerebellar ataxia and CoQ deficiency (87)(88)(89) while mutations in *ADCK4* cause nephrotic damage associated with CoQ deficiency (90). Recent studies suggest that the other ADCK member has a role in the maintenance of CoQ level within the mitochondria (91), although their exact function has not been described yet.

Although little information is available on the *ADCK2* gene, our group has reported that *ADCK2* haploinsufficiency in humans is associated with hepatic dysfunction and mitochondrial myopathy characterized by progressive muscle wasting which leads to accumulation of lipid droplets in skeletal muscle, decreased CoQ and impairment in mitochondrial β-oxidation (77). Particularly, the 50 years old male patient suffered progressive skeletal muscle degeneration that resulted in myalgia and permanent disability requiring permanently a wheelchair. Muscle Magnetic Resonance Imaging (MRI) showed damage in the shoulder girdle, deltoid, biceps, hamstring and calf muscles. Interestingly, the patient had a normal cognitive function and no sign of ataxia discarding an alteration of the CNS. Sequencing of the patient revealed a heterozygous NM_052853.3:c.997C>T p. (Arg333*) mutation in exon 2 of the *ADCK2* gene, which produces a stop codon that reduces *ADCK2* mRNA and protein. This mutation has a minor allelic frequency of (MAF) of 2:251,006. Temporal CoQ_{10} administration produced biochemical improvements in symptoms associated with muscle damage and mitochondrial diseases such as a reduction in lactate and myoglobin levels. However, after cessation of CoQ_{10} intake, muscle-related symptoms rapidly worsened. One year later, non-invasive ventilation was necessary due to global respiratory failure and twelve years after the presentation of the first symptoms the patient died (77).

We have developed a heterozygous *Adck2* knockout mouse that reproduced the heterogenic mutation of this patient (77). The phenotype of mutant mice showed affected fatty acids β-oxidation, liver damage and mitochondrial myopathy in skeletal muscle. The analysis revealed that *ADCK2* was involved in lipid homeostasis, controlling the CoQ pool in skeletal muscle and affecting the transport of lipids into the mitochondria, which is required for fatty acids β-oxidation and CoQ biosynthesis.

A recent review examined the different mutant animal models generated to understand the biological functions of CoQ (92). The authors explained that the phenotype found in the mutant *Adck2* mouse that includes an altered mitochondrial respiratory chain function and mitochondrial dysfunction in skeletal muscle associated with a decrease in CoQ_9 and CoQ_{10} supports the idea that the *ADCK2* gene plays a role in mitochondrial lipid metabolism in skeletal muscle and CoQ levels (92).

1.3.2 *Adck2* in yeast

A recent study deposited in bioRxiv analysed the role of *ADCK2* in CoQ mobilization from its site of synthesis on the IMM to other places where displays a crucial function using yeast genetics and lipid analyses (91). Loss of *ADCK2* in yeast (Ypl109c) results in CoQ getting away from mitochondria reducing CoQ levels inside of mitochondria, which was accompanied by impairment of polyunsaturated fatty acids (PUFAs) resistance. Additionally, the same study reported that other ADCK genes (*Adck1* and *Adck5*) were also involved in maintaining the proper CoQ levels in the mitochondria. Particularly, the absence of both genes led to an excessive CoQ accumulation inside of the mitochondria in yeast.

1.3.3 *Adck2* and skeletal muscle

Mitochondria are highly plastic organelles that play a crucial role in skeletal muscle metabolism, maintenance and physiology such as contributing with ATP to skeletal muscle contraction or modulating either redox homeostasis, cellular quality or cell death through mitophagy (93)(94). Organization and control of mitochondrial function are coordinately regulated by a protein quality control system, mitochondrial dynamics, biogenesis and precise degeneration (93). Therefore, mitochondrial dysfunction in muscle cells such as myocytes leads to muscle degeneration (95). Particularly, mitochondria play a regulatory role in the myonuclear domain in skeletal muscle myofibers in ageing and atrophy (94) (96). Mitochondria in skeletal muscle can be separated into two different populations presenting different bioenergetic (97) and structural functions (98). Mitochondria located under the sarcolemma, subsarcolemmal mitochondria (SSM), are involved mainly in signalling and providing energy for the initiation of contraction whereas mitochondria located between the myofibrils, intermyofibrillar mitochondria (IFM), are involved in providing ATP for contraction directly. Regarding the essential role of mitochondria in muscle energy production and redox homeostasis, impairment of mitochondria induces myocyte atrophy and muscle wasting (95).

Thus, mitochondria are essential organelles in skeletal muscle, consequently, mitochondrial dysfunction leads to muscle weakness and damage. As has been mentioned above, the human

patient that presents a mutation on the *ADCK2* gene developed a mitochondrial dysfunction characterized by a decrease in CoQ_{10} levels associated with a progressive skeletal muscle myopathy and an impairment in fatty acids metabolism (77). The high importance of mitochondria and CoQ in muscle metabolism suggest that the mutation of the *ADCK2* gene could lead to progressive skeletal muscle damage due to the high energy demands of skeletal muscle. Additionally, the impairment of fatty acids metabolism that presented to the patient could also influence muscle degeneration (77).

1.4 Skeletal muscle

1.4.1 General introduction

All eukaryotic cells present a contractile architectonic system including actin and myosin, but muscle cells possess an evolution version of this model more specialized. Mammals present four categories of cells specialized for contraction: skeletal muscle cells, heart (cardiac) muscle cells, smooth muscle cells and myoepithelial cells. All these kinds of cells produce contractile forces based on actin and myosin II. Skeletal muscle cells contraction under voluntary control produces movement converting chemicals into physical energy (2). Skeletal muscle is a biomechanical tissue constituted by innervated bundles of myofibers that presents voluntary contraction and high energy requirements, whose main function is to generate contraction, force and movement (99). Besides, skeletal muscle presents other functions such as thermogenesis, metabolism and the excretion of peptides for connection with other tissues (100). Particularly, skeletal muscle myofibers are formed by the fusion of myoblasts, consequently, skeletal myofibers are multinucleated cells that contain postmitotic nuclei and share a common cytoplasm (Figure 4) (2)(101). Skeletal muscle is also formed by the extracellular matrix (ECM) a three-dimensional network composed of different kinds of collagens, proteoglycans, glycoproteins and elastin. ECM participates in several processes such as connection with the immune system, regulation of muscle development, muscle growth, and repairment. ECM also works as a support structure for myofibers contraction and force transmission (100).

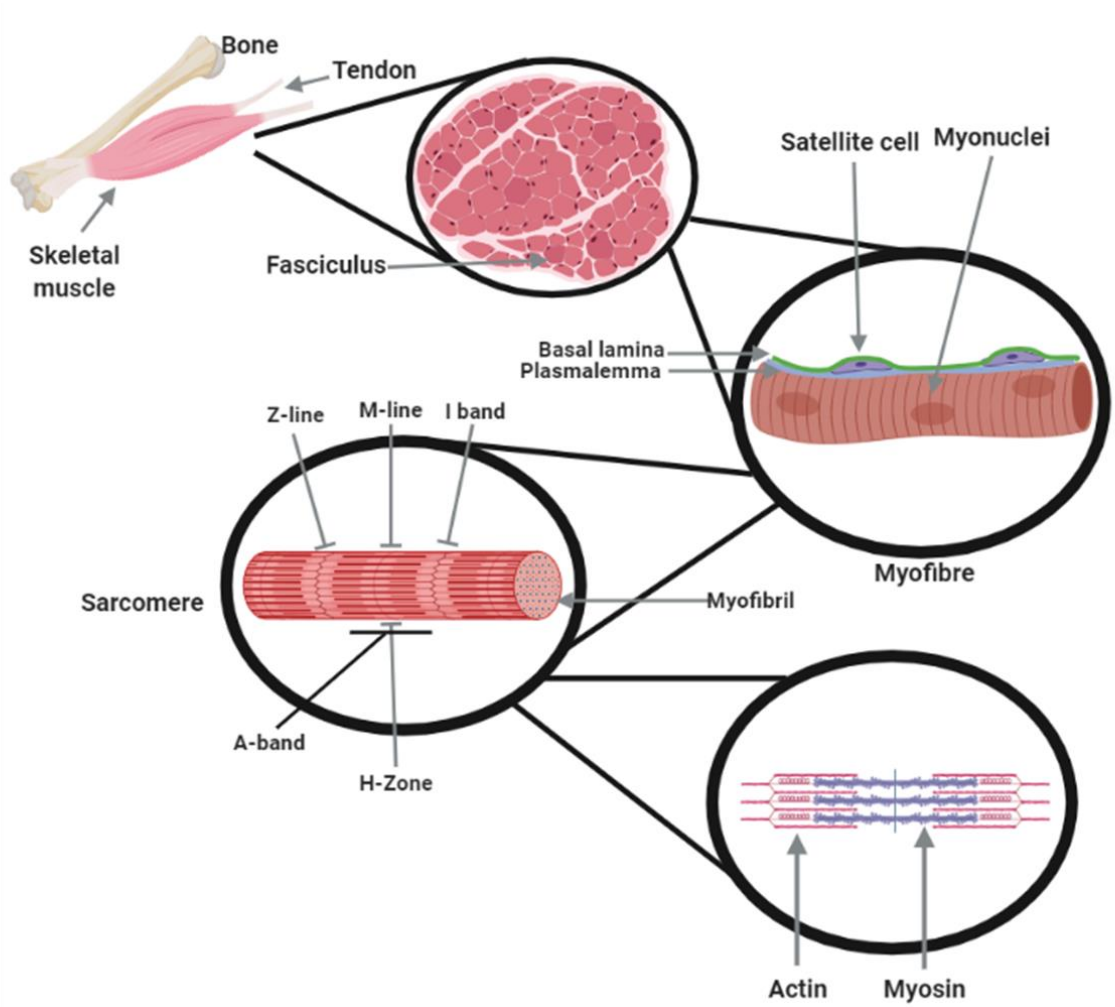

Figure 4. Structure of skeletal muscle, schematic representation of myofiber and sarcomere.
Every circular zoom shows a different component of skeletal muscle structure. The picture described from macrostructures to microstructures, from skeletal muscle tissue to actin and myosin bands. (Image elaborated by the PhD candidate).

For their part, myoblasts are precursors of skeletal muscle myofibers and present a period of proliferation after which they would experience a conformational change starting differentiation, fusing with other myoblasts to form multinucleate skeletal muscle fibres. Fusion occurs coordinately by the actions of several muscle-specific genes. After differentiation, the cells will never divide again and the nucleus will no longer replicate DNA, which means that they cannot proliferate to expand or restored their population after damage, repair skeletal muscle, or contribute to skeletal muscle growth neither (2). Particularly in mice, neoformation of muscle myofibers will stop by birth, after that postnatal and juvenile muscle growth will occur by progressive addition of myonuclei and the enlargement of the sarcoplasmic space. The incorporation of new myonuclei is completed by 3-4 weeks of age, doubling the number of myonuclear per myofiber. After the 4-week, muscle growth will continue increasing sarcoplasmic space and fusion of myonuclear, but at a lower rate (ten per cent). Each muscle will contain around 5-10 satellite cells (SCs) per myofiber influenced by the myofiber type (101).

1.4.2 Skeletal muscle dystrophy.

About the organizational complexity that skeletal muscle shows, any alteration leads to muscular dystrophies (MDs), which are severe myogenic syndromes associated with mutations in structural genes that produce progressive muscle wasting, weakness and dystrophic pathological aspect of skeletal muscle. MDs are usually related to mutations in genes that encode structural proteins of the dystrophin-glycoprotein complex generating skeletal muscle necrosis and sarcolemma disequilibrium. MDs disorders are characterized by continuous cycles of degeneration and regeneration obtaining unsuccessful repairment, loss of muscle, and fibrosis (102)(103)(104). More significantly, there is no possible therapeutic approximation to repair muscle damage when skeletal muscle myofibers have been destroyed and replaced by fibrotic deposits, therefore this scenario opens a new possibility for strategies to counteract muscle degeneration and promote muscle regeneration by SCs action (102)(105)(106). Several laboratory tests have been proposed for MDs diagnosis, such as quantification of serum creatine kinase levels because it is increased in severe dystrophies from birth. Electromyography is used to define the nature of the dystrophy, muscle histology to study muscle features and define the MDs, and immunochemistry is used to study proteins associated with MDs (104). MDs can be grouped in Duchenne and Becker, Emery-Dreifuss, distal, facioscapulohumeral, oculopharyngeal, and limb-girdle dystrophies (103). Last genetic technologies have allowed the identification of more than 40 genes associated with MDs, which are usually implicated in the basement membrane and extracellular matrix proteins, proteins related to the sarcolemma, proteins with putative enzymatic function, sarcomeric proteins, proteins from the nuclear membrane, and proteins from the reticulum endoplasmic among other (107).

Patients that suffer from Duchenne MD normally show symptoms after the first years of life, showing difficulties in movements, such as running or climbing stairs, and speaking ability, or mental delay in some cases (108). After 7 years of life approximately, the patient suffers a rapid decline including scoliosis, respiratory insufficiency and cardiomyopathy, which conditions survival (107). Duchenne MD patients also suffer from myofiber degeneration, SCs exhaustion and impaired self-renewal (101). Limb-girdle MDs group are considered a heterogenic group of MDs that shared muscle weakness and dystrophy appearance in muscle biopsy, while respiratory and cardiac systems could be affected in some subtypes (107).

Emery–Dreifuss MD patients normally present an advancing muscle system wasting and weakness in the biceps and calves, despite other tissues can be also secondary affected such as elbows, Achilles tendons, neck and spines. The cardiac system can be also affected due to

muscle-derived damage that can determine survival (107). These patients also suffer impaired SCs proliferation (101).

Facioscapulohumeral MDs present a growing asymmetric muscle waste and weakness, specifically affecting the face, scapular, and limb muscles. In contrast with other MDs syndromes, cardiac function and walk capacity are often maintained and creatine kinase levels can be also normal. Genetic diagnosis is normally required for these patients (107). Facioscapulohumeral MD is also characterized by myoblast apoptosis (101).

Regarding muscle regeneration usually takes place in response to damaged myofibers where SCs are activated, proliferate and are displaced to the damaged area, where they will fuse with the surviving myonuclei of the damaged myofiber (101). Especially in muscular dystrophies, chronic regeneration takes place as a continuous response to necrosis of muscle myofibers, altering align of precursor cells with nuclei from the damaged myofiber (101). Other elements involved in muscular regeneration in MDs are inflammatory cells, fibroblasts, fibro-adipogenic cells, and the genetic background (101).

1.5 Prenatal myogenesis and embryo development in mice

Mammalian embryogenesis includes processes of cell division, cellular proliferation, and differentiation through the time of early prenatal development. Fertilization, cleavage, differentiation of the first embryonic cells and blastocyst implantation into the uterus are essential for proper embryogenesis. Initially, sperm fertilizes a specialized oocyte leading to a zygote formation, a totipotent embryonic cell, initiating the way from oocyte to embryo transition. This process groups symmetric mitotic divisions, organelles redistribution in the cytoplasm, histone alterations, DNA methylation and changes in the transcriptomic profile (109)(110). At that time, a morula will be formed. After morula compaction, blastocysts will be formed and implanted in the uterine wall where gastrulation will take place indicating the end of the germinal stage of embryogenesis. Gastrulation will occur with up to 1000 cells and a limited number of cells types (111). Blastocysts will be differentiated into trophoblasts, surrounding cells such as the placenta and associated tissues and embryoblast, the inner cells (112). Inner cells present two layers: the hypoblast and the epiblast. Epiblast region will result in endoderm, ectoderm, and mesoderm formation. The identities and position of the primary cells that will constitute the three germ layers (ectoderm, endoderm, and mesoderm) are established during the early stages of gestation (113). The endoderm will lead to the digestive tract, liver, pancreas, auditory tube, trachea, bronchi, and the bladder among others, ectoderm

will form the epidermis, hair, mouth, nose, and nervous system among others; and the mesoderm will generate muscles, bones, adipose tissues and dermis among other.

Somites are formed during somitogenesis from the mesoderm along with the ais head to tail (Figure 5A). Mesoderm is anatomically divided into paraxial, intermediate, and lateral mesoderm in the function of the position from the midline to the neural tube and it is separated in blocks known as somites that will appear on both sides of the neural tube. Somites at the paraxial mesoderm of the vertebrate's embryos hold the precursors of the axial skeleton, skeletal muscles, and dermis. Particularly, the skeletal muscle tissue in the limbs and trunk are derived from somites that are formed gradually by segmentation of the paraxial mesoderm (myotome) on both sides of the neural tube (114). A myotome is composed of myogenic precursor cells (MPCs) that arrive from all lips of the dermomyotome to lead to the formation of myocytes (115) and it is surrounded by a laminin-rich membrane that disconnects it from the underlying sclerotome (116). Myoblasts, the precursors of skeletal muscle myofibers, are derived from mesodermal precursors that emerged from the myotome (111)(2).

Secondly, the assembly of the laminin in the myotome matrix takes place when epaxial myogenic precursor cells go into the myotome. Laminins are extracellular glycoproteins that guide cellular movements through the extracellular matrix. When the Myf5 positive cells colocalize with assembled laminins, they express integrin α6β1 to anchor itself to the extracellular matrix to be able to move, due to Myf5 is needed for α6β1 integrin expression on myogenic precursor cells and laminin is the main regulator of myotomal extracellular matrix assembly and cell guidance into myotome (117). In terms of time, the mean duration of mice gestation is 20-21 days including embryonic and fetal development. From 0 DPC to 5 DPC groups the pre-embryonic development until the blastocyst formation and the period from 5 DPC until 10 DPC includes embryo elongation and gastrulation. Organogenesis starts at 10.5 DPC until 12.5 DPC and after the embryonic period of 10 DPC, embryos are considered fetuses until birth (118).

On the other hand, somites formation, segmentation and myogenesis are carefully modulated by genes that are implicated in different pathways such as WNT, FGF or NOTCH. WNT pathway modulates proteins that transfer signals into a cell through different cell surface receptors. FGF modulates development in animal cells. NOTCH pathway constitutes a cell signalling system controlling another different signalling. WNT controls early cell activation in the epaxial dermomyotome (119), FGF maintains a balance between myogenesis and self-renewal of progenitor cells (120), and NOTCH signalling induces self-renewal along with the four Myogenic Regulatory Factors (MRFs): Myf5, MyoD, Myogenin and Mrf4, the transcription factors that control determination and differentiation of skeletal muscle cells during embryogenesis and

postnatal myogenesis (121). The MRFs function leads to the activation of muscle gene expression (122). MyoD, Myf5 and Mrf4 are determinant factors in embryonic myogenesis due to their absence precludes muscle formation. Particularly, Myf5 and MyoD activation in myoblasts modulate the specification of the head, epaxial, hypaxial and limb body muscle progenitors of the vertebrate embryo development, while Myogenin modulates the differentiation process from myoblasts to myofibers that are also regulated by Mrf4 and MyoD (123) (99). Pax3 is a transcription factor that regulates muscle precursor cells migration during embryogenesis (124), and a decisive element in the advancement from multipotent somatic cells to a tissue-specific myoblast at the beginning of myogenesis (114). About myogenic regulation, the Pax family of paired domain transcription factors have an essential role in tissue specification and organ development. Initially, cells that fuse collectively together expressed the paired box transcription factors $Pax3^{+}$ and $Pax7^{+}$ along the primary skeletal muscle myofibers that are considered the initial structure for the primary skeletal muscle (125). Then, the second group of $Pax3^{+}$ and $Pax7^{-}$ skeletal muscle cells will fuse to form the secondary myofibers starting in the middle of the primary myofiber and they will advance until the two ends of the primary myofibers (125). In the end, a subpopulation of myoblasts derived from precursor cells enters a quiescent undifferentiated state highly related to myofibers, becoming adult muscle stem cells (126). Although the molecular mechanism that controls myocytes fusion remains unclear, two elements have been proposed recently for myocytes fusion: Minion, a fundamental microprotein, and Myomarker, a transmembrane protein (127)(128)(129).

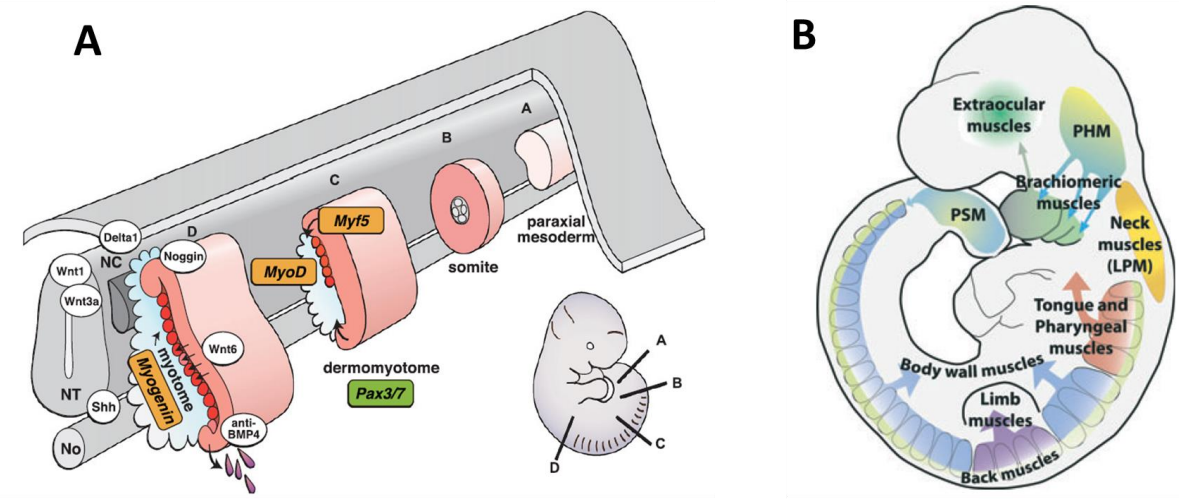

Figure 5. Prenatal myogenesis schematic representation.
(A) Schematic view of mammals' prenatal myogenesis. Myotomes mature following a rostrocaudal grade on either side of the axial structures (130). (B) Origins of skeletal muscles from four main mesodermal progenitor populations: the presomitic mesoderm, the lateral plate mesoderm, the posterior head mesoderm and the anterior head mesoderm (123).

1.6 Postnatal myogenesis

Satellite cells (SCs) are small, flattened, and quiescent stem cells located close to mature skeletal muscle below the basal lamina ready to be a self-renewing source of differentiated skeletal muscle cells. When skeletal muscle suffers damage or has a stimulus to growth, SCs rapidly activate, proliferate and differentiate to replace muscle cells that have been lost and damaged. Then, the progeny of primary SCs fuse to fix damaged skeletal muscle and contribute subsequently to muscle growth. SCs express receptors for growth factors such as FGF-receptor 2 that focus its proliferation on the release of growth factors from damaged muscle or inflammatory cells (101)(2). The immediate activation of SCs after the damage is referred to as the release of RNA coding for the Myf5 from cytoplasmic granules (131) and a rapid expression of MyoD (101). Through the process of SCs activation until myotubes, a series of transformational changes occur, which can be monitored by a series of transcriptional regulatory factors activation and deactivation. Active SCs will express Pax7 and myoblasts derived from SCs present active Myf5 and MyoD. Myocytes precedent from myoblast express MyoD, Mef2 and MyoG. Differentiated myotubes are positive for Mef2, MyoG and Mrf4 (99). SCs activation and proliferation will lead to fusion with other cells promoting myofibers regeneration while a small subgroup of SCs will inactivate MyoD expression to re-enter a quiescent state (132).

About MDs, a genetic defect affects differentiated skeletal muscle cells. In these pathologies, SCs are activated and proliferate to recover skeletal muscle-damaged myofibers. Nevertheless, SCs regenerative action is unable to repair completely the damages and consequently, connective tissue replaces muscle cells, blocking further repairment. Thus a progressive decline in regeneration and the exhaustion of regeneration capacity contribute to muscle weakness in the elderly (2).

In the mice model of MD, skeletal muscle regenerates differently: large^{myd} mice present a low regeneration capacity (133)(134) while mdx mice show a higher regeneration grade (134). If a defective gene is normally expressed in SCs or their progeny, these cells can be directly influenced by the genetic defect. However, defects in genes that are not usually expressed in muscle myofibers, or connective tissue could have an indirect effect on SCs function. Moreover, it has been proposed that SCs are dysfunctional in chronic muscle diseases, which increases the decline associated also ageing (101).

As can be visualized below during a normal process of muscle regeneration (postnatal myogenesis) sequential steps would take place where initially there is an activation of SCs in

response to the damage, going through a proliferation phase and a posterior differentiation that results in small newly formed myofibers that present centralized nuclei that would replace the damaged myofibers (135) the number of centrally located nuclei is an indicator of myofiber repair (136). Finally, regenerate myofibers would present no central myonuclei and would have their peripheral quiescent SCs for future activation.

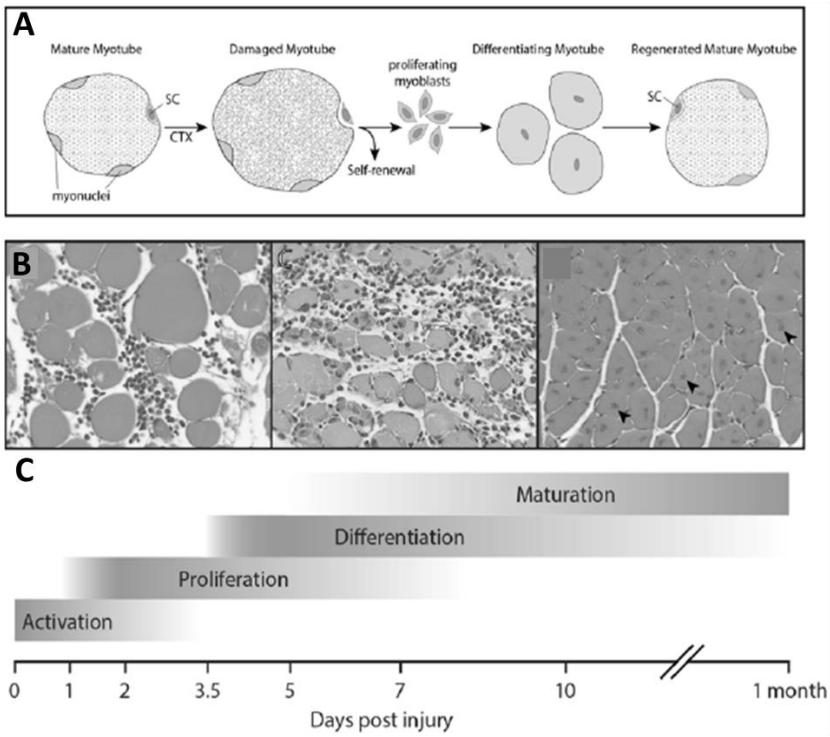

Figure 6. Skeletal muscle regeneration dynamics post-injury.
(A) Myofiber regeneration process displayed by satellite cells. (B) Histological section of skeletal muscle along the regeneration process (24 hours, 2- and 10-days post-injury). (C). Time course of satellite cells during skeletal muscle resulting in regenerated mature myotubes. (Adapted from (137)).

As is displayed in the Figure 6 during the maturation phase newly myofibers that present central myonuclei would experience a process of displacement to the periphery.

1.6.1 Why use SCs to study embryonic myogenesis?

Prenatal myogenesis and postnatal myogenesis in muscle regeneration by SCs activation in mature skeletal muscle share a lot of elements, transcription factors and signalling molecules (138). The transcription factors that modulate differentiation in the precursor cells population in mammalian skeletal muscle are similar to those observed during the initial muscle embryogenesis, the development of skeletal muscle in postnatal and juvenile periods and skeletal muscle repairment (101). Consequently, analyses of SCs activation, specification, proliferation, and differentiation in postnatal stages seem to be an adequate method to understand the myogenesis process.

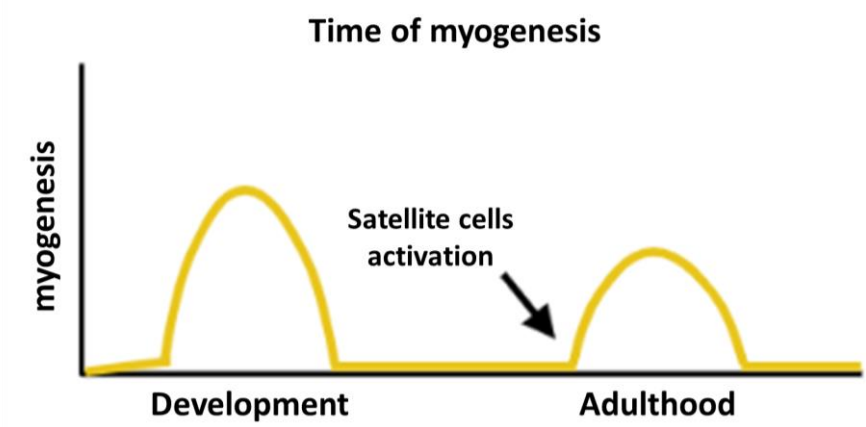

Figure 7. Prenatal and postanal myogenesis time points.
Skeletal muscle formation time points during development and adulthood in mammals, including prenatal and postnatal myogenesis. (Image elaborated by the PhD candidate).

1.7 Caloric restriction, skeletal muscle and mitochondria

Caloric restriction (CR) could be defined as a reduction of 10 to 40% of food intake without malnutrition. CR is a powerful method to increase lifespan and healthspan, but also delay the onset of chronic diseases associated with ageing such as diabetes, hypertension or cancer (139). In addition, mitochondrial dysfunction has been proposed as a crucial hallmark to explain the molecular and physiological basis of ageing (140). Although the mechanisms that explain the benefits attributed to CR are still unclear, it has been proposed that could be based on suppression of oxidative stress and maintenance of cellular redox balance that facilitate optimal cell signalling and adequate gene expression where mitochondria would play a key role (141). Moreover, TOR-S6K and AC-PKA pathways, IGF-I like receptors and several transcription factors (GIS1, DAF-16 and FOXO) delay ageing under CR (142). Regarding mitochondria and CoQ, CR has been shown to modify CoQ_9 and CoQ_{10} ratio and COQ gene expression in mice under CR in different tissues such as the kidney and heart (143). Even another study in rodents suggested that CR could increase the mitochondrial fraction of CoQ (144).

For skeletal muscle, CR has been proved to induce a reduction in skeletal muscle weight where fast myofibers were more susceptible to suffer alterations affecting myofibers composition (93). Particularly, CR has been shown to improve SCs availability and activity in muscles of young and old mice along with more mitochondrial levels and metabolic and longevity factors (145). These results could help to elucidate the metabolic factors that may modulate stem cells function and the impact of ageing on the impairment of the stem cells. CR could be a promising therapy to improve muscle stem cells in the context of muscle disease or muscle dysfunction. Additionally, an increase in SCs under CR in response to injury has been reported (146).

In summary, CR could be defined as a metabolic modulator that increases lifespan and affects skeletal muscle and adult muscle stem cells, which provides enough evidence to propose CR as an intervention in our *Adck2* mutant mouse to understand how CR could modulate the metabolism under mitochondria dysfunction, specifically in skeletal muscle.

Project Aims

2 Project Aims

The main aim of this project is to study the etiology, pathophysiology, and progression of the disease in our *Adck2* knockout mice during all its life stages and to check the effect of CoQ administration and CR intervention, focusing on skeletal muscle because it is the main tissue affected in mice and human patient. For this purpose, the following specific aims have been planned:

1. Study of embryonic development of *Adck2* knockout mice to understand the etiology to determine if alterations start during the embryonic development and to examine if a prenatal CoQ_{10} administration could regulate these alterations (described in chapter 1).

2. Study of postnatal myogenesis in *Adck2* knockout mice to examine if damages could be associated with an affected myogenesis process and analyse the effect of CoQ_{10} administration on postnatal myogenesis (described in chapter 2).

3. Study of skeletal muscle during ageing in *Adck2* knockout mice to determine the progression of the phenotype through ageing and the effect of CoQ_{10} over the ageing process in our mouse model (described in chapter 3).

4. Assess the effect of caloric restriction on the phenotype of our mouse model, focusing on skeletal muscle to understand the mechanism by which caloric restriction could modulate mitochondrial metabolism (described in chapter 4).

Materials and Methods

3 MATERIALS AND METHODS

3.1 Mice specifications and experiments.

3.1.1 Mouse model generation

The *Adck2* knockout mouse model was produced in the Transgenic Animal Model Core, Biomedical Research Core Facilities, the *University of Michigan* as illustrated in Figure 7 (77). Chimaeras were produced by microinjection of C57BL/6J-derived mutant ES cells into albino C57BL/6J host blastocysts obtained from the mating of C57BL/6J-BrdCrHsd-Tyrc females with C57BL/6J-BrdCrHsd-Tyrc males (Figure 8). Any white pups from chimaera breeding have a contribution to both the ES cells and the host embryos and were labelled as C57BL/6-BrdCrHsd. The ES cell clone *Adck2* 12053 was obtained from the KOMP repository, Mouse Biology Program, University of California. These cells are heterozygous for the *ADCK2* deletion, and the host blastocysts are wild type for the introduced mutation. The breeding of chimeric males with albino C57BL/6 females has produced black pups, which were derived from the ES cells. Because the ES cells are heterozygous for the mutation, half of the black pups were expected to be positive for the mutation. Heterozygous mutant mice were used for germline production and colony expansion. Particularly, the *ADCK2* gene in mice is located in chromosome 6 where present 8 exons. Our mutant mice present a deletion that starts at 39.574.304 bp and finishes at 39.587.522 bp with a deletion size of 13.219 bp affecting 8 exons of the *ADCK2* gene in mice. For this purpose, a BAC vector was introduced into the ES cells to generate knockout *Adck2* mice. BAC vector included LacZ and Neo.

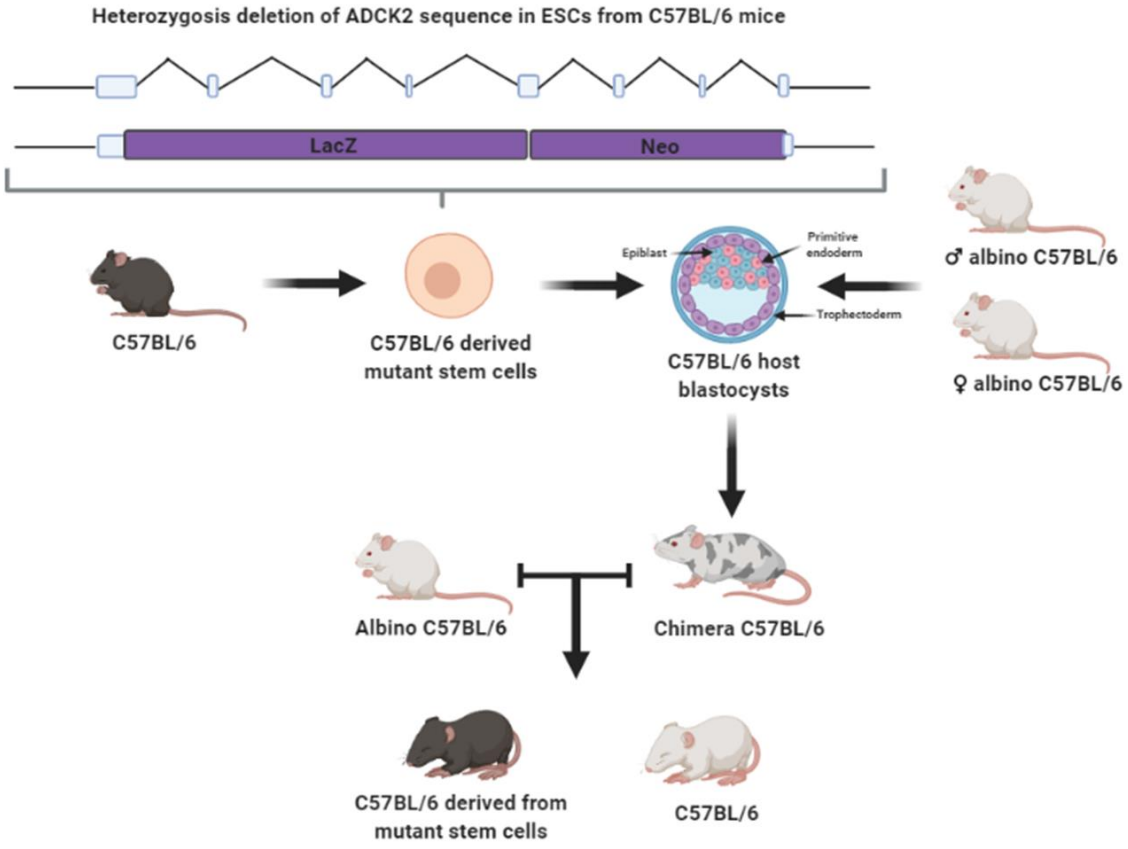

Figure 8. Schematic representation of mutant mice generation.
Mutant mouse production by microinjection of mutant ES cells into blastocysts. Chimeras obtained were crossed with wild type Albino C57BL/6J, black offspring mice were derived from ES cells. (Image elaborated by the PhD candidate).

3.1.2 Mouse environmental conditions

Mouse housing and tissue collection were performed using protocols approved by the Universidad Pablo de Olavide Ethics Committee (Seville, Spain; protocols 12/03/2021/033) by Spanish Royal Decree 53/2013, European Directive 2010/63/EU, and other relevant guidelines. Mice were bred and raised in the animal facility at the Centro Andaluz de Biología del Desarrollo (CABD). Mice were housed in autoclavable polycarbonate cages respecting the minimum space requirements per animal. The environmental conditions of housing were of 12 hours light / dark cycle. The light period was from 8:00 until 20:00. Temperature and humidity oscillated within the range of 22 ± 2ºC and 54 ± 1% respectively.

Sawdust was placed in the cages and enriched with polycarbonate toys and autoclaved papers. The animals were fed *ad libitum* with a standard laboratory mouse diet, SAFE D40 (Scientific Animal Food and Engineering) (composition: cereals 84.6% w/w, vitamin and mineral 3.9% w/w and vegetable proteins 11.5% w/w). Mice were sacrificed by cervical dislocation.

3.1.3 Mice breeding for embryos extraction.

Mice crosses were carefully planned, three days before the mice mating, the male mouse were relocated to a new box and female mice were placed in the old box of the male mouse that contain the faeces and urine of the male mouse to synchronize the estrus cycle in female mice (Whitten effect). Two female mice were crossed with a male mouse every time. Female mice were in estro on Monday afternoon and cross start on Thursday afternoon for four nights. To determine female mice fecundation plug was checked the first time in the morning (09:00 am), positive plug female mice were separated and the rest on mice were maintain on breeding. Mice were separated on Monday morning and negative female mice for plug were left in quarantine for two additional weeks before setting up a new cross.

Embryo's development stage was determined with plug-check control, positive plug in the early morning (09:00 am) was assigned as 0-day post coitum (DPC). Mice breeding was carefully established the day before in the afternoon (05:00 pm).

3.1.4 Skeletal system staining in embryos.

The skeletal system was examined to determine bone abnormalities and the embryo's development stage using the tibia length. Results were normalized with *Adck2*$^{+/+}$ embryos data from the same litter.

Embryos at 17 DPC were fixed in paraformaldehyde (PFA) 4% w/v and used to study developmental markers. Embryos were immersed in glass tubes in water at 70ºC for 5 minutes to allow the removal of skin. Also, fat from the chin, back, legs and organs from the abdomen were removed. Then, embryos were dehydrated in ETOH 100% for 3 days, washed with acetone for 2 days and stained with Alcian Blue for 3 days. At this time, embryos were re-hydrated with washings in decreasing ETOH solutions (100% v/v, 75% v/v, 50% v/v and 25% v/v ETOH 3 days in each solution). After that, embryos were washed in *mili*Q H_2O 3 times for 5 minutes, stained with Alizarin Red for 2 days and washed in a solution of increasing glycerol concentration (20% v/v, 50% v/v, 80% v/v and 100% 3 days in each solution). Finally, embryos were conserved in glycerol 100%.

Alcian Blue 86x	3.75 mg of Alcian Blue in 25 mL of a solution 80%ETOH/20% Glacial acetic acid v/v
Alizarin Red	1.25 mg of Alizarin Red in 25 mL of a solution 2%KOH/H_2O v/v

3.1.5 Size and weight analyses in embryos

Weight and size of embryos at 17 DPC on standard conditions and under CoQ_{10} administration were assessed. Previously, the umbilical cord, placenta and yolk sac were removed, and embryos were washed in phosphate-buffered saline (PBS) and dried in absorbent paper. Weight was measured in high precision balance (four decimals) and size was determined by measuring the distance between the head and the tail of the embryos. Results were normalized with *Adck2*$^{+/+}$ embryos data from the same litter to reduce the differences between litters. Embryos were photographed using scopes with DDC digital camera at CABD Functional Genomics Facility using Leica Software for images acquisition and analysis.

3.1.6 Muscle progenitors' analyses in embryos

Somites analyses were performed through the analysis of the expression of Myf5 and Mrf4, two Myogenic Regulatory Factors involved in skeletal myogenesis in vertebrate embryos (147). A wild type male mouse that contains a LacZ reporter to study transcriptional regulation of Myf5 and Mrf4 was crossed with one female mouse *Adck2*$^{+/-}$. The reported LacZ allows the analysis of the expression of Mrf4 and Myf5 through different enzymes, alkaline phosphatase or B-Galactosidase, thus it was possible to study the expression of both transcription factors with the same reporter. This technique was used to drive Myf5 or Mrf4 expression in epaxial and hypaxial somites, branchial arches and the central nervous system in our knockout *Adck2* mice.

For Myf5 staining, embryos were fixed overnight in Mirsky's fixative (National Diagnostics, HS-102) at 4ºC and washed three times in PBS. Then, embryos were placed in 3-5 ml of staining solution (5 mM $K_3Fe(CN)_6$ v/v, 5 mM $K_4Fe(CN)_6$ v/v, 2 mM $MgCl_2$,v/v, 40 mg/ml X-Gal v/v in PBST 0.02% v/v) at 37ºC in moving for 3-4 hours until staining was completed, and post-fixed in Mirsky's fixative. The next day, pictures of the embryos were taken to examine in detail the Myf5 expression.

For Mrf4 staining, embryos were fixed in Mirsky's and then postfix in fresh PFA 4% w/v overnight at 4ºC. Embryos were washed 3 times in 2 mM $MgCl_2$ PBS v/v and heated in 2 mM $MgCl_2$ PBS v/v 65ºC for 2 hours. Later, embryos were cooled and washed with AP staining buffer for 20 minutes. Then new AP stain buffer + 10 µl BCIP (50 µg/mL) v/v and 50 µl (100 µg/mL NBT) v/v were added, and embryos were placed in a covered black bucket with ice on the shaker. When Mrf4 expression was completely visualized, staining buffer was removed, and embryos were washed with PBS plus 20 mM EDTA to stop the reaction. Finally, embryos were postfixed in Mirsky. Embryos were photographed using scopes with DDC digital camera at CABD Functional Genomics Facility.

1X AP staining buffer	100 mM Tris-HCL pH 9.5, 100 mM NaCl, 50 mM $MgCl_2$, 0.1% Tween 20 v/v and miliQ H_2O.

3.1.7 CoQ_{10} supplementation in mice

Reduced CoQ_{10} (Kaneka QH stabilized powder type P30) (Kaneka Pharma Europe, Brussels, Belgium) was formulated in nanoparticles to be dissolved in water. CoQ_{10} final concentration was 33.33-50 mg/kg/day of CoQ_{10} (23). Previously, it was calculated the mean water consumption of a mouse (2-3 ml/day/mouse), CoQ_{10} was dissolved at 0.5 mg/ml for a final concentration of 1-1.5 mg/day (33.33-50 mg/kg/day). CoQ_{10} oxidation rate in water through time was evaluated (Figure 9). As CoQ_{10} suffers progressive oxidation in water, CoQ_{10} was replaced three times per week (Mondays, Wednesdays and Fridays) to prevent oxidation. Additionally, as the expected life span of CoQ in muscle from rodents is 50 hours (148) with our system new CoQ_{10} was continuously supplied to the mice muscle by this time.

CoQ_{10} administration started on adult mice (generation 0) and it was implemented in the progeny during the next two generations. Mice were supplemented with CoQ_{10} during their entire life.

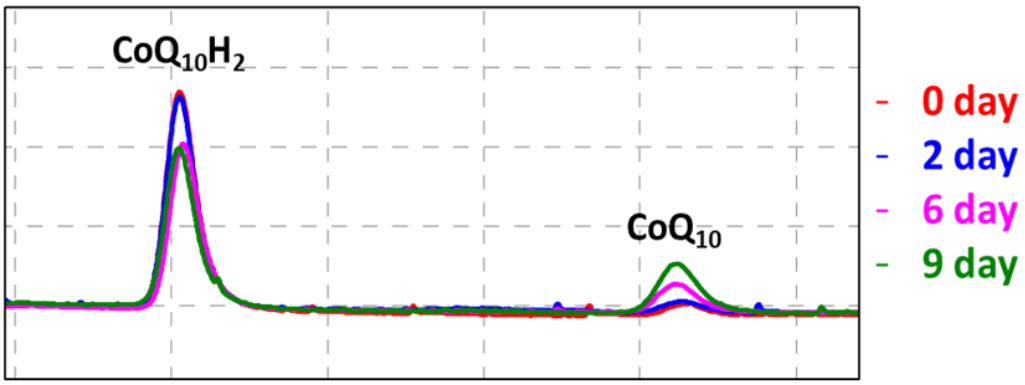

Figure 9. CoQ_{10} oxidation rate in water is associated with time.
$CoQ_{10}H_2$ in nanoparticles oxidation into CoQ_{10} in nanoparticles from 0 to 9 days dissolved in distilled water. Reduced and oxidized forms of CoQ_{10} in water were measured by HPLC. The graph shows the progressive oxidation of $CoQ_{10}H_2$ over time and the production of CoQ_{10}. (Image elaborated by the PhD candidate).

3.1.8 Mice ageing experiment

Mice used for experiments were classified into different groups based on their age: young (3-6 month-old), adult (10-12 month-old), old-adult (16-18 month-old) and old (22-24 month-old). These periods were established due to their similarity to age groups in humans as shown in Figure 10.

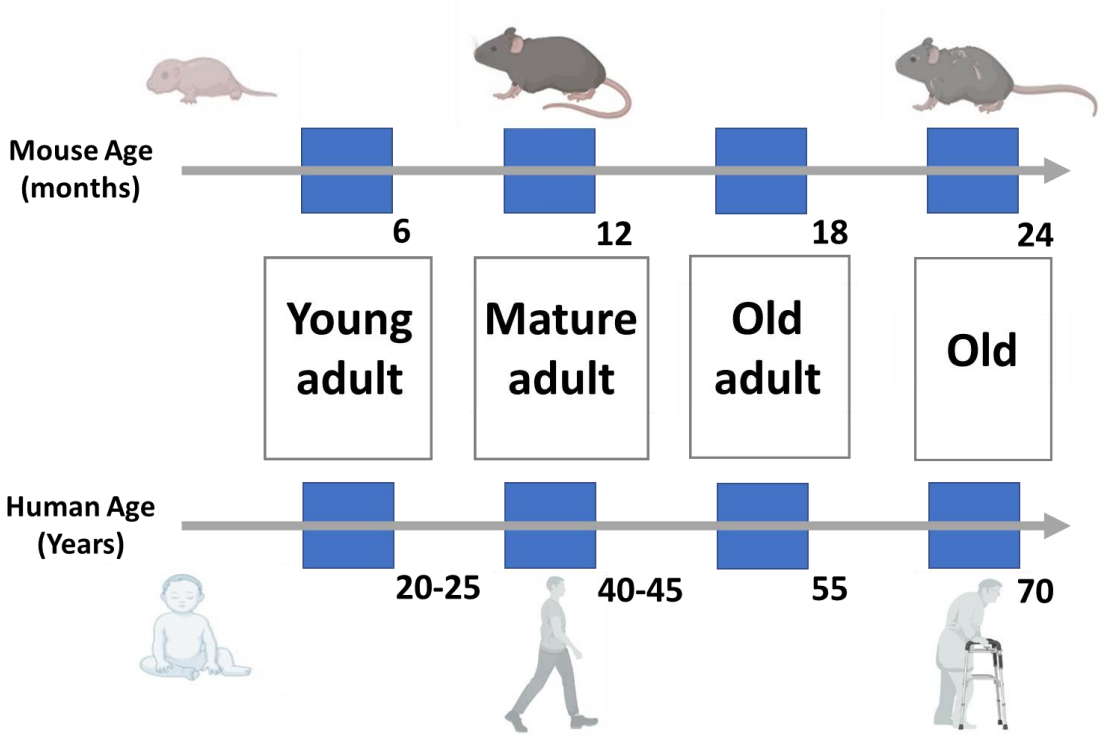

Figure 10. Schematic correlation of ageing between mice and humans.
Lifetime-points in mice and humans, comparison of life stages between both species to assess growth and ageing. This figure allows us to establish time points to perform experiments during the ageing process and to assess the decline and incapability inherent to ageing in mice and humans. (Image elaborated by the PhD candidate).

3.1.9 Caloric restriction conditions

Mice on CR underwent a 40% reduction in daily food intake, establishing a regimen by which 60% of ad libitum diet was added to the cages each day at 09:00 am. Basal food intake was determined over 2 months before CR was determined, and it was established to be approximately 4 grams per day. Therefore, mice in CR were fed 2.4 grams daily of the standard diet for laboratory mice.

For CR experiments, 6 month-old male mice were maintained on CR for 7 months. After that, 13 month-old mice were sacrificed by cervical dislocation. Age-matched male mice fed *ad libitum* were used as control. A standard chow diet (D40 SAFE) (Scientific Animal Food and Engineering) (composition: cereals 84.6% w/w, vitamin and mineral 3.9% w/w and vegetable proteins 11.5% w/w) was used and mice received water *ad libitum*.

3.1.10 Tibia length in young and old mice

Tibia length was determined in young and old mice to assess anatomical general development. The right lower limb was segmented from each animal, and then, skin, skeletal muscles and fat were removed. After that, the limb was immersed in NaOH 2% w/v solution in agitation for 7-9 days, revising the status every 2 days and, when all tissue was eliminated, tibias were stored at

RT and photographed using scopes with a DDC digital camera at CABD Functional Genomics Facility.

3.2 *In vivo* mice tests

3.2.1 Glucose and insulin levels in fasting conditions

Both fasting glucose and insulin levels were determined after the mice had fasted for 12 hours (08:00 pm to 08:00 am). Glucose measurement was performed in blood samples taken by venipuncture and using an Accu chek Performa glucometer. For insulin determinations, blood samples were collected in heparin treated tubes and centrifuged at 2000 g for 10 minutes at 4ºC to isolate the plasma fraction from the transparent upper phase. Insulin levels were determined using a Mouse Insulin Elisa kit from Mercodia (10-1247-01/10-1247-10). Insulin resistance was calculated from the Homeostatic model assessment (HOMA) index was calculated considering glucose and insulin values.

3.2.2 Glucose tolerance test (GTT)

For the glucose tolerance test, mice were fasted for 12 hours (08:00 pm to 08:00 am), body weight (BW) was recorded at the time of fast and received an intraperitoneal (IP) injection of glucose (2 g/kg weight) using a solution of 200mg/ml D-glucose w/v. For IP injections, insulin syringes (1/2cc, 281/2G) were used. Before glucose injection, fasting blood glucose was measured and recorded as Timepoint 0. After that, glucose was intraperitoneally injected, and the time started to count. Each mouse was staggered by at least 1 minute to manage time. Successive measures were performed every 15 minutes (15, 30, 45 and 60 minutes) for the first hour, and every 30 minutes (90 and 120 minutes) for the second hour. This test was used to evaluate the response to glucose injection and to examine the glucose entry into the cell and glucose homeostasis.

Additionally, insulin homeostasis after glucose load was also calculated. Mice were fasted, weighed and injected with D-glucose as previously described. Right before glucose injection, plasma was collected to measure basal insulin levels. Then, two successive measures were performed to analyse insulin production (20 and 40 minutes post glucose load). Blood collection was performed at the submandibular vein, blood was stored in heparin treated tubes and centrifuged at 2000 g for 10 minutes at 4ºC. Finally, insulin levels were determined using a Mouse Insulin Elisa kit from Mercodia (10-1247-01/10-1247-10).

3.2.3 Insulin Tolerance Test (ITT)

The response to exogenous insulin injection was also determined using the insulin tolerance test (ITT). Mice were fasted for 5 hours (from 10:00 am to 3:00 pm), the time of fasting was reduced to avoid hypoglycemia, and BWs were recorded at the time of fasting. The dose of insulin used was 0.75 U of insulin per kg/BW. Before the injection, fasting blood glucose was determined, and insulin was injected intraperitoneally. Successive measures were performed every 15 minutes (15, 30, 45 and 60 minutes) for 1 hour. At the end of the test, food box cages were refilled, and in case of low glucose levels, an oral glucose load was administered to the mice to avoid problems associated with hypoglycemia. This test evaluates the response to insulin injection focusing on glucose entry into the cell and insulin homeostasis.

3.2.4 Intraperitoneal pyruvate tolerance test (IPPTT)

The response to sodium pyruvate was assessed to evaluate glucose homeostasis, particularly, gluconeogenesis from non-carbohydrate carbon substrates (pyruvate). Mice were fasted for 5 hours (from 10:00 am to 3:00 pm) and BWs were recorded at the time of fasting. Fasting glucose was determined and immediately, pyruvate was intraperitoneally injected (2g per kg/BW dissolved in *Mili*Q water). Successive measures were performed every 15 minutes (15, 30, 45 and 60 minutes) for the first hour, and after that, two additional determinations were done every 30 minutes (90 and 120 minutes) for the second hour. Glucose increase after pyruvate injection represents hepatic gluconeogenesis, which means the rate of novo glucose synthesis using pyruvate as a substrate.

Physical performance assessment

All tests were started at the same time of the day (02:00 pm) to reduce variability associated with ageing in circadian rhythm. To reduce manipulator variation physical tests were performed by the same person. Mice were introduced into the experimental room 30 minutes before starting any behavioural test for acclimatization. Mice temperature and humidity were maintained during physical tests, and to avoid noise, people not involved in the test did not go inside the experimental room.

3.2.5 Grip Strength test

The grip strength test was used to examine *in vivo* muscle force (Grip Strength Columbus apparatus, Gibertec SA, Madrid, Spain) as indicated (149). The test is based on the tendency of a mouse to instinctively grasp a grid when suspended by the tail. The BM of the mouse was assessed before the test. When the manipulator holds the mouse by the middle tail and lowered it over the grid, the mouse grasps the grid tightly with the upper and four paws. Each mouse

performed 5 trials with upper both and with fours paws. The three trials most similar for two and four paws were used for data analysis. After each pull mice could rest for 30 seconds. Before the test, animals were revised to find any potential injury or damage that could influence the result of the test, and if that was the case, the mouse was not tested. The decline in strength associated to aging was calculated for each group individually using the values from the different life-points studied through the equation of the graph and the slope of the line.

Grip strength test was used to assess strength along the ageing process and to evaluate skeletal muscle function. When too many mice were studied, analyses were performed on two or three consecutive days. When mice on CR were tested, mice were fed at 09:00 am and the test started at 2:00 pm.

3.2.6 Weights test

The weight-lifting test indicates *in vivo* force production, seven grasp steel mesh balls attached to increasingly heavier weights are used for the test. Mice are held by the middle tail and lower over the grip to allow them to grasp the first weight, which is lied on a cork platform to avoid making noises. As it grasps the wire scale collector with its forepaws, start a stopped clock and raise the mice until the link is clear of the bench. The test was considered passed after 3 seconds and a new heavier weight was offered to the mouse. If the mouse drops the weight in less than 3 seconds, it was recorded the time and the weight held (16g, value = 1; 32g, value = 2; 48g, value = 3; 64g, value = 4; and 80g, value = 5). Rest the mouse for about 10 seconds and try it on the same weight once again. If it falls three times, the total time (in seconds) was noted, the trial terminates, and the mouse is assigned to the maximum time/weight achieved. If the mouse lifts the weight for three seconds, the mouse was tested on the next heavier weight. Again, it is given three attempts to hold the weight for 3 seconds. The final total score is calculated as the product of the value for the heaviest weight held for more than 1 second, multiplied by the time (seconds), and normalized by body weight. (150). The decline in strength associated to aging was calculated for each group individually using the values from the different life-points studied through the equation of the graph and the slope of the line.

The weight-lifting test was used to assess strength along the ageing process and to evaluate skeletal muscle. When mice on CR were tested, mice were fed at 09:00 am and the test started at 2:00 pm.

3.2.7 Treadmill aerobic test

The treadmill exercise test was used to determine aerobic capacity. Mice were forced to run until exhaustion using a mild electric shock on a 10° uphill open treadmill (Treadmill Columbus

1055M-E50; Cibertec SA, Madrid, Spain). Based on previous protocols tested for aerobic capacity (151)(152)(153) the protocol was elaborated.

This test should be performed after two pieces of training on previous days for acclimatization, then the task can be performed appropriately. Mice were acclimated for two days, with a regime of 5 min running at 8 m/min, plus an additional 5 min at 10 m/min on the second day. The day after the second training was considered a resting day. For the test, mice underwent a single bout of running for 60 minutes starting at 10 m/min for 20 min and increasing the speed by 1 m/min every 4 min for the remaining 40 min. Exhaustion was achieved when animals who quit running refused to move back to the treadmill 5 seconds after receiving a mild electric shock (154) (intensity was at 6 Hz and frequency at 8). When mice on CR were tested, mice were fed at 09:00 am and the test started at 2:00 pm.

3.2.8 Metabolic Cages

Mouse free physical performance and metabolism were assessed *in vivo* using automated home cage phenotyping (PhenoMaster TSE system, TSE Systems GmbH, Hessen, Germany) to fully characterize mice under controlled conditions, to obtain high quality and reproducible data with a high throughput because it is possible to run a large number of cages in parallel (155). The first 36 hours were considered the acclimatization period and were not used for the analysis. When mice on CoQ_{10} administration were tested, CoQ_{10} was dissolved in water as mentioned above and used in the water bottles of the PhenoMaster. When mice on CR were tested, food was added to the cage on mice on CR at 09:00 am every day of the experiment.

Data analyses were initially screened using an R script designed by Cristina Vicente Garcia and after the initial previsualization, the data was graphed using Prism – GraphPad.

The parameters collected for analysis were Z (Cnts), VO_2, VCO_2, RER, H and SumR+L. The Z (Cnts) counts break Z-beam which means a break of a beam of light at the upper-level Z. The VO_2 (ml/h/kg): O_2 consumption takes weight into account. The VCO_2 (ml/h/kg): CO_2 production taking weight into account. The Respiratory Exchange Rate: VCO_2 / VO_2. The H (kcal/h/kg): Heat production expressed by BW. The Running wheel is the SumR+L (cm). For running SumR+L and Z counts accumulative representation was displayed.

3.2.9 Study of *in vivo* adult muscle satellite cell and muscle regeneration

Satellite cells are adult muscle stem cells that regenerate muscle damage, to induce *in vivo* SCs activation and skeletal muscle regeneration we used a well-established barium chloride ($BaCl_2$) model of muscle injury. $BaCl_2$ was chosen because it is highly reproducible, cheap and easy to

use, and what is more important $BaCl_2$ injection mimics pathological elevations in intracellular Ca^{2+} that results in degeneration of myofibers and the subsequent activation of SCs for muscle regeneration (156). Firstly, mice were anaesthetized with an IP injection of ketamine (65 mg/kg BW), xylazine (13 mg/kg BW) and acepromazine (2 mg/kg BW), after 10-15 minutes the mice were anaesthetized. Next, the skin was shaved over the tibialis anterior (TA) muscle and then, 50 µL of 1.2% w/v $BaCl_2$ prepared in sterile H_2O was injected unilaterally into the TA (157). Mice were kept warm during recovery and returned to their cage, 14 days post-injection (dpi) mice were sacrificed by cervical dislocation and the TA was carefully dissected and properly frozen using the instructions described in the tissue freezing section, this time-point was selected to analyse muscle regeneration advanced-final stages (Figure 11).

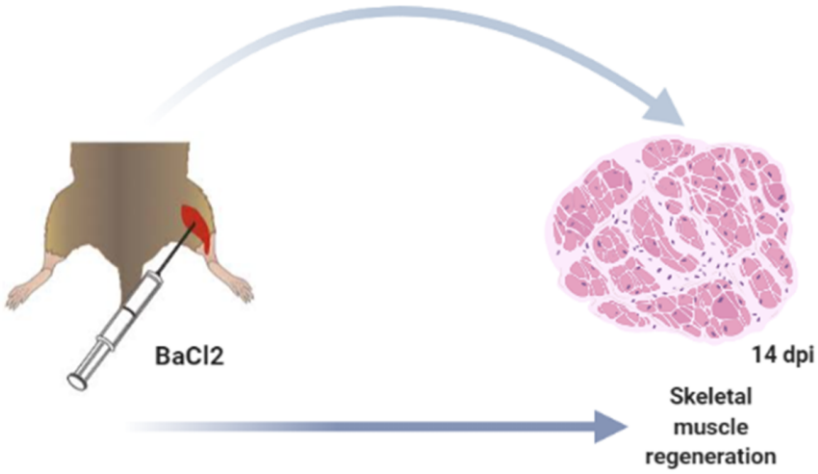

Figure 11. Study of in vivo skeletal muscle damage and regeneration.
Injection of $BaCl_2$ constituted a well-known method to study *in vivo* postnatal myogenesis. The chemical injection would induce satellite cells activation and the initiation of the regenerative response to muscle damage. The election of the precise time point to study is crucial to assess a specific stage of skeletal muscle regeneration. Mice were sacrificed 14 days post-injection to assess long term regeneration stages. (Image elaborated by the PhD candidate).

3.3 Biochemical methods

3.3.1 CoQ levels determination

Mitochondria from skeletal muscle were isolated through serial centrifugations under osmotic conditions as we previously described (158). Pellets of 100 µg of protein of enriched mitochondria solution were resuspended in 170 µl of PBS. CoQ_6 (10 µl of 10 µM solution [100 pmol]) was added to the initial mixture as standard to determine losses along with the extraction. Membranes and tissues were dissolved with 1% w/v SDS (20 µl of 20% solution) and vortex for another 1 minute. Then, a mixture of ethanol-isopropanol (90:10 v/v) (300 µl) was added and samples were vortexed for 1 minute. Finally, lipids were extracted with hexane (700 µl) and vortex for 1 minute. The mixture was centrifuged at 1000 g for 5 minutes at 4º C, to separate the hydrophobic upper phase that contains lipids, which was carefully transferred into

a 2 ml Eppendorf. The hexane extraction was repeated twice. The hexane phase was evaporated using SpeedVac Vacuum concentrators. The lipid extract was resuspended in methanol-isopropanol (85:15) and the lipid extract was injected into high-performance liquid chromatography (HPLC) as previously described (159).

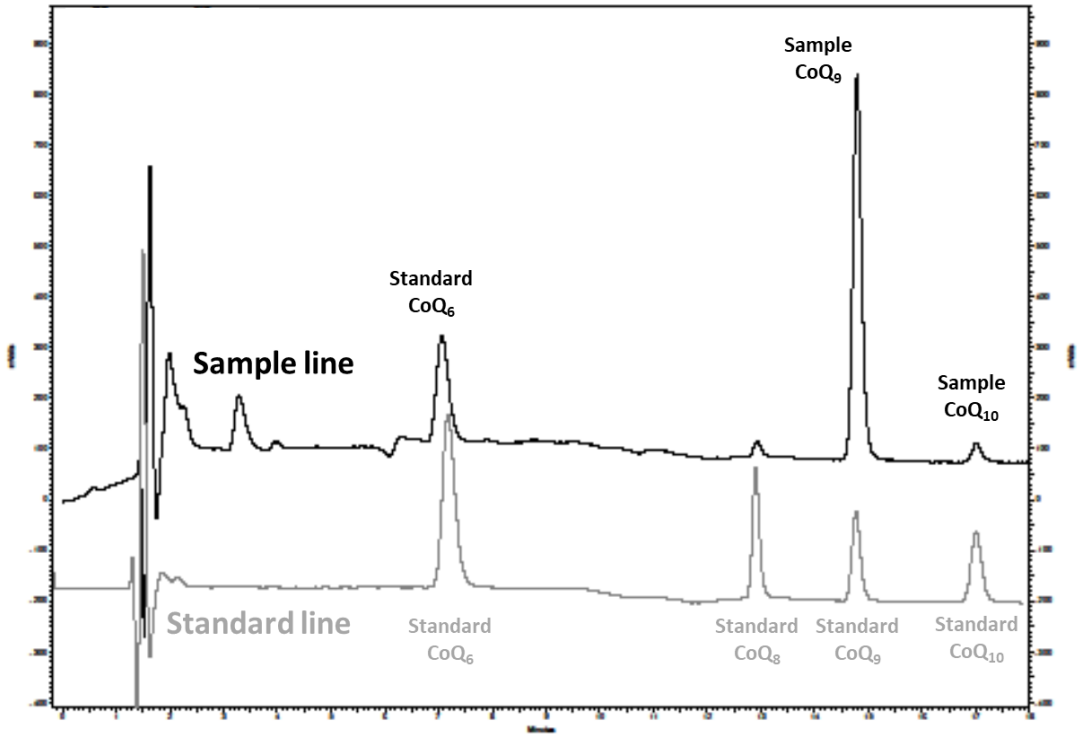

Figure 12 Standard visualization of a chromatogram of the HPLC system
The graph above represents a classical chromatogram view. The Standard line shows the different CoQ isoforms (CoQ_6, CoQ_8, CoQ_9 and CoQ_{10}) that are normally used to calibrate the system and assess the retention time of the different isoforms. The sample line shows the CoQ_6 standard that is added to the sample at the beginning of the lipids extraction to evaluate the loss of CoQ during the extraction process. CoQ_9 and CoQ_{10} isoforms are also shown indicating that the samples are from mice. Mice show 80-90% of CoQ_9 isoform and 10-20% of CoQ_{10} isoform, justifying the higher size of the CoQ_9 peak compared with the CoQ_{10} peak in the sample line.

3.3.2 Fatty acids β-oxidation metabolites analysis

Ketones bodies, plasma free fatty acids and acyl-carnitine were quantified in plasma. Mice fasted for 12 hours (from 08:00 pm to 08:00 am), blood was extracted from the submandibular plexus and stored in heparin treated tubes. Samples were centrifuged at 2000 g for 10 minutes at 4ºC and plasma was collected from the transparent upper phase. Beta-hydroxybutyrate and plasma free fatty acids were measured with an enzymatic method (spectrophotometry).

Analysis of acyl-carnitines in plasma was determined using HPLC, electrospray ionization and tandem mass spectrometry in the underivatized form using a commercial kit of deuterated acyl-carnitines (Perkin Elmer, Barcelona, Spain).

The non-targeted metabolomics studies were performed on mouse liver, skeletal muscle and plasma (stored at -80ºC until processed) by the University of California Davis, West Coast

Metabolomics Center (Davis, CA, USA). Thirteen-month-old *Adck2*$^{+/-}$ and wild type mice on *ad libitum* or CR were used. Analyses were performed using Gas chromatography coupled to mass spectrometry (GC-MS) methods. Results were obtained using the following chromatographic parameters. Column: Restek corporation Rtx-5Sil MS (30 m length x 0.25 mm internal diameter with 0.25 µm film made of 95% dimethyl/5% diphenylpolysiloxane w/w). Mobile phase: Helium. Column temperature: 50-330°C Flow-rate: 1 mL min-1. Injection volume: 0.5 µL. Injection: 25 splitless times into a multi-baffled glass liner Injection temperature: 50°C ramped to 250°C by 12°C s-1. Oven temperature program: 50°C for 1 min, then ramped at 20°C min-1 to 330°C, held constant for 5 min. This method yields excellent retention and separation of primary metabolite classes (amino acids, hydroxyl acids, carbohydrates, sugar acids, sterols, aromatics, nucleosides, amines and miscellaneous compounds) with narrow peak widths of 2–3 seconds and very good within-series retention time reproducibility of better than 0.2 s absolute deviation of retention times. Mass spectrometry parameters are used as follows: a Leco Pegasus IV mass spectrometer is used with unit mass resolution at 17 spectra s-1 from 80-500 Da at -70 eV ionization energy and 1800 V detector voltage with a 230°C transfer line and a 250°C ion source.

3.3.3 Western blotting and immunodetection

Gastrocnemius muscle (500 mg) was homogenized through sonication in RIPA buffer (TrisHCL 50mM pH=7.4, NaCl 150 mM, EDTA 1mM, 1%NP40, Na3VO4 5mM, $Na_4P_2O_7$ 10 mM, protease inhibitor cocktail (PIC) 1X), the lysate was centrifugated 10000 x g at 4ºC for 10 minutes and the supernatant was saved in a new tube. After protein quantification, 40 µg were mixed with LB 1X (10% SDS, dithiothreitol (DTT) 500mM, 50% Glycerol, Tris-HCL 250mM and 0.5% bromophenol blue dye, pH6.8.) and dithiothreitol [200 mM], heated for 5 minutes at 95ºC and loaded in a polyacrylamide gel electrophoresis in denaturing conditions (SDS-Page), using the Mini-PROTEAN Tetra cell (Bio-Rad) with 1X Tris/Glycine/SDS (TGS) buffer (25 mM Tris, 192 mM glycine, 0.1% w/v SDS pH 8.3) for 1 hour at 100 V. The first well of the gel was loaded with 4 µl of All Blue Marker (Bio-Rad). After electrophoresis was finished, the gel was activated by ultraviolet (UV) exposure using a Bio-Rad ChemiDoc imager and a Stain-Free image was used as load control.

The gel was blotted onto 0.2 µm nitrocellulose membrane previously soaked in transfer buffer (transfer buffer recipe) for 5 minutes. Transference was performed with a Trans-Blot Turbo Transfer System Bio-Rad (10-minute protocol). Then, the membrane was blocked with 5% w/v milk (Blotting-Grade Blocker #1706404, Bio-Rad) in Tween-Tris-buffered saline (TTBS) for 1 hour at RT, and subsequently, the membrane was incubated overnight with the specific primary antibody (Table 3) diluted in 5% w/v milk (Blotting-Grade Blocker #1706404, Bio-Rad) in TTBS.

The membrane was washed three times in TTBS to eliminate the unattached primary antibody and incubated with the specie-appropriate secondary antibody (Table 4) conjugated with horseradish peroxidase (HRP) for 2 hours at RT. Later, the membrane was washed three more times with TTBS. Finally, the membrane was incubated with Crescendo Western HRP substrate (Millipore) and examined with ChemiDocTM XRS+ Imaging System (BioRad). Band intensity was determined with Image Lab Software.

Transfer Buffer 1X	200 ml Transfer buffer 5X, 200 ml ethanol, 600 ml mili Q H_2O.
TTBS	20 mM Tris, 150 mM NaCl, 0.1% v/v Tween 20, pH 7.4–7.6 adjusted with HCl

3.3.4 Blue Native-PAGE

Blue native polyacrylamide gel (BN-PAGE) technique was used to examine the different complexes at the electron transport chain assembly in non-denaturing conditions by solubilization of the mitochondrial membranes with a neutral mild detergent (digitonin) that permeabilizes cell membranes and conserves the structure of the complexes (160) (161) (162).

Solubilization step: pellets enriched in mitochondria (50 µgs) were obtained through fragmentation and centrifugation process as described (158) and kept at -80ºC. Digitonin was dissolved in BT+AC buffer v/v (75 mM Bis-Tris pH=7.4 plus Aminocaproic 1.5 M) and heated for 2 minutes at 95ºC. The mitochondrial pellet was resuspended in 30 µl of digitonin solution and incubated for 10 minutes on ice. After that, the solution was centrifuged at 16000 g for 20 minutes at 4ºC and 25 µl of the supernatant was transferred to a new tube.

For sample preparation, 2 µl of Coomassie Blue 5% w/v and 9 µl of sample buffer 4X (Invitrogen) were added to the sample and mixed. For Native electrophoresis, NativePage 3-12% v/v Bis-Tris gels (Invitrogen) were used, and both Cathode and Anode buffers (Invitrogen) were used for electrophoresis, which was performed at 150 V during the first 30 minutes and 200V for the rest of the electrophoresis until the front of samples reaches the end of the gel.

Gel activity measures the working capacity of the mitochondrial complexes. Gels obtained from electrophoresis were washed with distilled water and incubated with specific substrates (160). Once the specific bands were visible, the gel was scanned.

- Gel activity of complex I. The gel was incubated in 20 ml of a 2mM Tris-HCl solution, pH = 7.4; 2.5 mg / ml NTB and 0.1 mg / ml NADH, w/v for a minimum of one hour.

- Gel activity of complex II. The gel was incubated in 10 ml of a 5 mM Tris-HCl solution, 1M sodium succinate, 25 mg NTB and 250 mM PES, w/v for a minimum of two hours.
- Gel activity of complex IV. The gel was incubated in 20 ml of a 50 mM NaPi solution, pH = 7.4, 0.5 mg/ml DAB and 1 mg/ml Cytochrome C, w/v for a minimum of two hours.

Native gel transference

After BlueNative electrophoresis, proteins can be transferred to a polyvinylidene difluoride (PVDF) membrane (Immobilon. Millipore) to study complexes assembly with specific antibodies. "Joe Carrol" Bicarbonate Transfer Buffer (100 mM $NaHCO_3$ and 30 mM $NaCO_3$) 10X has to be diluted to 1X, the gel must be immersed for 20 minutes in Transfer Buffer and the PVDF membrane must be activated by immersion in methanol for 5 minutes. Transference was done at 200 mA for 2 hours. Next, the membrane was immersed in 7% v/v acetic acid and 10% v/v methanol for 15 minutes and washed 4 times with double distillate water for 5 minutes each wash. Total protein load was visualized for further normalization by incubation of the membrane in Sypro Ruby Blot solution for 15 minutes in darkness. The membrane was revealed with the Sypro Ruby Blot programme in the ChemiDoc MP Imaging System (BioRad). To continue, membranes were blocked for 1 hour with 5% v/v milk (Blotting-Grade Blocker #1706404, Bio-Rad) on TTBS and after that, primary antibodies for the different complexes were used (Table 3) were incubated overnight. The next day, the membrane was washed three times with TTBS for 10 minutes and incubated with the species-appropriate secondary antibody (Table 4) conjugated with HRP for two hours in 5% v/v milk (Blotting-Grade Blocker #1706404, Bio-Rad) on TTBS solution for 5 minutes. The membrane was visualized with ChemiDocTM XRS+ Imaging System (Bio-Rad) and densitometry was calculated with Image Lab software.

3.3.5 Protein quantification

Protein content was quantified to normalise different experiments or for sample preparation, Bradford Protein Assay (BioRad) was the method selected for protein quantification. The analysis was performed triplicate in a 96 well microplate with a flat bottom. Bovine serum albumin (BSA) was used as standard curve (Thermo Fischer Scientific), several points were prepared for the calibration line: 1 mg/ml, 0.5 mg/ml, 0.25 mg/ml, 0.125 mg/ml, 0.0625 mg/ml and 0 mg/ml. BSA was dissolved in the same substance in which samples were prepared. Firstly, 2.5 µl of the sample was added to each well, after that 10 µl of NaOH 1M and 200 µl of 1X Bradford were successively introduced to each well and incubated for 5 minutes at RT in

darkness. Absorbance was read at 595 nm in a POLARstar Omega microplate Reader Spectrophotometer (BMG Labtech).

Table 3 Primary antibodies

Antigen	Mono/polyclonal	Host	Dilution	Company	Reference	Application
MyHC	Monoclonal	Mouse	1:300	DSHB	MF20-c	IHC
Dystrophin	Monoclonal	Mouse	1:100	DSHB	MANDRA4(5H7)	IHC
Myosin heavy chain Type IIB	Monoclonal	Mouse	1:100	DSHB	BF-F3	IHC
Myosin heavy chain Type IIA	Monoclonal	Mouse	1:600	DSHB	SC-71	IHC
Pax7	Monoclonal	Mouse	1:100	SC	sc-81648	IHC
Calnexin	Monoclonal	Mouse	1:1000	Thermo	MA3-027	WB
Na+/K+ ATPase alpha1	Monoclonal	Mouse	1:1000	Novus	NB300-146	WB
AKT	Monoclonal	Rabbit	1:1000	CS	C67E7	WB
LDH-A	Polyclonal	Goat	1:1000	SC	Sc-27230	WB
Tomm20	Monoclonal	Mouse	1:1000	Abcam	Ab56783	WB
Timm23	Polyclonal	Rabbit	1:1000	Abcam	Ab230253	WB
mtTFA	Polyclonal	Goat	1:1000	SC	Sc-23588	WB
VDAC	Polyclonal	Rabbit	1:1000	Abcam	Ab15895	WB
NDUFA9	Monoclonal	Mouse	1:1000	Abcam	Ab14713	WB
MT-CO1	Monoclonal	Mouse	1:1000	Invitrogen	459600	WB
MT-ATP6	Monoclonal	Mouse	1:1000	Abcam	Ab14748	WB
UQCRC2	Monoclonal	Mouse	1:1000	Abcam	Ab14745	WB
Bactin	Polyclonal	Goat	1:1000	MyBioSource	MBS448085	WB
HSP70	Polyclonal	Rabbit	1:1000	Proteintech	10995-1-AP	WB
PGC1α	Polyclonal	Rabbit	1:1000	Abcam	Ab191838	WB
AMPKα	Polyclonal	Rabbit	1:1500	SC	sc-25792	WB
ERK 1	Polyclonal	Rabbit	1:1500	SC	sc-93	WB
Foxo-1	Polyclonal	Rabbit	1:1000	SC	sc-49437	WB
Foxo-4	Polyclonal	Goat	1:1000	SC	sc-34899	WB
Sirt1	Monoclonal	Mouse	1:1000	Sigma	04-1557	WB
Sirt3	Polyclonal	Rabbit	1:1500	Thermo	PA5-13222	WB
PPARα	Monoclonal	Rabbit	1:1500	Thermo	MA1-822	WB

AACA2	Monoclonal	Mouse	1:1000	SC	100847	WB

Myosin Heavy Chain (MyHC), Developmental Studies Hybridoma Bank (DSHB), Immunohistochemistry (IHC), Western Blot (WB), Santa Cruz (SC), Cell Signaling (CS).

Table 4 Secondary antibodies

Antigen	Host species	Dilution	Company	Reference	Application
Anti-Goat	Rabbit	1:5000	Sigma	401504	HRP
Anti-Rabbit	Goat	1:5000	CS	7074	HRP
Anti-Mouse	Goat	1:5000	JL	115-035-006	HRP
Anti-Mouse IgG (H+L)	Goat	1:1000	Thermo	A-11001	Alexa 488
Anti-Mouse IgG1	Goat	1:500	Thermo	A-21121	Alexa 488
Anti-Mouse IgM	Goat	1:500	Thermo	A-21426	Alexa 555

Horseradish Peroxidase (HRP), Cell Signalling (CS), Jackson Laboratory (JL).

3.4 Molecular biology methods

3.4.1 Mice genotyping

Mice ear biopsies coming from ear metal identification tags were used to genotype, genotyping protocol consists of two steps: DNA extraction and Polymerase Chain Reaction (PCR). For the first part, mice ear biopsy was placed in an Eppendorf with 50 µl of tail-buffer and heated at 98ºC for 5 minutes and at 55 ºC for 7 minutes. Next, 50 µl of tail-buffer plus proteinase K (50:1) (v/v) were added and heated at 55ºC for 20 minutes, and at 98ºC for 4 minutes to inactivate proteinase K. After that samples were centrifuged at 16000g for 10 minutes at RT and 50 µl of the upper phase was transferred to a new Eppendorf plus 50 µl of isopropanol to precipitate DNA and centrifugated at 16000g for 10 min at 4ºC. The supernatant was discarded, and the Eppendorf was placed on ice, 100 µl ethanol 70% v/v was added to clean the pellet. Finally, the ethanol was removed, the pellet was dry on a filter paper for 20 minutes and then resuspended in 50 µl of TE-buffer.

Tail-buffer	Tris-HCL 100 mM, EDTA 5 mM, SDS 0.2% (w/v) and NaCl 200 mM.
TE-buffer	Tris-HCL 10 mM and EDTA 1 mM.
Proteinase K	40 mg/ml

PCR was used to detect the presence of the LacZ cassette found in mutant mice and the wild type *Adck2* allele. Multiple components for each PCR reaction were included 1 µl of DNA extracted from mice ear biopsy, 2 µl of buffer 10X (Canvax), 2 µl of $MgCl_2$ [25 mM] (Canvax), 2 µl of DNTPs [8mM] (Canvax), 10.8 µl of Mili Q water, 1 µl of forward primer [10 µM], 1 µl of reverse primer [10 µM] and 0.4 µl Taq polymerase enzyme (Canvax).

For the PCR reaction, samples were heated until 111ºC, and an initial denaturation step at 94ºC for 2 minutes was performed. Next, 30 cycles of denaturation, annealing and extension, including each cycle 30 seconds at 94ºC, 30 seconds at 58ºC and 60 seconds at 72ºC (programme 1) or 30 seconds at 72ºC (programme 2). Finally, samples were heated at 72ºC for 10 minutes.

Several pairs of primers were used to genotype the mice (Table 5). *ADCK2* primers detect the wild type allele of the gene *Adck2* (Figure 13). Either SU-LacZ or NeoSD, detect the transgene that substituted the *Adck2* gene (mutant DNA). B195APZ primers detect the positive embryos for histochemical analysis of Myf5 and Mrf4 genes.

Table 5 Primers used to genotype mutant mice

Name	Sequence (5' to 3')	Programme used	Fragment size
ADCK2-Forward	5' TGGTGGGTCAGAAGTGGGTGTGTC 3'	Programme 2	150 bp
ADCK2-Reverse	5' GGGTCTCTTTCGGATCTGGGGCAG 3'	Programme 2	150 bp
SU-Forward	5' TCTCTGCCTGGTTGTCACTG 3'	Programme 1	556 bp
LacZ-Reverse	5' GTCTGTCCTAGCTTCCTCACTG 3'	Programme 1	556 bp
Neo-Forward	5' TCATTCTCAGTATTGTTTTGCC 3'	Programme 2	304 bp
SD-Reverse	5' TTGTCGTCTTTAACAGACC 3'	Programme 2	304 bp
B195APZ-Forward	5' CAAGATGTGGCGTGTTACGGTG 3'	Programme 2	300 bp
B195APZ-Reverse	5' CCTGCCCATCGCAGTACTG 3'	Programme 2	300 bp

Base pair (bp).

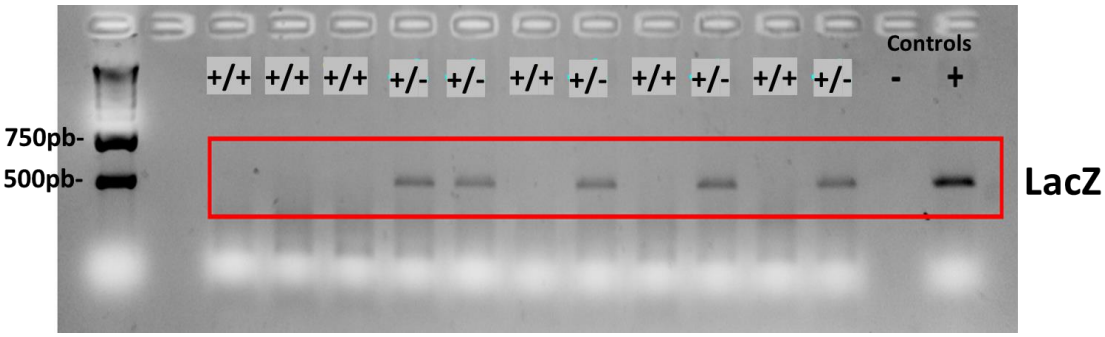

Figure 13 Representative gel to genotype mice

Samples studied in the gel came from the offspring between wild type and heterozygous mutant mice. LacZ bands were examined to genotype mutant *Adck2*$^{+/-}$ mice. Samples were loaded into a 2 per cent of acrylamide gel and the electrophoresis was run at 100 V for 15-20 minutes finally bands were examined with a UV gel reader (Gel Doc™ EZ imager BIO-RAD).

3.4.2 Microarrays analysis

Transcriptome analysis was performed in triplicate and realized on whole embryos at 9 days of development and the foetal liver, brain and skeletal muscles (extracted from the four limbs of the embryo) at 17 days of development. Comparing *Adck2*$^{+/-}$ mutant with *Adck2*$^{+/+}$ independently for each tissue and developmental point. These analyses are composed of five phases: sample collection, RNA extraction, analysis of its quality and RNA cleaning, hybridization with Clarion D arrays and the final statistical analysis.

Pregnant female mice were sacrificed for the first hour in the morning (09:00 am), embryos were carefully collected under a dissection microscope and placed on cold PBS. Embryos at 9 DPC were thoughtfully separated from the umbilical cord and placenta. Embryos at 17 DPC were meticulously separated from the umbilical cord and placenta. The four limbs of embryos were sectioned with a sharp scalpel, then the skin was meticulously removed, muscles were separated from bones and a pool of muscle from the four limbs per embryo was considered one biological replicate. From the same embryo, the liver was dissected through a scalpel incision at the abdomen. Finally, the brain from the same embryo was also collected, separating the brain from cranial bones. The dissection of the tissues of one embryo took around 3-5 minutes in the meantime the rest of the embryos were stored in cold PBS.

RNA was extracted with Trizol (Invitrogen) according to manufacturer instructions. Homogenization of 9-days embryos was done directly in 1 ml of Trizol by pipetting carefully up to the embryo was completely dissolved. Homogenization of tissues dissected from 17-days embryos was done in 1 ml Trizol using a FastPrep-24 5G homogenizer (MP Biolabs) with Lysing Matrix D tubes of 1.4 mm ceramic spheres. The samples homogenized were incubated on ice for 5 minutes to allow complete dissociation of the nucleoproteins complex. 0.2 ml of chloroform was added per 1 mL of Trizol ™ reagent used for lysis, the tube was closed and mixed well by

shaking, and incubated for 2-3 minutes at RT. The mix was centrifuged at 12000 g for 15 minutes at 4ºC to obtain three different phases: an aqueous colourless upper phase that contains the RNA, interphase that holds the DNA and a lower red phase that contains proteins. The upper phase was carefully transferred to a new tube. Next, 0.5 mL of isopropanol was added to precipitate RNA by mixing and incubated for 10 minutes at RT. Samples were centrifuged at 12.000 g for 10 minutes at 4ºC to precipitate the RNA and the supernatant was discarded. The pellet was washed with 1 mL of ethanol 75% v/v, briefly vortexed and centrifugated at 7500 x g for 5 minutes at 4ºC. The pellet was dry for 5-10 minutes and the RNA pellet was solubilized in 20-50 µl of free-RNase water. Finally, the RNA solution was stored at -80ºC until gene expression analysis.

Once RNA was extracted and previously to the hybridization, RNA concentration and purity were checked spectrophotometrically in a nanodrop and RNA quality was verified electrophoretically (Figure 14). Samples with either a low concentration rate, a signal of contamination or any signal of RNA degradation (visualized by the absence of any of the two bands of ribosomal RNA in an agarose gel) were discarded. Then, RNA was cleaned by running it through a column with the RNeasy MinElute Cleanup Kit (QUIAGEN) according to manufacturer instructions. Finally, RNA was quantified in a Bioanalyzer (Agilent) before starting the next phase.

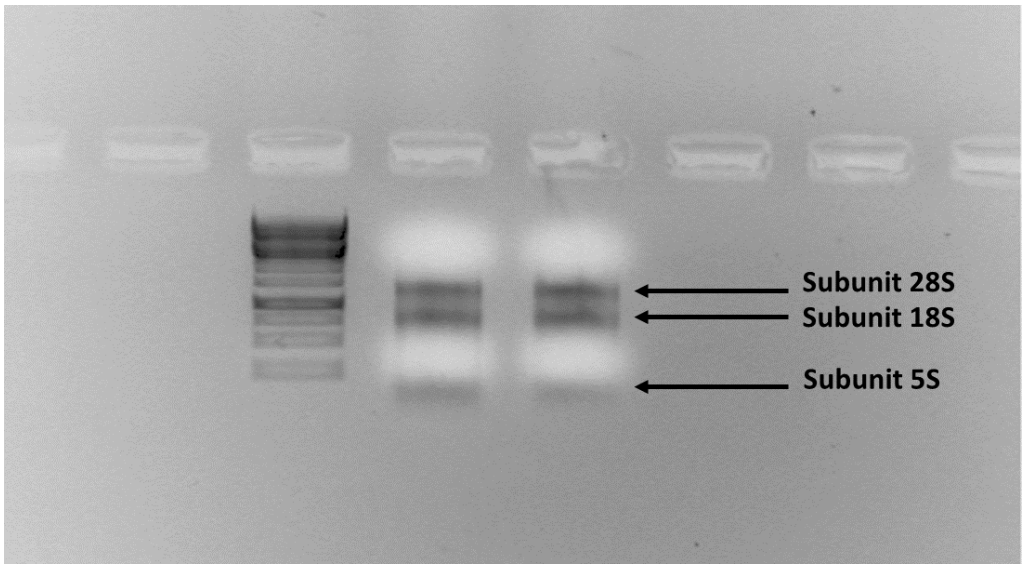

Figure 14. RNA sample electrophoresis to check RNA integrity
RNA extraction was performed in an RNAse free area in the lab. RNAse free spray was used to decontaminate appliances, worktables, glass, pipets and plastic instruments. Next, 0.5 µg of RNA, 1 µl of loading buffer and until 10 µl were completed with RNase-free water and loaded in a 1% acrylamide gel and run at 120V for 3 minutes and 100V for 10 minutes. Bands were visualized in a UV gel reader (Gelprinter Plus) with the ScnImage.lnk software.

For the synthesis and subsequent hybridization of the probes, samples were processed in the Genomic Unit of CABIMER (C/Américo Vespucio 24, 41092 Seville, Spain) where a cRNA probe was synthesized and fragmented from each RNA sample using Affymetrix/Thermofisher protocols and kits provided by QUIAGEN. Each cRNA probe was then hybridized to independent Mouse Clarion D arrays (previously known as GeneChip® Mouse Transcriptome Arrays 1.0). Hybridization and scanning of the arrays were performed according to manufacturer procedures. Arrays were used instead of RNA sequencing because our group has a previous agreement with the supplier.

The statistical analysis was performed in our laboratory, data extraction, cell intensity calculation and computational analysis were performed using the Transcriptome Analysis Console (TAC) Software (Affymetrix/ThermoFisher), which performs array quantification and data normalization, a statistical test for differential expression, look for pathways of interest, explore interactions between coding and non-coding RNA, and interpret complex alternative splicing events. Finally, data were prefiltered according to their fold-change (at linear scale) and their p-value and FDR p-value (163).

Then, regulated genes were selected and classified according to their Gene Ontology (GO). Gene Ontology Enrichment represents the selection of genes associated with a specific GO and is calculated by GORILLA software (Gene Ontology enrichment analysis and visualization tool at http://cbl-gorilla.cs.technion.ac.il/). Enrichment was calculated as follows: E=(b/n)/(B/N), being "N" the total number of annotated genes in the mouse genome, "B" the total number of genes associated with a particular GO, "n" the number of regulated genes in the *Adck2*$^{+/-}$ mouse and "b" the number of regulated genes in the *Adck2*$^{+/-}$ mouse associated with a particular GO.

Transcription factors enriched in the promoter regions of the deregulated genes were examined using Motif Databases included in HOMER conduct searches for known motifs. Data for analysis were prepared with Assembly data base.

Moreover, microRNAs were studied to examine potential factors that could modulate gene expression and explain CoQ_{10} regulation over gene expression. For each microRNA the regulated target genes were selected in each analysis, also the expected number of genes regulated were calculated and finally the effect of microRNA's deregulation on its target's gene expression modulation was determined.

3.4.3 Quantitative Real-Time PCR

Quantitative real-time PCR (qPCR) was used to analyse the expression of specific target genes. The HPRT gene was used as a normalization control.

RNA from embryos and mice tissues was isolated with Trizol and treated with DNase I following the manufacturer's instructions. 1 µg of DNase-treated RNA was retrotranscribed with IScript Kits (Bio-Rad) to produce complementary DNA (cDNA) by adding 4 µL 5x iScript Reaction Mix, 1µl iScript Reverse and Mili Q water to complete the final volume of 20 µl. The cDNA synthesis protocol included a priming step at 25ºC for 5 minutes, reverse transcription at 46ºC for 20 minutes, reverse transcription inactivation at 95ºC for 1 minute. qPCR was performed in CFX Connect Real-Time PCR Detection System (Bio-Rad) with iTaq Universal SYBR Green Supermix kit (Bio-Rad) in 96 wells reaction plates according to manufactured instructions.

3.5 Cell culture experiments

3.5.1 CoQ_{10} supplementation in cells

As CoQ_{10} is a lipid, it is not efficient to add it directly to an aqueous medium due to its difficulty to be dissolved. In complex organisms, CoQ_{10} is essentially imported to cells in lipoproteins. Consequently, to reproduce biological importation in cell culture conditions, we have developed a technique for CoQ_{10} administration in cells. The final concentration of CoQ_{10} in the medium was adjusted to 10 µM (MW=863.34 g/M), initially, 0.53 mg of CoQ_{10} were added to an Eppendorf with 50 µl of ethanol (Ethanol HPLC Grade) and heated at 40ºC to be dissolved. In parallel, aliquots of 0.5 ml of horse serum were heated at 37ºC. Once CoQ_{10} was completely dissolved in ethanol, it was added to the horse serum. Then, this supplemented aliquot is added to a 50 mL medium to get a final concentration of 10 µM. CoQ_{10} frozen supplemented aliquots of serum were heated and vortexed before adding them to the medium. In SCs studies, the medium has to be replaced every two days as it was previously recommended (164), thus CoQ_{10} was added to the new medium and replaced every two days.

The final concentration of CoQ_{10} was determined during a PhD to stay at Peter Zammit's lab (Randall Centre for Cell & Molecular Biophysics. King's College, London, UK) where I performed a screening study using myoblasts and myotubes from FSHD human patients and SCs , myoblasts and myotubes from mice, with different doses of CoQ_{10} and different formulations. Finally, we concluded that 10 µM was the most effective dose concerning the phenotype modulation and dilution grade for adult muscle stem cells.

3.5.2 Serum mice collection for cell culture experiments

Serum from mice blood was collected to examine the potential effects of serum components in the differentiation process of SCs and for the design of an *in vitro* model of CR using adult skeletal muscle stem cells. Blood samples were collected from the submandibular plexus in the first hour of the morning (09:00 am), mice on CR were in fasting condition because they did not receive food since the previous day, while *ad libitum* mice were in a postprandial state due to they have food available 24 hours per day.

Blood samples were left in Eppendorf for 1.5 hours for coagulation. After that, blood was centrifuged at 2000 g for 15 minutes at RT and serum was collected from the upper phase. Serum was stored at -80ºC until the moment when the medium was prepared. The complete medium plus the serum of the mice was filtered through a 0.45 µm filter to eliminate any potential contamination.

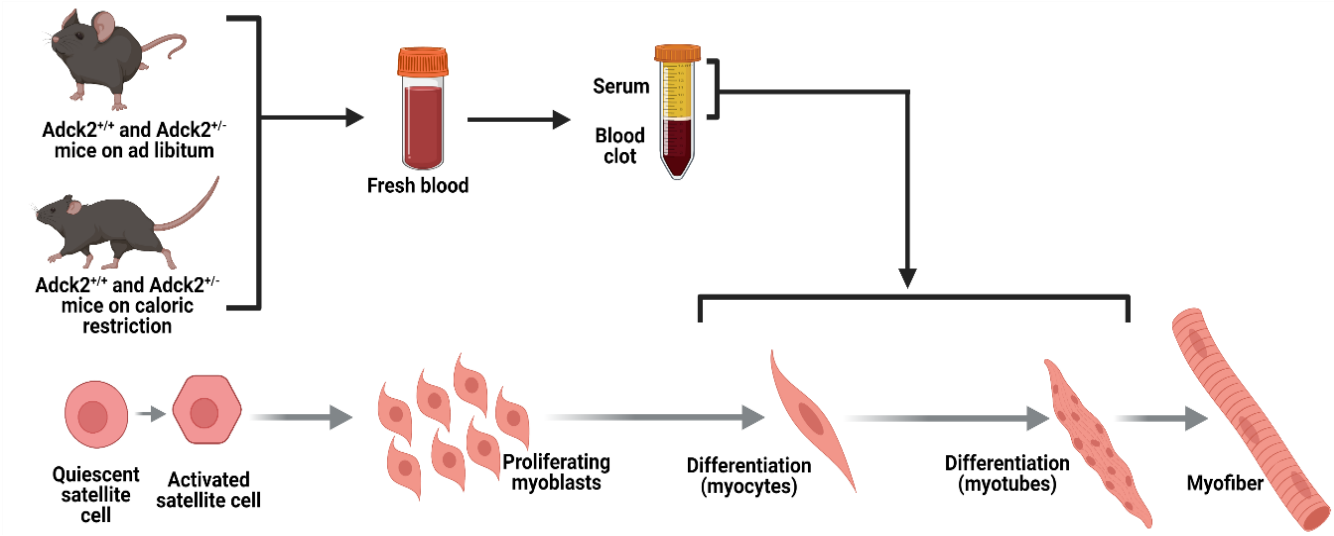

Figure 15 Schematic view of caloric restriction cell culture environment

Blood collected from mice was allowed to clot for 1.5 hours. Blood extraction was performed every two weeks first hour in the morning (09:00 am). Later clot was separated from serum through centrifugation for 2000 g 15 minutes at RT. Serum was stored in pools at -80ºC. Serum was added to the cell culture to induce satellite cells differentiation. Serum from wild type and *Adck2*$^{+/-}$ mice on CR or ad libitum could induce a microenvironment in the cell culture in the function of nutrients and elements composition. (Image elaborated by the PhD candidate).

3.6 Cell culture and myogenic differentiation of isolated Satellite cells

To study postnatal myogenesis, primary SCs cultures were established from EDL muscle. For this purpose, mice were sacrificed by cervical dislocation because carbon dioxide (CO_2) overdose induces myofibers to become hypoxic. The hind limbs were washed in 70% v/v ethanol and closely shave using a scalpel. Next, the mouse was pinned onto a cork dissection board and an incision was made with the scalpel through the skin from the knee to toe to ease the skin away from the underlying musculature and the connective tissue over the TA to expose the muscle.

Then, the TA muscle was removed by the tendons without damaging the EDL muscle. Four distal tendons of the EDL muscle were located on the dorsal side of the paw and were cut out from the hindlimbs proceeding with care to avoid myofiber contraction. EDL muscle was eased away from the rest of the musculature and bones by pulling them up, proximal EDL tendons were cut as close as possible to the kneecap. Both the proximal and distal tendons were kept to ensure that the EDL muscle was obtained intact and without damaging fibrous tissue. Also, blood vessels were carefully removed from the EDL muscle (164) (165).

EDL muscles were digested enzymatically with collagenase Type I (diluted 0.2% w/v in DMEM+glutamax medium) for two hours at 37ºC. Once muscles looked less defined and slightly swollen, they were transferred to a Petri dish with DMEM into the culture hood to preserve sterility and put back at 37ºC to rest for 20 minutes. Previously, Petri dishes were permeabilized with BSA 5% w/v to prevent myofibers from adhering. Meanwhile, the dissecting microscope was placed into the culture hood. Muscles were triturated repeatedly under the microscope with a heat-polished Pasteur pipette pre-coated with BSA 5% (w/v) in PBS to get single hairlike myofibers. Clean myofibers were separated from hypercontracted myofibers, fat droplets, tendons and debris (164)(165). Myofibers were transferred to a new Petri dish precoated with Matrigel (1:10 in DMEM+Glutamax v/v) (Sigma) containing plating medium and cultured for 72 hours with 5% CO_2 at 37ºC. Furthermore, to study SCs attached to myofibers, myofibers were collected and transferred to a 2 mL round-bottomed pre-rinsed with BSA 5% (W/V) in PBS for a wash. Then, the medium was carefully removed and filled with pre-warmed 4% PFA (w/v) and incubated for 10 minutes to fix the cells.

Myofibers were cultured for 72 hours with 5% CO_2 at 37 ºC in proliferation medium to allow SCs migration in a 10 cm diameter Petri dish coated with Matrigel (1:10 in DMEM+Glutamax v/v (164). After 72 hours, SCs were activated and migrated from the myofibers to the cell culture plate. Under a stereo dissecting microscope inside of a culture hood, attached myofibers were removed with a 1 mL pipette by agitating the medium over myofibers. After that, cells were washed twice with PBS and trypsinized for 5 minutes at 37ºC. Next, cells were transferred to a non-coated 10 cm Petri dish with fresh medium and incubated for 15 minutes at 5% CO_2 at 37ºC to remove contaminating fibroblasts, which remained attached to the plastic of the culture dish. At this time, non-adhered SCs were removed from the medium and plated on Matrigel-coated plates for proliferation and differentiation experiments (Figure 16).

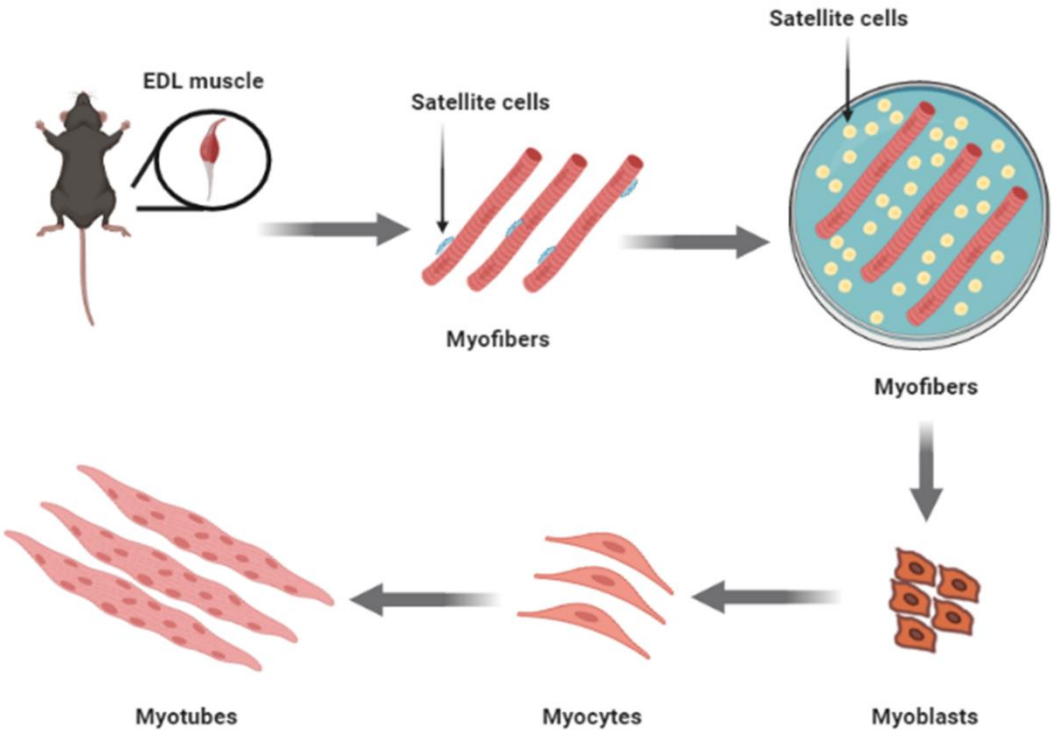

Figure 16. Satellite cells isolation, activation, proliferation and differentiation representation.
The steps of the primary cell cultures from isolated satellite cells are exhibited above: EDL muscle dissection, myofibers trituration, myofibers culture, satellite cells isolation and differentiation to myoblast, myocytes and myotubes. The different time points for each step were always carried out the same to compare experiments from different biological replicates. This protocol was used to assess postnatal myogenesis in satellite cells from young and old mice.

SCs can be passed 3-4 times and would remain in a proliferative status for 1.5 weeks. For all experiments performed using SCs, the medium was replaced carefully every 48 hours and cell culture plates were coated with Matrigel (1:10 in DMEM+Glutamax v/v) for at least 30 minutes at 37ºC.

SCs were plated in a 96-well plate previously coated with Matrigel (1:10 in DMEM+Glutamax v/v) for immunostaining in proliferation and differentiation. For proliferation assays, 20.000 cells per well were seeded, whereas, for differentiation assays, 10.000 cells per well were plated. For differentiation assays, the cells were allowed to grow for 1 day. During this initial day of seeding, SCs were in proliferation medium, and it was considered day -1, with no differentiation time. Differentiation was induced by a reduction of serum in the cell culture medium (Table 6). For Seahorse experiments, 30.000 SCs were seeded per well and allowed to differentiate until the specific time point.

Table 6 Mediums used for satellite cell experiments

PROLIFERATION MEDIUM			
Component	**Final concentration [%]**	**Volume for 50 mL**	**Reference**
DMEM+Glutamax	59	28.5 mL	Gibco. Dulbecco's Modified Eagle Medium: Ref 3196-021.
Fetal Bovine Serum (FBS)	30	15 mL	Gibco Ref 10500-064
Horse Serum (HS)	10	5 mL	Gibco by life technologies. Ref 16050-122
Chicken embryo extract (CEE)	1	500 µl	MP biomedicals 092850145, fisher scientific.
Fibroblast Growth Factor (FGF)	0.0001	5 µl	Prepotech Murine FGF-basic AF-450-33-10U
Penicillin-Streptomycin (PS)	0.001	50 µl	Sigma P0781
DIFFERENTIATION MEDIUM			
Component	**Final concentration [%]**	**Volume for 50mL**	**Reference**
DMEM+Glutamax	97.9	48.95 mL	Gibco. Dulbecco's Modified Eagle Medium: Ref 3196-021.
Horse Serum (HS)	2	1 mL	Gibco by life technologies. Ref 16050-122.
Penicillin-Streptomycin (PS)	0.001	50 µl	Sigma P0781
DIFFERENTIATION MEDIUM ON CR EXPERIMENTS			
Component	**Final concentration [%]**	**Volume for 50mL**	**Reference**
DMEM+Glutamax	97.9	48.95 mL	Gibco. DMEM: Ref 3196-021.
Mice serum	2	1 mL	Self-produced
Penicillin-Streptomycin (PS)	0.001	50 µl	Sigma P0781

3.7 Skeletal muscle histology and immunochemistry

3.7.1 Skeletal muscle dissection, freeze and section.

Hind limbs and lower body were saturated with 70 % v/v ethanol and shaved using a scalpel, shaved fur was removed with towel paper. The mouse was pinned onto a corkboard, pinned with one forelimb through the palm. The contralateral hind limb was pinned through the dorsal side of the paw. The tail was extended to the side and the contralateral hind limb to the opposite side. An incision was made through the skin from knee to toe and the skin was cut down to the paw, stopping just proximal to the digits. The skin and all connective tissue were removed to reveal the underlying musculature and tendons.

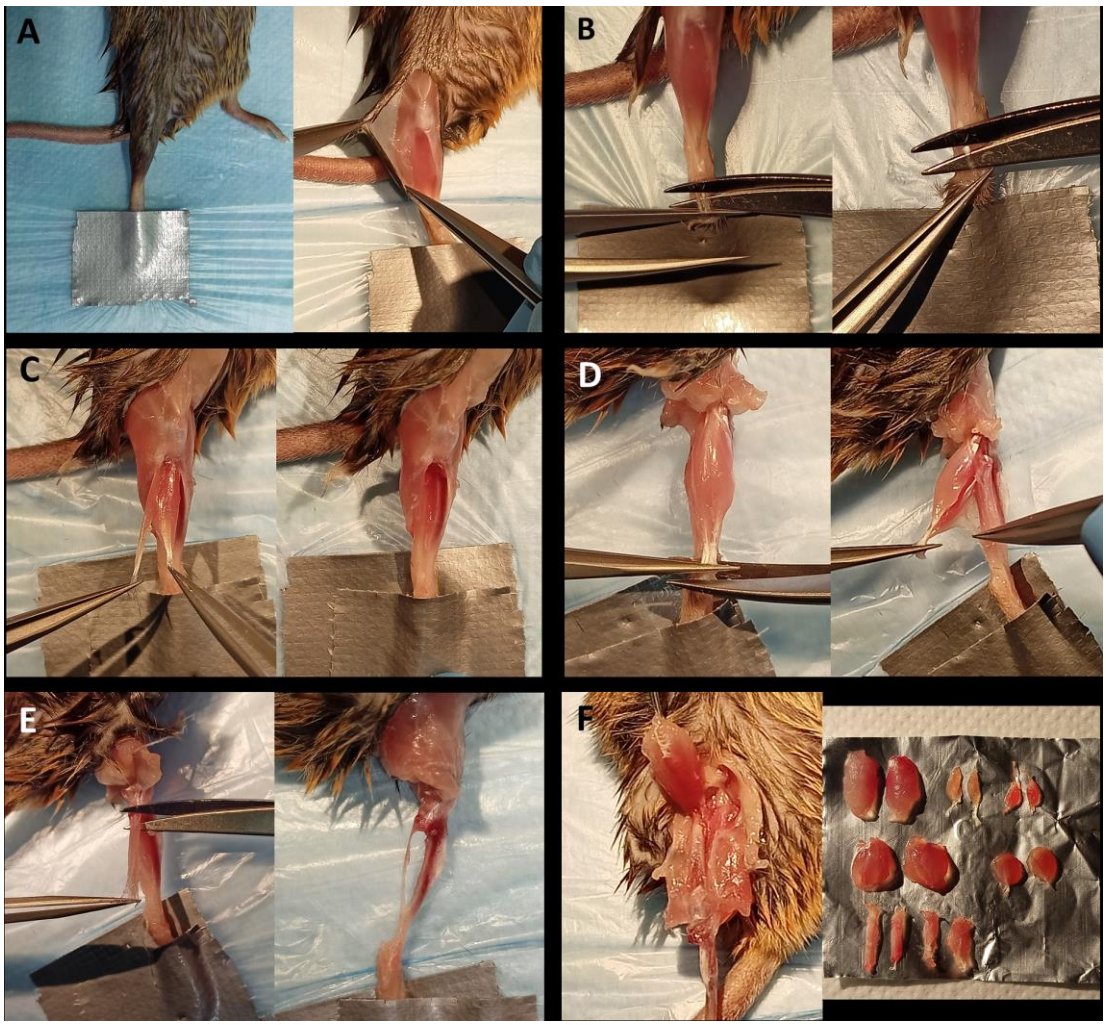

Figure 17. Dissection and isolation of murine skeletal muscles from hindlimbs.
(A) The mouse was pinned in a cross arrangement. An incision was made through the skin from next to the ankle stopping proximal to the knee. (B) TA and EDL tendons were sectioned close to their insertions. (C) The TA tendon was pulled up to ease the muscle away from the underlying musculature and bone. Then, the TA was cut proximally, close to the ventral crest to the tibia. Similarly, the EDL muscle was eased away, and the proximal tendon was meticulously cut at the side of the knee. (D) In the posterior hindlimb, gastrocnemius (GA) and soleus muscles were carefully liberated from the tibial bone after cutting the Achilles tendon. (E) The remaining muscles found from ankle to knee were collected until only the fibula and tibial bones remained. (F) Quadriceps were dissected as well and combined with the rest of the skeletal muscles collected for posterior mitochondrial isolation. Detailed representation of skeletal muscle dissection. (Adapted from (158)).

Carefully, the ends of the four distal tendons of the EDL muscle were cut out ensuring that all tendons were present (Figure 17). After that, the distal tendon of the TA in the anteromedial dorsal foot side was cut and gripped to carefully pull out the underlying musculature to finally cut the tendon close to the knee with a scalpel. After that, EDL was gripped by the underlying musculature by the distal tendon.

Muscles were embedded in Tissue-Tec® OCTTM (Sakura) in silver foil cubicles and frozen in liquid nitrogen-cooled isopentane for further immunostaining. Previously, a beaker filled with isopentane was introduced into a 1.8 L Dewar filled with liquid nitrogen until a frozen (white) layer of isopentane was formed at the bottom of the beaker while liquid isopentane was at the top of it. The foil cubicles held were submerged into the isopentane (only the base) until OCT was frosted and become white (Figure 18). The foil cubicles were stored in dry ice and finally at -80ºC.

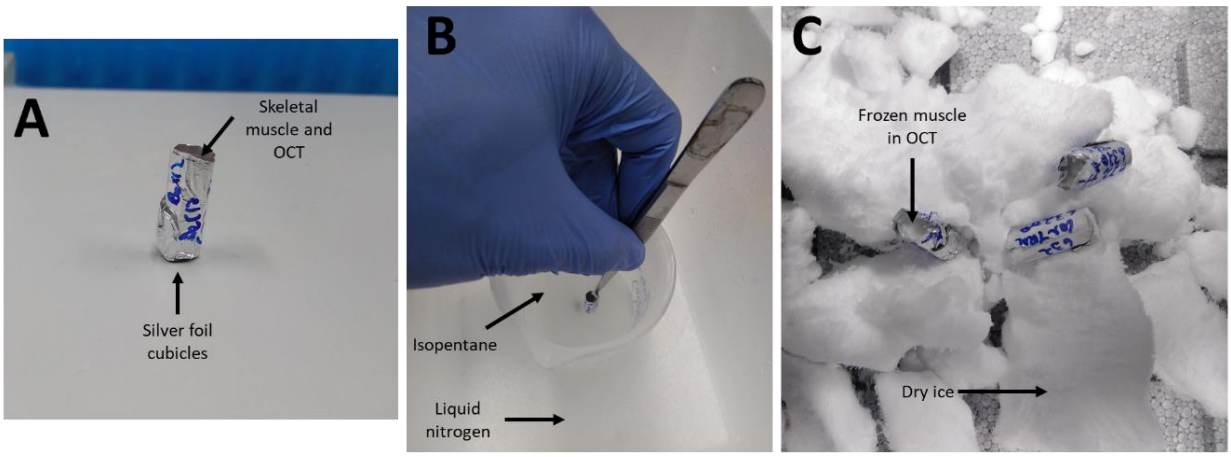

Figure 18. Skeletal muscle cryopreservation specifications
(A). Silver foil cubicles, skeletal muscle and OCT mounting avoiding OCT bubbles. (B). The skeletal muscle freezing method introduces only the base of the silver foil cubicles into the frozen nitrogen to prevent muscle damage by cold. (C). Skeletal muscle was cryopreserved in dry ice and stored at -80º degrees until cryosection was performed.

Previously to cryosection, frozen samples were equilibrated to the cryostat temperature (-20 ºC) for 1 hour. Excess OCT was carefully removed with a mounted razor blade and the frozen muscle was attached to a cryostat stub with extra OCT. Once, OCT added was frozen, the muscle was secured to the cryostat stub, and the stub was attached to the object holder where the muscle was localized in perpendicular to the cryostat blade (Figure 19).

Several sections of 60 µm of thickness were done and discarded to eliminate the excess of OCT and to reveal the muscle. Then, section thickness was adjusted to 12 µm and the muscle was sectioned until the whole transversal section of the tibial anterior was exposed. At this point, cryosections were cut, adhered and melted onto the warmer slide. Stretching and folding of the

cryosections were avoided by keeping a steady pressure. Muscle sections were revised under a light microscope to check orientation and quality. Only when high-quality cryosections were obtained, samples were collected for later analysis. Finally, dried slides were stored at -20ºC.

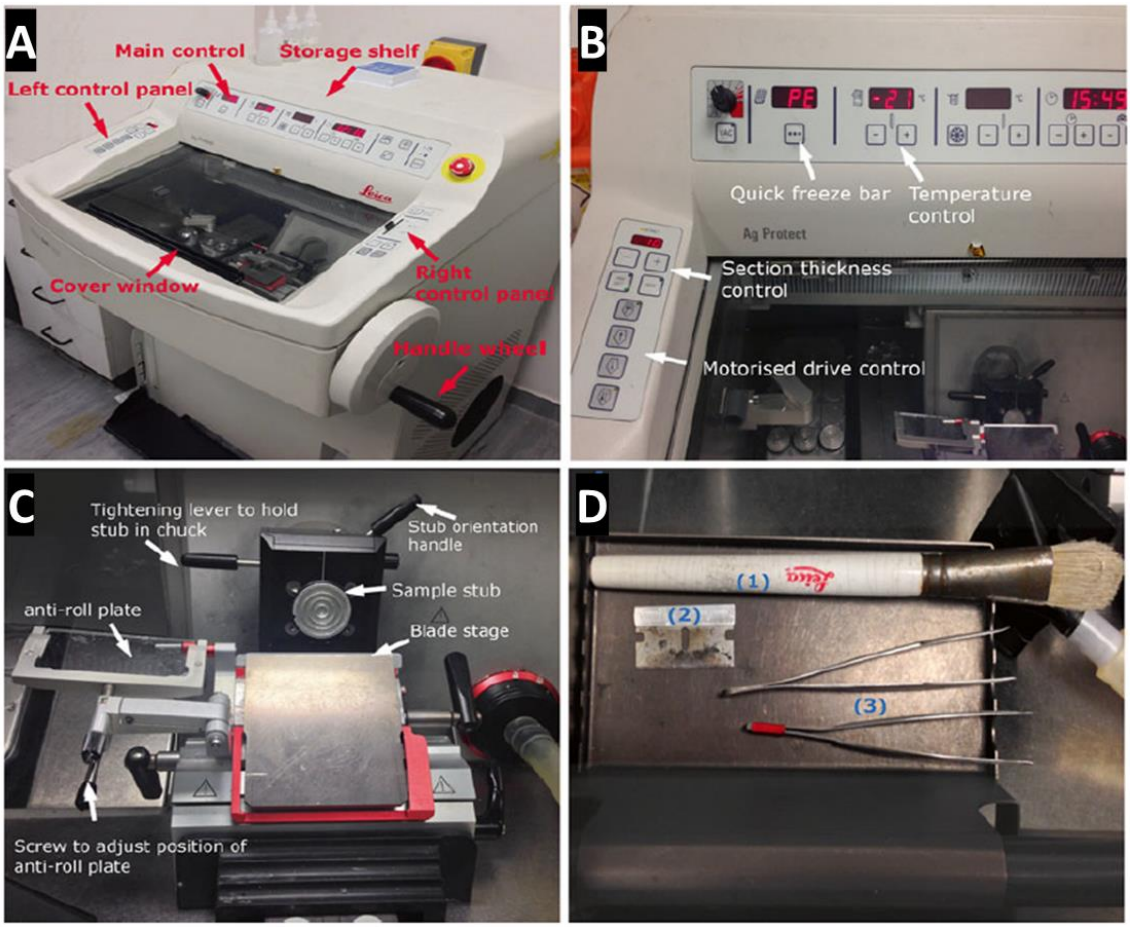

Figure 19. Cross-sectioning process in skeletal muscle.
(A). A Leica CM1950 cryostat highlighting external controls and components. (B). Zoom on control panels. (C) Sample holder and blade stage including controls to secure sample and blade orientation and position. (D) Tools needed for sectioning: (1) brush, (2) razor and (3) fine forceps. (Adapted from (166)).

3.7.2 Pax7 associated with myofibers immunostaining

For immunostaining of Pax7 positive satellite cells (SCs) attached to myofibers, between 15 and 25 myofibers were analysed per mouse. Myofibers were isolated from EDL muscle with enzymatic and mechanic digestion as detailed above and fixed with 1 mL of pre-warmed 4% PFA w/v for 10 minutes at RT with gentle agitation. Next, the tube was stood vertically to allow myofibers to settle and PFA was carefully removed. Fixed myofibers were washed three times with PBS for 8-10 minutes and myofibers were stored in PBS at 4ºC.

PBS was removed and 1 mL of 0.5% (v/v) Triton X-100/PBS solution was added and incubated for 10 minutes. Then, myofibers were washed three times with 1 mL of 0.5% (v/v) Tween/PBS

for 8 minutes and incubated for 90 minutes with a blocking solution (10% (v/v) goat serum in 0.25%(v/v) Tween/PBS) to avoid non-specific antibody binding. Myofibers were incubated with Pax7 antibody (1:100) overnight at 4ºC. The next day, myofibers were washed three times with 0.25% (v/v) Tween/PBS for 8-10 minutes and incubated with the secondary antibody (1:400 v/v) in 0.25% (v/v) Tween/PBS for 90 minutes at RT in dark. After that, myofibers were washed three times with PBS and incubated with 500 µl of DAPI solution (diluted 1:1000 in PBS) for 8 minutes at RT. Finally, myofibers were washed three times with PBS and transferred to a Petri dish containing PBS, where individual myofibers were collected and dropped over a glass slide trying that myofibers show a lineal orientation. The slides were placed on a flat surface and 50 µl of glycerol 50% (v/v) (diluted in ddH_2O) was added. A glass coverslip was lowered carefully over the myofibers, avoiding trapping air bubbles and secured with nail varnish. Slides were viewed under a fluorescence microscope.

3.7.3 Dystrophin immunostaining in muscle sections

Transversal cuts of TA muscle were prepared as described above. Slides were allowed to equilibrate for 5 minutes at RT and evaporate any condensation. The slides were dry with absorbent paper and the border was marked with a liquid-repellent slide marker pen. The rest of the protocol was performed over a humidified slide chamber. The slides were washed 3 times with PBS-T (0.1% v/v Triton X100) for 8 minutes. Muscle sections were blocked with blocking solutions (PBS plus FBS 10% v/v) for 1 hour at RT and incubated overnight with 150-200 µl primary antibody dissolved in blocking solution (Dystrophin 1:100 v/v). Next, slides were washed three times with PBS-Triton (0.1% Triton X100 v/v) for 10 minutes. From this point, the rest of the protocol was performed in darkness. The secondary antibody solution was added to the slides (Alexa Fluor 488, diluted 1:1000 in blocking solution v/v) and incubated for two hours at RT. Then, slides were washed three times with PBS-T (0.1% v/v Triton X100) for 5 minutes and incubated with DAPI solution (1:1000 v/v) for 8 minutes. Finally, slides were washed with PBS three times for 5 minutes, placed on a flat surface and mounted with 50 µl of glycerol 50% v/v (diluted in ddH_2O). A glass coverslip was lowered carefully over the stained section, avoiding trapping air bubbles and secured with nail varnish. Slides were viewed under a fluorescence microscope.

3.7.4 Myofibers typing immunostaining in muscle sections.

Slides from transversal TA muscle cut were obtained as previously detailed and stored at -80ºC. Slides were allowed to equilibrate for 5 minutes at RT and evaporate any condensation. The protocol was performed over a humidified slide chamber. Slides were washed for 5 minutes in PBS and incubated with blocking solution for 1 hour at RT (10% FBS diluted in PBS v/v). Next, a

cocktail of primary antibodies prepared in blocking solution was added (SC71 1:400 v/v and BFF3 1:100 v/v) and slides were incubated for 1 hour at RT. Then, slides were washed 3 times in PBS for 5 minutes, and the rest of the protocol was performed in darkness. Secondary antibodies cocktail was added to the slides and incubated for 1 hour at RT. After that, the slides were washed 3 times for 5 minutes with PBS. Finally, slides were placed on a flat surface and 50 µl of glycerol 50% v/v (diluted in ddH_2O) was added. A glass coverslip was lowered carefully over the stained section, avoiding trapping air bubbles. The coverslip was secured with nail varnish. Slides were viewed under a fluorescence microscope.

3.7.5 Immunostaining of cells differentiate from satellite cells

Freshly isolated SCs were plated in a 96-well plate previously coated with Matrigel (1:10 in DMEM+Glutamax v/v). SCs were cultured with the appropriate medium for each experiment performed and at the specific time point, the cell culture medium was replaced by 150 µl of 4% PFA w/v to fix the cells for 10 minutes on a rocker at RT.

Next, cells were washed with 200 µl PBS 1X three times for 5 minutes on a rocker to eliminate any rest of 4% w/v PFA. Cells were permeabilised with 150 µl 0.1% Triton in PBS v/v for 15 minutes on a rocker at RT. Next, 150 µl of blocking solution was added per well and incubated for 1 hour in a rocker at RT. The blocking solution was 5% FBS v/v in PBS. Subsequent, cells were incubated with 75 µl of primary antibody diluted in blocking solution v/v overnight on a rocker at 4ºC. The next day, cells were washed three times with PBS for 5 minutes. From this point, the rest protocol was performed in darkness. Next, 75 µl secondary antibody diluted in blocking solution was added per well and incubate for two hours on a rocker at RT. Finally, cells were washed three times with PBS for 5 minutes. Cells were incubated with DAPI solution (1:1000 v/v) in PBS for 10 minutes on a rocker at RT and cells were stored at 4ºC in darkness.

Particularly, satellite cells were incubated with MyHC antibody to assess the differentiation from SCs to myotubes. Several markers of differentiation were used to quantify the differentiation of satellite cells such MyHC area, differentiation index, myotube length and branching capacity. We also evaluate the growth of myotubes through the time-points studied with the equation of the graph and the slope of the line.

3.7.6 Image acquisition and image analysis.

Cell imaging was performed using a Fluorescence Microscopy Zeiss Axio Imager M2, with a Confocal Microscope Leica SPE and with a Stellaris Confocal Laser Scanning Microscope from Leica.

For image analysis, different automatic plugins or macros for analysis were used, as well as semiautomatic methods that included manual correction steps. Moreover, for some analyses where automatic or semi-automatic methods were not reliable, manual analyses were performed. The image analysis system used will be detailed above:

- Analysis of MyHC area in differentiated myotubes from SCs. Myotubes were stained with MyHC primary antibody and Alexa Fluor 488 was used as the secondary antibody. Myogenic nuclei were stained with DAPI. An automatic method for the MyHC area was used, the parameter was calculated with an R script recently published by the Peter Zammit group (167). The script analyses the percentage of the image that was occupied by MyHC which is a protein expressed in differentiated myotubes. The script reports an image to check the green area and blue nuclei analysed.
- Differentiation index was determined in myotubes from SCs. Myotubes were stained with MyHC primary antibody and Alexa Fluor 488 was used as the secondary antibody. Myogenic nuclei were stained with DAPI. An automatic method was used to analyse the fusion index in the myotubes differentiated from SCs. The method was recently published as an R script by the Zammit group (167).

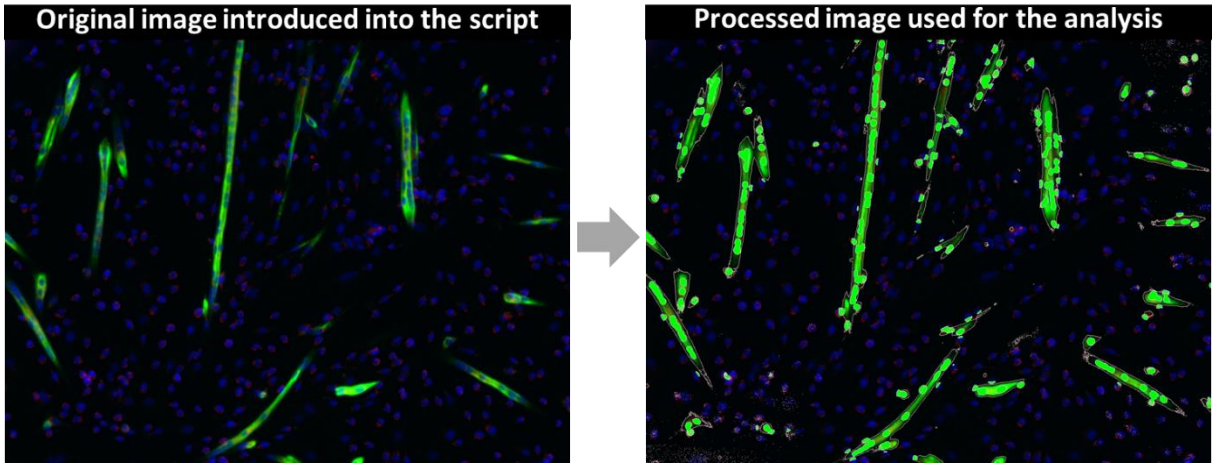

Figure 20 Analysis method of MyHC staining
Analysis of MyHC area in myotubes differentiated from primary satellite cells culture. The method that determines the MyHC area proportion and the differentiation index from images taken with the Fluorescence Microscopy Zeiss Axio Imager M2 (objective 10X).

- Positive nuclei for proliferation markers were examined using a Fiji plugin that automatically recognises positive nuclei for the specific marker and DAPI. It is necessary to set the intensity values from which positive nuclei from the selected channels would be quantified and apply the same settings to all images studied. The plugin was developed by Johanna Pruller from the Zammit group (unpublished plugin).
- Central nuclei in transversal TA muscle cuts were studied to examine skeletal muscle regeneration. Dystrophin was used to stain myofiber borders and DAPI was used to stain

central and peripheral nuclei. The analysis was performed with an automatic plugin for Fiji software that allows us to examine the number of central nuclei per myofiber. The plugin also included specific steps to check that the image masks were correctly performed. The plugin was developed by Alejandro Campoy from the Microscopy Unit at CABD (unpublished plugin).

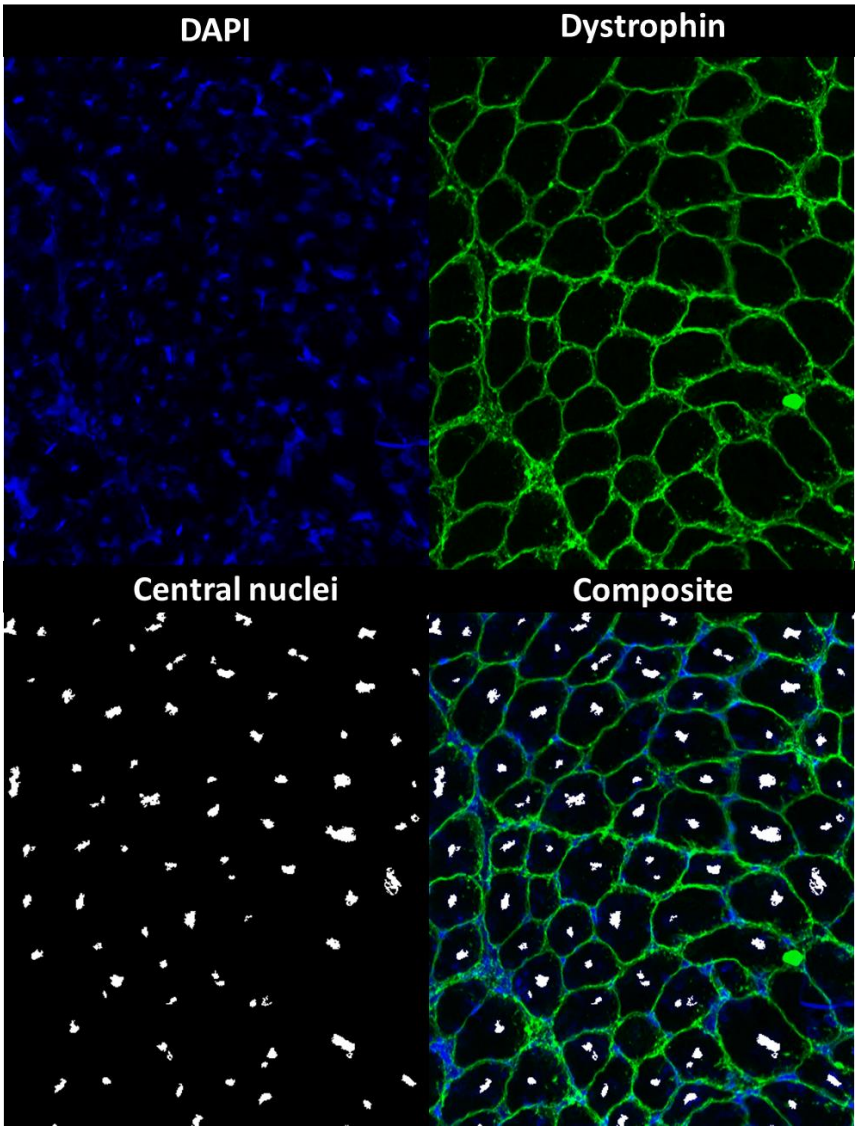

Figure 21 Analysis method of central myonuclei study
For analysis of myofibers, borders were stained with dystrophin antibody (in green) and nuclei from the myofiber were stained with DAPI (in blue). The complete transversal section was examined to assess the regeneration process in the whole muscle. After the analysis, only central myonuclei were quantified and referred to as the total number of myofibers.

- Analysis of Pax7 positive nuclei in isolated myofibers. Pax7 were stained with Pax7 antibody and incubated with Alexa Fluor 488 secondary antibody while nuclei were stained with DAPI. The analysis was performed to check that positive nuclei per DAPI were also positive for Pax7. The image acquired from the microscope was introduced in

Fiji. First, both channels were united: “Image→Colour→Merge channels”, to check that nuclei were positive in both channels: “Image→Colour→Channel tools”.

- For the analysis of myofiber typing, the same area (2000x2000 µm) was selected from each transversal TA muscle image including white and red TA area. Myofibers IIA were stained in green, myofibers IIB were stained in red and myofibers IIX were in black. To quantify the number of the different myofibers types (IIA, IIB and IIX) “oval” selection in Fiji was used.

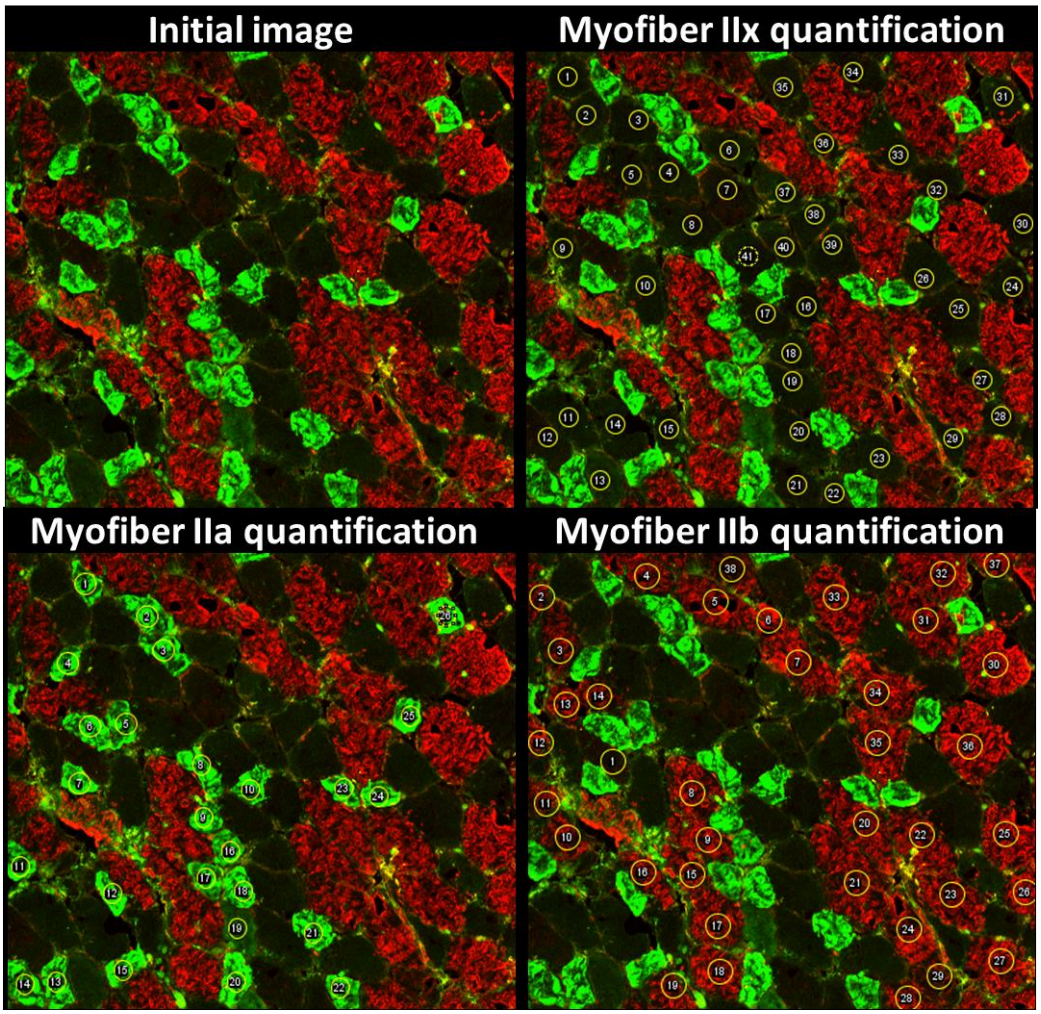

Figure 22 Analysis method of myofiber typing study
Immunostaining to assess myofiber typing in transversal TA muscle cuts. Myofibers type IIX are in black, type IIA in green and type IIB in red. A section (2000x2000 µm) from each mouse was quantified and the number of each myofiber type was referred to the whole number of myofibers to obtain the proportion of the different myofiber types.

- For the analysis of the cross-sectional area on transversal TA muscle cuts a segmentation process was implemented. Dystrophin was used to stain myofiber borders and DAPI was used to stain nuclei. First, channels were separated by “Image→Colour→Split channels” to select the dystrophin channel. The picture was improved if it was worth “Image→adjust→Brightness and contrast→auto”, “Process→Enhance local contrast

(not fast)", "Process→Noise→Remove NANDS or outliers". Next, the image was transformed to white-black "Image→adjust→threshold+click on dark background" and now to close the myofiber perimeter "Plugins→MorphoLibJ→Morphological Filters→Closing + Disk + 5 pixels". All myofibers from the muscle cuts were selected "Analyse→ analyse particles+ include the particles in the ROI record" and the ROI was loaded over the colour dystrophin image. The border of the myofiber was painted in white using the paint tool from Fiji and the myofibers sharp edges in red, to check that the mask was adequate to the original image. After that, the image was transformed to 8-bit type, the threshold was adjusted to select only what was painted in white or red. Then, new particles were selected and pasted in the mask (white-black image previously generated) to load the "Roi→More→fill". Finally, the analysis was done in the mask "Analyse→analyse particles→ select particle between 200-1500 um".

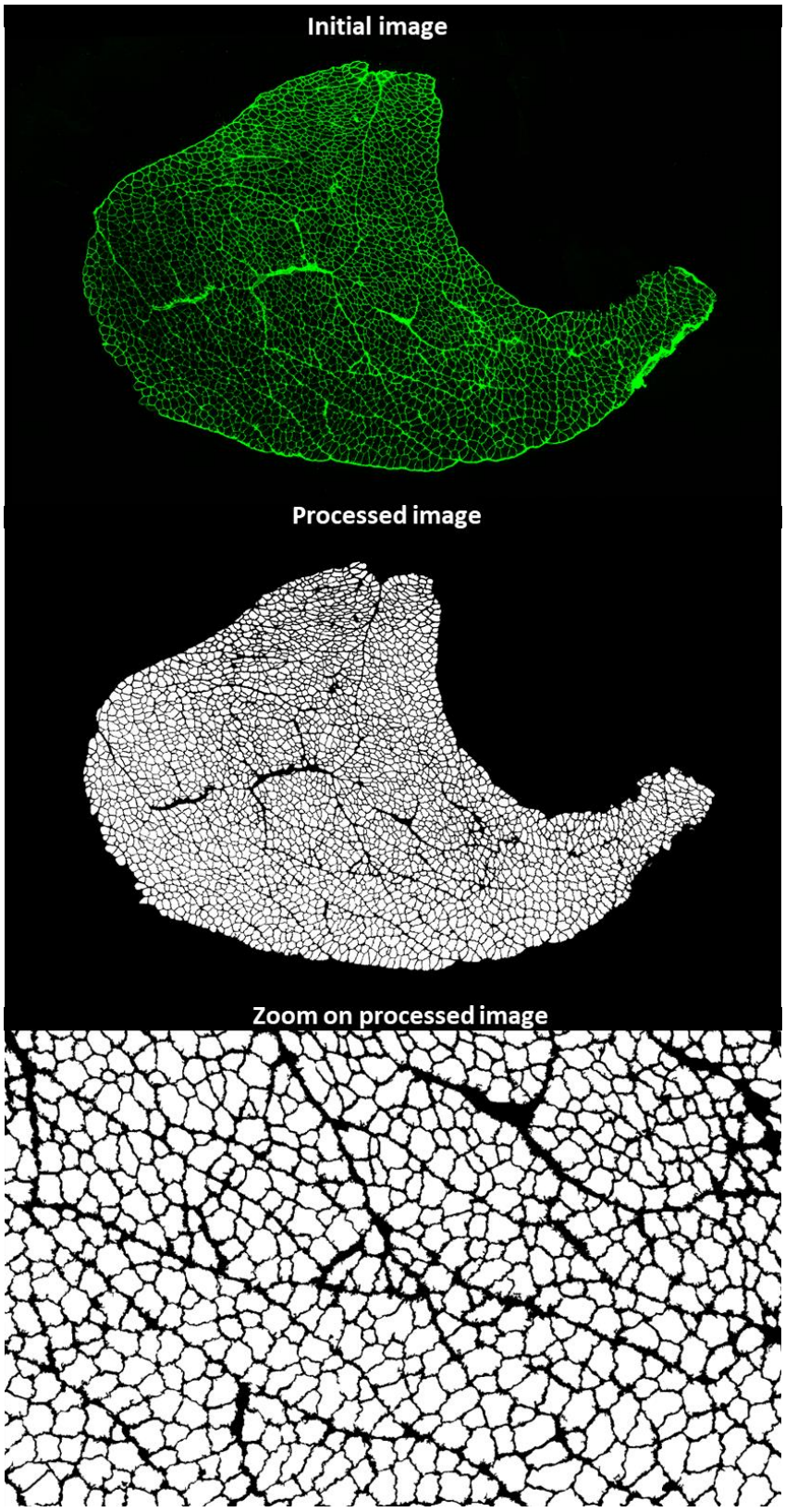

Figure 23 Analysis method of myofiber size

Method for myofiber size study includes an unprocessed image of the whole transversal section of TA muscle, a processed image after Fiji correction and a zoom image of the processed image where every myofiber can be individually analysed. The same analysis was perfect for the transversal muscle section of all mice studied to quantify the dimensions of every single myofiber of the TA muscle.

3.8 Mitochondrial respiration analysis.

3.8.1 Assessment of mitochondrial respiration in cells.

Seahorse was used to analyse the mitochondrial metabolism of myotubes derived from SCs. Freshly isolated SCs were seeded at an optimal density of 30.000 cells per well onto the Seahorse cell culture plate and allowed to grow for 24 hours in the proliferative medium. Then, this medium was replaced by differentiation medium and left for 48 hours before running the assay. Respiration experiments were determined with an XFe24 Extracellular Flux Analyzer (Seahorse Bioscience) following the manufacturer's instructions. To ameliorate the attachment of the cells to the Seahorse plate, plate wells were coated with 500 µl of Matrigel (1:10 in DMEM+Glutamax v/v) solution and incubated for 45 minutes at 37ºC to promote monolayer gel formation at the bottom of the well. Oxygen consumption rate (OCR) was assayed using glucose as an energy substrate while palmitoyl-DL-carnitine was used as an energy substrate in β-oxidation assays.

Oxygen Consumption Rate

The day before the assay, the cartridge was pre-hydrated with Seahorse XF Calibrant Solution and incubated overnight at 37ºC without CO_2. OCR assay was conducted in Agilent Seahorse XF base medium (bicarbonate-free medium), supplemented with 2 mM D-glucose, 1 mM sodium pyruvate and 2 mM L-glutamine. The medium was freshly prepared and adjusted to pH 7.4 with NaOH at 37°C before use. Cells were washed twice with the medium of the assay and after that, 500 µl of the medium of the assay was added to each well and the plate was incubated for 1 hour at 37ºC without CO_2. Meanwhile, the cartridge was loaded with the respiratory inhibitors oligomycin, carbonyl cyanide-p-trifluoromethoxyphenylhydrazone (FCCP), antimycin A and rotenone, which were diluted with assay medium and loaded respectively into ports A, B, C and D of the XFe24 sensor cartridge. The final working concentrations of oligomycin A, FCCP and antimycin A and rotenone were 4.0, 1.0, 5.0 and 1.0 µM, respectively. Finally, the cartridge was inserted into the Seahorse Analyzer and calibrated. After that, the cell plate was also introduced into the Seahorse Analyzer and the assay started.

OCR was measured on basal respiration and after consecutive injections of any of the different inhibitors. After assays completion, cells were lysed in RIPA buffer for protein quantification using the RC DC Protein Assay (Bio-Rad 5000122) was used to normalize the data and albumin used as standard (Bio-Rad 5000007) (168).

Parameters analysed:

- Non-Mitochondrial respiration: minimum rate measurement after injection of all inhibitors.
- Basal respiration: respiration values on resting conditions. It is calculated by subtracting the value of the last rate measurement before oligomycin injection from the non-mitochondrial respiration.
- Maximal respiration: oxygen consumption after the addition of the uncoupler element (FCCP), which allowed mitochondria to respire at maximum capacity, to compensate for the loss of mitochondrial membrane potential. It was calculated by subtracting the value of the maximum rate measurement after FCCP injection from the non-mitochondrial respiration rate.
- Spare respiratory capacity: measurement of the cell's capacity to respond to energetic demand. It was calculated by subtracting the value of the maximal respiration from the basal respiration
- Coupled or ATP-linked respiration: oxygen consumption coupled to ATP production. It was obtained by subtracting the value of the last rate measurement before oligomycin injection from the minimum measure after oligomycin injection.

The β-oxidation assay indicates the cell's capacity to use exclusively fatty acids as energetic substrates. The assay was performed in MAS buffer medium (sucrose [70mM], mannitol [440 mM], KH_2PO_4 [100 mM], $MgCl_2$ [50 mM], EGTA [10 mM] and HEPES [20 mM]) adjusting the pH to 7.2 with KOH at 37ºC before use. Cells were washed twice with the medium of the assay and after the second wash, 500 µl of the medium was left in each well. The first injection was digitonin plus malic acid [5 µg/µl and 2.5 mM]. The purpose of digitonin was to permeabilize the cell membrane and allow inhibitors and substrates to arrive at the mitochondria. In the second port, palmitoyl-DL-carnitine and ADP were injected [50 µM and 1mM] respectively. The third injection was oligomycin at [4 µM] and the last port was loaded with Antimycin A plus rotenone [5 µM and 1 µM] respectively. cells were lysed in RIPA buffer for protein quantification using the RC DC Protein Assay (Bio-Rad 5000122) to normalize the data and albumin was used as standard (Bio-Rad 5000007) (169). The fatty acid β-oxidation rate was calculated using the two-consecutive measurements after the first injection (digitonin plus malic acid) and two consecutive measurements after the second injection (palmitoyl plus ADP).

Table 7 Preparation of injection solutions for the respiration assays in cells.

Oxygen Consumption Assay						
Port	Compound	[Stock]	[Injection Port]	[Final]	Recipe	
					Inhib	Medium
A	Oligomycin	4 mM	40 µM	4 µM	14.30 µL	1421.7 µL
B	FCCP	20 mM	50 µM	5 µM	3.90 µL	1556.10 µL
C	Antimycin A	5 mM	50 µM	5 µM	16.90 µL	1551.94 µL
D	Rotenone	1 mM	10 µM	1 µM	4.22 µL	1672.26 µL
β-Oxidation Assay						
Port	Compound	[Stock]	[Injection Port]	[Final]	Recipe	
					Inhib	Medium
A	Digitonin // Malate	2.5 mg/ul //250 mM	25 ug/ul // 25 mM	2.5 ug/ul // 2.5 mM	20 µL // 200 µL	2000 µL
B	Palmitoyl // ADP	50 mM //100 mM	500 µM // 10 mM	50 µM // 1 mM	20 µL // 200 µL	2000 µL
C	Oligomycin	4 mM	40 µM	4 µM	20 µL	2000 µL
D	Antimycin A // Rotenone	5 mM // 1 mM	40 µM // 5 10 µM	4 µM // 1 µM	16.90 µL // 4.22 µL	1672.26 µL

Table 8 Protocol setting for the respiration assays in cells

Action	Time (minutes)	Repetition	Port
Calibrate	15-20		
Mix + Wait + Measure	3 + 2 + 3	X 3	
Inject			A
Mix + Wait + Measure	3 + 2 +3	X 2	
Inject			B
Mix + Wait + Measure	3 + 2 +3	X 2	
Inject			C
Mix + Wait + Measure	3 + 2 +3	X 2	
Inject			D
Mix + Wait + Measure	3 + 2 +3	X 2	

3.8.2 Assessment of mitochondrial respiration in isolated mitochondria from skeletal muscle.

To assess mitochondrial metabolism and bioenergetics, we have set up a new protocol to analyse respiration in freshly isolated mitochondria from mice's skeletal muscles (158).

Buffers for mitochondria isolation and protein quantification were prepared fresh on the day of the experiment. Maintaining the right pH throughout the whole procedure was crucial for obtaining successful results. Buffers were adjusted with KOH to pH 7.2 and BSA containing buffers were not measured with the pH meter. Commercial pure H_2O at pH 7 was used to prepare buffers.

Table 9 Buffers preparation for mitochondrial isolation

Buffers for mitochondria isolation	
10% (w/v) fatty-acid-free (FFA) BSA	150 mg FFA BSA in 1.5 mL H_2O by inversion/rotatory wheel.
1X Bradford reagent	Dilute the commercial solution according to 1X concentration.
8X Mitochondria buffer	4.112 grams of sucrose and 763 mg of HEPES were dissolved in 15 mL of H_2O. Adjust the pH to 7.2, 250 µl FFA BSA were added (stock at 10% v/v) and QS to 20 mL with H_2O
Isolation Buffer 1 (IB1)	400 µl of EDTA (stock at 0.5M), 784 mg of D-mannitol and 2.5 mL of 8X MB were dissolved in 15 mL of H_2O. Adjust the pH to 7.2 and QS to 20 mL with H_2O
Isolation Buffer 2 (IB2)	30 µl of EGTA (stock at 0.5 M), 196 mg of D-mannitol and 625 µl of 8X MB were dissolved in 4 mL of H_2O. Adjust the pH to 7.2 and QS to 5mL with H_2O.
Resuspension Buffer (RB)	120 mg of sucrose, 191.3 mg of D-mannitol, 50 µl HEPES (stock at 0.5M), 10 µl of EGTA (stock at 0.5M) were dissolved in 4 mL of H_2O. Adjust the pH to 7.2 and QS to 5 mL with H_2O.
2X MAS-1	1.199 grams of sucrose, 2.8 grams of mannitol, 1mL of KH_2PO_4 (stock 0.5M), 250 µl $MgCl_2$ (stock 1M), 200 µl of HEPES (0.5 M) and 100 µl of EGTA (0.5M) were dissolved in 20 mL of H2O. Adjust the pH to 7.2 and QS to 25 mL with H_2O
CAM+BSA	300 µL pyruvic acid (stock at 0.5 M), 30 µL of malic acid (stock at 0.5 M) and 7.5 mL of 2X MAS-1 were diluted in 6 mL of H_2O. Adjust the pH to 7.2. 300 µL of BSA (stock at 10% v/v) were added and QS to 15 mL with H_2O
CAM-BSA	120 µL of pyruvic acid (stock at 0.5 M), 12 µL of malic acid (stock at 0.5 M) and 3 mL of 2X MAS-1 were diluted in 2 mL of H_2O. Adjust the pH to 7.2 and QS to 6 mL with H_2O.
BOXM+BSA	12 µL of palmitoyl-L-carnitine (stock at 50 mM), 30 µL of malic acid (stock at 0.5 M) and 7.5 mL of 2X MAS-1 were diluted in 7 mL of H_2O. Adjust the pH to 7.2. 300 µL BSA (stock at 10% v/v) were added and QS to 15 mL with H_2O.
BOXM-BSA	4.8 µL of palmitoyl-L-carnitine (stock at 50 mM), 12 µL of malic acid (stock at 0.5 M) and 3 mL of 2X MAS-1 were diluted in 2 mL of H_2O. Adjust the pH to 7.2 and QS to 6 mL with H_2O

1X Coupling Assay medium (CAM): Two different MAS-1-based buffers need to be prepared: 1) CAM+BSA for proper CA assay, 2) CAM-BSA for preparing the assay inhibitors. It was important to keep the 10:1 pyruvate: malate ratio. Since BSA sticks and could clog the injection ports, inhibitors were diluted in BSA-free CAM.

1X β-oxidation medium (BOXM): As in the previous cases, BSA-containing and BSA-free BOXM solutions were prepared.

Table 10 Preparation of stocks of substrates and inhibitors for respiration assays

Stock concentration	Substance	Diluted in	Comments
0.5 M	Succinate	Mili-Q water	pH to 7.2 with KOH
0.5 M	Pyruvic acid	Mili-Q water	pH to 7.2 with KOH
0.5 M	Malic acid	Milli-Q water	pH to 7.2 with KOH
50 mM	palmitoyl-L-carnitine	100% DMSO	-
4 mM	rotenone	100% DMSO	-
20 mM	FCCP	100% DMSO	-
100 mM	ADP	Milli-Q water.	pH to 7.2 with KOH
4 mM	Oligomycin	100% DMSO	-
5 mM	Antimycin A	100% DMSO	-

Muscle dissection, homogenization and mitochondrial isolation.

Materials and buffers were placed on the ice during the whole procedure to protect mitochondria from damage. Three 50 mL beakers per sample were placed on ice and the following solutions were added: beaker 1 (10 mL of PBS), beaker 2 (10 mL of 10 mM EDTA/PBS) and beaker 3 (4 mL of IB1). Mice were euthanized by cervical dislocation. CO_2 euthanasia was avoided since it could interfere with respiration analyses. Next, the hind limbs and the lower half of the body were washed with 70% v/v ethanol. The hind limbs were carefully shaved using a scalpel. An incision was made with the scalpel through the skin as shown in Figure 17. The skin griped with toothed forceps and the underlying musculature eased away. All skeletal muscles from the ankle to the knee from both hindlimbs were dissected as is detailed in Figure 17.

Muscles were rinsed in Beaker 1, and then in Beaker 2. All muscles were transferred to Beaker 3 and finely muscles were minced with sharp scissors. Then, the suspension was transferred to a C Tube (purple lid, gentleMACS), always keeping it on ice. The C tube was tightly closed and attached upside down onto the sleeve of the gentleMACS Dissociator. Muscles were homogenized with the 1-minute program called m_mito_tissue_01. The homogenate was divided into two 2mL pre-chilled microcentrifuge tubes and centrifuged at 700 x g for 10 minutes at 4°C in a tabletop centrifuge to precipitate nuclei, cell debris and extracellular structures. Next, the supernatants were transferred to new 2mL pre-chilled tubes, carefully avoiding fat and non-homogenized tissue. The pellets were kept at -80°C for fragmentation purity determination (fraction N). The supernatants were centrifuged at 10,500 x g for 10 minutes at 4°C to precipitate mitochondria.

The supernatants were transferred to new 2mL pre-chilled tubes and labelled as SN1 (Supernatant Number 1). The pellets were resuspended and combine both in 500µL total of IB2 in ice to wash mitochondria and centrifuged at 10,500 x g for 10 minutes at 4°C. The supernatant was then transferred to a new 2mL pre-chilled tube and labelled as SN2 (Supernatant Numb 2). The final mitochondrial pellet was resuspended in 200µL of RB. Next, 10µL were quickly set aside for protein quantification and 10µL of 10% FFA-BSA w/v was immediately added to the remaining mitochondrial suspension to prevent damage. Protein concentration was determined with the Bradford assay.

Preparation of the Agilent Seahorse XFe24 Analyzer assays

Initially, the sorvall centrifuge was prechilled with the swinging bucket microplate rotor and the corresponding microplate adapters at 4ºC. The appropriate protocol was selected on the Wave software from the Agilent Seahorse XFe24 and the volume of each inhibitor was added in each port, the cartridge was introduced into the Seahorse Analyzer to start calibration. The concentrated mitochondria suspension was centrifuged at 10,500 g for 10 minutes at 4ºC and the mitochondria pellet was resuspended in 100 µL of 1X CAM+BSA or 1X BOXM+BSA, depending on the protocol to be performed. Further, the concentrated mitochondrial sample was diluted to a final concentration of 0.2 µg/µL in the corresponding assay medium. Next, 10 µg of mitochondrial protein was seeded per well (50 µL of 0.2 µg/µL) in a pre-chilled XF24 cell culture microplate placed on ice. In the background correction wells, just the corresponding assay medium was added. The plate was centrifuged at 2,000 g for 20 minutes at 4°C in the previously prechilled sorvall centrifuge and the remaining assay medium was warmed at 37ºC during microplate centrifugation. After centrifugation, the plate was left on the bench for 5 minutes to temper. 450 µL of warm assay medium was added for a final volume of 500 µL per well at RT and the selected assay was conducted.

Table 11 Protocol setting for the respiration assays in isolated mitochondria.

Action	Time (minutes)	Repetition	Port
Calibrate	15-20		
Wait	10		
Mix + Wait	1 + 3	X 2	
Mix	1		
Measure + Mix	3 + 1	X 2	
Inject			A
Mix	1		
Measure	3		
Mix	1		
Inject			B
Mix	1		
Measure	3		
Mix	1		
Inject			C
Mix	1		
Measure	3		
Mix	1		
Inject			D
Mix + Measure	1 + 3	X 2	

Table 12 Injection volumes in Seahorse for respiration assays

Port	Volume injected	Stock prepared (26 wells)
A	50 µl	1300 µl
B	55 µl	1430 µl
C	60 µl	1560 µl
D	65 µl	1690 µl

Table 13 Preparation of Injection solutions for the respiration assays in mitochondria.

Coupling Assay						
Poad	Compound	[Stock]	[Injection Port]	[Final]	Recipe	
					Inhib	CAM-BSA
A	ADP	100 mM	50 mM	5 mM	650 µL	650 µL
B	Oligomycin	4 mM	31.6 µM	3.16 µM	11.3 µL	1418.7 µL
C	FCCP	20 mM	60 µM	6 µM	4.68 µL	1555.32 µL
D	Antimycin A // Rotenone	5 mM // 4 mM	40 µM // 50 µM	4 µM // 5 µM	13.52 µL // 21.12 µL	1655.36 µL
β-Oxidation Assay						
Port	Compound	[Stock]	[Injection Port]	[Final]	Recipe	
					Inhib	BOX-BSA
A	ADP	100 mM	40 mM	4 mM	520 µL	780 µL
B	Oligomycin	4 mM	31.6 µM	3.16 µM	11.3 µL	1418.7 µL
C	FCCP	20 mM	60 µM	6 µM	4.68 µL	1555.32 µL
D	Antimycin A // Rotenone	5 mM // 4 mM	40 µM // 20 µM	4 µM // 2 µM	13.52 µL // 8.45 µL	1668 µL

Interpretation of the results

Performing respiration analysis of isolated mitochondria allows us to study different parameters of mitochondrial respiration:

- Basal respiration rate represents the mitochondrial respiration in the presence of the substrates added to the assay medium. It was calculated by subtracting the values after Antimycin A plus rotenone injection (non-mitochondrial O_2 consumption) from the basal values.
- Mitochondrial State III represents ATP production from ADP and inorganic phosphate. For State III calculation non-mitochondrial O_2 consumption values were subtracted from the values after ADP injection.
- Mitochondrial State IVo indicates the proton leak associated with the inhibition of ATP synthase by oligomycin injection. It was calculated by subtracting the non-mitochondrial O_2 consumption values from the respiration values post oligomycin injection.
- Mitochondrial State IIIu shows the maximal respiratory capacity that mitochondria can display. It was calculated by deducting non-mitochondrial O_2 consumption from respiration post-FCCP injection.
- Respiratory control ratio (RCR) indicates the mitochondrial coupling and it was obtained by division of State IIIu between State IVo values.

3.9 Statistical analysis

Data were expressed as mean ± SD. Data analysis was performed with GraphPad Prism 8.0 software. When a comparison between two groups was performed, an unpaired two-tailed t-test with Welch's correction was used. When more than two groups were studied, a one way (1 parameter studied) or two-way ANOVA (2 or more parameters studied) with Sidak's, Tukey's or Dunnett's multiple comparison *post-hoc* test was applied. P-values <0.05 were considered statistically significant.

4 Results

Chapter 1

4.1 CHAPTER 1: Embryonic development in *Adck2* mouse model.

4.1.1 Introduction

Coenzyme Q deficiencies are characterized by a decrease in CoQ levels associated with a mutation in any gene associated with the CoQ biosynthesis pathway (primary deficiency) or with a mutation in another gene that alters somehow this pathway and secondarily leads to a CoQ decrease (secondary deficiency), which could be related to respiratory chain defects, multiple acyl-CoQ dehydrogenase decrease, ataxia and oculomotor apraxia. Early diagnosis is crucial so that patients with CoQ deficiency can begin CoQ supplementation as soon as possible to reduce damage associated with these syndromes. However, the diagnosis is normally performed when the patients have already suffered damages and consequently, CoQ administration cannot recover these established damages, allowing only a partial recovery or a delay in the progression of the disease.

The main point of the present chapter is to check when the damages associated with a secondary CoQ deficiency start and if they do during embryonic development, to analyse if these alterations are already produced at the time of birth and to determine to what degree the damage has already occurred. This idea is supported by the fact that a decrease in CoQ levels during embryonic development could lead to a delay or an incomplete embryonic development (169) (170). This could give rise to a new scenario for this type of syndromes, which would justify the delay in diagnosis and the severe syndromes that some human patients present shortly after birth.

For that reason, we decided to study biochemically, genetically, and physiologically the embryogenesis and the development of our *Adck2* model to set up when the damages star, what is altered and how the organism is affected. To do that, two specific time points were established along with embryonic development: firstly, one point at early development, nine to ten days post coitum (DPC) depending on the test and the parameters to be analysed in the experiment, and secondly, one point at late development, seventeen DPC. We analysed late development instead of born pups to avoid loss of them during birth.

Moreover, we decided to study if a prenatal CoQ_{10} administration could prevent or reduce damages associated with a deficiency in our model. As epigenetics could play a role in disease progression through transgenerational inheritance (171)(172)(173), and to avoid such alterations could affect the effect of CoQ_{10} administration, we decided to apply CoQ_{10} supplementation during two generations so that progenitors used for the experiments and their offspring were maintained under CoQ_{10} supplementation during the full length of their life. To

our knowledge, this is the first study that analyses the longitudinal effect of CoQ_{10} using prenatal administration to evaluate the potential of CoQ_{10} in mitochondrial diseases.

Gene expression is altered at 9-days of development

Initially, we decided to perform an analysis of the transcriptomic profile at an early stage of development to explore if the mutation on the *ADCK2* gene could be affecting the transcriptomic profile of the mice since embryonic development.

All analysed embryos, both mutant and wild-type 9 DPC embryos, were obtained from the same cross to avoid differences in developmental stages if several crosses were performed, from which RNA and DNA were extracted independently with Trizol reagent. Once they were genotyped correctly, we obtained 5 mutant and 3 wild-type embryos. Then, each RNA was used to synthesize a cDNA probe to hybridise with independent Mouse Clarion D arrays from ThermoFisher. After normalization and statistical analysis, only 29 deregulated genes appeared deregulated significantly (p-value<0.05) more than 2-fold in the mutant (Figure 24A), although some of the genes were non-coding sequences or without a full description. So, to obtain a greater number of genes to be able for making the subsequent analysis to give a biological meaning, we lowered the threshold of detection to 50% and 20% dysregulation of gene expression, and we found that 118 genes were significantly deregulated more than 50% (figure 24B) and that more than 1000 genes appeared deregulated more than 20% (figure 24C).

We only found altered genes with small changes in the gene expression, although a functional enrichment analysis revealed that most of them clustered into Gene Ontologies related to structure and system development (figure 24D), indicating that gene dysregulation affected very specific biological processes even though the changes were very small.

We believe that these small changes in gene expression could be due to we performed the analysis in the whole embryo, thus we studied the whole cell population that would be involved in the development of all tissues in the adult while some tissues in the adult mice did not show damages.

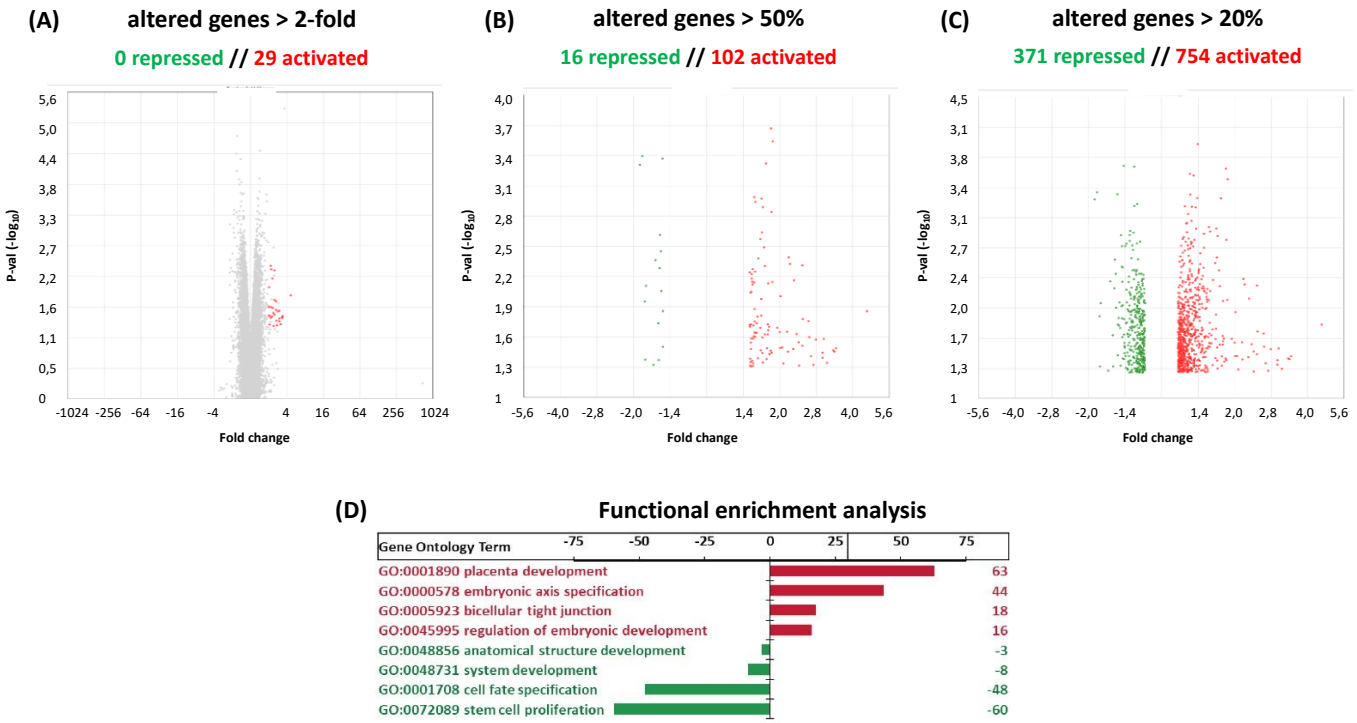

Figure 24. Gene expression analysis during the early development.
Gene expression of 9-DPC embryos was analysed by hybridization with Mouse Clarion D arrays (ThermoFisher). Transcriptome Analysis Console software was used for normalization and statistical analysis. (A, B and C) Volcano plot representing the Fold change versus p-value for each probe present in the array. Significant genes (p-value <0.05) with an altered gene expression higher than 2-fold (A), 50% (B) or 20% (C) are coloured in red if activated, or in green, if repressed. In grey, are coloured the non-significant genes and those significant genes with deregulation lower than the threshold used for the analysis (only represented in A). (D) Functional enrichment analysis performed with GORILLA software clusters the dysregulated genes into Gene ontologies: GO listed in green include repressed genes and those listed in the red group the activated genes.

Somitogenesis is altered in *ADCK2* mice and CoQ_{10} prevents alterations

We had demonstrated that the transcriptomic profile at 9 DPC was slightly affected, finding only small changes in the gene expression although most of the genes belong to Gene Ontologies related to structure and system development.

We think that such small changes in gene expression could be because we perform the analysis in the whole embryo, studying all cell populations involved in the development of all tissues, including tissues in the adult mice that did not show damage. So, we hypothesise that if we would have isolated cells that would develop skeletal muscle in adult mice, we would find more and higher differences. To corroborate this idea, we decided to study the somitogenic process to follow the progression and evolution of muscle progenitor cells.

We crossed our mutant mice with other mice that present an APZ reporter that allows the study and analysis of two MRFs (Myf5 and Mrf4) along with the embryonic development by staining at 10 DPC as has been described previously (147).

Myf5 is one of the four Myogenic Regulatory Factors that control and regulate myogenesis. Particularly Myf5 works as a transcriptional modulator controlling the transcription of genes associated with muscle and regulates muscle differentiation, thus, Myf5 is an essential factor in muscle formation. The dermomyotomal expression in the dorsal and ventral somites of Myf5 revealed aberrant development of some somites (figure 25). Particularly, we found that some embryos showed damage on somite formation that could indicate an alteration in somitogenesis, the process by which germ cells became body cells. We quantified the number of damaged somites, finding that heterozygous mutant embryos present between 1 and 3 damaged somites compared with wild type embryos, which were not damaged (no significant differences). Altered somites were not always the same, but they tend to be in the same region along the anterior-posterior axis. Interestingly, these damages were decreased under the CoQ_{10} administration. We also found that the homozygous mutant was considerably delayed and did not show nuclear staining of Myf5. These results indicate that mutant embryos at this developmental stage present an inadequate somitogenesis process, which is improved when embryos are supplemented prenatally with CoQ_{10}.

Figure 25. Myf5 expression in skeletal muscle progenitors during early embryonic development.
Somites damages were quantified per embryo as an alteration in somite structure. Embryos were collected at 10 DPC and fixed for posterior staining. Myf5 expression was studied by nuclear staining of the somites. CoQ_{10} in nanoparticles was dissolved in the water bottle, mean CoQ_{10} intake was estimated at 1-1.5 mg/day (33.33-50 mg/kg/day). Data represent the mean +/- SD. Unpaired two-tailed t-test and one-way ANOVA test were applied. P-values <0.05 were considered statistically significant.

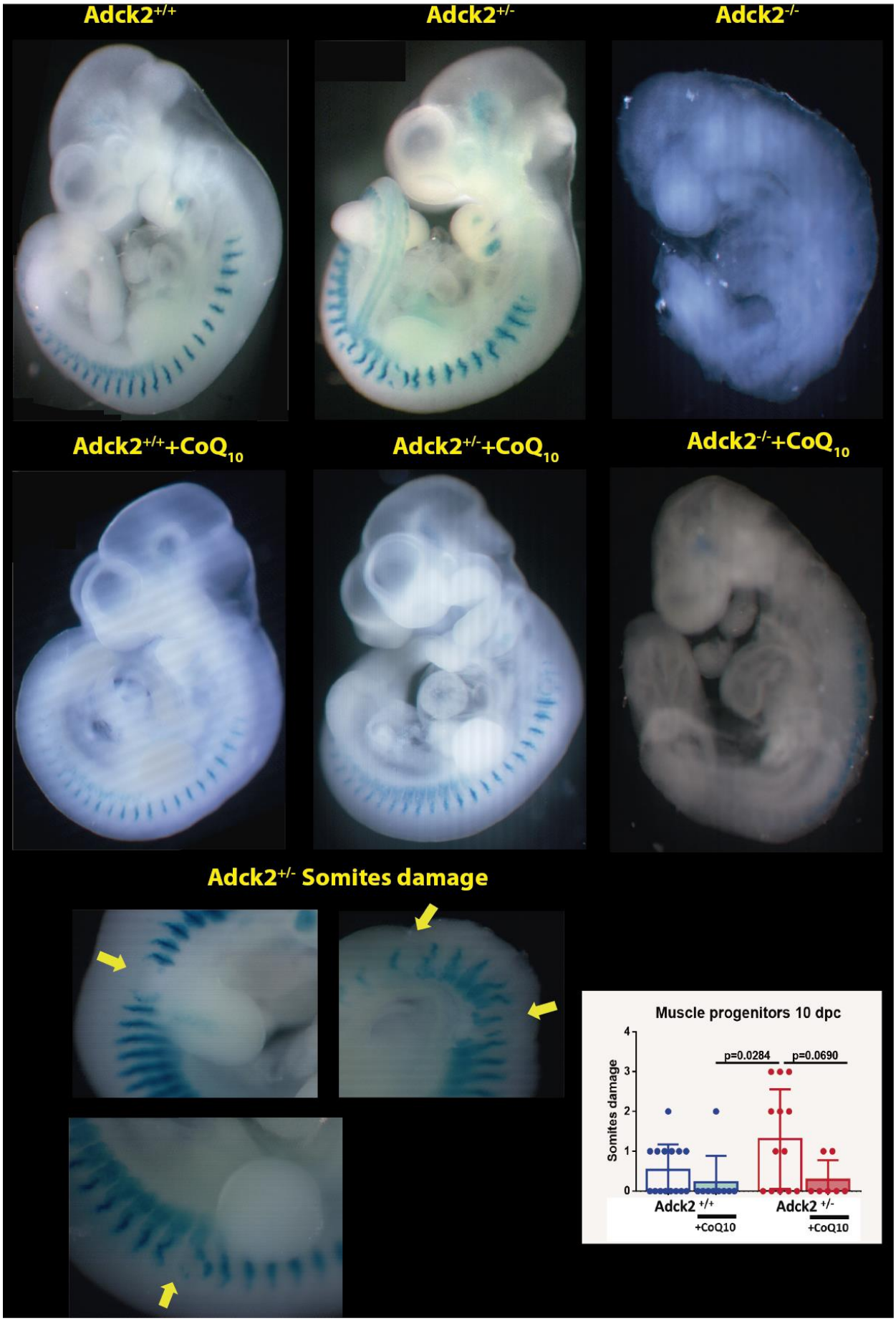
Adck2+/+
Adck2+/-
Adck2-/-
Adck2+/+ +CoQ10
Adck2+/- +CoQ10
Adck2-/- +CoQ10
Adck2+/- Somites damage
Muscle progenitors 10 dpc
Somites damage
p=0.0284
p=0.0690
Adck2 +/+
+CoQ10
Adck2 +/-
+CoQ10

In addition, we also study Mrf4 expression at 10 DPC, by which cytoplasmic staining of muscle progenitor cells can be detected using the reporter BAC195APZ (figure 26). Mrf4 is another transcription factor of the four Myogenic Regulator Factors, and it is a marker involved in muscle differentiation. We found that 10 DPC embryos show an early hypaxial expression plus the ventral and dorsal myotome and again, we found damages in somite structure indicating an alteration in somitogenesis that could lead to aberrant development. We decided to quantify the damages in the somites finding that the mutant embryos on standard conditions presented between 1 and 2 damaged somites compared to the wild type embryos, which did not present damage. *Adck2* knockout embryos supplemented with CoQ_{10} showed a reduction in somites damage. Altered somites were not exactly the same, but they tend to be in the same region.

Taking all these results together, mutant embryos show an incomplete somitogenic process at this developmental stage altering the myotome development from early embryonic development. Whereas when mutant embryos are supplemented prenatally with CoQ_{10}, these embryos show a normal progression of the muscle progenitor cells.

Figure 26. Mrf4 expression in skeletal muscle progenitors during early embryonic development
Somites damages quantified per embryo as an alteration in somite structure. Embryos were collected at 10 DPC and fixed for posterior staining. Mrf4 expression was studied by cytoplasmatic staining of the somites. CoQ_{10} in nanoparticles was dissolved in the water bottle, mean CoQ_{10} intake was estimated at 1-1.5 mg/day (33.33-50 mg/kg/day). Data represent the mean +/- SD. Unpaired two-tailed t-test and one-way ANOVA test were applied. P-values <0.05 were considered statistically significant.

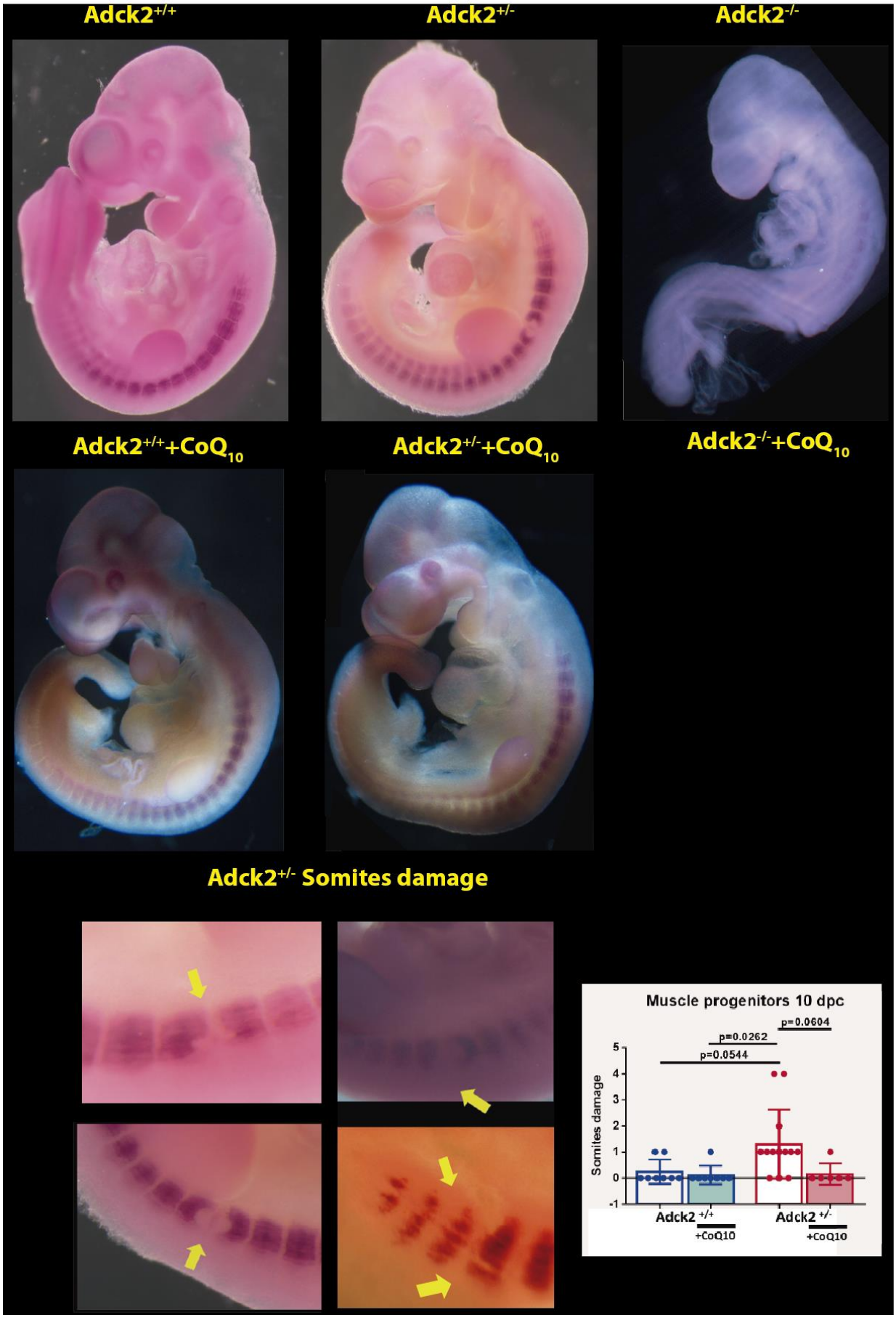
Adck2+/+
Adck2+/-
Adck2-/-
Adck2+/++CoQ10
Adck2+/-+CoQ10
Adck2-/-+CoQ10
Adck2+/- Somites damage
Muscle progenitors 10 dpc
p=0.0604
p=0.0262
p=0.0544
Somites damage
5
4
3
2
1
0
-1
Adck2 +/+
+CoQ10
Adck2 +/-
+CoQ10

Alteration of gene expression becomes tissue-specific as the development progresses

The results obtained lead us to analyse the transcriptomic profile in the later developmental stage to set up the alteration degree on gene expression and the disease progression. So, we decided to analyse these parameters at 17 DPC, and not in newborn pups to avoid loss of offspring during birth.

Because the development is very advanced at 17 DPC and the organs are already formed, we decided to perform the study in skeletal muscle, liver and brain due to the main tissue affected in the adult mice is the skeletal muscle, the liver suffers metabolic mild damages and mice did not suffer any damages in the brain (147).

First, we studied the transcriptomic profile in the skeletal muscle of embryos (Figure 27A) where we observed that there was a significant (p-value < 0.05) huge gene deregulation with 814 genes repressed more than 2-fold and 384 genes activated more than 2-fold. Then, we performed a functional enrichment analysis with these genes finding a correlation between the Gene Ontologies and the mutant phenotype (figure 27B). Activated genes were clustered into genes ontologies related to the control of myogenesis control and oxygen transport, whereas repressed genes were associated with structural components in the skeletal muscle such as "cell-cell adhesion" or "keratin filament", also, gene ontologies related to metabolic processes and fatty acids metabolism were repressed including "fatty acid biosynthetic process" or "fatty-acyl-CoA metabolic process". In general, we could mention that the transcriptomic profile represents changes that could indicate a bioenergetic alteration and deregulation of myogenesis management and, that these alterations could potentially be affecting prenatal myogenesis, which in turn would subsequently affect primary and secondary skeletal muscle formation.

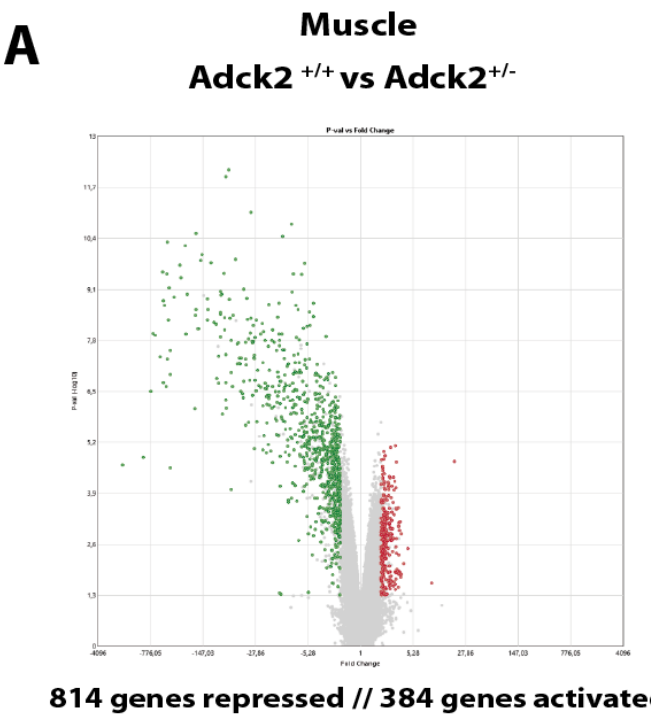

Figure 27. Gene expression in skeletal muscle during late embryonic development.

Gene expression of skeletal muscle in 17-DPC embryos was analysed by hybridization with Mouse Clarion D arrays (ThermoFisher). Transcriptome Analysis Console software was used for normalization and statistical analysis. (A) Volcano plot representing the Fold change versus p-value for each probe present in the array. Significant genes (p-value <0.05) with an altered gene expression higher than 2-fold are coloured in red if activated, or in green if repressed. In grey, are coloured the non-significant genes and those significant genes with deregulation lower than the threshold used for the analysis. (B) Functional enrichment analysis performed with GORILLA software clusters the deregulated genes into Gene ontologies: GO listed in green include repressed genes and those listed in the red group contain activated genes.

Transcriptomic profile in the brain showed an alteration in a very small number of genes (Figure 28A). 16 genes were repressed significantly (p-value <0.05) more than 2-fold and only 8 genes appeared activated, with these genes any Gene Ontology appeared deregulated after clustering the deregulated genes in the Functional Enrichment analysis. The lack of alterations found in the brain highlight the idea that modifications could be tissue-specific, some tissues would be affected, and other tissues would not. Additionally, it would be necessary to highlight that no neurological damage has been reported in adult mutant mice (147).

The transcriptomic profile on the liver showed eighty-seven genes repressed and twenty-three genes activated (Figure 28B). Gene ontologies deregulation analysis reveals that there was an activation of gene ontologies associated with enzyme activities, cell cycle, or development. However, gene ontologies repressed showed an important suppression of gene ontologies related to fatty acids, cholesterol triglyceride process, or lipid transport such as “fatty acid metabolic process”, “cholesterol metabolic process” or “plasma lipoprotein particle assembly”, but we also found gene ontologies from other pathways repressed including “urea cycle”, “tyrosine metabolic process” or “L-phenylalanine catabolic process” meaning that the repression found in the liver could be also affecting other metabolic pathways (Figure 28C). In general, the deregulation that the liver shows on gene expression was related to metabolic processes and pathways. As skeletal muscle and liver share multiple pathways and are closely connected, it could be proposed that changes found in liver gene expression could be derived from the deep deregulation that suffers the skeletal muscle, as a consequence of the important changes that occurred in skeletal muscle.

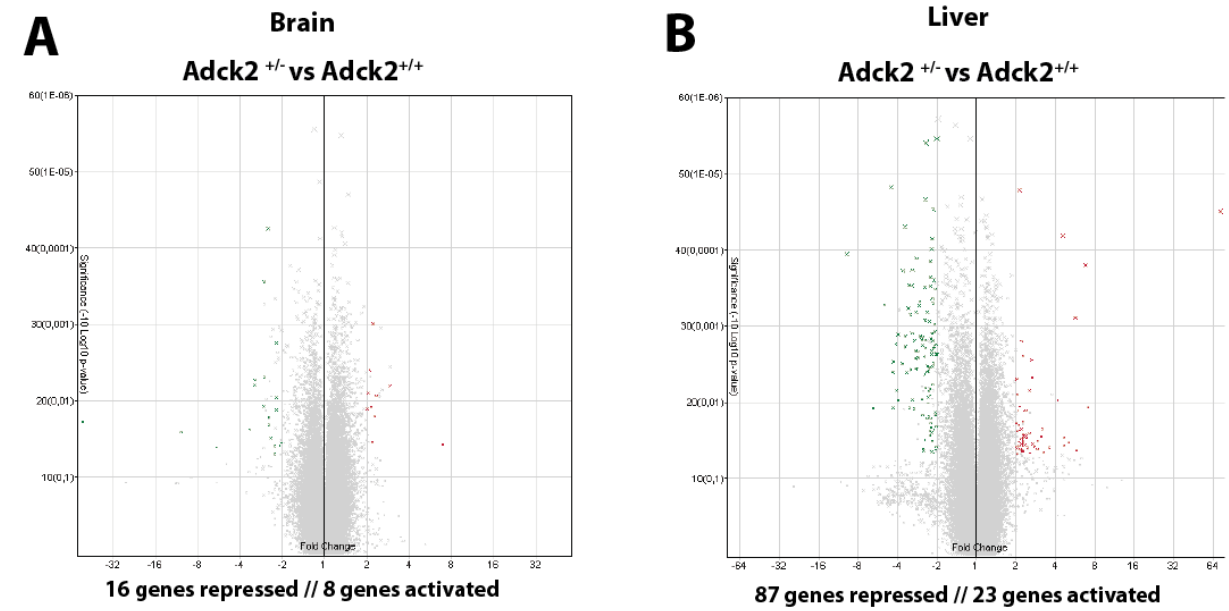

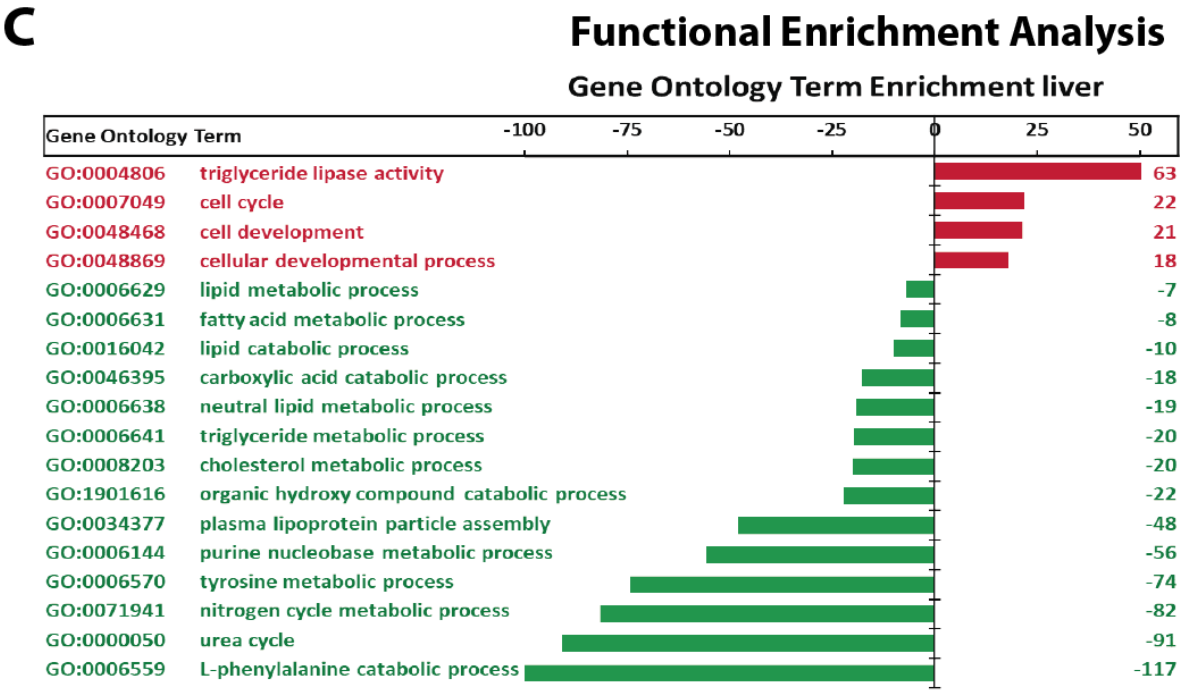

Figure 28. Gene expression in liver and brain during late embryonic development.

Gene expression in the brain and liver of 17-DPCdpc embryos was analysed by hybridization with Mouse Clarion D arrays (ThermoFisher). Transcriptome Analysis Console software was used for normalization and statistical analysis. (A and B) Volcano plot representing the Fold change versus p-value for each probe present in the array. Significant genes (p-value <0.05) with an altered gene expression higher than 2-fold (A and B) are coloured in red if activated, or in green, if repressed. In grey, are coloured the non-significant genes and those significant genes with deregulation lower than the threshold used for the analysis. (C) Functional enrichment analysis performed with GORILLA software clusters the dysregulated genes into Gene ontologies: GO listed in green include repressed genes and those listed in the red group the activated genes.

CoQ_{10} administration modulates skeletal muscle transcriptomic profile of 17-DPC embryos

As the main tissue affected was the skeletal muscle, we decided to study more deeply the transcriptomic profile of skeletal muscle at seventeen DPC. First, we analysed the effect of CoQ_{10} treatment on the transcriptomic profile of mutant embryos. We found that 412 genes were repressed while 865 were activated more than 2-fold significantly (p-value). Considering the previous analysis reported (wild type versus mutant), we could say that CoQ_{10} administration can activate a lot of genes that previously were repressed (including GO collagen-containing extracellular matrix or GO fatty acids metabolic process) while also could be modulating genes that previously shown a neutral status (such as GO brown fat cell differentiation or GO cell differentiation). After that, we decided to analyse the transcriptomic profile of mutant embryos supplemented with CoQ_{10} versus wild type embryos to examine the recovery grade of the genic expression in mutant embryos after CoQ_{10} administration. We found 625 repressed genes and 629 activated, indicating that CoQ_{10} administration led to the activation of a lot of genes in mutant embryos, although some of the genes that were previously repressed are still downregulated.

The modulation of GO by CoQ_{10} administration was also quantified in the Functional Enrichment Analysis (figure 29) where can be observed the recovery of gene expression by CoQ_{10} supplementation in the GO that initially was deregulated and now show a no deregulate status. Some GO showed that CoQ_{10} administration recovers gene expression to wild type levels such as in “collagen-containing extracellular matrix”. In other Gene Ontologies, we found an increase in gene expression without reaching the wild type levels, such as the “intermediate filament-based process”. More significantly, some Gene Ontologies that were not deregulated in mutant embryos are now modulated by CoQ_{10} administration such as “brown fat cell differentiation” or “cell differentiation”. These facts indicated that CoQ_{10} prenatal administration could be recovering wild type gene expression and regulating new pathways to compensate for the *ADCK2* phenotype.

The transcriptomic profile of wild type embryos supplemented with CoQ_{10} was also studied to examine the effect of CoQ_{10} over a no deregulate transcriptomic profile, the pathways that were specifically modulated by CoQ_{10} independently of the genotype and the effect of *ADCK2* mutation over the CoQ_{10} administration.

Interestingly, the comparison of wild type embryos versus wild type embryos plus CoQ_{10} revealed important changes in gene expression where nine hundred thirty-three genes were repressed and six hundred seventy-one were activated, highlighting the idea that CoQ_{10}

administration during embryonic development can modulate gene expression. Finally, we also compared wild type mice supplemented with CoQ_{10} versus mutant embryos plus CoQ_{10} to check if CoQ_{10} was able to modulate gene expression specifically in a function of the genotype of the embryos. We observed that one hundred twenty-nine genes were upregulated while five hundred eleven were down-regulated indicating that CoQ_{10} administration regulates gene expression differently in mutant and wild type embryos that independently regulation could explain some specific changes in the phenotype of the embryos or mice associated with CoQ_{10} administration that only occurred in mutant or wild type mice.

We also performed an intergroup comparison of gene ontologies to check the effect of CoQ_{10} administration on the different groups representing the number of the genes from the GOs that were modulated and the enrichment. Particularly some gene ontologies such as “collagen-containing extracellular matrix” or “fatty acid metabolic process” that initially were repressed in mutant embryos versus wild type embryos while when CoQ_{10} is administrated we can observe that there is an upregulation in gene ontologies in mutant embryos supplemented with CoQ_{10}. However, we found that other gene ontologies that previously were repressed in the mutant embryo, such as the “intermediate filament-based process”, were lightly activated when CoQ_{10} was administrated, although this gene activation was not enough to reach the wild type expression levels and consequently, the gene ontology remains repressed when it was compared to wild type embryos. More importantly, some gene ontologies that previously were not deregulated, such as “brown fat cell differentiation” or “cell differentiation” are now modulated by CoQ_{10} administration. These new regulations on GO could indicate that CoQ_{10} intake could be working two ways, on the one hand, it can restore wild type expression in the gene ontologies that previously were deregulated, but what is more significant is that CoQ_{10} administration could modulate other pathways that are independently regulated by CoQ_{10}.

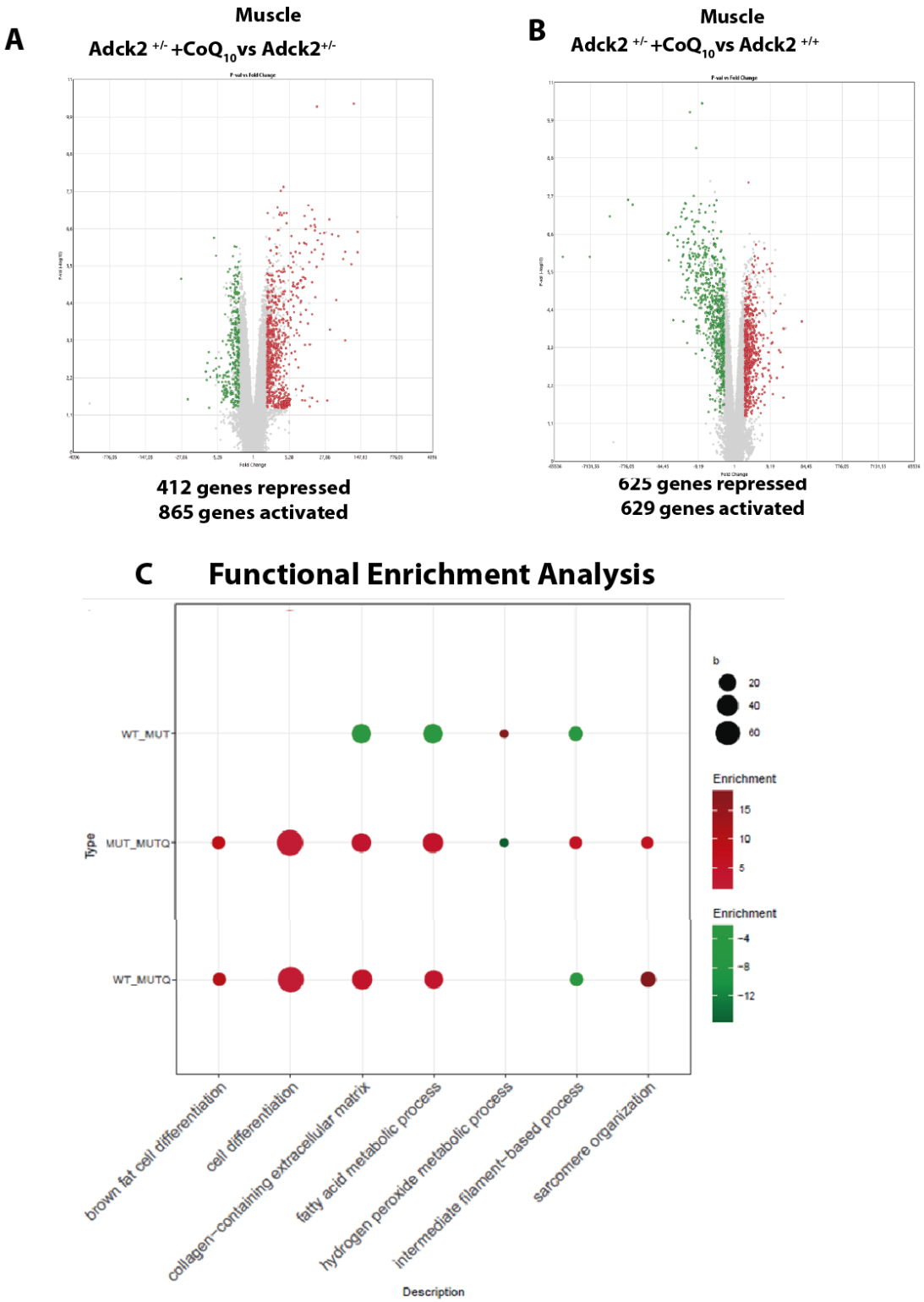

Figure 29. Gene expression in muscle under CoQ_{10} administration during late embryonic development.

The figure above represents the transcriptomic profile of skeletal muscle from wild type embryos and mutant embryos under standard conditions and supplemented prenatally with CoQ_{10} where we have done different comparative analyses between the groups studied. Gene expression in skeletal muscle of 17-DPC embryos was analysed by hybridization with Mouse Clarion D arrays (ThermoFisher). Transcriptome Analysis Console software was used for normalization and statistical analysis. (A and B) Volcano plot representing the Fold change versus p-value for each probe present in the array. Significant genes (p-value <0.05) with an altered gene expression higher than 2-fold (A and B) are coloured in red if activated, or in green, if repressed. In grey, are coloured the non-significant genes and those significant genes with deregulation lower than the threshold used for the analysis. (C) Functional enrichment

analysis performed with R software clusters the dysregulated genes into Gene ontologies: GO listed in green include repressed genes and those listed in red grouped the activated genes.

Later, we performed another functional enrichment analysis to determine the metabolic and signalling pathways that were altered in the skeletal muscle of 17 DPC embryos and that could be modulated by CoQ_{10} treatment (Figure 30). The analyses compared mutant versus wild type (in black), mutant versus mutant supplemented with CoQ_{10} (in orange), and mutant supplemented with CoQ_{10} versus wild type (in yellow). Mutant embryos showed repression of metabolic pathways associated with mitochondrial metabolism such as "Fatty acid biosynthesis", "Fatty acid transporters" and "Fatty acyl-CoA biosynthesis", as well as repression in metabolic pathways related to oxidative stress and redox capacity. In contrast, mutant embryos supplemented with CoQ_{10} showed a general upregulation in the metabolic pathways that previously were repressed, and specific activation of pathways highly associated with mitochondria, such as "TCA cycle", "Electron transport chain" o "NAD metabolism, sirtuins and ageing", suggesting that CoQ_{10} administration could be activating mitochondria pathways.

However, when mutant embryos plus CoQ_{10} are compared with wild type embryos, we observed an upregulation of different metabolic pathways that were not so clear as in the previous comparison, suggesting that CoQ_{10} was able to at least partially reverse gene expression in most of the metabolic pathways. Moreover, CoQ_{10} could exert its function by activating the mitochondria, since we found an activation of "Mitochondrial biogenesis", "Assembly of mitochondrial Complexes I and IV", "ETC", both "TCA and Urea cycles" and "the metabolism of amino acids and glycogen". Also, the "NAD metabolism, sirtuins and ageing" was highly activated.

This analysis confirmed that mutant embryos presented repression in pathways associated with mitochondria, energetic metabolism, and oxidative stress. Besides, mutant embryos prenatally supplemented with CoQ_{10} activated these pathways and others associated with mitochondria.

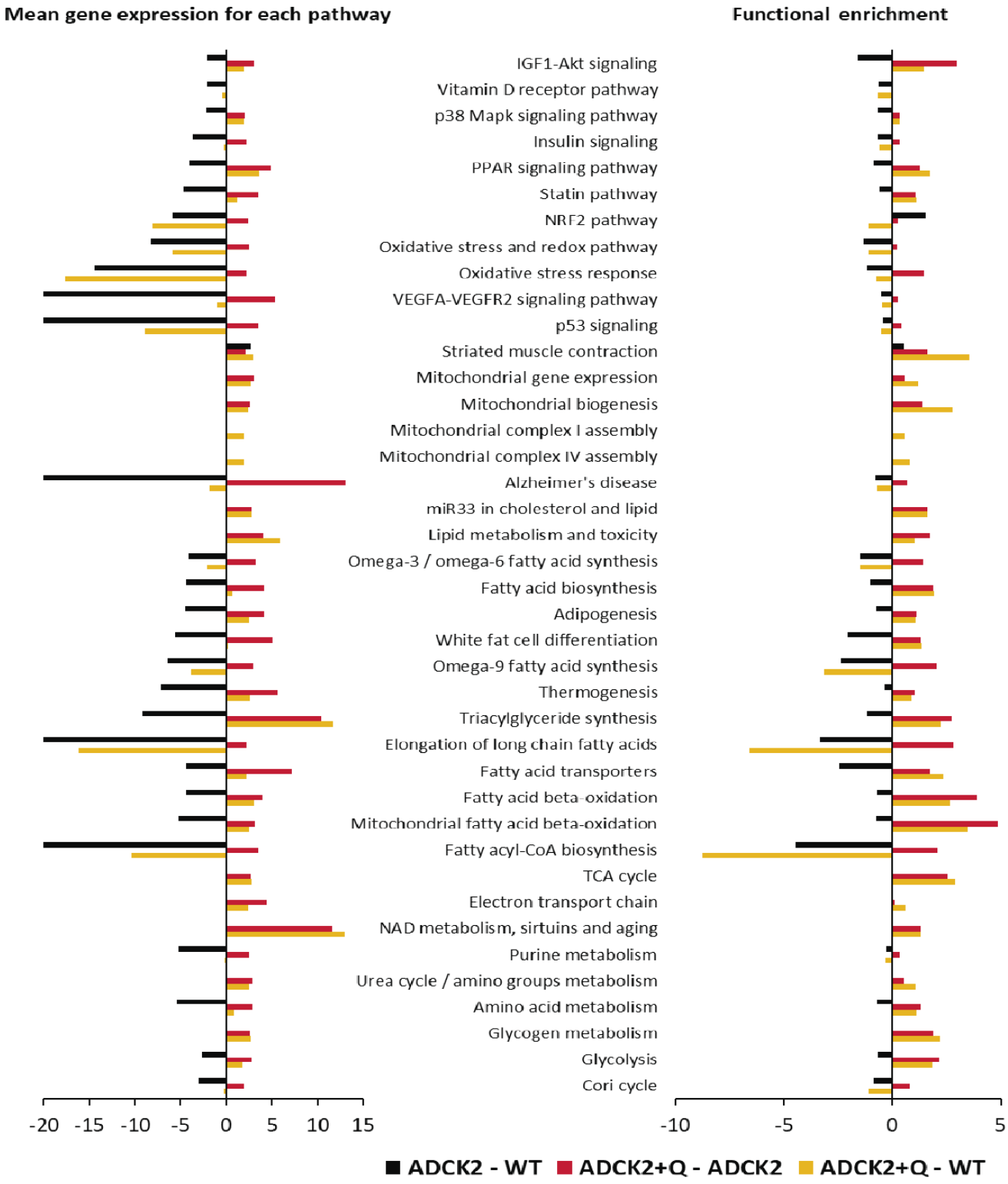

Figure 30. Functional enrichment analysis of signalling and metabolic from skeletal muscle of embryos at 17 DPC.
Analysis of mean gene expression and the enrichment of different metabolic pathways in skeletal muscle from *Adck2*$^{+/+}$, *Adck2*$^{+/-}$ and *Adck2*$^{+/-}$ +CoQ. Analysis was performed using gene expression obtained in the microarray experiments to assess the potential effect of CoQ administration.

To understand the mechanisms that drive the altered gene expression to be muscle and mitochondria specific in the mutant embryo, we analysed the sequence of the promoter regions of each regulated gene using the HOMER Motif Analysis to find the regulatory elements that could play a role in this specific modulation of the gene expression (Figure 31) and the RNA silencing by which gene expression is negatively regulated by non-coding RNAs (Figure 32).

First, we analysed the promoter regions of deregulated genes in mutant embryos compared with wild type (Figure 31A) and we obtained that they were enriched in transcription factors related to metabolisms such as VDR, Nr5a2 or Sf1 and in transcription factors that modulate myogenesis such as Pax7, Myf5, MyoD, ZBTB18, Hand2, Pitx1. Particularly, Nr5a2 regulates the expression of cholesterol homeostasis and triglyceride synthesis. Pax7 modulates muscle stem cells, myogenesis, and muscle regeneration. Myf5 and MyoD are two of the four Myogenic Regulatory Factors that control myogenesis and skeletal muscle formation. Next, we analysed the activated genes separately from the repressed genes. Promoter regions of repressed genes were enriched in metabolic modulators, such as MaFA and Bach2, and regulators of myogenesis, including MyoG. MaFA is related to insulin expression, while MyoG is another Myogenic Regulatory Factor crucial for embryonic skeletal muscle formation and muscle cell differentiation, which is also involved in atrophy in denervated muscle. Additionally, the promoter region of upregulated genes was enriched in transcription factors associated with myogenesis such as MyoD, Mef2c, Mef2a and MyF5. Mef2c controls myogenesis and regulatory regions of muscle genes, Mef2a is related to muscle growth and Myf5 and MyoD control myogenesis and skeletal muscle cell differentiation. Promoter regions of deregulated genes in mutant embryos supplemented with CoQ_{10} compared to mutant embryos without treatment were enriched in myogenesis modulators, such as Mef2c or Mef2d, and in embryonic regulators, including Pitx1 or KLF14 (Figure 31B). Pitx1 is related to the development of the hindlimb while Mef2c and Mef2d participated in muscle growth. Also, we analysed the activated genes separately from the repressed ones, finding that only upregulated genes shared promoter regions were enriched in Mef2d, Mef2c and Nr5a2. Nr5a2 is a nuclear receptor that acts as a key metabolic sensor by regulating the expression of genes involved in lipid metabolism.

In summary, we found that promoters regions of deregulated genes were generally enriched in transcription factors associated with metabolism and more importantly in myogenesis and skeletal muscle formation supporting our previous results that indicate that mutant embryos suffer alteration in prenatal myogenesis that lead to an incomplete skeletal muscle formation. These changes in regulatory elements could explain the alterations found in gene expression and the effect of CoQ_{10} administration.

A

Comparison skeletal muscle embryo Adck2$^{+/-}$ versus Adck2$^{+/+}$ (UP and DOWN):

Motif	Name	P-value	log P-pvalue	q-value (Benjamini)	# Target Sequences with Motif	% of Targets Sequences with Motif	# Background Sequences with Motif	% of Background Sequences with Motif
	ZBTB18	1e-5	-1.270e+01	0.0002	7299	34	2984	31
	Pax7	1e-4	-9.221e+00	0.0024	1619	7	605	6
	VDR	1e-3	-8.291e+00	0.0042	3336	15	1332	14
	Nr5a2	1e-3	-8.180e+00	0.0044	9757	45	4121	43
	SF1	1e-2	-6.579e+00	0.0146	6537	30	2735	28
	Pitx1	1e-2	-5.505e+00	0.0338	21022	98	9275	98
	Myf5	1e-2	-5.465e+00	0.0338	9473	44	4043	42
	RXR	1e-2	-5.246e+00	0.0391	13677	64	5914	62
	MyoD	1e-2	-4.772e+00	0.0522	10353	48	4447	47

Comparison skeletal muscle embryo Adck2$^{+/-}$ versus Adck2$^{+/+}$ (DOWN):

Motif	Name	P-value	log P-pvalue	q-value (Benjamini)	# Target Sequences with Motif	% of Targets Sequences with Motif	# Background Sequences with Motif	% of Background Sequences with Motif
	MafA	1e-3	-7.031e+00	0.0179	476	56	14874	50
	Bach2	1e-2	-6.290e+00	0.0270	135	16	3646	12
	MyoG	1e-2	-4.784e+00	0.0895	568	67	18484	63

Comparison skeletal muscle embryo Adck2$^{+/-}$ versus Adck2$^{+/+}$ (UP):

Motif	Name	P-value	log P-pvalue	q-value (Benjamini)	# Target Sequences with Motif	% of Targets Sequences with Motif	# Background Sequences with Motif	% of Background Sequences with Motif
	MyoD	1e-3	-7.396e+00	0.1287	156	61.42	15432	51
	Mef2c	1e-2	-6.849e+00	0.1287	93	36	8320	27
	Mef2a	1e-2	-4.969e+00	0.1807	89	35	8387	27
	Myf5	1e-2	-4.691e+00	0.2221	137	53	13992	46

B

Comparison skeletal muscle embryo Adck2$^{+/-}$ +CoQ$_{10}$ versus Adck2$^{+/-}$ (UP and DOWN):

Motif	Name	P-value	log P-pvalue	q-value (Benjamini)	# Target Sequences with Motif	% of Targets Sequences with Motif	# Background Sequences with Motif	% of Background Sequences with Motif
	Pitx1	1e-3	-7.028e+00	0.1614	1349	99	28851	98
	Mef2c	1e-2	-6.165e+00	0.2550	439	32	8404	28
	Mef2d	1e-2	-5.894e+00	0.2550	209	15	3730	12
	KLF14	1e-2	-5.559e+00	0.2550	1209	89	25379	86

Comparison skeletal muscle embryo Adck2$^{+/-}$ +CoQ$_{10}$ versus Adck2$^{+/-}$ (UP):

Motif	Name	P-value	log P-pvalue	q-value (Benjamini)	# Target Sequences with Motif	% of Targets Sequences with Motif	# Background Sequences with Motif	% of Background Sequences with Motif
	Mef2d	1e-3	-8.029e+00	0.0395	137	17	3777	12
	Mef2c	1e-3	-7.045e+00	0.0481	271	33	8449	28
	Nr5a2	1e-2	-6.158e+00	0.0732	418	52	13874	46

Figure 31. Analysis of regulatory elements enriched on promoter regions of deregulated genes.

(A). *Adck2$^{+/+}$* versus *Adck2$^{+/-}$*. (B). *Adck2$^{+/-}$* versus *Adck2$^{+/-}$* +CoQ$_{10}$ analysis. Analysis of the promoter regions was performed with the gene expression levels from the microarray experiment in skeletal muscle from embryos at 17 DPC. HOMER Motif Analysis software was used for promoter regions analysis in the deregulated genes. More significant transcription factors found are shown.

On the other hand, we found activation of a lot of small RNAs and microRNAs in mutant embryos, which could be associated with the general gene repression that is shown in the skeletal muscle of mutant embryos (Figure 32A). However, mutant embryos under CoQ_{10} administration exhibited repression of these small RNAs and microRNAs, which was accompanied by an activation of the coding genes. These findings suggest the idea that the gene repression found in mutant embryos depends at least on the action of small RNAs and microRNAs, while CoQ_{10} could be modulating gene expression through small RNAs and microRNAs repression.

RNA silencing refers to a family of gene silencing effects by which gene expression is negatively regulated by non-coding RNAs. The mechanism by which RNA interferes with gene expression is highly conserved in most eukaryotes and implies an endogenously expressed microRNA (miRNA) that induces the degradation of messenger RNA with a complementary sequence. So that, to quantify the implication of this mechanism in the modulation of gene expression we looked for the putative miRNA that could modulate the repressed genes based on the sequence that could be interfered with. Next, we performed the same search for the putative miRNA that could regulate the activated genes. To continue, we clustered each miRNA with its putative genes and compared the expression level of each miRNA with the mean gene expression of their corresponding target genes (Figure 32B). These analyses were performed with the regulated genes in mutant embryos compared to wild type, with the modulated genes by CoQ_{10} in the mutant embryo, and with the regulated genes in mutant embryos treated with CoQ_{10} compared to wild type. We can observe that mutant embryos presented a group of microRNAs active such as mir125b, mirlet7c, mirlet7f, mir143, mir146b, mir15a, mir532, mir674 and mir3079, whereas their target genes were repressed. Interestingly, CoQ_{10} administration induced repression of these microRNAs that lead to the activation of their target genes, reaching wild type expression levels in some cases. These analyses present a potential way by which CoQ_{10} administration could be modulating gene expression during embryogenesis, skeletal muscle formation, and contributing to the amelioration of the phenotype in mutant mice.

A

muscle(ADCK2) vs muscle(WT)				
Group	Total	Passed Filter	Up-Regulated	Down-Regulated
Coding	11264	447	54	393
Multiple_Complex	15332	435	33	402
Small_RNA	2728	283	280	3
Precursor_microRNA	1729	17	13	4
Ribosomal	388	1	1	0
Pseudogene	2758	0	0	0
NonCoding	31717	0	0	0
Unassigned	24	0	0	0
tRNA	16	0	0	0

muscle(ADCK2)+CoQ_{10} vs muscle(ADCK2)				
Group	Total	Passed Filter	Up-Regulated	Down-Regulated
Coding	11264	597	529	68
Multiple_Complex	15332	346	286	60
Small_RNA	2728	267	18	249
Precursor_microRNA	1729	35	9	26
Ribosomal	388	7	1	6
tRNA	16	5	5	0
Pseudogene	2758	0	0	0
NonCoding	31717	0	0	0
Unassigned	24	0	0	0

B

Figure 32. Analysis of miRNAs.

(A) Gene expression analysis of skeletal muscle of embryos at 17 DPC data obtained from the microarray experiments in skeletal muscle from embryos at 17 DPC. (B) miRNAs regulation by *Adck2* mutation and by CoQ_{10} obtained from the microarray experiment. Figure 32B shows the association between microRNAs and the expression of the target genes expression in skeletal muscle of 17 DPC wild type embryos versus mutant embryos in blue, mutant embryos versus mutant embryos supplemented with CoQ_{10} in orange and wild type embryos versus mutant embryos plus CoQ_{10} in grey.

Finally, we analysed the transcriptomic profile of wild type embryos prenatally supplemented with CoQ_{10} (Figure 33). CoQ_{10} administration modulates specifically some GO in wild type embryos producing the activation of the same GO previously altered in mutant embryos under the treatment, such as “cell differentiation”, while others were repressed like “intermediate filament-based process”.

Interestingly, the analysis of mutant embryos supplemented with CoQ_{10} compared to wild type under the same treatment revealed a wide gene activation in terms of several activated genes and the degree of their activation compared to the repressed genes. This result could indicate that some of the gene modulation displayed by CoQ_{10} supplementation could be specific to the genotype of the embryos.

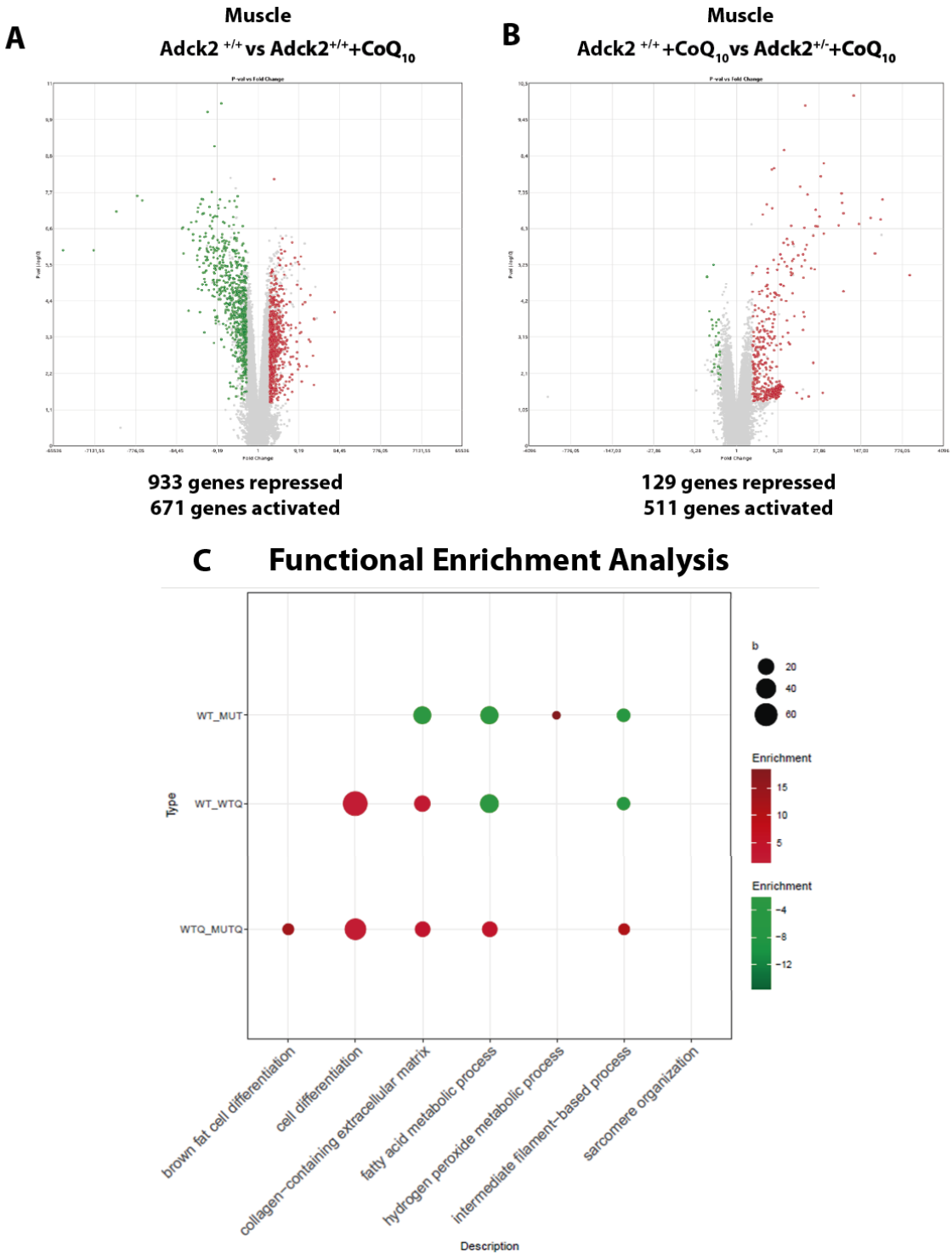

Figure 33 Gene expression in muscle from wild type embryos under CoQ_{10} administration during late embryonic development.

The figure above represents the transcriptomic profile of skeletal muscle from wild type embryos and mutant embryos under standard conditions and supplemented prenatally with CoQ_{10} where we have done different comparative analyses between the groups studied. Gene expression in skeletal muscle of 17-DPC embryos was analysed by hybridization with Mouse Clarion D arrays (ThermoFisher). Transcriptome Analysis Console software was used for normalization and statistical analysis. (A and B) Volcano plot representing the Fold change versus p-value for each probe present in the array. Significant genes (p-value <0.05) with an altered gene expression higher than 2-fold (A and B) are coloured in red if activated, or in green, if repressed. In grey, are coloured the non-significant genes and those significant genes with deregulation lower than the threshold used for the analysis. (C) Functional enrichment analysis performed with R software clusters the dysregulated genes into Gene ontologies: GO listed in green include repressed genes and those listed in the red group the activated genes.

Embryo's development status of embryos at 17 DPC

Finally, we performed a descriptive analysis of embryos through development. The visual aspect of mutant embryos at 17 DPC on standard conditions showed several alterations (Figure 34A), most of them related to the size, although they were also related to structural parts of the head, like the eye. All these alterations were more pronounced in the homozygotic mutant, indicating that development was more altered or highly delayed. In contrast, mutant mice on CoQ_{10} administration did not show these pronounced alterations, although some of them seemed to be also smaller than wild type embryos. Therefore, it seems that CoQ_{10} could be reversing the alterations previously found during embryonic development.

To evaluate these changes during embryonic development, the embryos were weighed and measured (Figure 34B). Weight analyses revealed that mutant embryos under standard conditions had a lower weight compared with wild type embryos whereas mutant embryos under CoQ_{10} administration tended to have a higher weight. Heterozygotic and homozygotic mutant embryos on standard conditions were smaller than wild type embryos while again mutant embryos with CoQ_{10} supplementation tended to be bigger. Consequently, we can propose that mutant embryos are smaller than wild type while prenatal CoQ_{10} administration tends to normalize the size and weight. We also analysed tibia length because it has been reported to be a marker of body development (Figure 34C). Mutant embryos tended to have a lower tibia length while mutant embryos under CoQ_{10} treatment normalized the tibia length by the rest of our results.

Interestingly, we did not find differences in the tibia length in young mice after birth, although old mice under treatment showed longer tibia in both genotypes, wild type and mutant (Figure 34D). This increase could be a consequence of the activation of gene expression related to growth and differentiation, which is accentuated more with age.

A

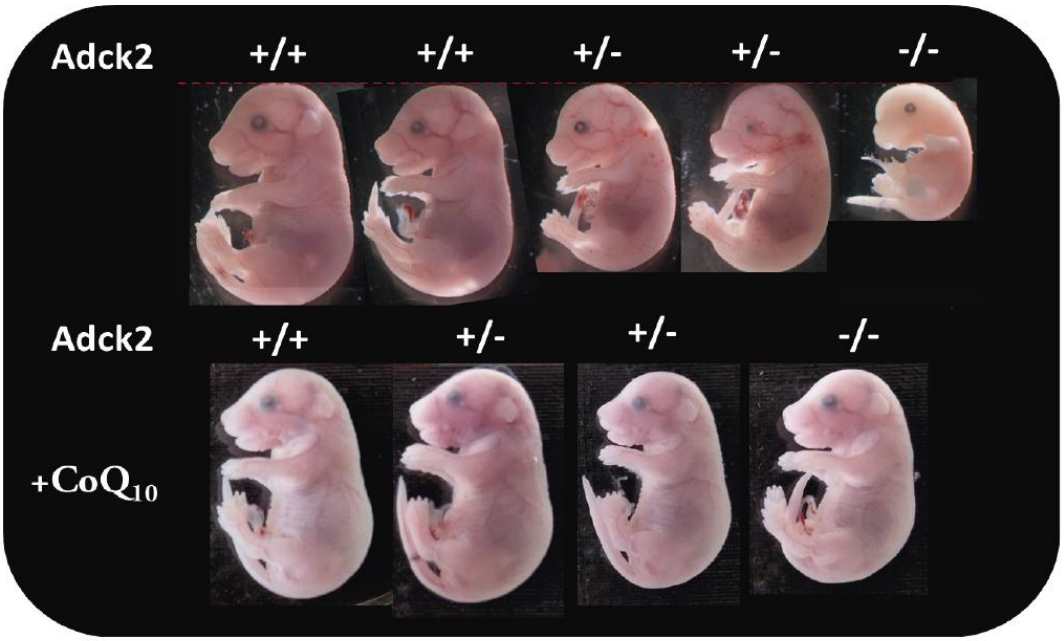
Adck2
+/+
+/+
+/-
+/-
-/-
Adck2
+/+
+/-
+/-
-/-
+CoQ10

B

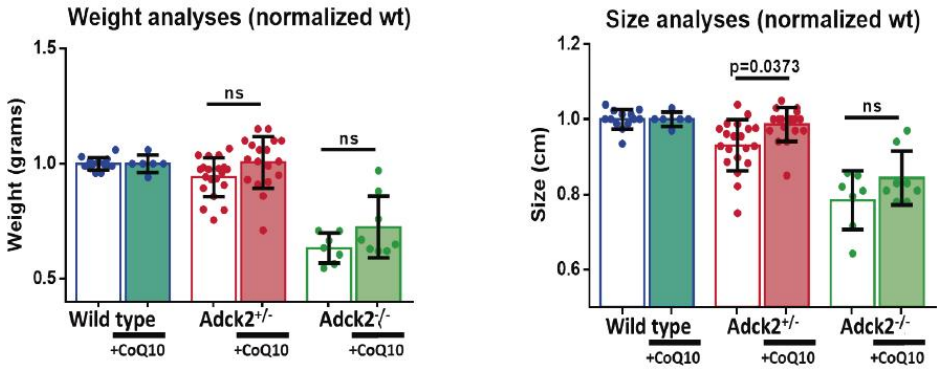
Weight analyses (normalized wt)
Weight (grams)
1.5
1.0
0.5
ns
ns
Wild type
Adck2+/-
Adck2-/-
+CoQ10
+CoQ10
+CoQ10
Size analyses (normalized wt)
Size (cm)
1.2
1.0
0.8
0.6
p=0.0373
ns
ns
Wild type
Adck2+/-
Adck2-/-
+CoQ10
+CoQ10
+CoQ10

C

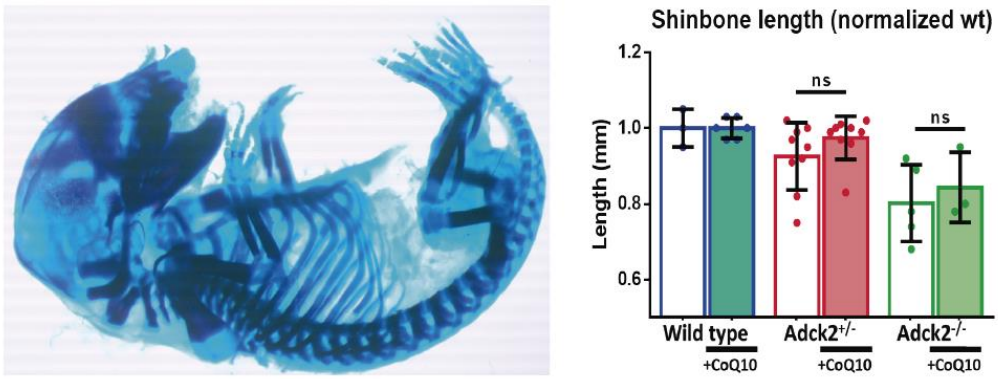
Shinbone length (normalized wt)
Length (mm)
1.2
1.0
0.8
0.6
ns
ns
Wild type
Adck2+/-
Adck2-/-
+CoQ10
+CoQ10
+CoQ10

D

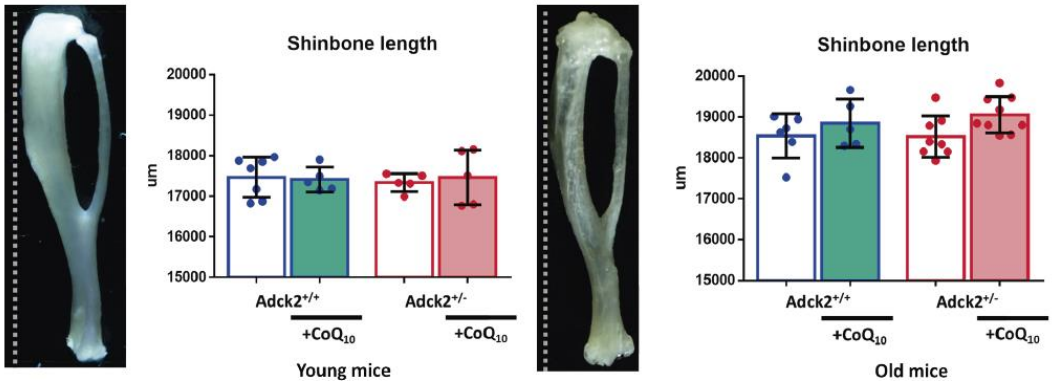
Shinbone length
um
20000
19000
18000
17000
16000
15000
Adck2+/+
Adck2+/-
+CoQ10
+CoQ10
Young mice
Shinbone length
um
20000
19000
18000
17000
16000
15000
Adck2+/+
Adck2+/-
+CoQ10
+CoQ10
Old mice

Figure 34. Analysis of late embryonic development.
(A) General aspect of embryos at 17 DPC including wild type, heterozygotic and homozygotic mutant embryos and also supplemented with CoQ_{10}. Embryos were photographed with a Leica DMC6200 camera coupled to an Olympus SZX16 laboratory magnifier. Images were acquired a few minutes after embryos dissection. (B) Size and weight measurements at 17 DPC. Size and weight were calculated from the images obtained using Fiji software for analysis. (C) Tibia length at 17 DPC. The skeletal system was stained to study tibia length in embryos at 17 DPC. Embryos were photographed with an OptikamB3 Digital Camera SN 558231 coupled to a Nikon SMZ1500 laboratory magnifier. (D) Tibia length at three-month-old and two-year-old. Right lower limb was segmented from each animal and immersed in NaOH 2% w/v for 7-9 to remove the skin, skeletal muscle and fat from the bones. CoQ_{10} in nanoparticles was dissolved in the water bottle, mean CoQ_{10} intake was estimated at 1-1.5 mg/day (33.33-50 mg/kg/day). Data represent the mean +/- SD. A one-way ANOVA test was applied. P-values <0.05 were considered statistically significant.

CoQ_9 and CoQ_{10} levels during the embryonic development

Also, we measured the CoQ levels through development in mutant embryos at ten and seventeen DPC (Figure 35). CoQ_9 and CoQ_{10} were higher on 10-days embryos under prenatal CoQ_{10} administration, although we did not find differences between mutant and wild type at this developmental stage.

Also, CoQ_9 and CoQ_{10} levels were higher in skeletal muscle of 17-days embryos under CoQ_{10} administration. The fact that CoQ_9 and CoQ_{10} levels were higher on embryos under CoQ_{10} administration demonstrates that mammals' embryos are capable of synthesizing their own CoQ_9.

Additionally, no significant differences were found between wild type and mutant embryos on standard conditions on skeletal muscle at 17-days of development. This may be because it has never been investigated whether CoQ deficiency begins during embryonic development or because CoQ_9 and CoQ_{10} levels were measured in the total homogenate and not in an isolated mitochondrial extract, where CoQ quantification could have been more precise.

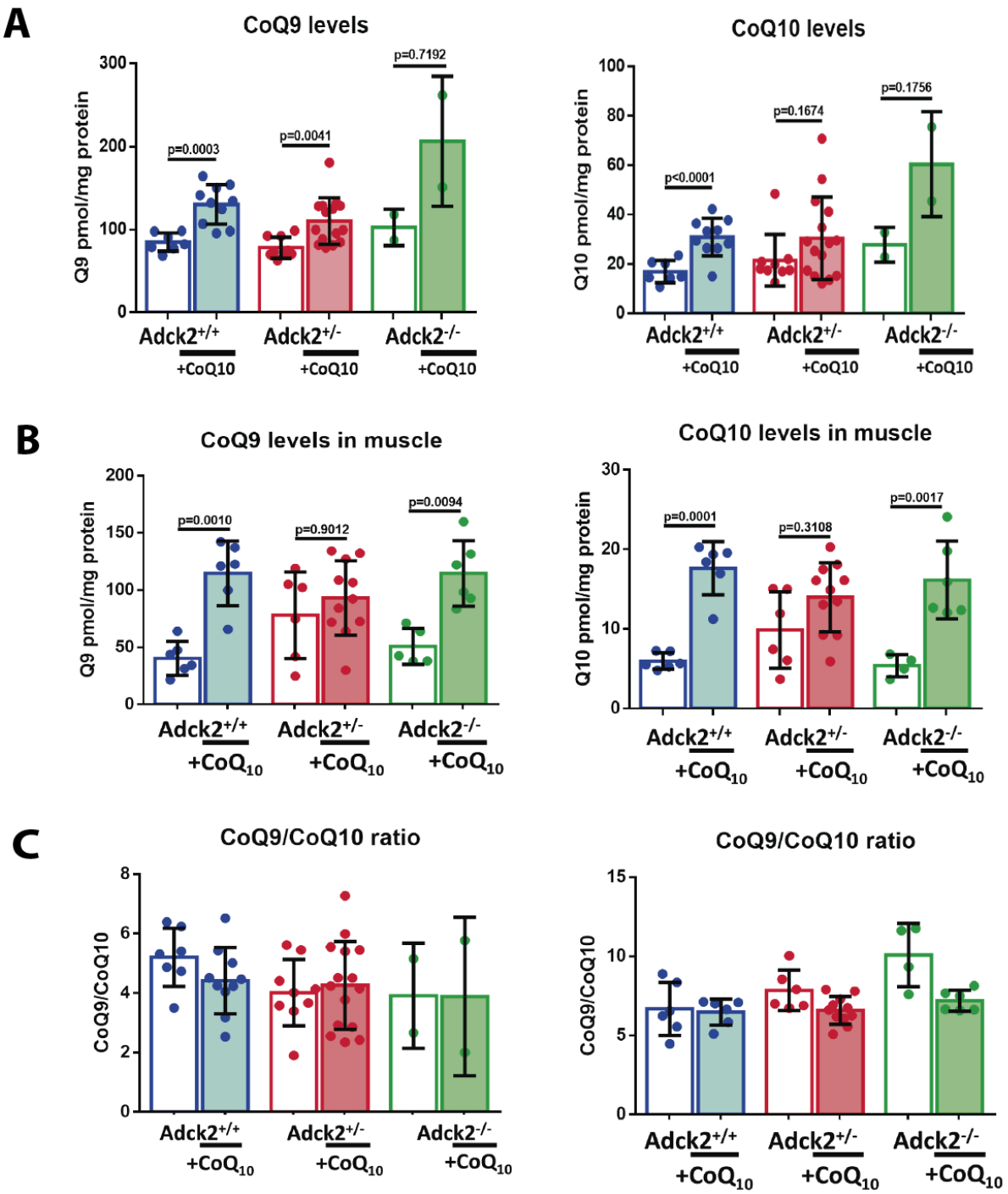

Figure 35. CoQ_9 and CoQ levels in embryos.

(A) CoQ_9 and CoQ_{10} levels in embryos at 10 DPC. CoQ was extracted from the whole wild type, *Adck2*$^{+/-}$ and *Adck2*$^{-/-}$ embryos at 10 DPC on standard conditions and under CoQ_{10} supplementation. (B) CoQ_9 and CoQ_{10} levels in skeletal muscle from wild type, *Adck2*$^{+/-}$ and *Adck2*$^{-/-}$ embryos at 17 DPC. Skeletal muscle from the four limbs was dissected at 17 DPC, skeletal muscle was meticulously separated from skin and bones. CoQ_9 and CoQ_{10} levels were examined by HPLC after lipids extraction. (C) Ratio CoQ_9/CoQ_{10} in embryos at 10 DPC and in skeletal muscle from embryos at 17 DPC. The study of CoQ_9 and CoQ_{10} proportion was examined with the ratio CoQ_9/CoQ_{10}. Data represent the mean +/- SD. Unpaired two-tailed t-test and one-way ANOVA test were applied. P-values <0.05 were considered statistically significant.

4.1.2 Discussion chapter 1:

The main objective of the present chapter was to determine if pathological phenotype found in the adult mice could start during embryonic development. Consequently, if damages of these mitochondrial syndromes would start during embryonic development, the moment when clinicians perform the diagnosis usually after birth, childhood or adulthood some irreparable damages would have already occurred and the treatments could only recover partially or delay the disease's progress (174). Our hypothesis is in line with a previous study (170) where a knockout mouse model for PDSS2 with a delay in glial cell growth and neuron progenitor migration leads to an impairment on cerebellum formation during embryonic development, even with an increase in apoptosis of neuroblasts. PDSS2 gene is involved in CoQ biosynthesis, and it is associated with ataxia and central nervous system damage in adulthood in both patients and mice. In our case, the phenotype of our mutant mice model is established during adulthood where the main tissue affected is the skeletal muscle suffering a mitochondrial dysfunction. For these reasons, we focus our study on this tissue during embryogenesis development. Furthermore, we decided to establish two specific time points during embryonic development for our study. Firstly, one point at early development, 9 DPC, and secondly, one point at late development, 17 DPC.

It has been reported the potential usefulness of transcriptomic analysis on mouse models in the design of disease diagnosis and treatments (175). So, we decided to perform such as analysis at nine DPC to explore if the mutation on the *ADCK2* gene could be affecting the transcriptome profile of mice. We only found small changes in the gene expression and most of the genes clustered on GO were related to structure and system development. We think that these small changes in gene expression were due because we performed the analysis in the whole embryo, including the whole cell population involved in the development of all tissues, although some tissues did not show damage in the adult mice. We believe that if we would have isolated cells that would develop skeletal muscle in adult mice, we would find more differences.

To corroborate this idea, we crossed our mutant mice with other mice that present an APZ reporter that allows the study and analysis of two MRFs (Myf5 and Mrf4) along with the embryonic development by colorimetric staining (176). Nuclear staining of MyF5 revealed dermomyotomal expression in the dorsal and ventral somites at 10 DPC, whereas Mrf4 expression was cytoplasmic and showed an early hypaxial expression plus the ventral and dorsal myotome at 10 DPC. In both cases, we found between 1 and 3 damaged somites in mutant embryos, possibly due to inadequate somitogenesis, whereas these alterations were practically absent in wild type. Embryos under CoQ_{10} administration did not present any of these

alterations, indicating that CoQ_{10} treatment was able to restore the altered myotome development since early developmental stages.

Next, we performed a transcriptomic study on skeletal muscle, liver and brain in a later stage of development (17 DPC). We decided to focus on these tissues because the skeletal muscle was the main tissue affected in the adult mice, the liver was mild-affected maybe due to the metabolic compensation, and the brain did not suffer any damage (77).

Mutant embryos suffered important gene deregulation in skeletal muscle. The 814 repressed genes were associated with structural development and bioenergetic metabolism, such as “fatty acid biosynthesis process”, “fatty-acyl-CoA metabolic process”, “cell-cell adhesion” or “Keratin filament”. However, the 384 activated genes were associated with “skeletal muscle differentiation and “myoblast fusion”. These results demonstrated that the transcriptomic profile of the skeletal muscle was already altered on 17-days embryos, indicating that the damages found in adult mice could have been initiated during embryonic development.

However, the transcriptomic profile of skeletal embryos from 17 DPC embryos prenatally supplemented with CoQ_{10} revealed that most of the GO previously repressed were activated, and even some GO reached wild type levels. Interestingly, CoQ_{10} activated new pathways indicating that CoQ_{10} was able to modulate gene expression in a specific way.

Later, we explored the factors that could be modulating the altered gene expression in the muscle of 17-days embryos, and we found a correlation between activation of miRNA and gene repression. Also, promoter regions of deregulated genes in mutant embryos were enriched in transcription factors that modulate myogenesis including Pax7, Myf5, or MyoD and others involved in metabolisms such as VDR, Nr5a2 or Sf1, whereas modulated genes by CoQ_{10} in mutant embryos were enriched in transcription factors that regulate myogenesis including Mef2c and Mef2d. These results support the idea that transcription alterations could be modulated by transcription factors that control the myogenesis process.

The transcriptomic profile in the liver from mutant embryos at 17 DPC showed weak deregulation with 87 genes repressed and 23 genes activated. Most of the Gene Ontologies deregulated were associated with metabolic process indicating that the metabolic deregulation found in mice are mainly related to fatty acids accumulation. The alteration found in the liver could be associated with the huge deregulation presented by skeletal muscle and could be a side effect of the damage to the skeletal muscle due to the close relationship between these two tissues.

The transcriptomic profile of the brain in 17-days embryos showed small gene deregulation with only 16 repressed genes and 8 activated. We consider that the lack of deregulation of brain tissue could also be associated with the lack of symptoms in the CNS described in adult mice (77), indicating that the damage would be tissue-specific.

All these results together could explain the smaller size and the visual defects of the mutant embryos, which could be related to delayed development, and emphasized the benefits of a prenatal CoQ_{10} treatment that tend to recover these defects. Furthermore, the evaluation of the tibia length as a marker of development corroborated that mutant embryos tend to have potential decreased development. All gene expression analysis were performed in heterozygous mutant embryos due to homozygous mutant embryos were no viable and they died before birth, also the human patient was heterozygous for the mutation, for these reasons we focused on the heterozygous mutant mice.

Finally, we could conclude that mutant embryos suffer alterations during embryonic development that condition the proper embryonic development resulting in an impairment of prenatal myogenesis.

Chapter 2

4.2 CHAPTER 2: Postnatal myogenesis in the *Adck2* mouse model.

4.2.1 Introduction

The results found during the study of embryonic development suggest that skeletal muscle formation could be compromised. Consequently, to perform a close approximation to skeletal muscle formation, we decided to study postnatal myogenesis using the primary culture of adult muscle stem cells as a model. Embryonic myogenesis and adult muscle stem cell activation share elements such as transcription factors and signalling molecules (138). Transcription factors that regulate myogenic differentiation of the precursor cells in mammalian skeletal muscle are similar to those observed during skeletal muscle development, including embryogenesis, postnatal and juvenile stages, and skeletal muscle repairment and regeneration (101).

Furthermore, stem cells have important metabolic flexibility that allows them to shift from glycolysis to oxidative phosphorylation during quiescence, self-renewal and differentiation, highlighting the importance of different metabolic pathways in skeletal muscle stem cell metabolism (177). As our heterozygous *Adck2* knockout mice present a mitochondrial dysfunction characterized by a decrease in CoQ levels, an impairment in the ETC and a defect in fatty acids β-oxidation (77). We proposed that the different metabolic pathways that are regulated during the myogenesis process could potentially be altered in SCs from our mutant mice.

So, to determine how an altered metabolism can affect the myogenesis process, we decided to study the proliferation and differentiation stages of SCs isolated from our mutant mice. Additionally, as it was reported that clinical manifestations were more severe in the human patient during ageing (77), analyses of postnatal myogenesis were performed on SCs from young mice (three-month-old) and SCs from old mice (two-year-old). Furthermore, as we have described in chapter 1 that the compromised prenatal myogenesis in *ADCK2* embryos was improved under CoQ_{10} administration, we decided to check the effect of CoQ_{10} administration on SCs. Therefore, we described in this chapter SCs activation, proliferation, differentiation, and specification from wild type and mutant mice, treated or not with CoQ_{10} during both youth and old ages.

Finally, we decide to support our *in vitro* analysis with *in vivo* study of postnatal myogenesis. For this purpose, we studied skeletal muscle regeneration after 14 days post $BaCl_2$ injection into the TA muscle. We used this approach due because $BaCl_2$ mimics the pathological elevations of intracellular Ca^{2+}, resulting in degeneration of myofibers and their posterior regeneration by SCs (137). Again, based on the progressive clinical manifestations reported in the human patient, we

decided to perform this experiment in young mice (three-month-old) and old mice (two-year-old) treated or not with CoQ_{10} administration. In all cases, mice were sacrificed 14 days after $BaCl_2$ injection and TA muscle was carefully dissected and frozen for immunohistochemical analysis.

On balance, the present chapter is focused on the study of postnatal myogenesis through *in vitro* and *in vivo* approaches, including ageing as a factor that could increase the severity of the phenotype.

***ADCK2* mice have fewer satellite cells attached to myofibers**

First, we studied SCs when they were still attached to myofibers to quantify the number and status of SCs in old mice. To do that, isolated and collagen free myofibers from the EDL muscle were stained to quantify the SCs on their surface. SCs were distinguished from the rest because they were Pax7 positive (Figure 36A).

Myofibers from aged wild type mice had almost twice as many SCs as those from the mutant (mean value for WT was 4.08 and for mutant, 2.72), whereas myofibers from mutant mice supplemented with CoQ_{10} showed an increase in the number of SCs (mean value was 4.18). No differences were found between the number of SCs attached to myofibers in mutant mice supplemented with CoQ_{10} showed compared to wild type animals (Figure 36B), which showed the effectiveness of the treatment in the loss of SCs during ageing.

Next, we represented the distribution of the number of SCs per myofibers finding that mutant mice had a higher proportion of myofibers with a lower number of SCs compared with wild type (Figure 36B). More significantly, the profile of mutant myofibers supplemented with CoQ_{10} was more similar to wild type. Wild type animals under CoQ_{10} supplementation very slightly increased the number of SCs per myofibers without reaching significant differences.

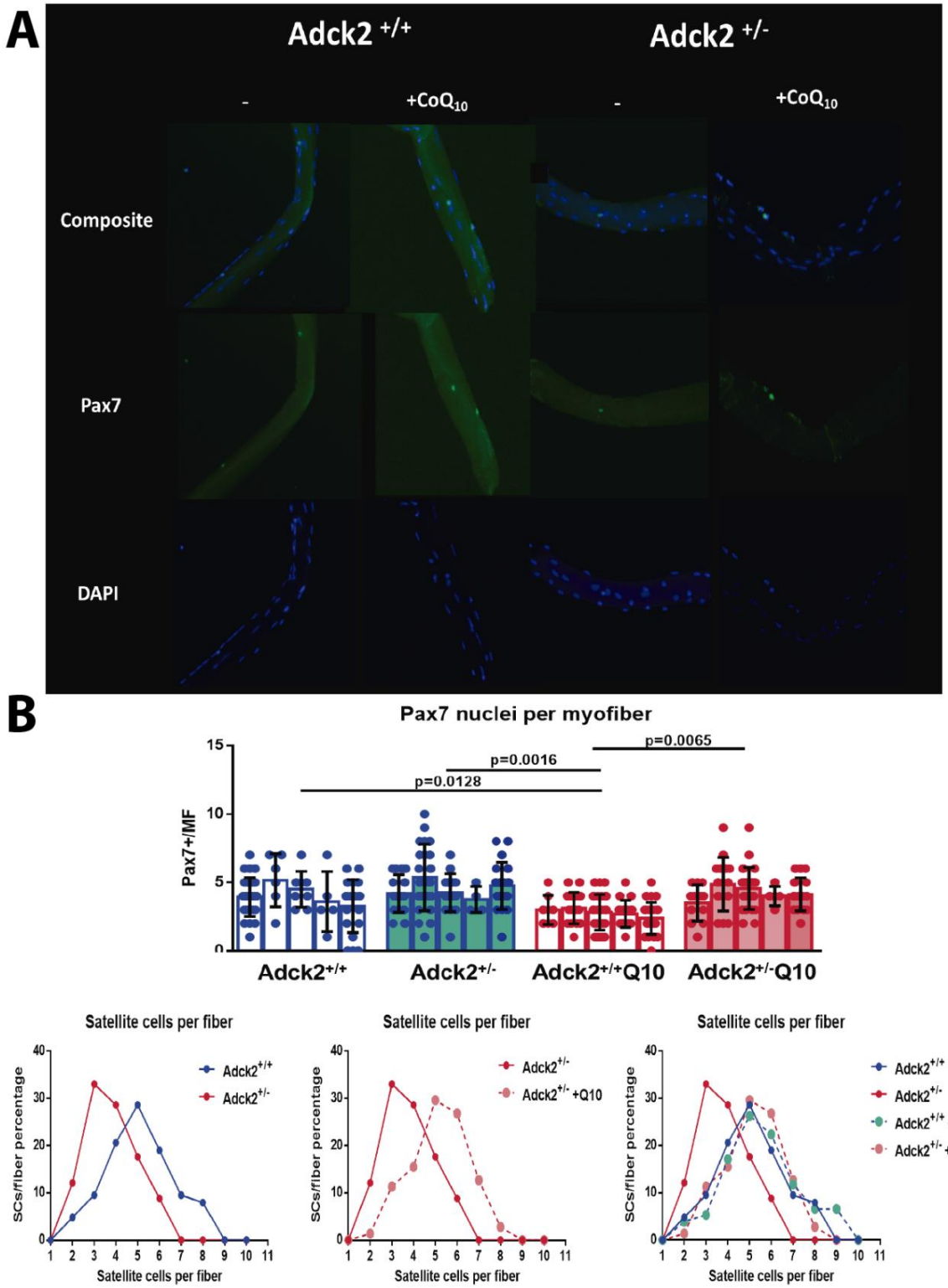

Figure 36. Satellite cells on myofibers from old mice.

(A) Representative images of Pax 7 staining for SCs quantification. DAPI was used to stain in blue all the nuclei from the myofiber, whereas Pax7 was used to stain in green the nuclei of satellite cells. Myofibers were fixed in 4% PFA after myofibers isolation. (B) Quantification and distribution of the number de SCs attached to myofibers. Each dot represents the number of SCs per myofiber. Each bar shows the mean of SCs found in all myofibers extracted from each EDL muscle. Five animals were used for this quantification. Data represent the mean +/- SD. A one-way ANOVA test was applied. P-values <0.05 were considered statistically significant. Satellite cells population analysis in the different groups studied. The global mean and mode for each genotype and treatment was for wild type, 4.08 SCs per myofiber (mode=4); for *Adck2*$^{+/-}$, 2.78 (mode= 2), for wild type supplemented with CoQ_{10}, 4.53 (mode=4); and for *Adck2*$^{+/-}$ supplemented with CoQ_{10}, 4.18 (mode=4).

***In vitro* analysis reveals an alteration of myogenesis**

We had demonstrated that myofibers of mutant mice had fewer SCs. To determine if this reduction could affect myogenesis, we isolated SCs from young and old mice and we plated them in a proliferative medium that contains high serum concentration to allow them to grow and divide. Active SCs were distinguished from the rest because they were Pax7 positive, whereas DAPI was able to stain the nuclei of all cells present in the culture (Figure 37A). Next, we quantified the proportion of Pax7 positive cells along the time to determine the proliferative status of SCs, which was defined as the Pax7/DAPI ratio. The study did not prolong more than 72 hours because SCs would start to differentiative after 3 days of culture.

No differences were found between SCs isolated from wild type and SCs from heterozygous *Adck2* knockout mice for 72 hours neither in young mice (Figure 37B) nor old mice (Figure 37C). However, the number of Pax7 positive cells was higher in young mice compared with old mice at all time points studied, indicating that SCs from young mice presented a higher proliferative status.

To mimic CoQ_{10} administration in the *in vitro* assays, 10 µM CoQ_{10} was added to the culture medium of SCs extracted from supplemented animals. The proliferative status of SCs under CoQ_{10} supplementation seemed to be 10-20% higher in both genotypes, although the increase was not significant concluding that CoQ_{10} administration to SCs could tend to intensify SCs proliferative status.

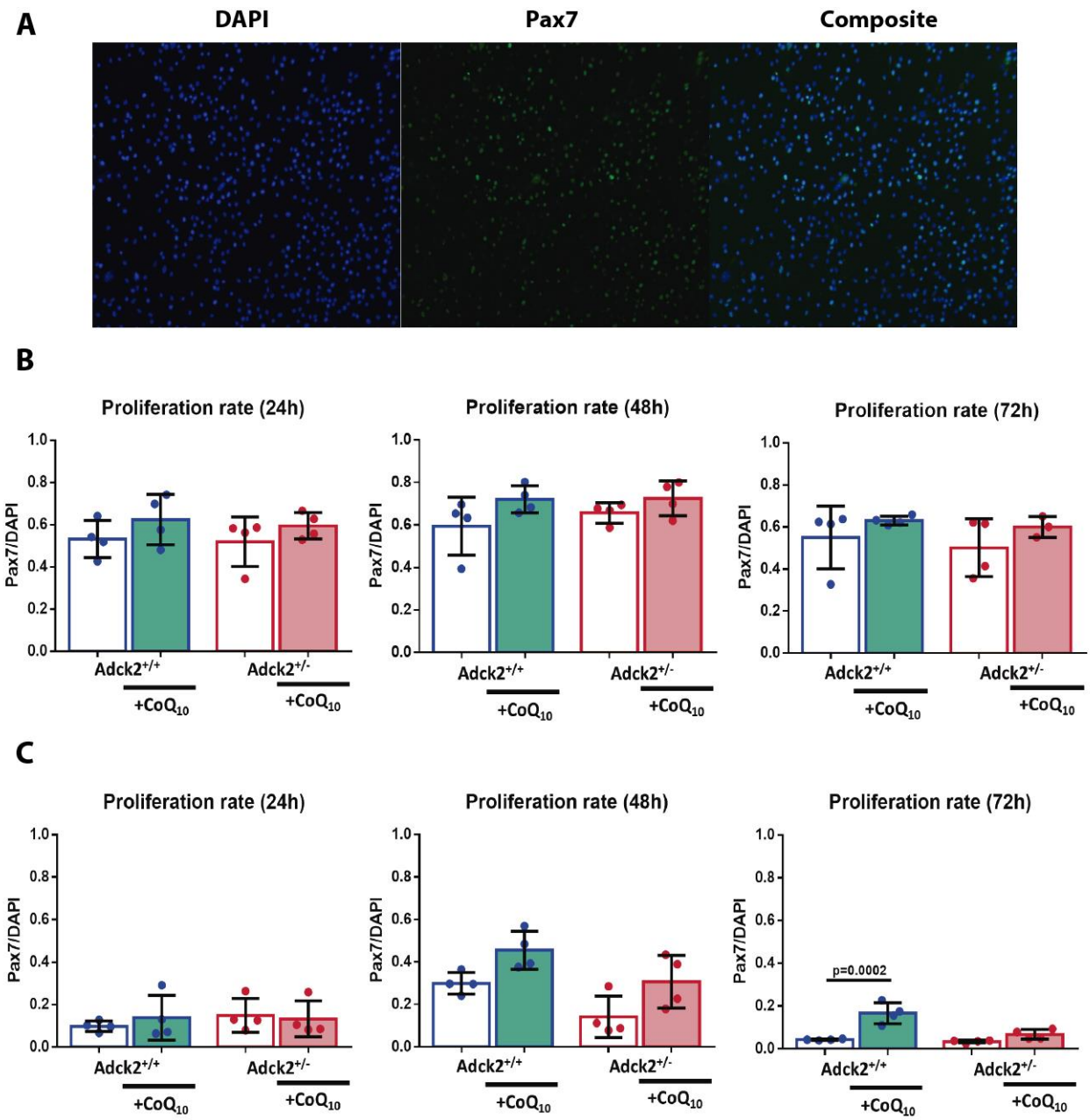

Figure 37. Myogenic proliferation on satellite cells.

Pax7 antibody staining was used to distinguish proliferative satellite cells and to determine stem cell identity through consecutive cell division in proliferation conditions. Satellite cells were cultured with the proliferative medium. (A) Representative images of Pax7 and DAPI positive cells. (B) Proliferation analysis during 72 hours in cells from young mice. (C) Proliferation analysis during 72 hours in cells from young mice and old mice. The mean value was calculated from 4 different wells and each dot represents the mean value of five random pictures taken from the same culture well. Data represent the mean +/- SD. A one-way ANOVA test was applied. P-values <0.05 were considered statistically significant.

Next, we determined the differentiation process of SCs by following the expression of the MyHC protein, which allowed us to quantify the increase in the size of the newly formed myotube once SCs started to differentiate. The differentiation was induced by a decrease in the serum concentration in the medium and was followed every 24 hours for 5 days so that 5-time points

were assayed (24, 48, 72, 96 and 120 hours). SCs were isolated from EDL muscle dissected from three-month-old mice, both wild type and mutant in standard conditions and under CoQ_{10} administration. Then, individual myofibers were separated from the EDL muscle and later plated to induce SCs activation. Finally, SCs were separated from myofibers and plated for differentiation experiments. To mimic CoQ_{10} administration in the *in vitro* assays, 10 µM CoQ_{10} was added to the culture medium of SCs extracted from animals under treatment. The differentiation process was quantified by measuring several markers of myotubes differentiation, such as the increase in size (growth) and ramification. Representative images of the differentiation process along the time for each of the groups studied are shown in young (Figure 38) and old mice (Figure 40). The differentiation status was determined by quantification of the MyHC area, length of the myotubes and their ramification capacity. Figure 39 shows the differentiation parameters studied of myotubes from young mice, whereas Figure 41 represents the results of myotubes from old mice.

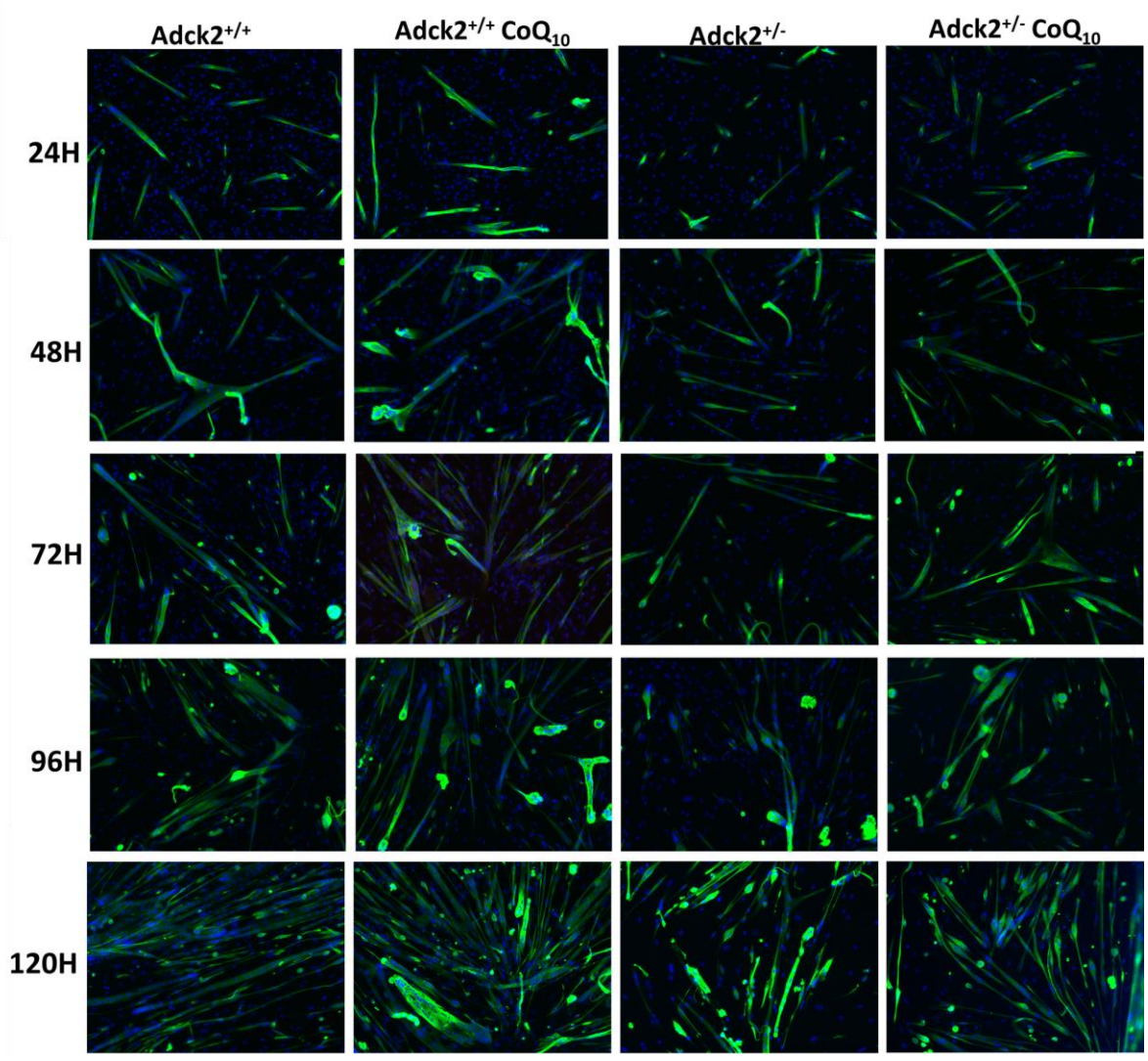

Figure 38. Differentiation process of satellite cells isolated from young mice.
Representative images of satellite cells differentiate into myotubes, differentiation to myotubes was induced by a reduction in serum concentration. Fresh medium was replaced in each well every 48 hours to avoid nutrient depletion. The final concentration of CoQ_{10} was adjusted to 10 μM and it was replaced every 48 hours. DAPI was used to stain in blue the nuclei of the myotubes, while differentiated myotubes were stained in green with a MyHC antibody. The differentiation process was determined by following the increase of the MyHC area in myotubes at 24 (A), 48. (B), 72 (C), 96 (D) and 120 hours (E).

Cells from mutant mice presented lower MyHC area compared with those isolated from wild type mice, and this difference became bigger as the differentiation progressed (Figure 39A). However, the differentiation index did not show differences between mutant and wild type cells. We did not find any significant effect associated with CoQ_{10} administration in these two parameters.

We also analysed the length of the myotubes over 120 hours as another marker of differentiation and myotube growth (Figure 39B), finding that myotubes from mutant mice were shorter compared with myotubes from wild type mice. What is more spellbinding was that CoQ_{10} supplementation increased the length of myotubes in mutant mice, while the treatment did not show any effect on the length of myotubes in wild type mice.

Finally, we also quantified the ramification capacity in the myotubes for 120 hours as another marker of myotubes differentiation and growth (Figure 39C). Particularly, we quantified the proportion of myotubes with two branches (linear myotubes without ramification), three branches (1 ramification) or four branches (2 ramifications) in these samples. In agreement with the rest of the measures performed, statistical analysis is shown in Table 14. We found that mutant myotubes present a lower branching capacity and consequently a lower number of ramifications compared with wild type myotubes in the final time points of the period studied. Additionally, myotubes supplemented with CoQ_{10} isolated from mice treated with CoQ_{10} showed an increase in the branching capacity in the final points of the period studied. Branching capacity occurred in mature myotubes and thus it was necessary to study this parameter longitudinally to detect defects in the final stages of myotube differentiation. Initially, we did not find any difference in the branching capacity of the myotubes of the different groups studied (Figure 39C), although it seems that mutant increases the proportion of ramified myotubes slower compared to wild type myotubes, indicating impairment on differentiation in terms of ramification capacity. Besides, CoQ_{10} addition increased the velocity of generated ramifications in myotubes and, thus, could accelerate the differentiation process.

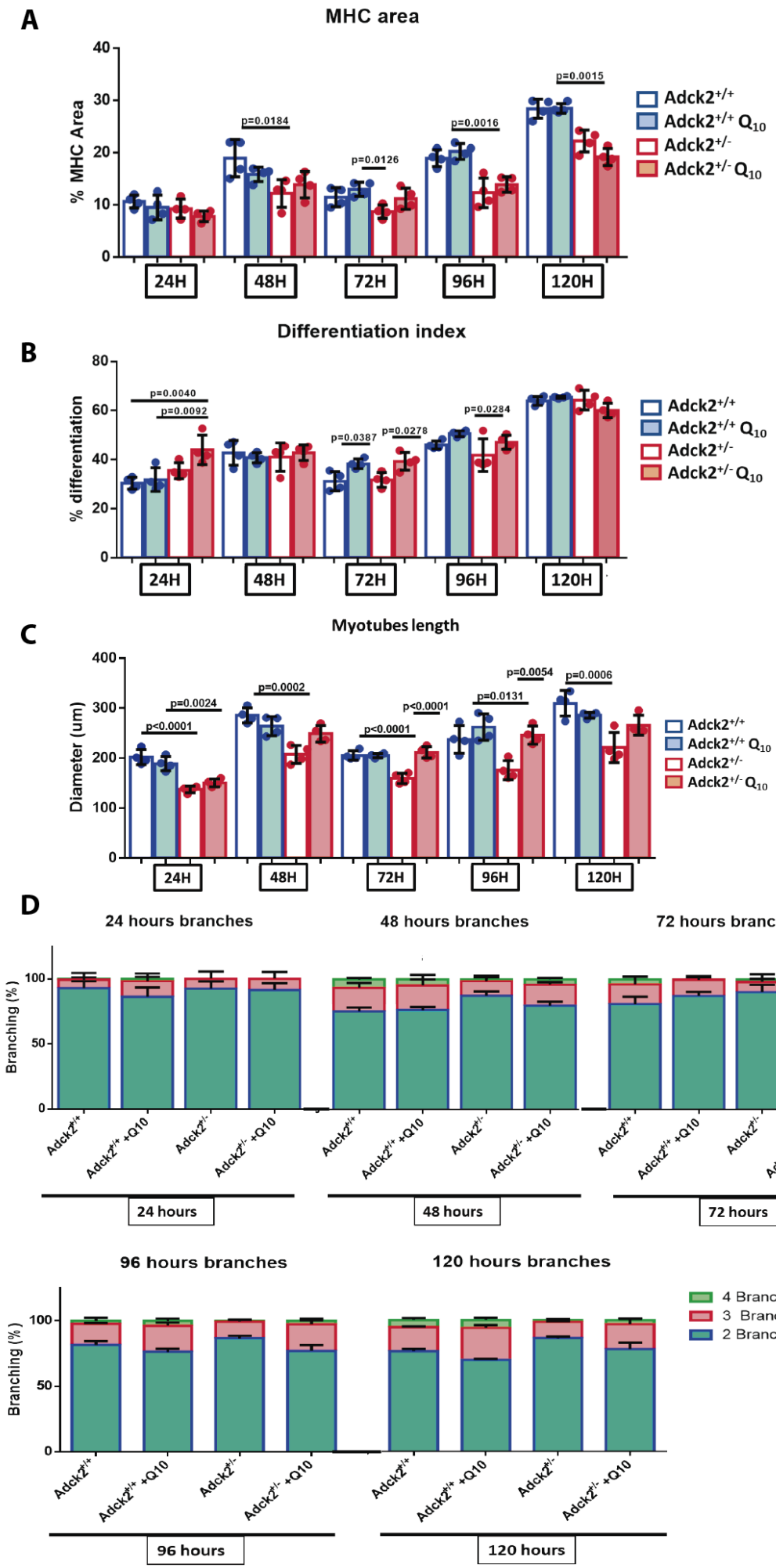
A
MHC area
% MHC Area
p=0.0184
p=0.0126
p=0.0016
p=0.0015
24H
48H
72H
96H
120H
Adck2+/+
Adck2+/+ Q10
Adck2+/-
Adck2+/- Q10
B
Differentiation index
% differentiation
p=0.0040
p=0.0092
p=0.0387
p=0.0278
p=0.0284
C
Myotubes length
Diameter (um)
p<0.0001
p=0.0024
p=0.0002
p<0.0001
p<0.0001
p=0.0131
p=0.0054
p=0.0006
D
24 hours branches
48 hours branches
72 hours branches
Branching (%)
24 hours
48 hours
72 hours
96 hours branches
120 hours branches
4 Branches
3 Branches
2 Branches
96 hours
120 hours

Figure 39. Figure differentiation process analysis of satellite cells isolated from young mice.
Satellite cells from young mice were isolated and differentiated to myotubes for 120 hours. DAPI was used to stain in blue the nuclei of the myotubes, while differentiated myotubes were stained in green with Myosin heavy chain (MyHC) antibody. The differentiation process was determined by following the increase of MyHC expression by immunostaining. Differentiation of satellite cells to myotubes is induced by a reduction in serum concentration. (A) MyHC area. (B) Differentiation index. (C) Myotubes length. (D) Branching capacity. Data represent the mean +/- SD. One-way ANOVA test was applied. P-values <0.05 were considered statistically significant.

Table 14 Statistic analysis of branching capacity in myotubes from young mice

Time point 24 hours					
Branches 2		**Branches 3**		**Branches 4**	
Comparison	**Significance**	**Comparison**	**Significance**	**Comparison**	**Significance**
$Adck2^{+/+}$ vs $Adck2^{+/+}$ CoQ_{10}	ns	$Adck2^{+/+}$ vs $Adck2^{+/+}$ CoQ_{10}	ns	$Adck2^{+/+}$ vs $Adck2^{+/+}$ CoQ_{10}	ns
$Adck2^{+/+}$ vs $Adck2^{+/-}$	ns	$Adck2^{+/+}$ vs $Adck2^{+/-}$	ns	$Adck2^{+/+}$ vs $Adck2^{+/-}$	ns
$Adck2^{+/+}$ vs $Adck2^{+/-}$ CoQ_{10}	ns	$Adck2^{+/+}$ vs $Adck2^{+/-}$ CoQ_{10}	ns	$Adck2^{+/+}$ vs $Adck2^{+/-}$ CoQ_{10}	ns
$Adck2^{+/+}$ CoQ_{10} vs $Adck2^{+/-}$	ns	$Adck2^{+/+}$ CoQ_{10} vs $Adck2^{+/-}$	ns	$Adck2^{+/+}$ CoQ_{10} vs $Adck2^{+/-}$	ns
$Adck2^{+/+}$ CoQ_{10} vs $Adck2^{+/-}$ CoQ_{10}	ns	$Adck2^{+/+}$ CoQ_{10} vs $Adck2^{+/-}$ CoQ_{10}	ns	$Adck2^{+/+}$ CoQ_{10} vs $Adck2^{+/-}$ CoQ_{10}	ns
$Adck2^{+/-}$ vs $Adck2^{+/-}$ CoQ_{10}	ns	$Adck2^{+/-}$ vs $Adck2^{+/-}$ CoQ_{10}	ns	$Adck2^{+/-}$ vs $Adck2^{+/-}$ CoQ_{10}	ns
Time point 48 hours					
Branches 2		**Branches 3**		**Branches 4**	
Comparison	**Significance**	**Comparison**	**Significance**	**Comparison**	**Significance**
$Adck2^{+/+}$ vs $Adck2^{+/+}$ CoQ_{10}	ns	$Adck2^{+/+}$ vs $Adck2^{+/+}$ CoQ_{10}	ns	$Adck2^{+/+}$ vs $Adck2^{+/+}$ CoQ_{10}	ns
$Adck2^{+/+}$ vs $Adck2^{+/-}$	p=0.0005	$Adck2^{+/+}$ vs $Adck2^{+/-}$	ns	$Adck2^{+/+}$ vs $Adck2^{+/-}$	p=0.0240
$Adck2^{+/+}$ vs $Adck2^{+/-}$ CoQ_{10}	ns	$Adck2^{+/+}$ vs $Adck2^{+/-}$ CoQ_{10}	ns	$Adck2^{+/+}$ vs $Adck2^{+/-}$ CoQ_{10}	ns
$Adck2^{+/+}$ CoQ_{10} vs $Adck2^{+/-}$	p=0.0011	$Adck2^{+/+}$ CoQ_{10} vs $Adck2^{+/-}$	p=0.0485	$Adck2^{+/+}$ CoQ_{10} vs $Adck2^{+/-}$	ns
$Adck2^{+/+}$ CoQ_{10} vs $Adck2^{+/-}$ CoQ_{10}	ns	$Adck2^{+/+}$ CoQ_{10} vs $Adck2^{+/-}$ CoQ_{10}	ns	$Adck2^{+/+}$ CoQ_{10} vs $Adck2^{+/-}$ CoQ_{10}	ns
$Adck2^{+/-}$ vs $Adck2^{+/-}$ CoQ_{10}	p=0.0175	$Adck2^{+/-}$ vs $Adck2^{+/-}$ CoQ_{10}	ns	$Adck2^{+/-}$ vs $Adck2^{+/-}$ CoQ_{10}	ns
Time point 72 hours					
Branches 2		**Branches 3**		**Branches 4**	
Comparison	**Significance**	**Comparison**	**Significance**	**Comparison**	**Significance**
$Adck2^{+/+}$ vs $Adck2^{+/+}$ CoQ_{10}	ns	$Adck2^{+/+}$ vs $Adck2^{+/+}$ CoQ_{10}	ns	$Adck2^{+/+}$ vs $Adck2^{+/+}$ CoQ_{10}	p=0.0099
$Adck2^{+/+}$ vs $Adck2^{+/-}$	ns	$Adck2^{+/+}$ vs $Adck2^{+/-}$	ns	$Adck2^{+/+}$ vs $Adck2^{+/-}$	ns
$Adck2^{+/+}$ vs $Adck2^{+/-}$ CoQ_{10}	ns	$Adck2^{+/+}$ vs $Adck2^{+/-}$ CoQ_{10}	ns	$Adck2^{+/+}$ vs $Adck2^{+/-}$ CoQ_{10}	p=0.0137
$Adck2^{+/+}$ CoQ_{10} vs $Adck2^{+/-}$	ns	$Adck2^{+/+}$ CoQ_{10} vs $Adck2^{+/-}$	ns	$Adck2^{+/+}$ CoQ_{10} vs $Adck2^{+/-}$	ns
$Adck2^{+/+}$ CoQ_{10} vs $Adck2^{+/-}$ CoQ_{10}	ns	$Adck2^{+/+}$ CoQ_{10} vs $Adck2^{+/-}$ CoQ_{10}	ns	$Adck2^{+/+}$ CoQ_{10} vs $Adck2^{+/-}$ CoQ_{10}	ns
$Adck2^{+/-}$ vs $Adck2^{+/-}$ CoQ_{10}	ns	$Adck2^{+/-}$ vs $Adck2^{+/-}$ CoQ_{10}	ns	$Adck2^{+/-}$ vs $Adck2^{+/-}$ CoQ_{10}	ns
Time point 96 hours					
Branches 2		**Branches 3**		**Branches 4**	
Comparison	**Significance**	**Comparison**	**Significance**	**Comparison**	**Significance**

Adck2$^{+/+}$ vs Adck2$^{+/+}$ CoQ$_{10}$	ns	Adck2$^{+/+}$ vs Adck2$^{+/+}$ CoQ$_{10}$	ns	Adck2$^{+/+}$ vs Adck2$^{+/+}$ CoQ$_{10}$	ns
Adck2$^{+/+}$ vs Adck2$^{+/-}$	ns	Adck2$^{+/+}$ vs Adck2$^{+/-}$	ns	Adck2$^{+/+}$ vs Adck2$^{+/-}$	ns
Adck2$^{+/+}$ vs Adck2$^{+/-}$ CoQ$_{10}$	ns	Adck2$^{+/+}$ vs Adck2$^{+/-}$ CoQ$_{10}$	ns	Adck2$^{+/+}$ vs Adck2$^{+/-}$ CoQ$_{10}$	ns
Adck2$^{+/+}$ CoQ$_{10}$ vs Adck2$^{+/-}$	p=0-0026	Adck2$^{+/+}$ CoQ$_{10}$ vs Adck2$^{+/-}$	p=0-0014	Adck2$^{+/+}$ CoQ$_{10}$ vs Adck2$^{+/-}$	ns
Adck2$^{+/+}$ CoQ$_{10}$ vs Adck2$^{+/-}$ CoQ$_{10}$	ns	Adck2$^{+/+}$ CoQ$_{10}$ vs Adck2$^{+/-}$ CoQ$_{10}$	ns	Adck2$^{+/+}$ CoQ$_{10}$ vs Adck2$^{+/-}$ CoQ$_{10}$	ns
Adck2$^{+/-}$ vs Adck2$^{+/-}$ CoQ$_{10}$	p=0.0044	Adck2$^{+/-}$ vs Adck2$^{+/-}$ CoQ$_{10}$	p=0.0009	Adck2$^{+/-}$ vs Adck2$^{+/-}$ CoQ$_{10}$	ns
Time point 120 hours					
Branches 2		**Branches 3**		**Branches 4**	
Comparison	**Significance**	**Comparison**	**Significance**	**Comparison**	**Significance**
Adck2$^{+/+}$ vs Adck2$^{+/+}$ CoQ$_{10}$	p=0.0283	Adck2$^{+/+}$ vs Adck2$^{+/+}$ CoQ$_{10}$	p=0.0110	Adck2$^{+/+}$ vs Adck2$^{+/+}$ CoQ$_{10}$	ns
Adck2$^{+/+}$ vs Adck2$^{+/-}$	p=0.0014	Adck2$^{+/+}$ vs Adck2$^{+/-}$	p=0.0129	Adck2$^{+/+}$ vs Adck2$^{+/-}$	p=0.0091
Adck2$^{+/+}$ vs Adck2$^{+/-}$ CoQ$_{10}$	ns	Adck2$^{+/+}$ vs Adck2$^{+/-}$ CoQ$_{10}$	ns	Adck2$^{+/+}$ vs Adck2$^{+/-}$ CoQ$_{10}$	ns
Adck2$^{+/+}$ CoQ$_{10}$ vs Adck2$^{+/-}$	p<0.0001	Adck2$^{+/+}$ CoQ$_{10}$ vs Adck2$^{+/-}$	p<0.0001	Adck2$^{+/+}$ CoQ$_{10}$ vs Adck2$^{+/-}$	p=0.0044
Adck2$^{+/+}$ CoQ$_{10}$ vs Adck2$^{+/-}$ CoQ$_{10}$	p=0.0070	Adck2$^{+/+}$ CoQ$_{10}$ vs Adck2$^{+/-}$ CoQ$_{10}$	p=0.0255	Adck2$^{+/+}$ CoQ$_{10}$ vs Adck2$^{+/-}$ CoQ$_{10}$	ns
Adck2$^{+/-}$ vs Adck2$^{+/-}$ CoQ$_{10}$	p=0.0053	Adck2$^{+/-}$ vs Adck2$^{+/-}$ CoQ$_{10}$	p=0.0056	Adck2$^{+/-}$ vs Adck2$^{+/-}$ CoQ$_{10}$	ns

Non significant (ns); Versus (vs).

To quantify this, we correlated these parameters along time to calculate the slope of the line as a marker to measure the velocity of differentiation (Table 15). The slope of the line was always slightly smaller in mutant myotubes than in the wild type, indicating that differentiation could be affected in mutant mice. The effect of CoQ$_{10}$ supplementation on mutant myotubes was only clear in the myotube length and their ramification capacity.

Table 15 Differentiation analysis in myotubes from young mice

Parameter: MyHC area		
Group	The slope of the line	R squared on the graph
Adck2$^{+/+}$	0.1478	R^2 = 0.5633
Adck2$^{+/+}$ +CoQ$_{10}$	0.1763	R^2 = 0.7982
Adck2$^{+/-}$	0.1082	R^2 = 0.4945
Adck2$^{+/-}$ +CoQ$_{10}$	0.0948	R^2 = 0.6329
Parameter: Differentiation Index		
Group	The slope of the line	R squared on the graph
Adck2$^{+/+}$	0.2929	R^2 = 0.6292
Adck2$^{+/+}$ +CoQ$_{10}$	0.3208	R^2 = 0.8363
Adck2$^{+/-}$	0.2426	R^2 = 0.4681
Adck2$^{+/-}$ +CoQ$_{10}$	0.1507	R^2 = 0.4143
Parameter: Myotubes length		
Group	The slope of the line	R squared on the graph
Adck2$^{+/+}$	0.6961	R^2 = 0.2606
Adck2$^{+/+}$ +CoQ$_{10}$	0.7997	R^2 = 0.4621
Adck2$^{+/-}$	0.5693	R^2 = 0.3094
Adck2$^{+/-}$ +CoQ$_{10}$	0.9511	R^2 = 0.5591
Parameter: Ramificated myotubes		
Group	The slope of the line	R squared on the graph

Adck2$^{+/+}$	0.112	$R^2 = 0.2857$
Adck2$^{+/+}$ +CoQ_{10}	0.1381	$R^2 = 0.3998$
Adck2$^{+/-}$	0.0552	$R^2 = 0.1998$
Adck2$^{+/-}$ +CoQ_{10}	0.1251	$R^2 = 0.441$

We also studied the differentiation process of SCs isolated from old mice in both wild type and mutant mice under standard conditions and under CoQ_{10} administration. Figure 40 showed representative images of the myofibers along the differentiation process.

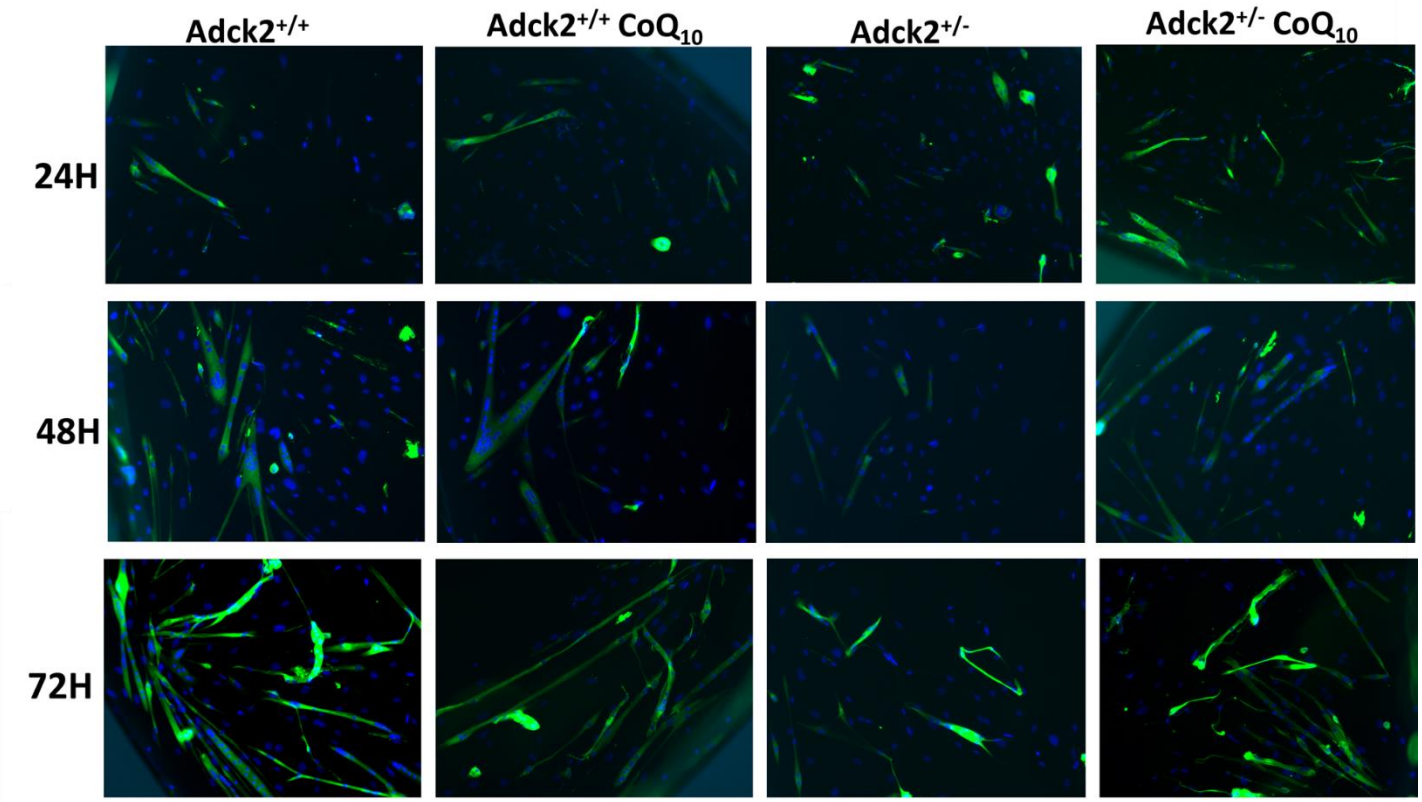

Figure 40. Differentiation process of satellite cells isolated from old mice.
Representative images of satellite cells differentiate into myotubes, differentiation to myotubes was induced by a reduction in serum concentration. Fresh medium was replaced in each well every 48 hours to avoid nutrient depletion. The final concentration of CoQ_{10} was adjusted to 10 µM and it was replaced every 48 hours. DAPI was used to stain in blue the nuclei of the myotubes, while differentiated myotubes were stained in green with a MyHC antibody. The differentiation process was determined by following the increase of the MyHC area in myotubes. (A) Differentiation at 24 hours. (B) Differentiation at 48 hours. (C) Differentiation at 72 hours.

The analysis from old mice revealed that differentiated mutant cells presented a much lower MyHC area compared with myotubes from wild type mice and that such differences got bigger as differentiation progressed (Figure 41A). We also found that the differentiation index was reduced in mutant cells indicating a lower proportion of differentiated cells. When mutant cells were treated with CoQ_{10}, they showed similar values to wild type cells in both parameters.

We also determined myotubes length as another marker of differentiation and myotube growth. Myotubes from mutant mice showed a decrease in myotubes length compared with myotubes

from wild type cells at later stages of differentiation (Figure 41B). Again, myotubes from mutant mice supplemented with CoQ_{10} that also received CoQ_{10} during the differentiation showed an increase in myotubes length, reaching wild type myotubes levels.

Finally, branching capacity was also quantified as another marker of myotubes differentiation and growth in terms of ramification. Initially, there were no differences between the groups analysed, but as differentiation progresses, we discovered that myotubes from mutant mice hardly branch out and still maintain a linear shape with only 2 ends compared with wild type myotubes (Figure 41C), statistical analysis is shown in Table 16. In addition, mutant myotubes treated with CoQ_{10} displayed a ramification process similar to that of wild type myotubes with also a similar proportion of branched myotubes.

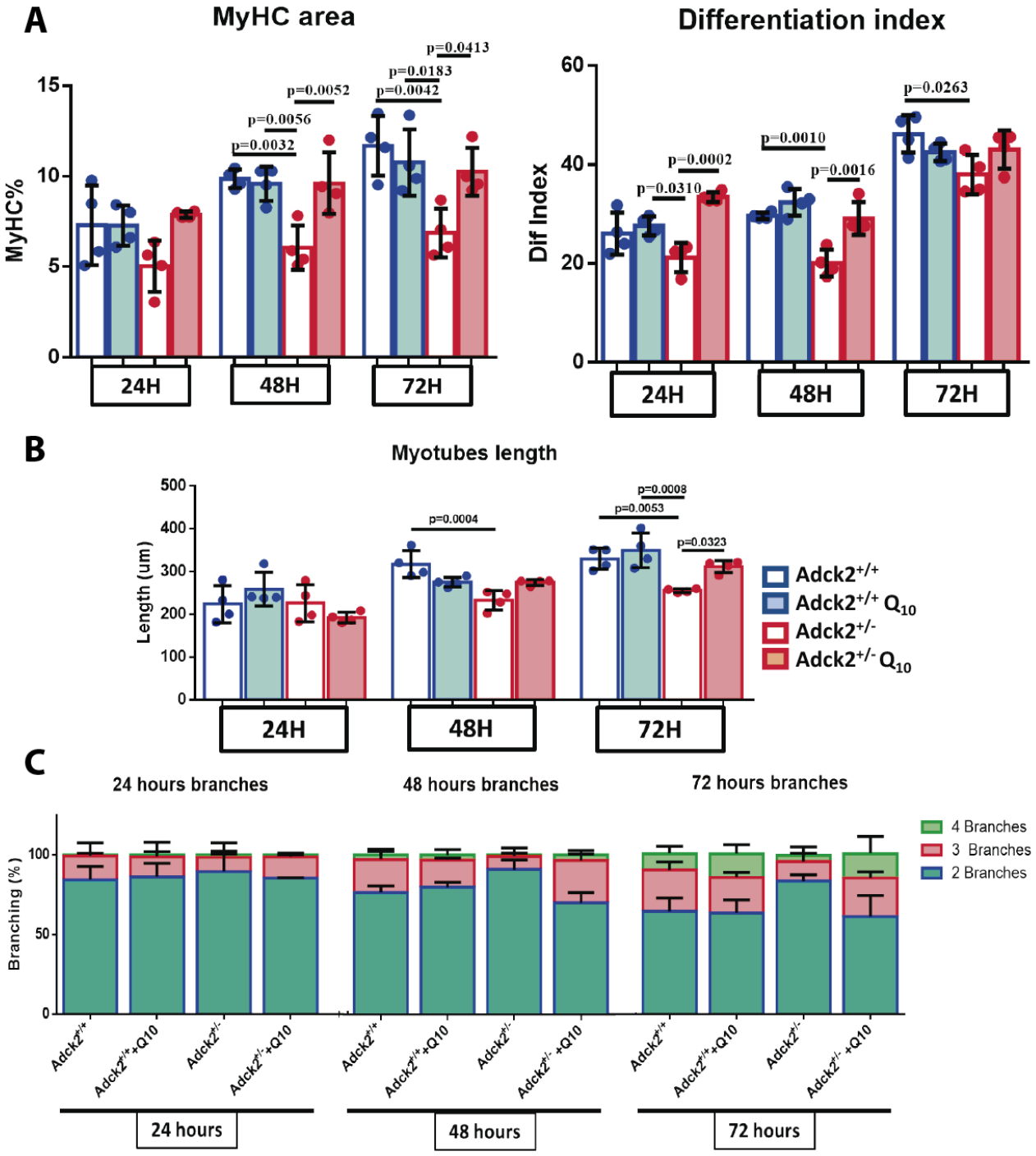

Figure 41. Differentiation process analysis of satellite cells isolated from old mice.
Satellite cells from old mice were isolated and differentiated to myotubes for 72 hours. DAPI was used to stain in blue the nuclei of the myotubes, while differentiated myotubes were stained in green with Myosin heavy chain (MyHC) antibody. The differentiation process was determined by following the increase of MyHC expression by immunostaining. Differentiation of satellite cells to myotubes is induced by a reduction in serum concentration. (A) MyHC area and differentiation index. (B) Myotubes length. (C) Branching capacity. Data represent the mean +/- SD. A one-way ANOVA test was applied. P-values <0.05 were considered statistically significant.

Table 16 Statistic analysis of branching in myotubes from old mice

Time point 24 hours					
Branches 2		**Branches 3**		**Branches 4**	
Comparison	**Significance**	**Comparison**	**Significance**	**Comparison**	**Significance**
$Adck2^{+/+}$ vs $Adck2^{+/+}$ CoQ_{10}	ns	$Adck2^{+/+}$ vs $Adck2^{+/+}$ CoQ_{10}	ns	$Adck2^{+/+}$ vs $Adck2^{+/+}$ CoQ_{10}	ns
$Adck2^{+/+}$ vs $Adck2^{+/-}$	ns	$Adck2^{+/+}$ vs $Adck2^{+/-}$	ns	$Adck2^{+/+}$ vs $Adck2^{+/-}$	ns
$Adck2^{+/+}$ vs $Adck2^{+/-}$ CoQ_{10}	ns	$Adck2^{+/+}$ vs $Adck2^{+/-}$ CoQ_{10}	ns	$Adck2^{+/+}$ vs $Adck2^{+/-}$ CoQ_{10}	ns
$Adck2^{+/+}$ CoQ_{10} vs $Adck2^{+/-}$	ns	$Adck2^{+/+}$ CoQ_{10} vs $Adck2^{+/-}$	ns	$Adck2^{+/+}$ CoQ_{10} vs $Adck2^{+/-}$	ns
$Adck2^{+/+}$ CoQ_{10} vs $Adck2^{+/-}$ CoQ_{10}	ns	$Adck2^{+/+}$ CoQ_{10} vs $Adck2^{+/-}$ CoQ_{10}	ns	$Adck2^{+/+}$ CoQ_{10} vs $Adck2^{+/-}$ CoQ_{10}	ns
$Adck2^{+/-}$ vs $Adck2^{+/-}$ CoQ_{10}	ns	$Adck2^{+/-}$ vs $Adck2^{+/-}$ CoQ_{10}	ns	$Adck2^{+/-}$ vs $Adck2^{+/-}$ CoQ_{10}	ns
Time point 48 hours					
Branches 2		**Branches 3**		**Branches 4**	
Comparison	**Significance**	**Comparison**	**Significance**	**Comparison**	**Significance**
$Adck2^{+/+}$ vs $Adck2^{+/+}$ CoQ_{10}	ns	$Adck2^{+/+}$ vs $Adck2^{+/+}$ CoQ_{10}	ns	$Adck2^{+/+}$ vs $Adck2^{+/+}$ CoQ_{10}	ns
$Adck2^{+/+}$ vs $Adck2^{+/-}$	p=0.0100	$Adck2^{+/+}$ vs $Adck2^{+/-}$	p=0.0141	$Adck2^{+/+}$ vs $Adck2^{+/-}$	ns
$Adck2^{+/+}$ vs $Adck2^{+/-}$ CoQ_{10}	ns	$Adck2^{+/+}$ vs $Adck2^{+/-}$ CoQ_{10}	ns	$Adck2^{+/+}$ vs $Adck2^{+/-}$ CoQ_{10}	ns
$Adck2^{+/+}$ CoQ_{10} vs $Adck2^{+/-}$	p=0.0465	$Adck2^{+/+}$ CoQ_{10} vs $Adck2^{+/-}$	ns	$Adck2^{+/+}$ CoQ_{10} vs $Adck2^{+/-}$	ns
$Adck2^{+/+}$ CoQ_{10} vs $Adck2^{+/-}$ CoQ_{10}	ns	$Adck2^{+/+}$ CoQ_{10} vs $Adck2^{+/-}$ CoQ_{10}	ns	$Adck2^{+/+}$ CoQ_{10} vs $Adck2^{+/-}$ CoQ_{10}	ns
$Adck2^{+/-}$ vs $Adck2^{+/-}$ CoQ_{10}	p=0.0005	$Adck2^{+/-}$ vs $Adck2^{+/-}$ CoQ_{10}	p=0.0008	$Adck2^{+/-}$ vs $Adck2^{+/-}$ CoQ_{10}	ns
Time point 72 hours					
Branches 2		**Branches 3**		**Branches 4**	
Comparison	**Significance**	**Comparison**	**Significance**	**Comparison**	**Significance**
$Adck2^{+/+}$ vs $Adck2^{+/+}$ CoQ_{10}	ns	$Adck2^{+/+}$ vs $Adck2^{+/+}$ CoQ_{10}	ns	$Adck2^{+/+}$ vs $Adck2^{+/+}$ CoQ_{10}	ns
$Adck2^{+/+}$ vs $Adck2^{+/-}$	ns	$Adck2^{+/+}$ vs $Adck2^{+/-}$	p=0.0035	$Adck2^{+/+}$ vs $Adck2^{+/-}$	ns
$Adck2^{+/+}$ vs $Adck2^{+/-}$ CoQ_{10}	ns	$Adck2^{+/+}$ vs $Adck2^{+/-}$ CoQ_{10}	ns	$Adck2^{+/+}$ vs $Adck2^{+/-}$ CoQ_{10}	ns
$Adck2^{+/+}$ CoQ_{10} vs $Adck2^{+/-}$	p=0.0401	$Adck2^{+/+}$ CoQ_{10} vs $Adck2^{+/-}$	p=0.0271	$Adck2^{+/+}$ CoQ_{10} vs $Adck2^{+/-}$	ns
$Adck2^{+/+}$ CoQ_{10} vs $Adck2^{+/-}$ CoQ_{10}	ns	$Adck2^{+/+}$ CoQ_{10} vs $Adck2^{+/-}$ CoQ_{10}	ns	$Adck2^{+/+}$ CoQ_{10} vs $Adck2^{+/-}$ CoQ_{10}	ns
$Adck2^{+/-}$ vs $Adck2^{+/-}$ CoQ_{10}	p=0.0210	$Adck2^{+/-}$ vs $Adck2^{+/-}$ CoQ_{10}	p=0.0099	$Adck2^{+/-}$ vs $Adck2^{+/-}$ CoQ_{10}	ns

To quantify the differentiation process over time, we also correlated these parameters over time to calculate the slope of the line as a marker to measure the velocity of differentiation (Table 17). Myotubes from old mutant mice present a much slower slope compared to wild type in all the parameters analysed. And again, the differentiation was improved under the CoQ_{10} administration.

Table 17 Differentiation analysis in myotubes from old mice

Parameter: MyHC area		
Group	The slope of the line	R squared on the graph
Adck2$^{+/+}$	0.0913	$R^2 = 0.617$
Adck2$^{+/+}$ +CoQ_{10}	0.0724	$R^2 = 0.583$
Adck2$^{+/-}$	0.0383	$R^2 = 0.2971$
Adck2$^{+/-}$ +CoQ_{10}	0.0493	$R^2 = 0.4292$
Parameter: Differentiation Index		
Group	The slope of the line	R squared on the graph
Adck2$^{+/+}$	0.4199	$R^2 = 0.7942$
Adck2$^{+/+}$ +CoQ_{10}	0.3087	$R^2 = 0.8805$
Adck2$^{+/-}$	0.3498	$R^2 = 0.6258$
Adck2$^{+/-}$ +CoQ_{10}	0.2004	$R^2 = 0.3784$
Parameter: Myotubes length		
Group	The slope of the line	R squared on the graph
Adck2$^{+/+}$	2.2062	$R^2 = 0.5995$
Adck2$^{+/+}$ +CoQ_{10}	1.8922	$R^2 = 0.5727$
Adck2$^{+/-}$	0.6097	$R^2 = 0.1867$
Adck2$^{+/-}$ +CoQ_{10}	2.4841	$R^2 = 0.9203$
Parameter: Ramificated myotubes		
Group	The slope of the line	R squared on the graph
Adck2$^{+/+}$	0.4264	$R^2 = 0.6259$
Adck2$^{+/+}$ +CoQ_{10}	0.4835	$R^2 = 0.6755$
Adck2$^{+/-}$	0.1382	$R^2 = 0.1292$
Adck2$^{+/-}$ +CoQ_{10}	0.5153	$R^2 = 0.6430$

On balance, these results demonstrated that myotubes from old mutant mice presented a delay in differentiation compared with wild type, which led to smaller myotubes, and what is more significant, administration of CoQ_{10} produced an increase in all the differentiation markers analysed.

Mitochondrial respiration in differentiated myotubes from satellite cells

Next, we analysed the mitochondrial respiratory activity in differentiated myotubes from primary SCs obtained from young (Figure 42) and old mice (Figure 43). We analysed in both cases wild type and mutant myotubes, including also cells from mice supplemented with CoQ_{10}. To do that, freshly isolated SCs were directly plated in the chamber of the Seahorse cell culture plate and then differentiated to myotubes in the same plate of the assay. On the day of the assay, myotubes were washed carefully with a washing medium, and once the experiment was complete, cells were trypsinized and collected for protein quantification. So, we performed the analysis on *in vitro* differentiated myotubes from SCs using different energy substrates to stimulate the mitochondrial energetic metabolism, specifically glucose to stimulate the Krebs cycle plus the ETC (Figure 42A and 43A), and palmitoyl-DL-carnitine to stimulate fatty acids oxidation plus the ETC (Figure 42B and 43B).

Myotubes from young mutant mice showed a decrease in oxygen consumption when glucose was used as an energetic substrate (Figure 42A). CoQ_{10} administration restored mitochondrial respiration. However, no differences were found in basal respiration, neither proton leak nor ATP between the different groups studied. Differences were found in the maximum respiratory capacity and the spare capacity, while CoQ_{10} supplementation produced an increase in both parameters in wild type and mutant myotubes.

When fatty acids oxidation was measured, we found a huge decrease in myotubes from mutant mice (reduction of 80%) compared to those from wild type (Figure 42B), corroborating the defect in β-oxidation that we previously described (77). CoQ_{10} supplementation increased 3-times oxygen consumption and the use of palmitoyl as an energetic substrate in mutant myotubes, although the treatment did not get the myotubes to reach the levels of the wild type and the respiration was kept 40% lower. CoQ_{10} supplementation did not affect the respiration of wild type myotubes.

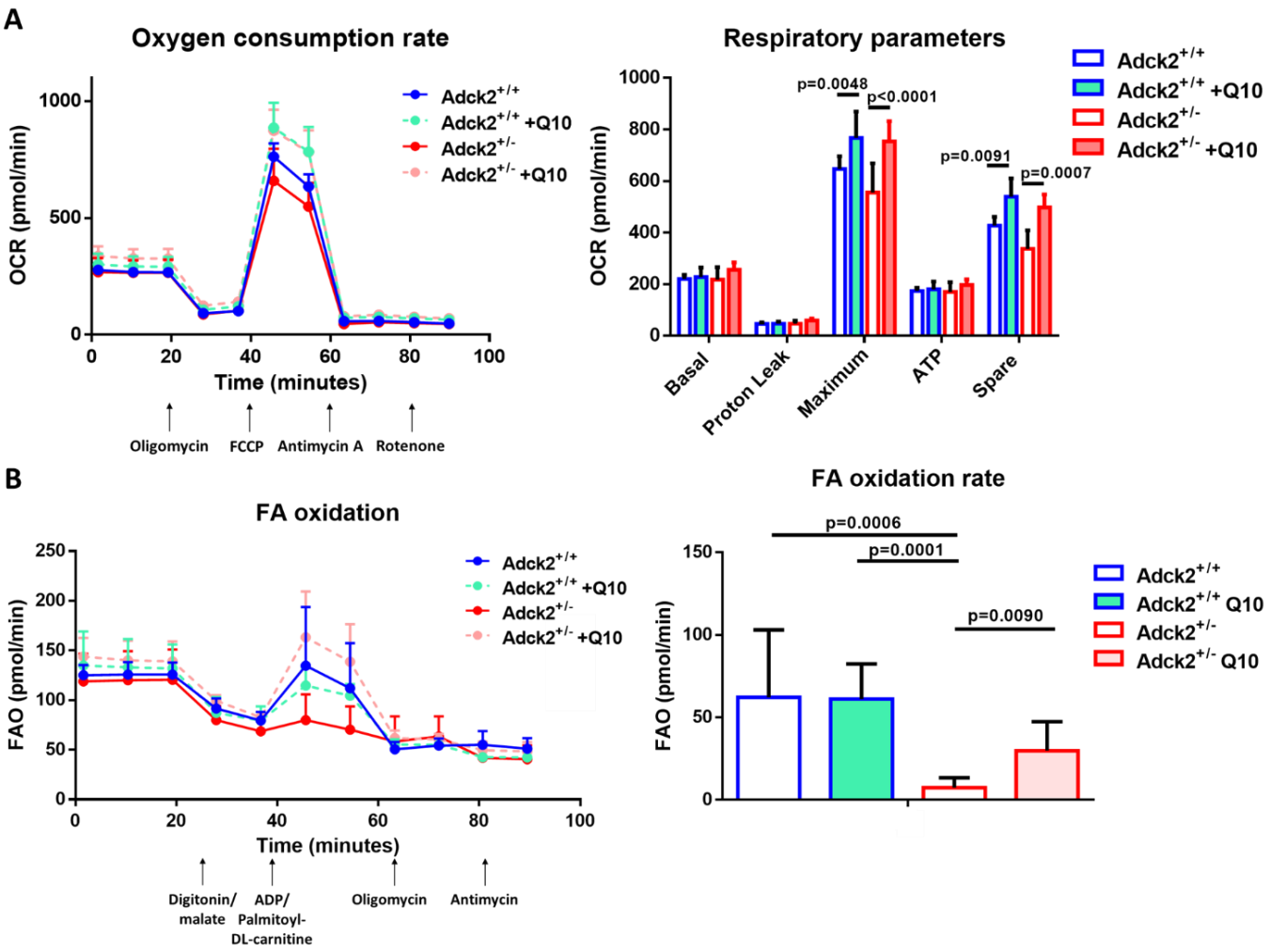

Figure 42. Analysis of mitochondrial respiration in myotubes from young mice.
(A) Oxygen consumption rate in myotubes isolated from young mice. (B) Fatty acids β-oxidation in myotubes isolated from young mice. One representative experiment of two or three independent experiments is shown for each assay. Oxygen consumption studies were performed in a Seahorse XFe24 Analyzer. The final concentration of CoQ_{10} was adjusted to 10 µM and it was replaced every 48 hours. Oligomycin is an inhibitor of complex V. FCCP is a potent mitochondrial oxidative phosphorylation uncoupler. Antimicyn A is an inhibitor of complex III. Rotenone is an inhibitor of complex I. Digitonin was used to permeate the cell plasma membrane. Malate is a Krebs cycle intermediary and an NADH inductor. ADP is a substrate of complex V. Palmitoyl-l-carnitine chloride is a substrate of fatty acids β-oxidation. FA, fatty acids; FAO, fatty acids oxidation; OCR, oxygen consumption rate; FCCP, Carbonyl cyanide-p-trifluoromethoxyphenylhydrazone. Data represent the mean +/- SD. One-way or two-way ANOVA tests were applied. P-values <0.05 were considered statistically significant.

These differences got bigger when myotubes from old mutant mice were analysed. The oxygen consumption rate using glucose as energy substrate demonstrated that mutant myotubes from old mice have practically no basal respiration nor proton leak as OCR kept linear after the addition of the inhibitors (Figure 43A). Also, the maximum respiration was 3-times lower than control and there was no ATP production, whereas the spare capacity was reduced to half the value shown by wild type myotubes. CoQ_{10} supplementation restored all these parameters allowing mutant myotubes to reach the wild type values. CoQ_{10} supplementation also improved these parameters in wild type myotubes.

We also found a huge reduction when palmitoyl was used as an energetic substrate (Figure 43B). In contrast, myotubes obtained from old mice supplemented with CoQ_{10} experimented with an improvement in mitochondrial respiration and practically reached the wild type values.

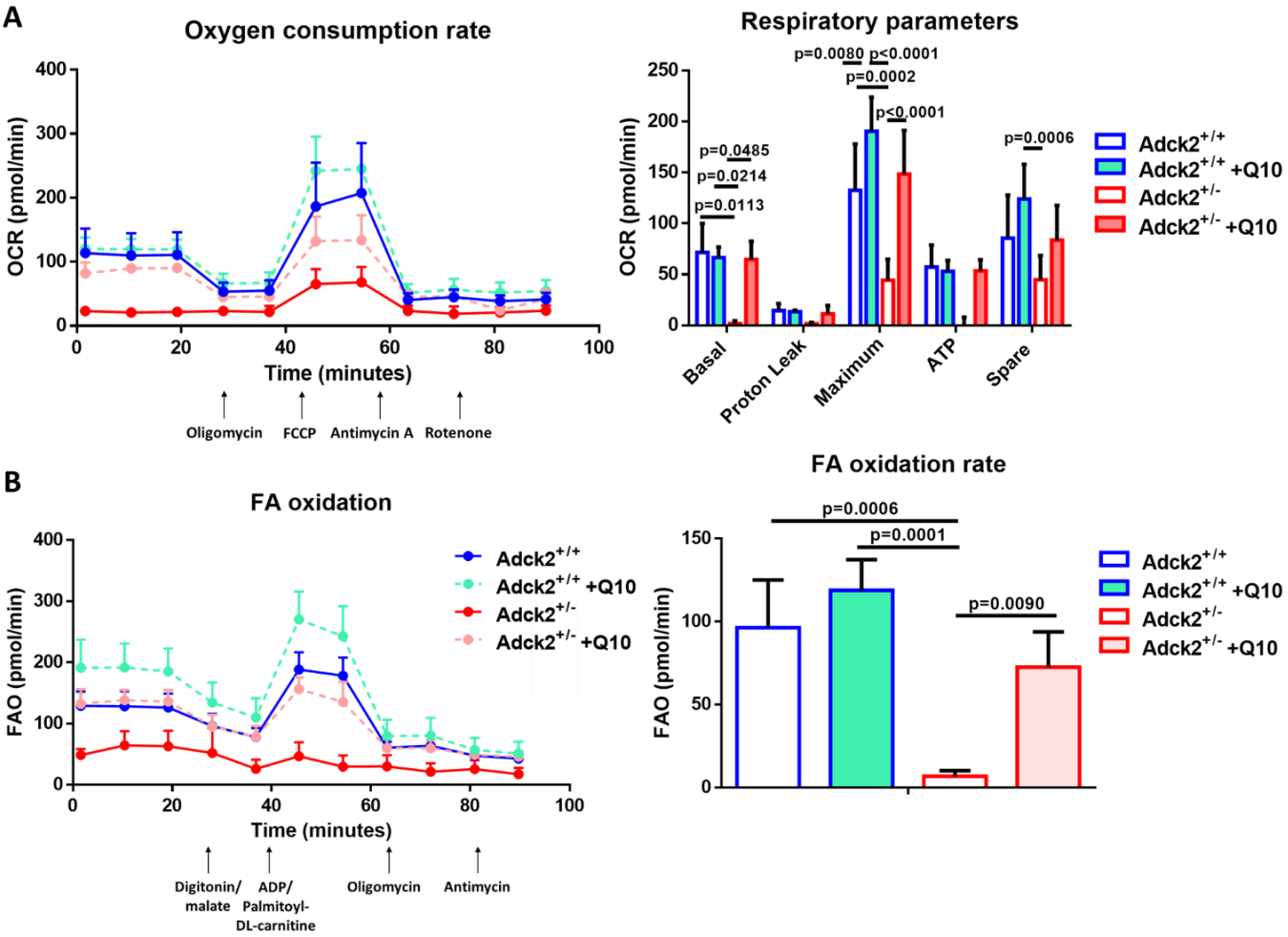

Figure 43 Analysis of mitochondrial respiration in myotubes from old mice

(A) Oxygen consumption rate in myotubes in myotubes isolated from young mice. (B) Fatty acids β-oxidation in myotubes isolated from young mice. One representative experiment of two or three independent experiments is shown for each assay. Oxygen consumption studies were performed in a Seahorse XFe24 Analyzer. The final concentration of CoQ_{10} was adjusted to 10 µM and it was replaced every 48 hours. Oligomycin is an inhibitor of complex V. FCCP is a potent mitochondrial oxidative phosphorylation uncoupler. Antimicyn A is an inhibitor of complex III. Rotenone is an inhibitor of complex I. Digitonin was used to permeate the cell plasma membrane. Malate is a Krebs cycle intermediary and an NADH inductor. ADP is a substrate of complex V. Palmitoyl-l-carnitine chloride is a substrate of fatty acids β-oxidation. FA, fatty acids; FAO, fatty acids oxidation; OCR, oxygen consumption rate; FCCP, Carbonyl cyanide-p-trifluoromethoxyphenylhydrazone. Data represent the mean +/- SD. One-way or two-way ANOVA tests were applied. P-values <0.05 were considered statistically significant.

Analysing all these results together, differences seem to be bigger in old mice, suggesting that ageing could be making the phenotype in mutant cells more severe. On balance, mutant myotubes present a defect in oxygen consumption using glucose or palmitoyl as substrates and the defect is clearer when we analysed myotubes isolated from old mice. Interestingly myotubes

treated with CoQ_{10} that were isolated from mutant mice treated with CoQ_{10} showed an increase in respiration using both substrates.

***In vivo* assessment of postnatal myogenesis in young and old mice**

We have demonstrated that the myogenesis was altered in mutant myotubes. To evaluate if the myogenesis process is compromised *in vivo*, we analysed the regeneration process after skeletal muscle damage fourteen days after $BaCl_2$ injection. As it was mentioned before, $BaCl_2$ injection into the skeletal muscle induced skeletal muscle damage and regeneration. $BaCl_2$ mimics the pathological elevations of intracellular Ca^{2+}, induces massive necrosis of myofibers, and migration of neutrophils and macrophages that lead to inflammation and subsequent SCs activation, which will grow into the damaged area to regenerate myofibers. Initially, SCs will be activated, proliferate, and differentiate into myotubes. During this process, SCs occupy a central position in the transversal section of the myofiber, being this a signal of regeneration. Finally, the nuclei of matured myotubes in regenerated myofibers will be displaced into the periphery and then myofibers will not show central myonuclei.

To perform the experiments, mice were anaesthetized for $BaCl_2$ injection and when they did not show reflex response, which consists of evaluating if there is a loss of reflex on limb retraction followed by relaxation of the abdominal muscles, then mice were prepared for injection. As we previously found that alteration in *in vitro* studies was bigger when differentiation was assayed for a longer time, we decided to study a later stage of *in vivo* regeneration, so that mice were sacrificed 14 days post-injection (dpi) and TA muscles were dissected for immunostaining analysis. Particularly, we decided to assess the final stage of the regenerative process by analysing the presence and the number of central nuclei as markers of skeletal muscle regeneration. Transversal cuts of TA muscle 14 days after $BaCl_2$ injection were stained using dystrophin antibody to show the basal lamina in green, and with DAPI to stain the myonuclei in blue. The whole transversal section was analysed to have a global vision of the muscle during the regeneration process and to avoid problems related to the selection of specific areas of the muscle section. We performed this assay to determine the effect of *ADCK2* mutation over *in vivo* skeletal muscle regeneration and the potential effect of CoQ_{10} administration. Also, as we found that ageing could be a modulator in the severity of the phenotype of our mutant mice, we decided to study 3-month-old young (Figure 44) and 2-year-old mice (Figure 46). Fourteen days after $BaCl_2$ injection, myofibers that did not show central myonuclei could not have been damaged, whereas myofiber with 2, 3 or 4 central myonuclei could be in the middle of the regenerative process.

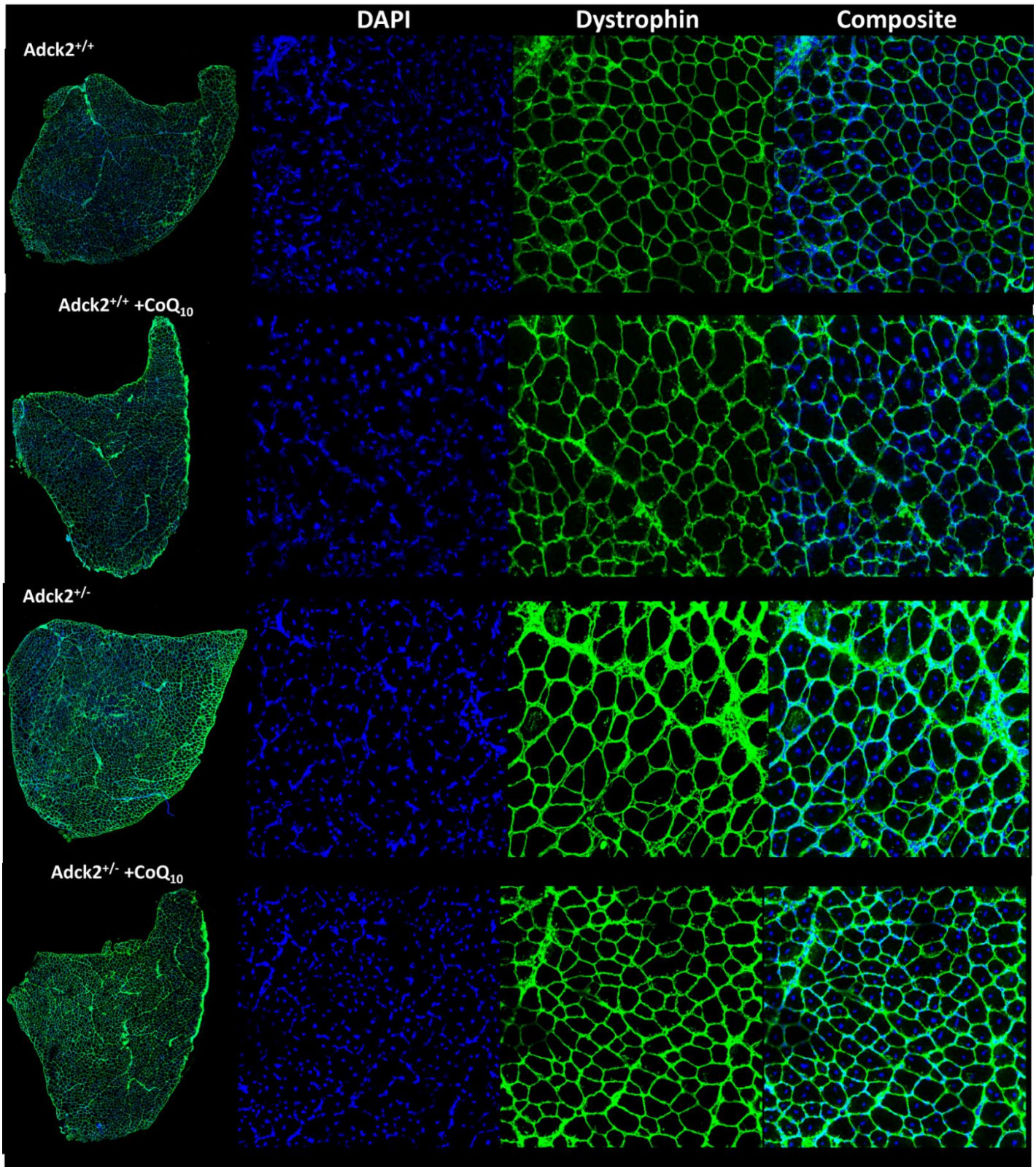

Figure 44. In vivo assessment of satellite cell regeneration capacity in young mice

Representative images. Nuclei of the TA muscle sections were stained with DAPI in blue. The extracellular matrix of the myofiber membrane was stained with an antibody that localizes dystrophin protein in green. When the immunostaining where finished we carried the image acquisition with a Stellaris Confocal Laser Scanning Microscope from Leica, for image analysis we perform an image segmentation analysis that allow us to study every single myofiber of the whole skeletal muscle section (2000-2500 myofibers per muscle) and for myonuclei quantification, we used a Fiji macro by which we can isolate and quantify the number of central myonuclei in every single myofiber of our muscle image what ensure an automatic and quick method for analysis. CoQ_{10} in nanoparticles was dissolved in the water bottle, mean CoQ_{10} intake was estimated at 1-1.5 mg/day (33.33-50 mg/kg/day).

Initially in young mice, we did not find differences in the proportion of central myonuclei between wild type and mutant mice because both groups showed the same proportion of myofibers with zero, one, two, three and four central myonuclei (Figure 45A). Nevertheless, we detected that both groups under CoQ_{10} administration presented a lower proportion of myofibers that exhibited two, three or four central myonuclei indicating that CoQ_{10} could be either protecting against skeletal muscle damage or accelerating the dynamics of regeneration.

Later, myofiber cross-sectional area (Figure 45B), ferret diameter (Figure 45C) and perimeter (Figure 45D) were determined in each myofiber that showed no central myonuclei, myofibers that potentially would have been protected from $BaCl_2$. No differences were found between wild type and mutant mice under standard conditions, but interestingly an increase in cross-sectional area, ferret diameter and perimeter were found in mice supplemented with CoQ_{10}. The increase in the skeletal muscle size could be an indicator of accelerated skeletal muscle regeneration or higher protection against muscle damage under CoQ_{10} administration.

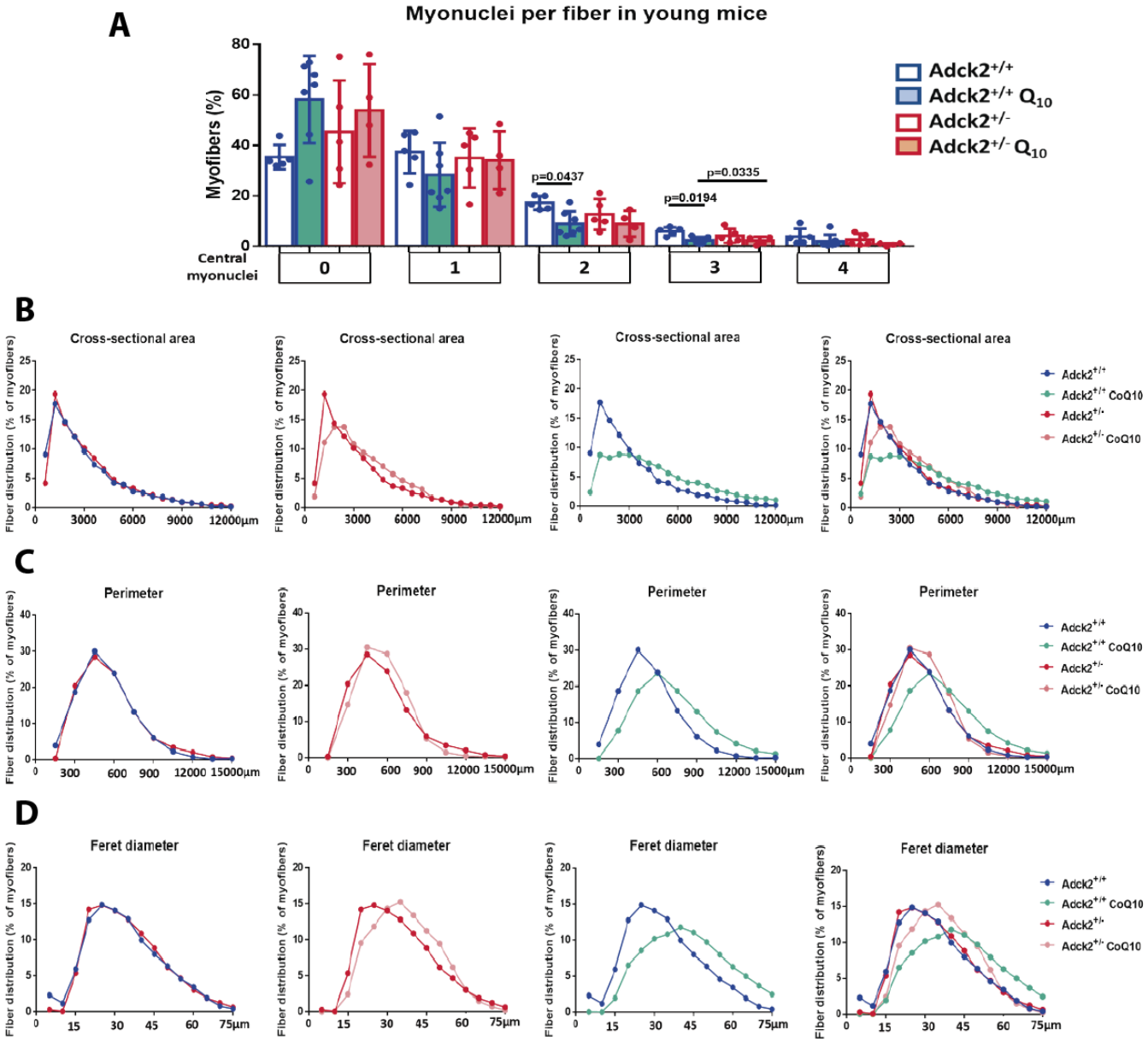

Figure 45. Distribution of central myonuclei and size analysis of myofibers with no central myonuclei in young mice.
(A) Distribution of central myonuclei. Nuclei of the TA muscle sections were stained with DAPI in blue. The extracellular matrix of the myofiber membrane was stained with an antibody that localizes dystrophin protein in green. Figures 40B, C and D also show the analysis of the myofibers size of myofibers that no present central myonuclei and are considered matured regenerated myofibers. (B) CSA in young mice. (C) Feret diameter in young mice. (D) Perimeter in young mice. Data represent the mean +/- SD. A one-way ANOVA test was applied. P-values <0.05 were considered statistically significant.

Additionally, we decided to perform the same experiment using two-year-old mice to analyse the response of our old heterozygous *Adck2* knockout mice to $BaCl_2$ injection and also the effect of longitudinal CoQ_{10} administration in response to skeletal muscle damage in old mice (Figure 46).

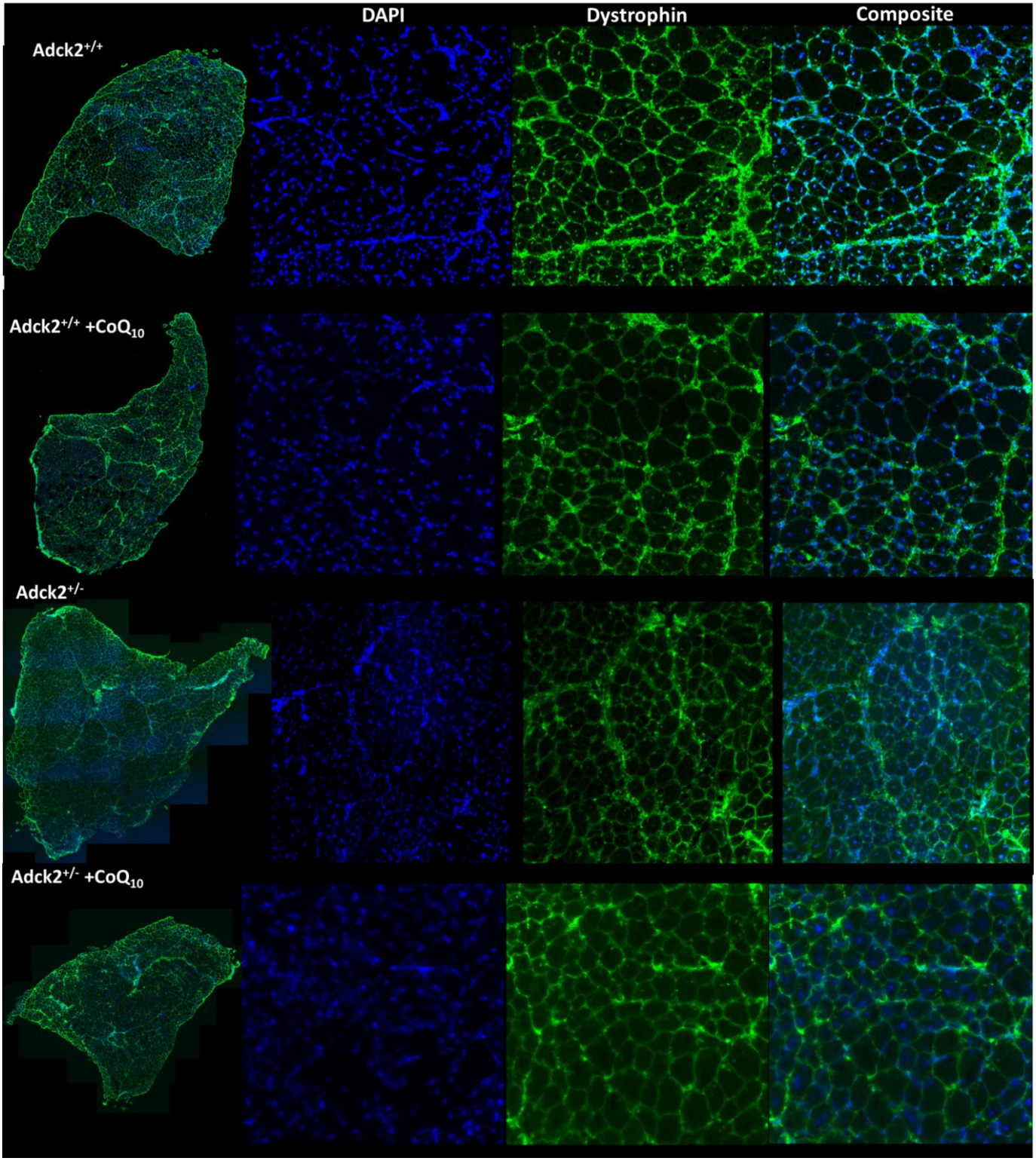

Figure 46. In vivo assessment of satellite cell regeneration capacity in old mice.

Representative images. Nuclei of the TA muscle sections were stained with DAPI in blue. The extracellular matrix of the myofiber membrane was stained with an antibody that localizes dystrophin protein in green. When the immunostaining where finished we carried the image acquisition with a Stellaris Confocal Laser Scanning Microscope from Leica, for image analysis we perform an image segmentation analysis that allow us to study every single myofiber of the whole skeletal muscle section (2000-2500 myofibers per muscle) and for myonuclei quantification, we used a Fiji macro by which we can isolate and quantify the number of central myonuclei in every single myofiber of our muscle image what ensure an automatic and quick method for analysis. CoQ_{10} in nanoparticles was dissolved in the water bottle, mean CoQ_{10} intake was estimated at 1-1.5 mg/day (33.33-50 mg/kg/day).

The proportion of central myonuclei in old mice after 14 days post $BaCl_2$ injection showed that mutant mice presented a higher proportion of myofiber with 2, 3 or 4 central myonuclei compared with wild type mice, whereas mutant mice supplemented with CoQ_{10} presented a lower proportion of myofiber with 2, 3 or 4 central myonuclei (Figure 47A). No differences were found between mutant mice under CoQ_{10} treatment and wild type animals. These results suggest that a higher proportion of myofibers from mutant animals are still in the regeneration process while a higher proportion of myofibers from both wild type and mutant mice under CoQ_{10} administration have been regenerated or another explanation could be that fewer myofibers have been damaged by $BaCl_2$ under CoQ_{10} supplementation.

Also, myofiber cross-sectional area (Figure 47B), ferret diameter (Figure 47C) and perimeter (Figure 47D) were determined in each myofiber that showed no central myonuclei. And again, no differences were found between wild type and mutant mice under standard conditions, but interestingly an increase in cross-sectional area, ferret diameter, and perimeter were found in mice supplemented with CoQ_{10}. These results could indicate that the accelerated skeletal muscle regeneration was maintained through ageing in mice under CoQ_{10} supplementation.

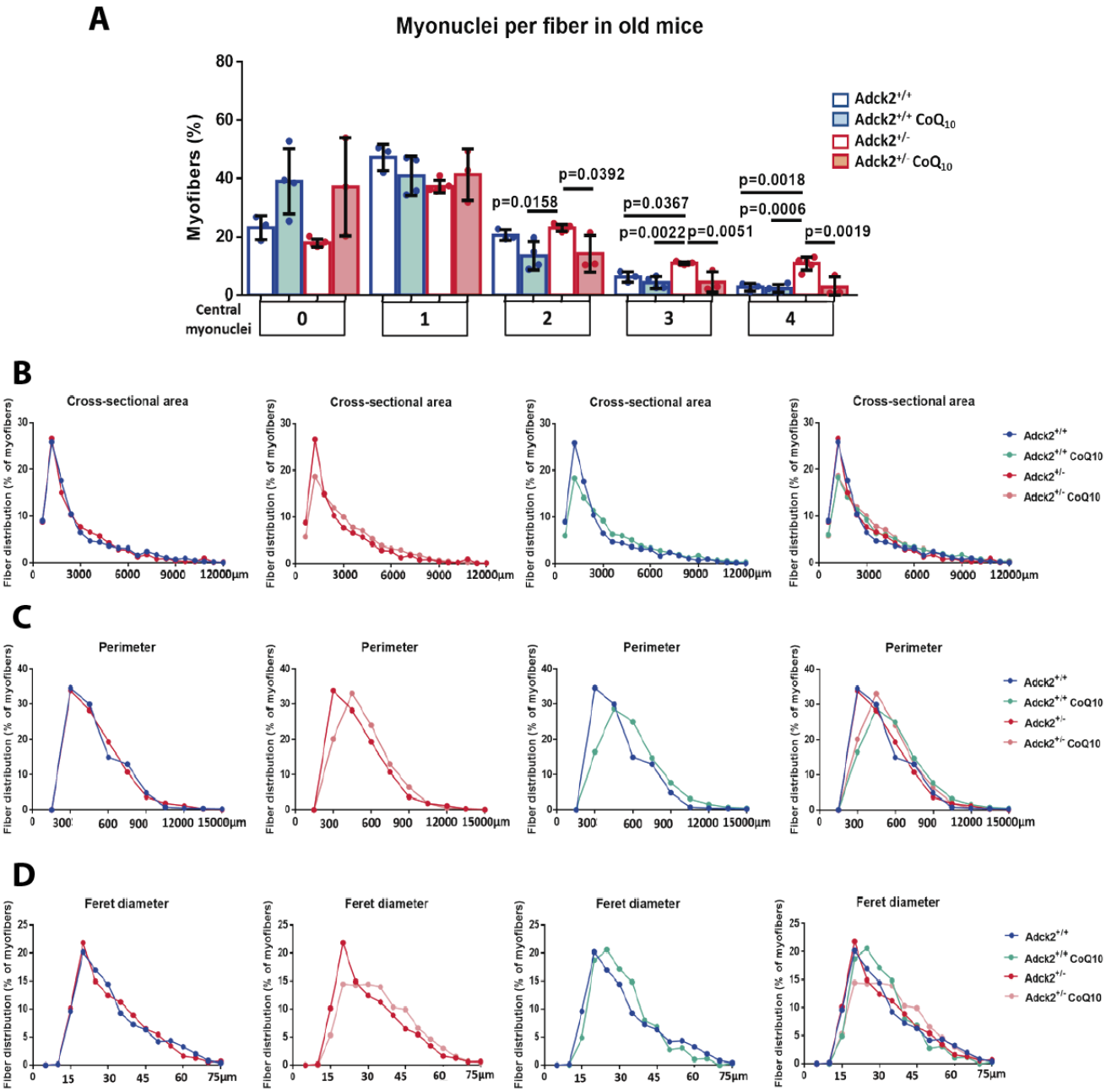

Figure 47 Distribution of central myonuclei and size analysis of myofibers with no central myonuclei in old mice.
(A) Distribution of central myonuclei. Nuclei of the TA muscle sections were stained with DAPI in blue. The extracellular matrix of the myofiber membrane was stained with an antibody that localizes dystrophin protein in green. Figures 47B, C and D also show the analysis of the myofibers size of myofibers that no present central myonuclei and are considered matured regenerated myofibers. (B) CSA in young mice. (C) Feret diameter in young mice. (D) Perimeter in young mice. Data represent the mean +/- SD. A one-way ANOVA test was applied. P-values <0.05 were considered statistically significant.

4.2.2 Discussion of chapter 2:

The present chapter studied myogenesis using adult muscle stem cells as a model where the focus was to determine if alterations reported during embryonic myogenesis shown in the first chapter would be reflected in postnatal myogenesis.

We studied SCs when they are still attached to myofibers to quantify the number and status of SCs in young and old mice. After that, we isolated SCs and seeded them in a proliferative medium that contains a high serum concentration. SCs were distinguished because they were Pax7 positive. We plated freshly SCs in a medium containing low serum to study the differentiation process through several markers of myotubes differentiation, growth and ramification. As we found differences during differentiation, we decided to perform bioenergetic analysis in these cells, particularly, we chose to focus on respiration assays using different energetic substrates to stimulate the Krebs cycle plus the ETC using glucose as substrate in the medium of the assay or inciting β-oxidation plus the ETC using palmitoyl-L-carnitine as substrate. Finally, as we discovered some differences in the last stages of myotubes differentiation probably associated with the bioenergetic defect previously described in the mutant mice, we decided to support our *in vitro* results with an *in vivo* experiment where we injected $BaCl_2$ in the TA muscle and after fourteen days mice were sacrificed, and the regeneration status was examined. We chose a later stage of *in vivo* regeneration experiment because differences found in the *in vitro* approach were higher in the later time points studied.

A previous study reported that SCs isolated from patients that suffer facioscapulohumeral muscular dystrophy (FSHD) presented a defective myogenic differentiation leading to smaller myotubes (167), particularly they performed a morphological study of the myotubes showing hypotrophic myotubes with lower MyHC area. More importantly, in our project, we found that myotubes differentiated from SCs of our mutant mice presented a lower MyHC area, but also a lower myotubes length and a reduced branching capacity associated with a ramification defect. Therefore, we think that these data could support the idea that myotubes from mutant mice presented a morphological defect that results in hypotrophic myotubes. The alterations could be associated with the defect reported in skeletal muscle formation during embryonic development setting a reflection of embryonic myogenesis in our postnatal myogenesis approximation. Besides, the differences reported were higher in myotubes from old mice indicating that skeletal muscle from mutant old mice has a more severe phenotype suggesting the idea that ageing could be an important factor in the phenotype of our heterozygous *Adck2* knockout mice.

In addition, the same study conducted a sequencing screening during the differentiation process of myotubes obtained from FSDH patients to determine the establishment of the disease (167). They reported the suppression of mitochondrial biogenesis through the peroxisome proliferator-activated receptor-gamma coactivator 1-α (PGC1α) as the cause of the hypotrophic phenotype found in the myotubes from FSDH patients. This fact allows us to establish another link between the result found in our *in vitro* differentiation experiments and the results of this study suggesting that a decrease in the CoQ levels together with a defective fatty acids β-oxidation associated with *ADCK2* mutation leads to respiratory chain defects that could be the cause of the hypotrophic status reported in the mutant myotubes.

Also, they reported a screening test to rescue the hypotrophic characteristics of the myotubes using food supplements that counteract the defect found in their RNA-sequencing data, including biochanin A, daidzein, or genistein (167). In our case, as a decrease in CoQ levels has been previously associated with *ADCK2* mutation (77) (178), we decided to dose our SCs with CoQ_{10} using the procedure that we described in the method section. We studied SCs isolated from mice that have been supplemented with CoQ_{10} during their entire life, the SCs have been differentiated under CoQ_{10} administration. CoQ_{10} administration produced an increase in the parameters studied during the differentiation process and recovered the hypotrophic phenotype, suggesting the idea that CoQ_{10} administration improved the postnatal myogenesis defect report in our model.

To explain the mechanism by which mutant myotubes present a hypotrophic phenotype, a recent article suggests that the cause could be the metabolism of SCS and how it has to shift from glycolytic to oxidative as the SCs proliferate and differentiate into myotubes (177). Indeed, they first proposed that the metabolism of SCs has an impact on regeneration, muscle disorders, and ageing, and described that muscle SCs in proliferation present a glycolytic metabolism that switches to oxidative when they differentiate, including oxidative phosphorylation and β-oxidation (179) (180), and second, that mitochondrial oxidative metabolism could function as an indicator of differentiating state of stem cells and as a modulator of the stem cell fate.

The metabolism of SCs and how it shifts from glycolytic to oxidative as the SCs proliferate and differentiate into myotubes are summarized in Figure 48. Initially, the activation of SCs from quiescence to proliferation is associated with a metabolic reprogramming from fatty acids utilization to glycolysis characterised by a decrease in intracellular levels of $NAD(^{+})$ and the function of the histone deacetylase SIRT1 where alteration of this metabolic switch could impaired myofiber size and muscle regeneration (181). Additionally, quiescent stem cells

present activated genes related to fatty acids transport into the mitochondria and β-oxidation while genes involved in glycolysis are repressed. Moreover, fatty acids oxidation is associated with a low metabolic rate sustaining muscle stem cell regeneration capacity. Deregulation of fatty acids oxidation incite overproduction of ROS connected with a premature myotubes differentiation resulting in a hypotrophy phenotype, a reduction in differentiation markers and skeletal muscle regeneration impairment (182).

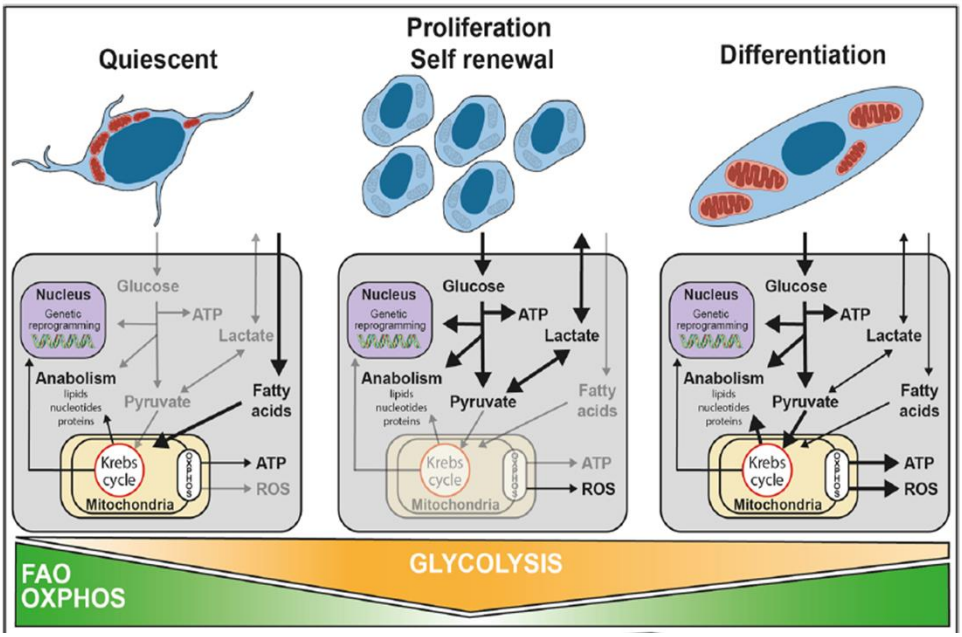

Figure 48. Myogenic metabolism of satellite cells during quiescence, activation, proliferation and differentiation.
Figure 49 shows the metabolic pathways used by satellite cells in quiescent, proliferation and differentiation. Quiescent satellite cells display an oxidative metabolism that mainly relies on fatty acids β-oxidation in the mitochondria leading to the synthesis of ATP, lipids, nucleotides and proteins. Satellite cells on proliferation are more dependent on glycolytic metabolism where glucose is the main substrate used to produce ATP, pyruvate, lactate and anabolic reactions. Proliferative cells show a non-active mitochondrion in this particular state. Satellite cells on differentiation show an increase in dependency on oxidative pathways where mitochondria are activated and fuelled by different substrates (Adapted from (177)).

In contrast, SCs in a proliferative state present anaerobic glycolysis associated with activation of anaerobic glycolysis gene expression (181). Besides, the glycolytic component of skeletal muscle stem cell is demonstrated by modulation of glycolysis through inhibition of lactate dehydrogenase (LDH) which result in a decrease in proliferation whereas an increase in the expression of lactate dehydrogenase A- subunit (LDHA) stimulate SCs proliferation and glycolysis (183). In addition during differentiation, myotubes experienced another metabolic switch promoting higher OXPHOS, mitochondrial biogenesis and fatty acids β-oxidation, even an improvement in respiration (181)(177). Besides, during differentiation SCs undergo high energy demands, an increase in mitochondria biogenesis, mitochondria net complexity, alteration of mitochondria ultrastructure that is supported by a more oxidative metabolism (184). An

increase in differentiation coexists with a bigger myofiber mass that required functional mitochondria to support a high energy demand (180).

Our results demonstrate that myotubes from mutant mice are smaller and present an impaired differentiation process compared with myotubes from wild type mice due to the metabolic shift that SCs must perform during differentiation could be compromised for the failure in the activation of OXPHOS and fatty acids oxidation that particularly suffer our mutant mice. Myotubes from mutant mice present lower respiration capacity indicating a defect in the OXPHOS system and fatty acids oxidation and lower metabolic flexibility. And what is more significant, we found that by supplementing the mutant mice and mutant myotubes with CoQ_{10}, we can improve mitochondrial respiration. Mutant plus CoQ_{10} present higher respiration levels using glucose and palmitoyl-L-carnitine as substrates, which results in a partial recovery of the respiration capacity. Fatty acid β-oxidation is crucial for ATP production, particularly during fasting periods, generating acetyl-CoA stimulating different pathways. Fatty acid β-oxidation is associated with the CoQ pool at ETC by the heterodimeric electron-transferring flavoprotein (ETF) and at the heterodimeric electron-transferring flavoprotein dehydrogenase (ETFDH) (185). That could explain why CoQ_{10} administration could improve ETC machinery and the electrons transport from fatty acyl-CoA to complex III.

Furthermore, our findings reported a lower capacity in old mutant myotubes in both assays, indicating that the phenotype is more severe in cells isolated from old mice and that ageing could make the phenotype more severe.

Additionally, we perform an *in vivo* approach to support our *in vitro* data to examine the skeletal muscle regeneration in our mice, for this purpose we injected $BaCl_2$ into the TA muscle to induce massive necrosis of myofibers and the subsequent migration of neutrophils and macrophages that will generate inflammation and later SCs activation, which will grow into the damaged area to regenerate myofibers (186). We let the mice recover for 14 days to study the later stages of myotubes differentiation where higher differences were found *in vitro.* In parallel, mice assigned to CoQ_{10} administration continued to receive CoQ_{10} during the time of recovery.

During a normal process of muscle regeneration, SCs undergo sequential steps where initially they are activated in response to the damage, proliferate, and differentiate later to replace the damaged myofibers, resulting in small newly formed myofibers with centralized nuclei (135). So, the number of centrally located nuclei is a well-established indicator of myofiber repair (136). Finally, regenerated myofibers do not present central myonuclei and have their peripheral

quiescent SCs for future activation. For that reason, the analysis of the dynamic central position of the myonuclei was used to assess the regeneration process induced by $BaCl_2$.

The result obtained suggests that old mutant mice present an impaired skeletal muscle regeneration which could indicate that mutant mice are more susceptible to muscle damage or that SCs regeneration could be affected. Considering our *in vitro* results, we can propose that myotubes of old mutant mice could present a hypotrophy phenotype that could result in impaired skeletal muscle regeneration, and it could be associated with the bioenergetic defects that we have previously shown with the *in vitro* respiration analysis. More significantly, mice under CoQ_{10} administration showed a profile similar to wild type mice in the dynamic of central myonuclei during skeletal muscle regeneration, with a higher proportion of zero or one central myonuclei and a lower proportion of two, three, or four central myonuclei. These results could indicate that longitudinal CoQ_{10} administration could result in higher protection against skeletal muscle damage and could improve skeletal muscle regeneration. As we demonstrated with our *in vitro* approach, CoQ_{10} administration could be modulating the myotube differentiation process resulting in bigger and more branched myotubes with a better bioenergetic profile, because they showed higher oxygen consumption rate using glucose and palmitoyl-L-carnitine as substrate. Consequently, we believe that CoQ_{10} administration could be improving skeletal muscle regeneration outcoming in a higher proportion of mature myofibers fourteen days after $BaCl_2$ injection.

As a summary, in this chapter, we have evaluated the postnatal myogenesis by *in vitro* and *in vivo* assays in young and old mice under both standard conditions and under CoQ_{10} administration. We obtained that heterozygous *Adck2* knockout mice suffer a defect in postnatal myogenesis, specifically in myotubes differentiation stages, and we showed that the defect is associated with reduced mitochondrial respiration. The results obtained in this chapter allow us to conclude that our heterogenic knockout *Adck2* mice undergo inadequate postnatal myogenesis due to an impairment in the mitochondrial oxidative metabolism.

Chapter 3

4.3 CHAPTER 3: Skeletal muscle decline in *Adck2* mouse associated with ageing.

4.3.1 Introduction

This chapter is focused on understanding the progressive establishment of the phenotype in our heterozygous *Adck2* knockout mice, specifically the skeletal muscle decline associated with ageing. For this objective, we performed experiments to determine skeletal muscle structure and function in young mice (three-month-old) and old mice (two-year-old) because the skeletal muscle was the main tissue affected in these mice (77). We hypothesized that the effect of ageing on muscle, including sarcopenia and skeletal muscle atrophy, could be more evident in mutant mice. A recent study that supports our hypothesis about the progressive decline, described the mutant mice model for PDSS2, which present a primary CoQ deficiency (170). These mutants were healthy at birth and even at 4.5 months old there was no evidence of phenotype associated with ataxia, but slowly develop alterations in the central nervous system and ataxia during adulthood around 1-year-old. This study supports our theory about progressive damage that results in a more severe phenotype during ageing, which could be standard in mitochondrial diseases characterized by a decrease in CoQ levels.

Moreover, due to the potential benefits of a prenatal CoQ_{10} administration during embryonic development described in chapter 1 and the improvement of mitochondrial energy metabolism and muscle stem cell's function described in chapter 2, we decided to perform the longitudinal study under CoQ_{10} administration to check if CoQ_{10} intake could delay the progressive decline that mutant mice could experience through ageing. Furthermore, we have studied mitochondrial function focusing on the analysis of oxygen consumption in isolated mitochondria from skeletal muscle, adding different substrates to the medium to promote different metabolic pathways. For the mitochondrial respiratory analysis, we analysed young and old mutant mice and animals supplemented with CoQ_{10}. There is preliminary evidence, as in senescence-accelerate mouse prone 8 (SAMP8) (187), to suggest a progressive age-associated muscle decline that could be treated with drugs that act on mitochondria, increasing OXPHOS activity and mitochondrial biogenesis. The idea that a supplement that stimulates mitochondrial respiration could preserve skeletal muscle and mitochondrial quality supports the idea that prolonged CoQ_{10} administration could help during the progressive decline that suffers *Adck2* mutant mice.

To our knowledge, this is the first longitudinal study to date that examines the effect of CoQ_{10} administration throughout the whole life of an organism including animals that suffer from

mitochondrial dysfunction syndrome. In this way, our project would report new results about CoQ_{10} treatment in mitochondrial diseases.

The present chapter discusses the progressive skeletal muscle decline in our mutant mice and the mitochondrial dysfunction, for this purpose, we decided to study the ageing process in our mice model focusing on young mice (three-month-old) and old mice (two-year-old mice), although for skeletal muscle function tests adult mice (10-12 month-old) and old adult mice (16-18 month-old) were also included.

General decline associated with ageing in mutant *Adck2* mice

Figure 49 shows the aspect of the mice through ageing, although there was no difference in young mice, old mutant mice were affected by the ageing process in comparison with wild type mice. Old mutant mice seemed to be more affected by ageing presenting bald spots on the fur over the body and the colour of hair was more irregular, supporting our hypothesis that the effect of ageing could be more severe in mutant mice. Moreover, old mutant mice on CoQ_{10} administration have a better aspect than mutant mice, CoQ_{10} administration could protect mutant mice from these effects.

Figure 49. The visual aspect of mice during the ageing process.
(A). Representative images of young mice (3 month-old). (B). Representative images of old mice (2-year-old). Photos of the animals were taken at the animal facility at CABD, UPO. Mice were lain face down to observe all bodies of mice. CoQ_{10} in nanoparticles was dissolved in the water bottle, mean CoQ_{10} intake was estimated at 1-1.5 mg/day (33.33-50 mg/kg/day).

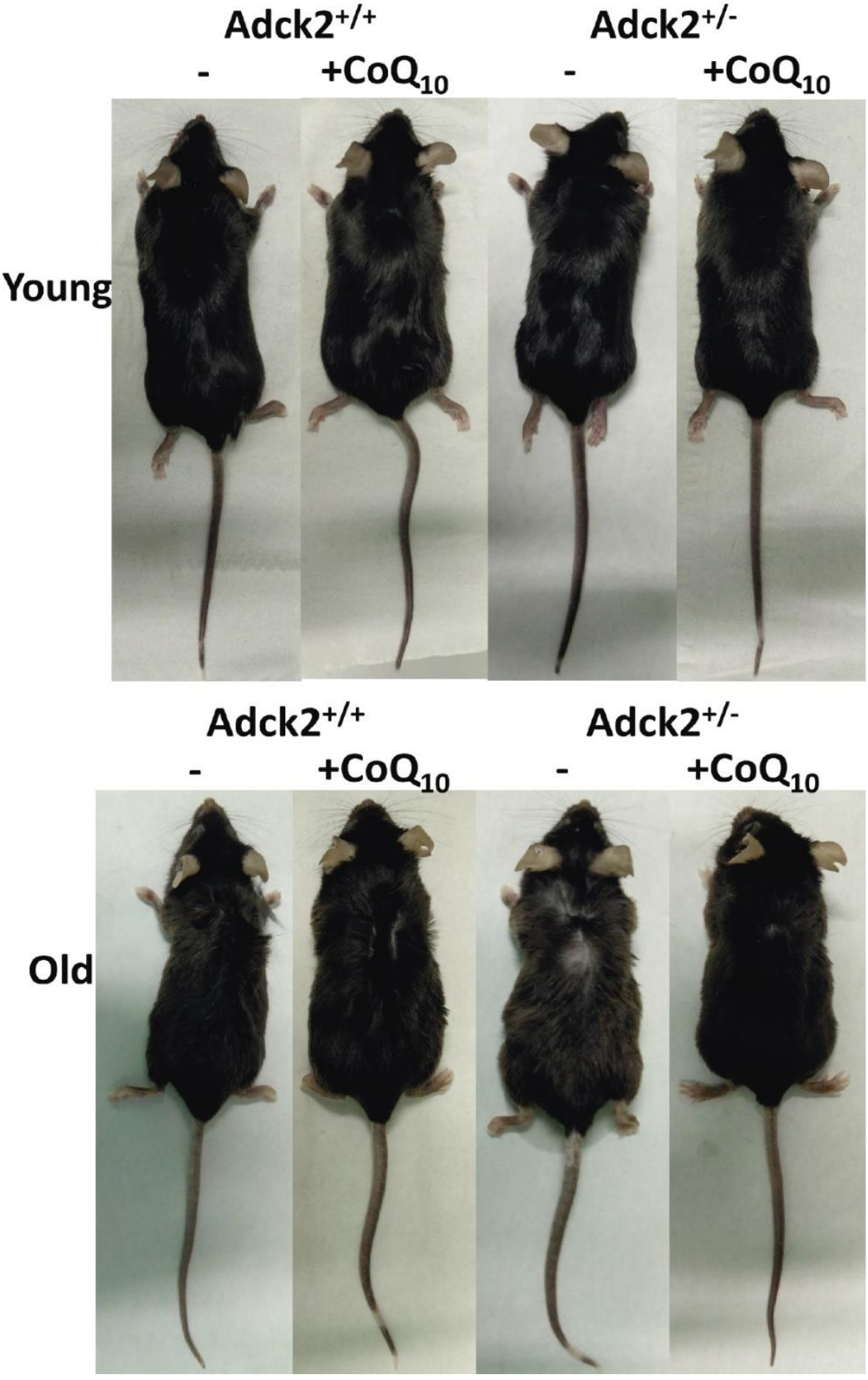
Adck2+/+
Adck2+/-
-
+CoQ10
-
+CoQ10
Young
Adck2+/+
Adck2+/-
-
+CoQ10
-
+CoQ10
Old

Myofiber typing analysis in TA muscle

To understand why heterozygous *Adck2* knockout mice are more affected by the ageing process, we decided to analyse the physiology and anatomy of these animals. Firstly, we focused on the structure of the skeletal muscle because of the myopathy that mutant mice suffer (77). Skeletal muscle is formed by myofibers with distinct morphological, functional and metabolic characteristics and myofibers can be categorised in function of specific features such as contractile speed, metabolic function and MyHC content. Particularly, muscles from mammals presents 4 different MyHC isoforms, three fast isoforms (MyHCIIA, MyHCIIX and MyHCIIB) and one slow isoform (MyHCI) (188). Classification of skeletal muscle myofibers depend on the speed of twitch and the metabolism of the myofibers: type I (slow-twitch and oxidative metabolism), type IIA (fast-twitch and oxidative-glycolytic metabolism), type IIB (fast-twitch and glycolytic metabolism) and type IIX that present intermediate properties between the type IIA and IIB with an intermediate metabolism and fatigue index (189). We studied the myofiber composition in TA muscle of young (Figure 50) and old mice (Figure 52). The staining allows the identification of myofibers type IIA, IIX and IIB. Myofibers type IIA is considered more oxidative while myofibers type IIB are considered more glycolytic. The myofibers type IIX are hybrid myofibers with an intermediate metabolism. We photographed the whole transversal section of the TA muscle and then we selected the same area (2000 um x 2000 um) of each image for quantification of the myofiber composition. The area selected included the red and white area of the TA muscle, so we could study the metabolism and the myofiber composition in both areas.

No significant differences were found in myofiber composition in young mice (Figure 51), but we could only report a tendency by which the mutant mice show a higher proportion of type IIB myofibers, probably because TA muscle from young mutant mice tends to present a more glycolytic metabolism. Additionally, CoQ_{10} administration was able to reverse this tendency, the TA muscle of mutant mice under CoQ_{10} supplementation a similar pattern to wild type mice.

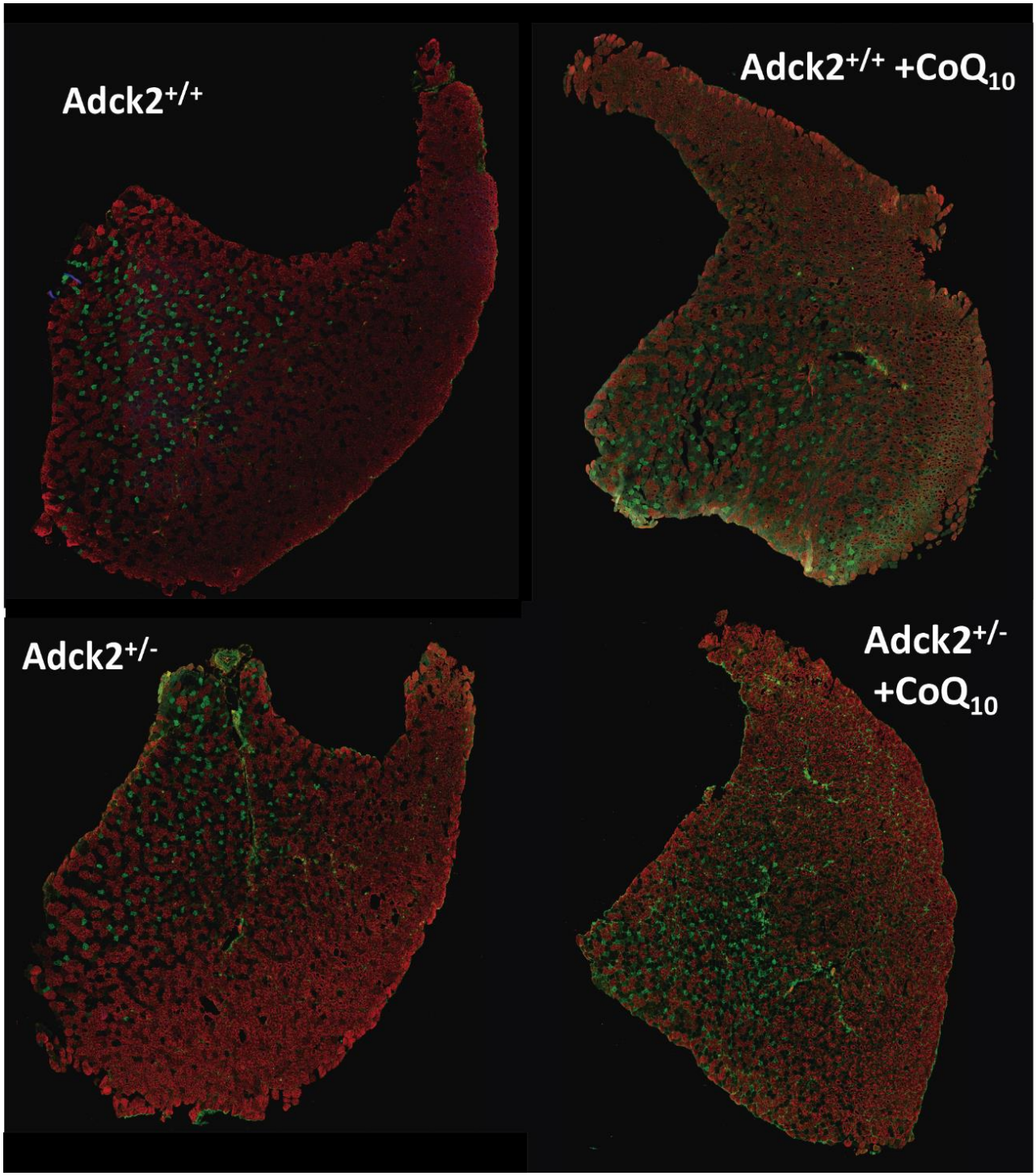

Figure 50. Representative images of myofiber typing in young mice.

Immunostaining analysis to determine myofiber composition in transversal sections from tibialis anterior (TA) muscle from young mice (three-month-old). Myofibers type IIA, IIB and IIX appear in green, in red and in black. Cryosections of TA muscle (12 µm) were used for the immunostaining.

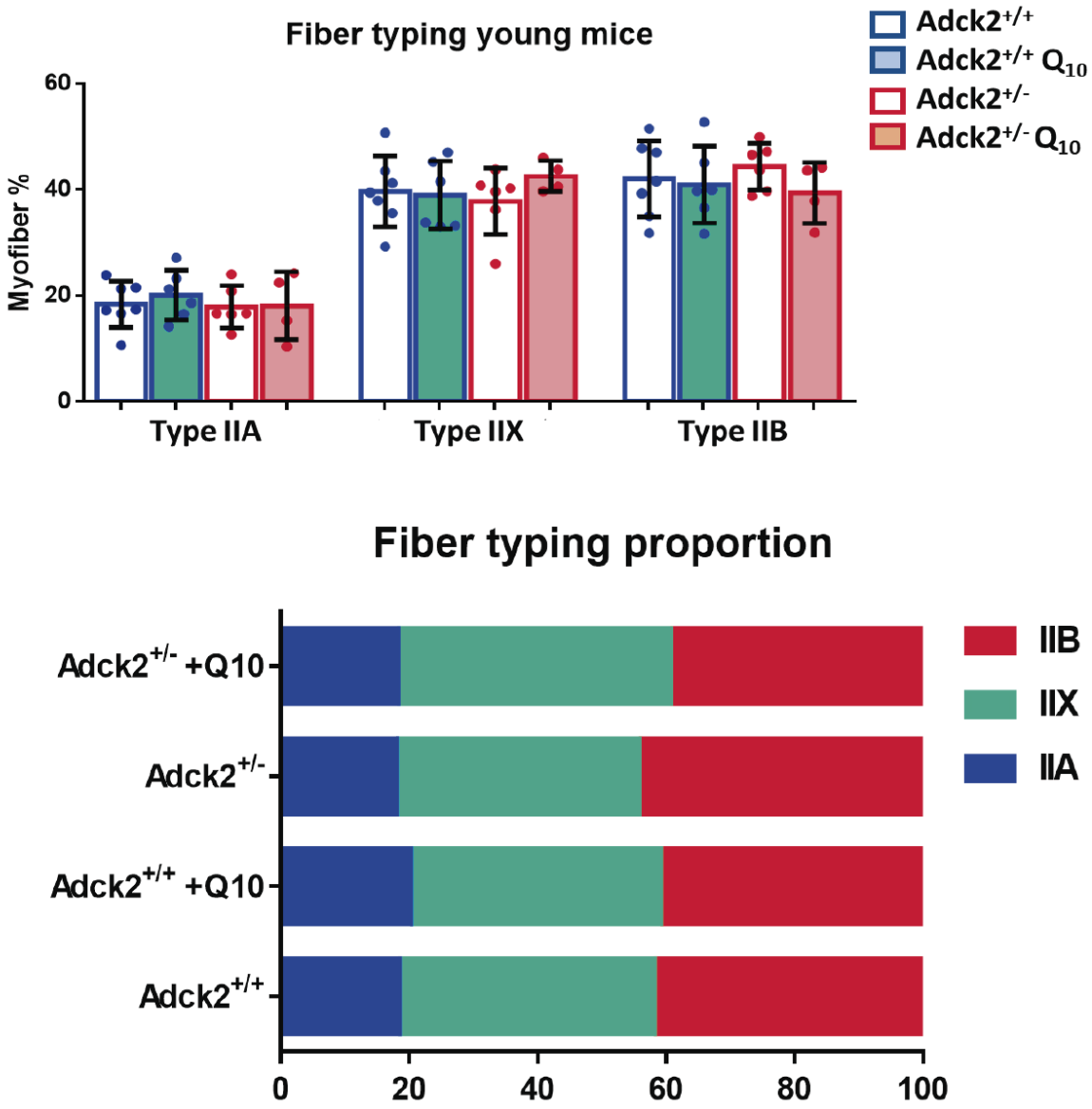

Figure 51 Myofiber typing analysis in TA muscle from young mice
Myofiber composition was analysed in TA muscle from three-month-old mice. Type IIA, IIB and IIX appear in green, red and black. Data represent the mean +/- SD (N=4-7). A one-way ANOVA test was applied. P-values <0.05 were considered statistically significant.

However, old mutant mice showed a decrease in oxidative myofibers type IIA and an increase in hybrid type IIX myofibers (Figure 53). These results demonstrated that old mutant mice have a higher glycolytic myofibers content in the TA muscle compared with old wild type mice. The point that young mutant mice present a higher number of myofibers type IIB while old mutant mice present a higher proportion of hybrid myofibers type IIX and less proportion of oxidative type IIA could indicate that ageing induces a change in myofiber typing in our mutant mice increasing hybrid type IIX myofibers to the detriment of oxidative IIA, probably due to the

impairment of mitochondrial oxidative metabolism. Interestingly, as with young mice, old mutant mice supplemented with CoQ_{10} present a composition similar to wild type mice, demonstrating that CoQ_{10} administration could prevent the myofiber change due to ageing in mutant mice.

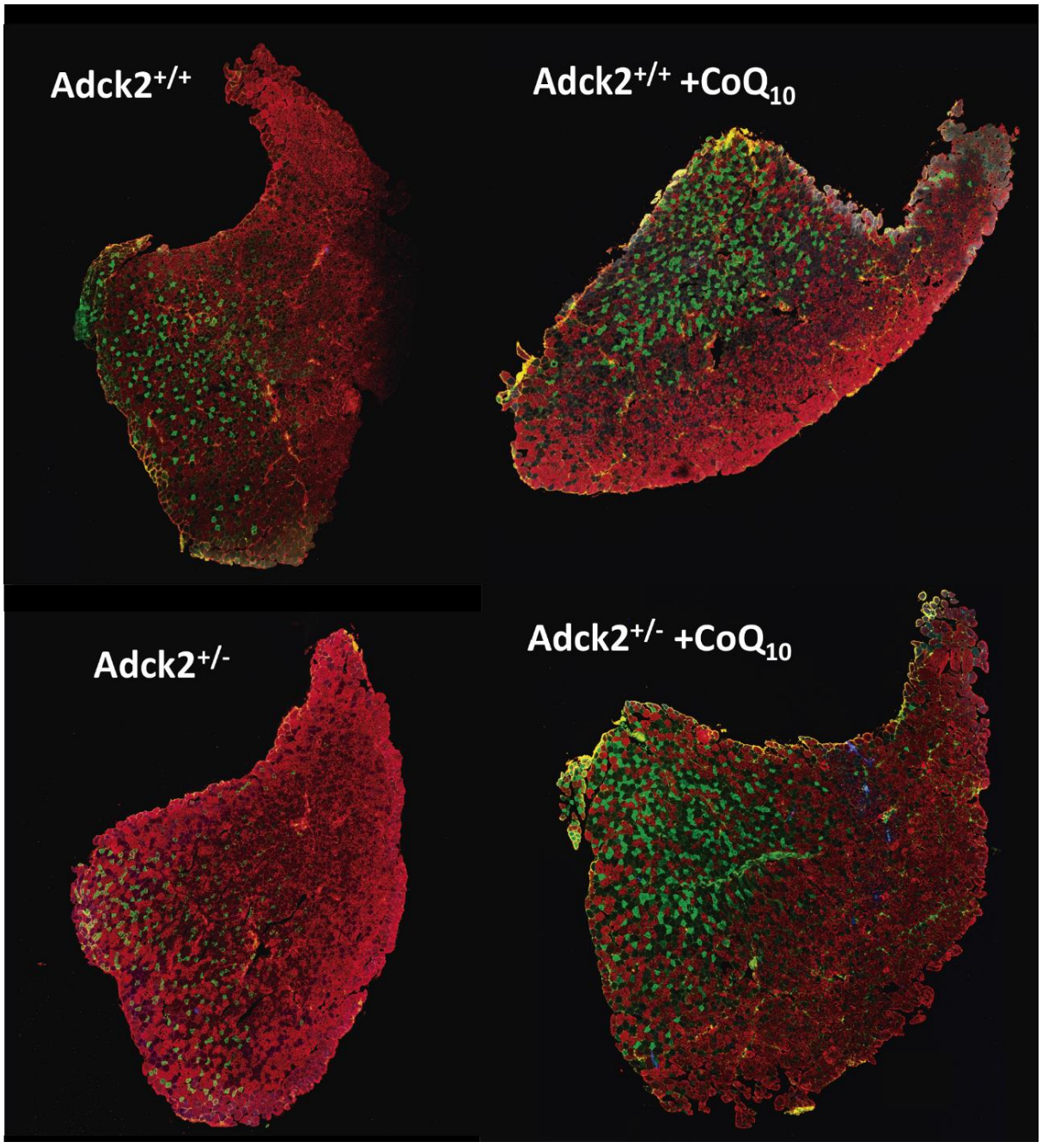

Figure 52. Representative images of myofiber typing in old mice.
Immunostaining analysis to determine myofiber composition in transversal sections from tibialis anterior (TA) muscle from old mice (two-years-old). Myofibers type IIA, IIB and IIX appear in green, in red and in black. Cryosections of TA muscle (12 µm) were used for the immunostaining.

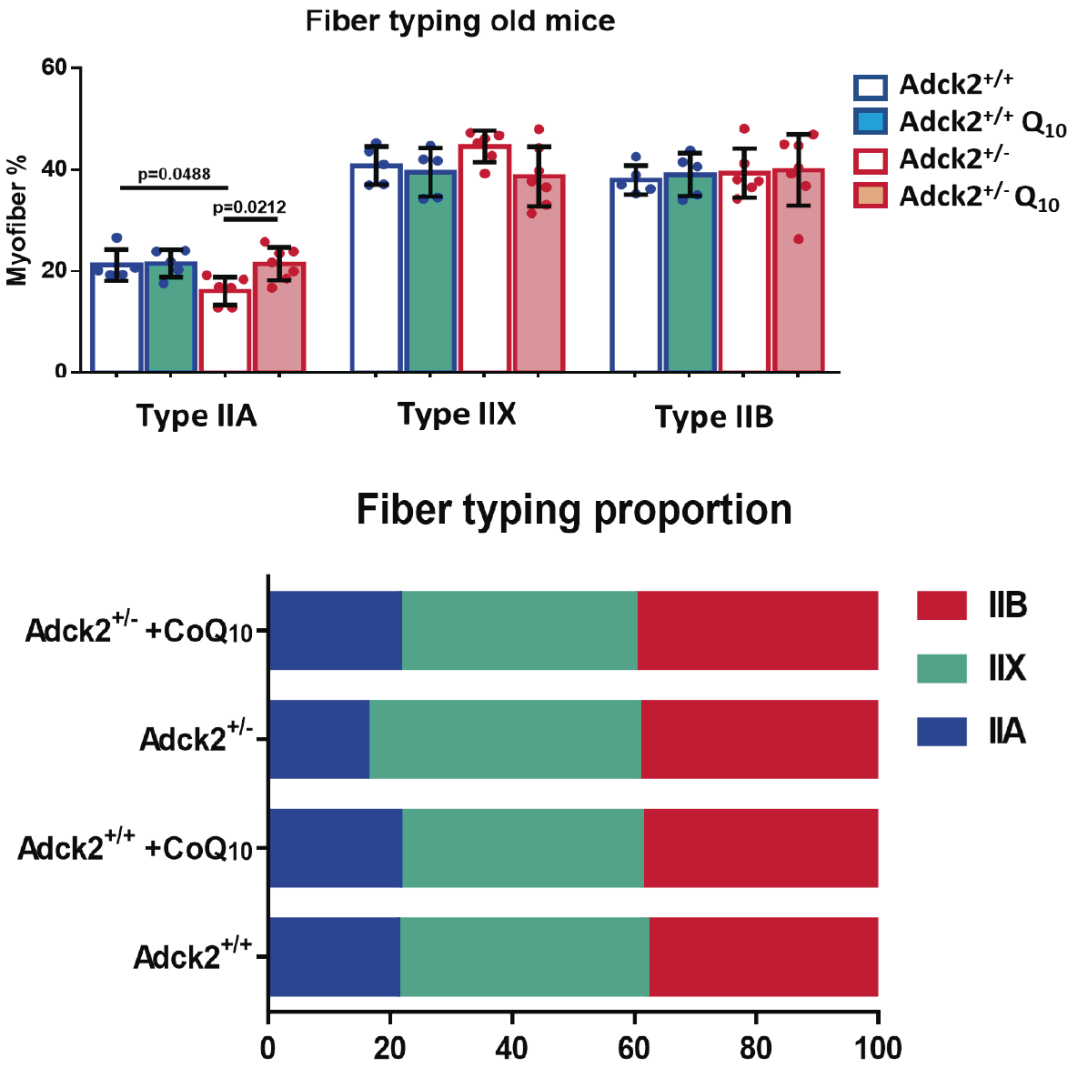

Figure 53 Myofiber typing analysis in TA muscle from old mice

Myofiber composition was analysed in TA muscle from two-years-old mice. Type IIA, IIB and IIX appear in green, red and black. Data represent the mean +/- SD (N=5-7). A one-way ANOVA test was applied. P-values <0.05 were considered statistically significant.

Cross-sectional analysis of TA muscle to determine myofibers size

Next, we performed a cross-sectional analysis of the myofibers of TA muscles. The analysis of myofiber size was performed by staining the basal lamina with dystrophin antibody and myonuclei with DAPI (Figure 54 for young mice and Figure 56 for old mice). After image acquisition in a fluorescence confocal microscope, a segmentation process was done as detailed in the Methods section to examine myofiber size. All the myofibers from the TA muscle were studied, and three parameters were determined for each myofiber: area, diameter and perimeter. However, there were no significant differences in young mice (Figure 55), indicating that there was no difference in the size of the muscle TA.

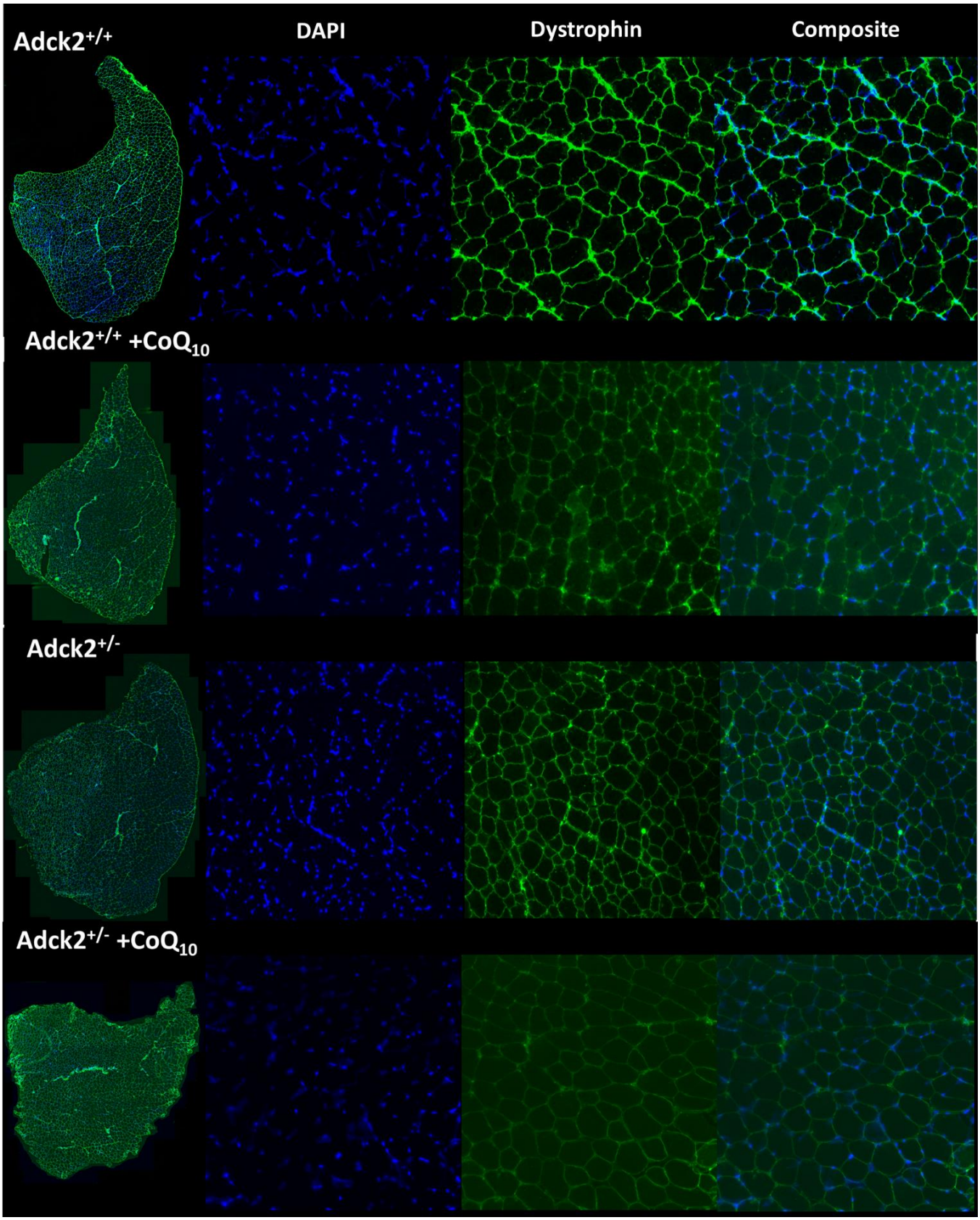

Figure 54. Representative images of tibialis anterior muscle in young mice.
Nuclei of transversal tibialis anterior (TA) muscle sections were stained with DAPI in blue. The extracellular matrix of the myofiber membrane was stained with an antibody that localizes dystrophin protein in green. Image acquisition was carried out in a Stellaris Confocal Laser Scanning Microscope from Leica, for image analysis we perform an image segmentation analysis that allows us to study every single myofiber of the whole skeletal muscle section (2000-2500 myofibers per muscle).

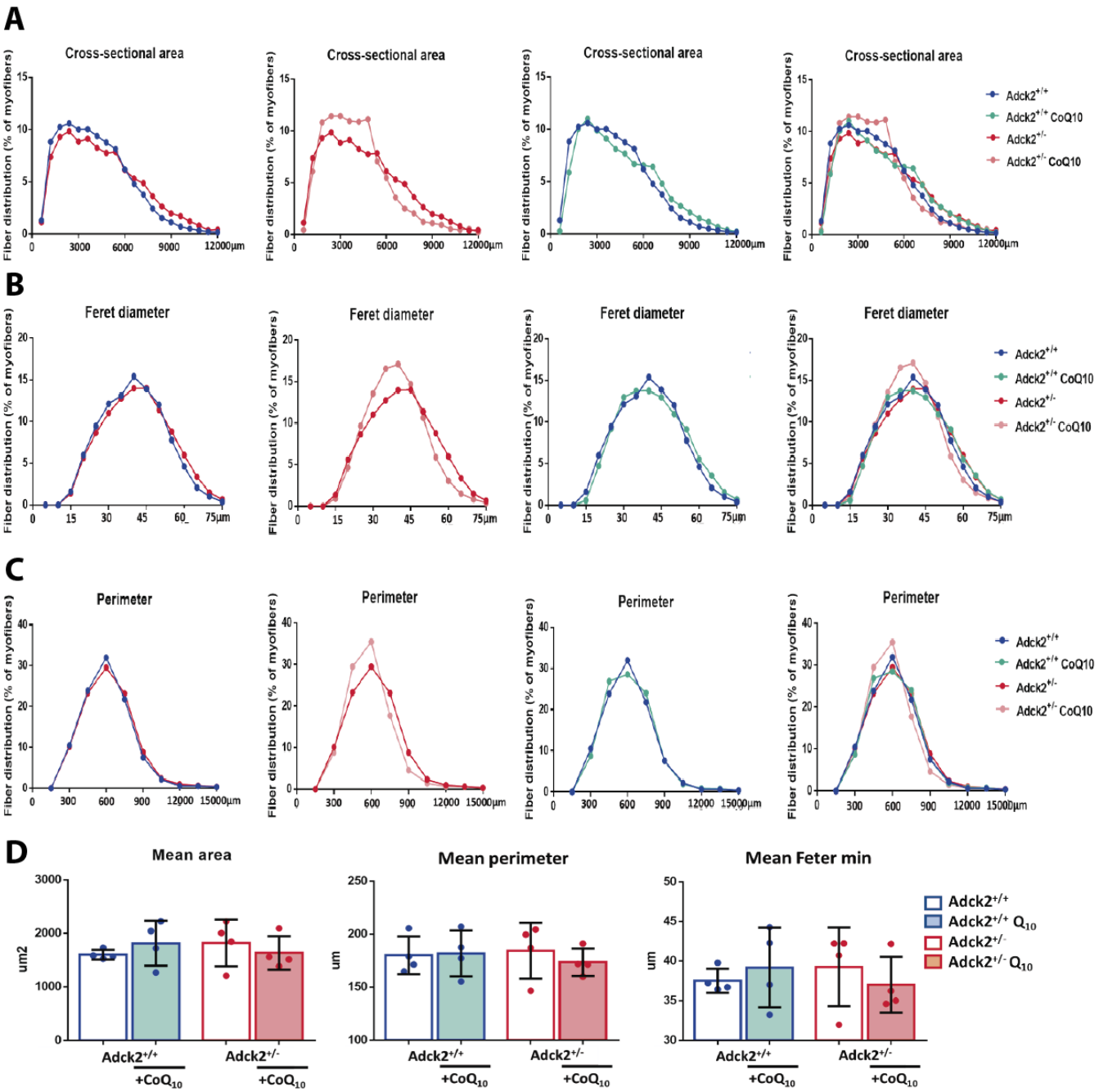

Figure 55. Analysis of myofiber size on transversal cuts from young mice.

(A) Cross-sectional area. (B) Feret diameter. (C) Perimeter. Analysis of 4-5 mice per group. Myofibers basal lamina was stained with dystrophin antibody while nuclei were stained with DAPI. Image acquisitions were performed using a Stellaris Confocal Laser Scanning Microscope from Leica. The whole section of the TA muscle was recorded and all the myofibers from the TA muscle were examined, around 2000-2500 myofibers were quantified and between four or five mice per group were studied. Data represent the mean +/- SD (N=4-5). A one-way ANOVA test was applied. P-values <0.05 were considered statistically significant.

To continue, we analysed the cross-sectional cuts of old mice. We found that the size of myofibers of mutant mice was smaller than myofibers from the wild type, whereas myofibers from old mutant mice under CoQ_{10} administration were bigger than myofibers from mutant mice without treatment and did not show any difference concerning the wild type. So, we can propose that old mutant mice suffer a decrease in myofiber size associated with ageing, which could be avoided under CoQ_{10} supplementation.

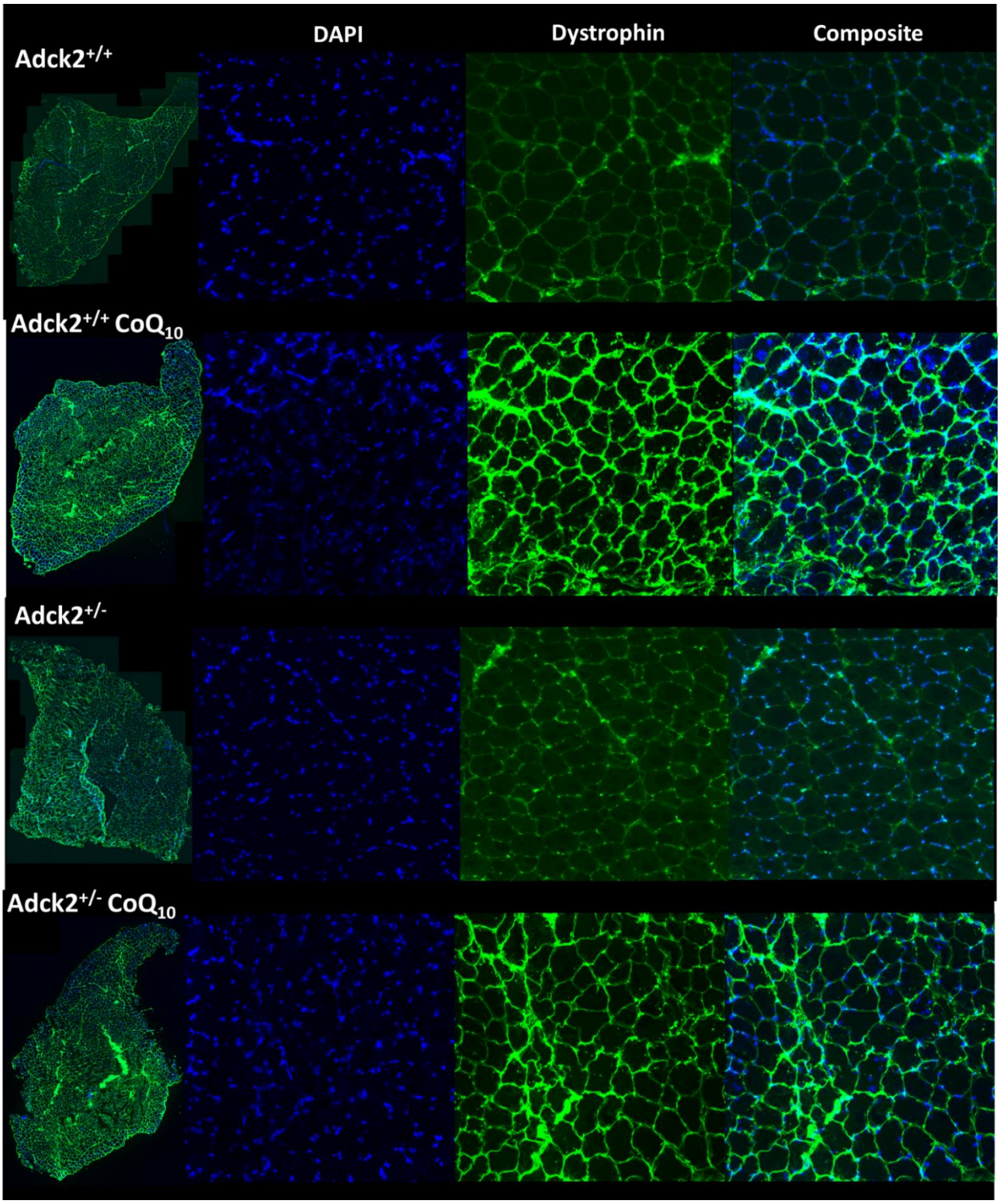

Figure 56. Representative images of tibialis anterior muscle in old mice
Nuclei of transversal tibialis anterior (TA) muscle sections were stained with DAPI in blue. The extracellular matrix of the myofiber membrane was stained with an antibody that localizes dystrophin protein in green. Image acquisition was carried out in a Stellaris Confocal Laser Scanning Microscope from Leica, for image analysis we perform an image segmentation analysis that allows us to study every single myofiber of the whole skeletal muscle section (2000-2500 myofibers per muscle).

On balance, we have found that the TA muscle of heterogenic knockout *Adck2* mice presents an age-dependent mitochondrial bioenergetic failure which leads to the TA muscle presenting a higher content of glycolytic myofibers, with a smaller myofiber size and a much less oxidative

metabolism. In contrast, CoQ_{10} administration can reverse the decline observed in the skeletal muscle.

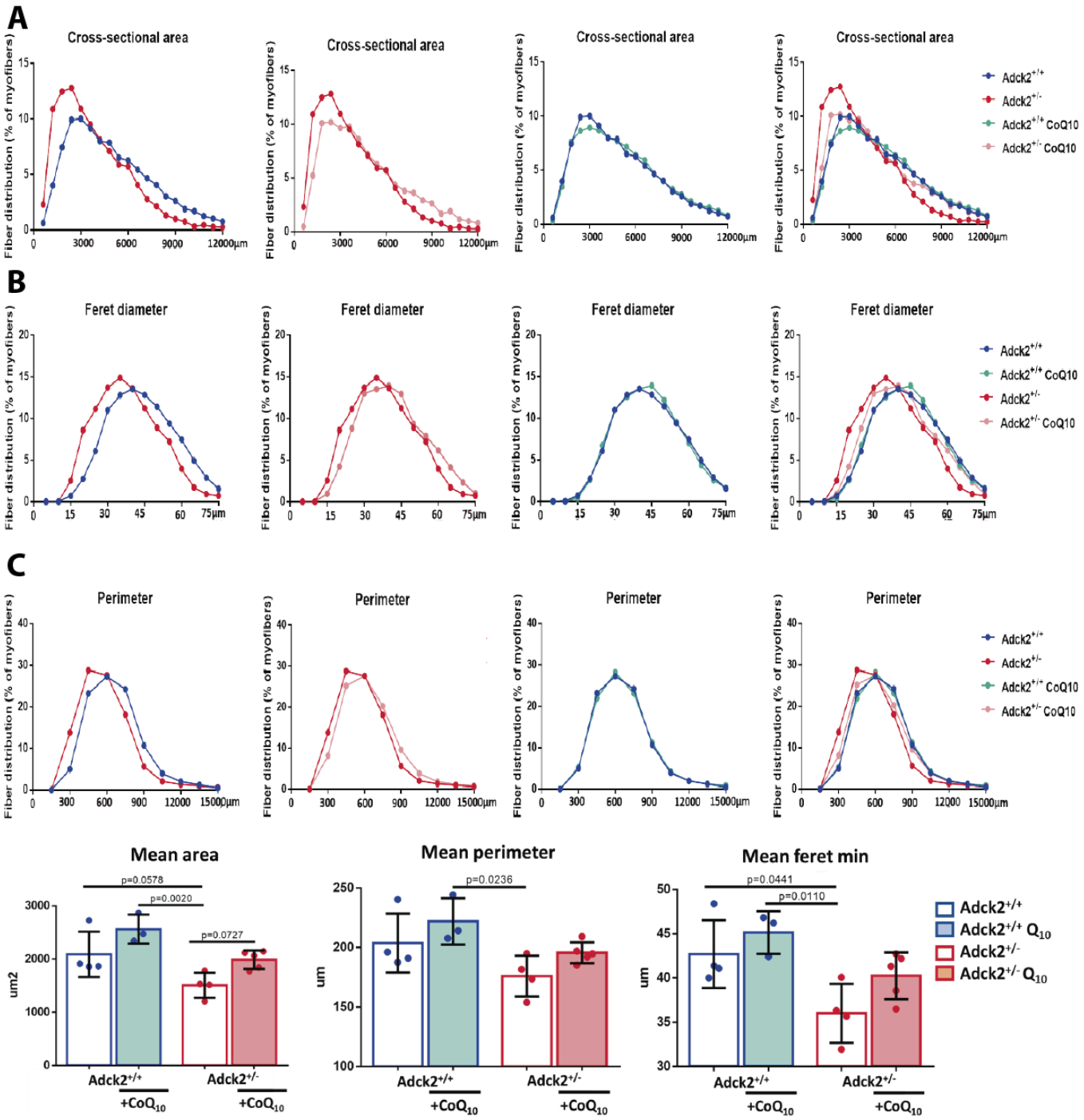

Figure 57. Analysis of myofiber size on transversal cuts from old mice.

(A). Cross-sectional area. (B) Feret diameter. (C). Perimeter. Analysis of 4-5 mice per group. Myofibers basal lamina was stained with dystrophin antibody while nuclei were stained with DAPI. Image acquisitions were performed using a Stellaris Confocal Laser Scanning Microscope from Leica. The whole section of the TA muscle was recorded and all the myofibers from the TA muscle were examined, around 2000-2500 myofibers were quantified and between four or five mice per group were studied. Data represent the mean +/- SD (N=4-5). One-way ANOVA test were applied. P-values <0.05 were considered statistically significant.

Adck2 mutant mice suffer a decline in exercise performance associated with ageing

Based on the previous results obtained in the present chapter, we decided to study muscle strength performance through ageing. Particularly, we have decided to focus on two different tests that evaluate muscle strength *in vivo* the weights test and the Grip Strength test for two and four limbs. We assumed the *in vivo* analysis was necessary because the main tissue affected in our mice model was skeletal muscle, thus we thought that these tests could be an appropriate approach to evaluate longitudinally skeletal muscle function throughout ageing. To avoid too much exposure of the mice to these tests and a potential learning experience, the test was performed every six months, first to the age of 3-6 month-old (young mice), secondly at 9-12 month-old (adults), thirdly at 15-18 month-old (old adult) and finally at 22-24 month-old (old mice).

The analyses revealed that there were not many differences between the young mice, although the decrease in strength associated with ageing mutant mice was more aggressive than in wild type mice, leading to old mutant mice with a significant decrease in strength. This fact agrees with the rest of the results obtained in this chapter, indicating that ageing could have more severe effects on mutant mice. Interestingly, longitudinal administration of CoQ_{10} reduced the decrease in strength as can be visualized in the grip strength and weights tests results (Figure 58).

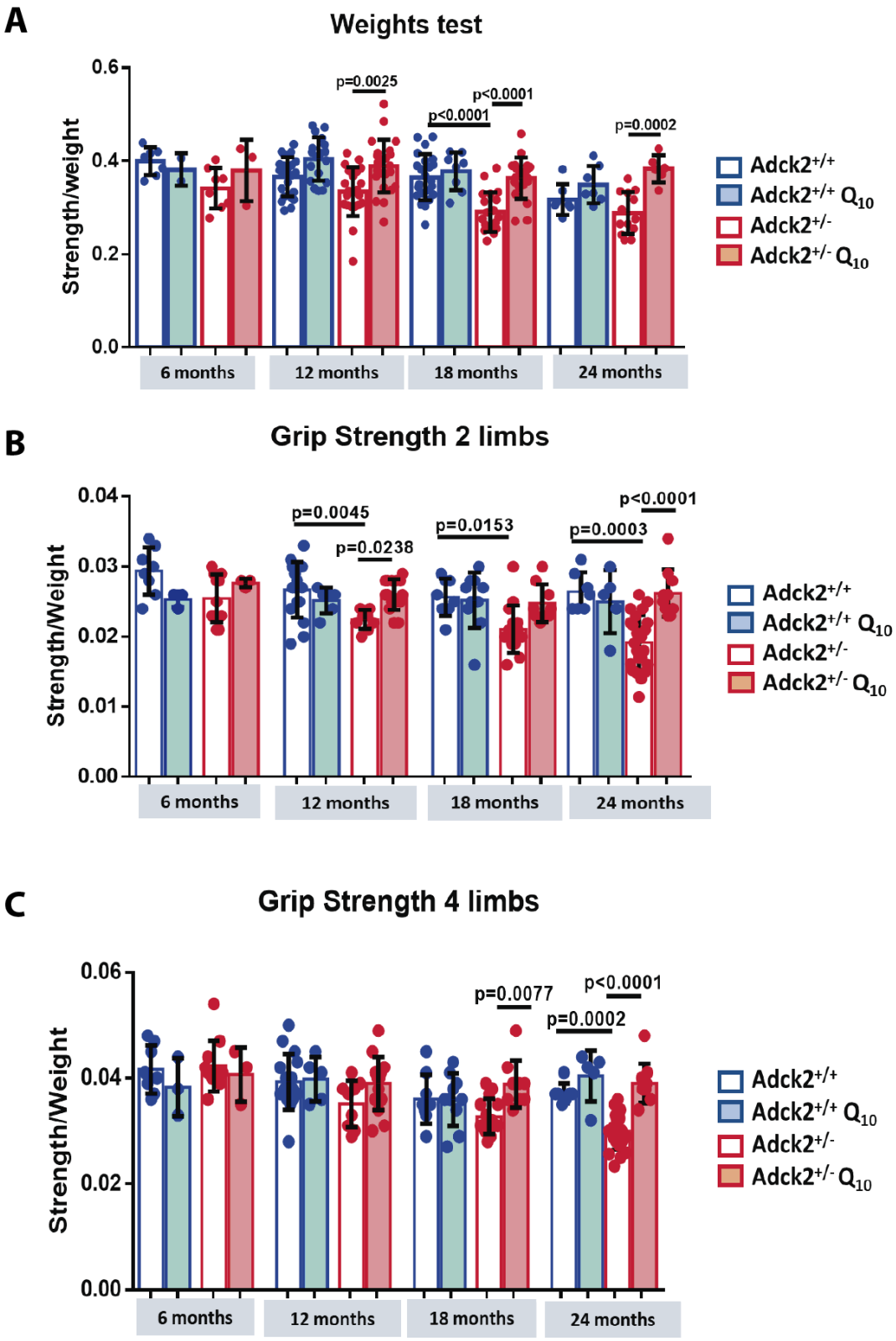

Figure 58. Skeletal muscle performance through the ageing process

(A). Weights test. (B) Grip strength test for two limbs. (C) Grip strength test for four limbs. All tests were performed under the same experimental conditions. Data represent the mean +/- SD (N=4-15). A one-way ANOVA test was applied. P-values <0.05 were considered statistically significant.

To quantify the decline in strength associated with ageing we correlated the mean value obtained in each test along the time and calculated the slope of the line (Table 15). We observed that the decline *in vivo* strength was more pronounced in mutant mice than in wild type. The values showed that mutant mice lost strength 9% faster than wild type in the weights test and more than 2-fold faster in the grip strength with two and four limbs. CoQ_{10} administration ameliorated the loss of strength in mutant mice under treatment so that these animals showed better strength values than non-supplemented wild type mice. The strength loss was more than 2-fold slower than wild type in the weights test and more than 3-fold and 7-fold slower in the grip strength with two and four limbs respectively. CoQ_{10} administration improved, even more, these parameters in the wild type and almost completely protected the animals against loss of strength because the slope of the line was almost cero in the grip strength.

Table 18 Physical exercise analysis in mice through ageing

Parameter: Weights test		
Group	The slope of the line	R squared on the graph
Adck2$^{+/+}$	-0.0034	$R^2 = 0.1411$
Adck2$^{+/+}$ +CoQ_{10}	-0.0036	$R^2 = 0.1626$
Adck2$^{+/-}$	-0.0037	$R^2 = 0.1751$
Adck2$^{+/-}$ +CoQ_{10}	-0.0013	$R^2 = 0.0136$
Parameter: Grip strength in two limbs		
Group	The slope of the line	R squared on the graph
Adck2$^{+/+}$	-0.00016x	$R^2 = 0.07622$
Adck2$^{+/+}$ +CoQ_{10}	-0.00001x	$R^2 = 0.00066$
Adck2$^{+/-}$	-0.00033x	$R^2 = 0.32095$
Adck2$^{+/-}$ +CoQ_{10}	-0.00005x	$R^2 = 0.00995$
Parameter: Grip strength in four limbs		
Group	The slope of the line	R squared on the graph
Adck2$^{+/+}$	-0.00028x	$R^2 = 0.12637$
Adck2$^{+/+}$ +CoQ_{10}	0.00001x	$R^2 = 0.00015$
Adck2$^{+/-}$	-0.00064x	$R^2 = 0.55984$
Adck2$^{+/-}$ +CoQ_{10}	-0.00004x	$R^2 = 0.00330$

Next, we also analysed the metabolic phenotype of our mice through ageing using the PhenoMaster from TSE Systems as is described in the material and methods section. The analysis was performed longitudinally in our mice colony including young, adult, old adult and old mice.

Figure 59 represents the oxygen consumption and Figure 60 carbon dioxide production normalized by BW. Young mice did not show much difference in the parameters studied, but interestingly when ageing progresses, we observed that mutant mice exhibit higher values than wild type mice, indicating bioenergetic deregulation associated with ageing (Figures 59D and 60D). The respiratory exchange ratio (RER) was also studied (figure 61). This value is calculated based on O_2 consumption and CO_2 production and indicated the energetic substrate that the organism is metabolizing. A higher RER value (close to 1) denoted that carbohydrates are being used as an energetic substrate while a lower RER (close to 0.7) demonstrates that fatty acids are being used. Again, mutant mice experienced a deregulation associated with ageing by which old mutant mice present a higher RER than wild type mice indicating a defect in fatty acids metabolism that promotes a higher use of carbohydrates (Figure 61D).

To continue, we examined heat production (Figure 62) and the voluntary physical activity of the mice (Figures 63 and 64). Initially, we examined the heat production by indirect calorimetry that could indicate a deregulated metabolism, old mutant animals present a higher heat production compared with wild type mice, suggesting the idea old mutant mice suffer potential bioenergetic deregulation (Figure 62D). Regarding the voluntary activity of mice, we quantified the number of times that mice break the beam of light at the upper-level Z (Figure 63). This measurement counts the number of times that the mice stand on their hind legs, being an indicator of skeletal muscle system health over ageing. We found that mutant mice presented a lower Z count over ageing compared with wild type mice (Figure 63D). Furthermore, mutant mice supplemented with CoQ_{10} presented a higher Z level over ageing suggesting a positive effect of CoQ_{10} on ageing.

Besides, we also studied the voluntary wheel running of our mice as a measurement of voluntary aerobic exercise capacity during ageing (Figure 64). Mutant mice present a lower physical capacity compared with our wild type mice during ageing whereas CoQ_{10} administration could counteract the decrease in voluntary running capacity (Figure 64D).

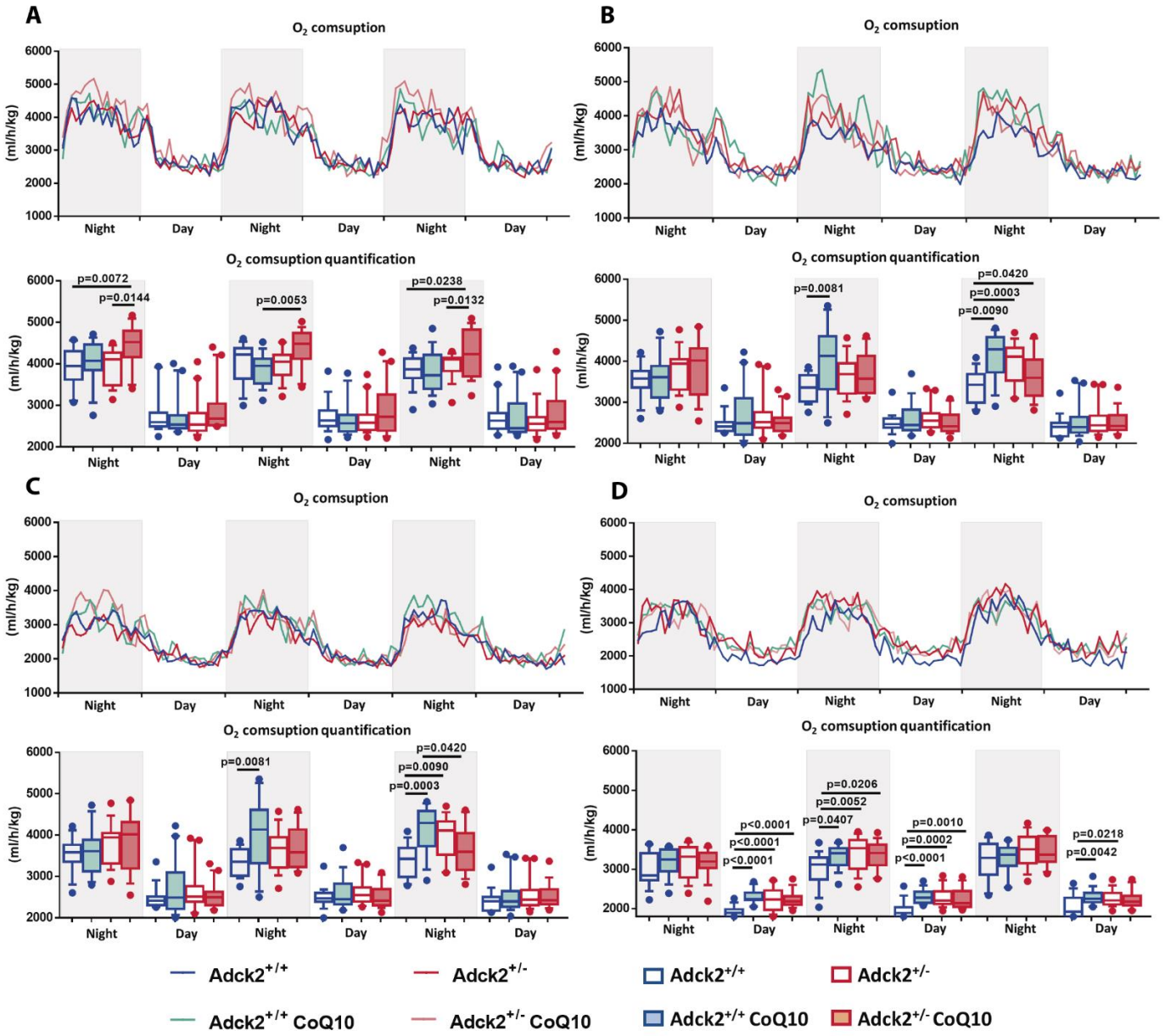

Figure 59 O2 consumption through the ageing process

O2 consumption measured with the automated home cage phenotyping system is shown for a three-night/day period. Young (A), adult (B), old-adult (C) and old (D) mice were studied. CoQ_{10} was added to the water bottle of mice under CoQ_{10} administration conditions. The first 36 hours from every experiment were considered the acclimatization periods and were not used for the analysis. Data represent the mean +/- SD (N=5-8). A one-way ANOVA test was applied. P-values <0.05 were considered statistically significant.

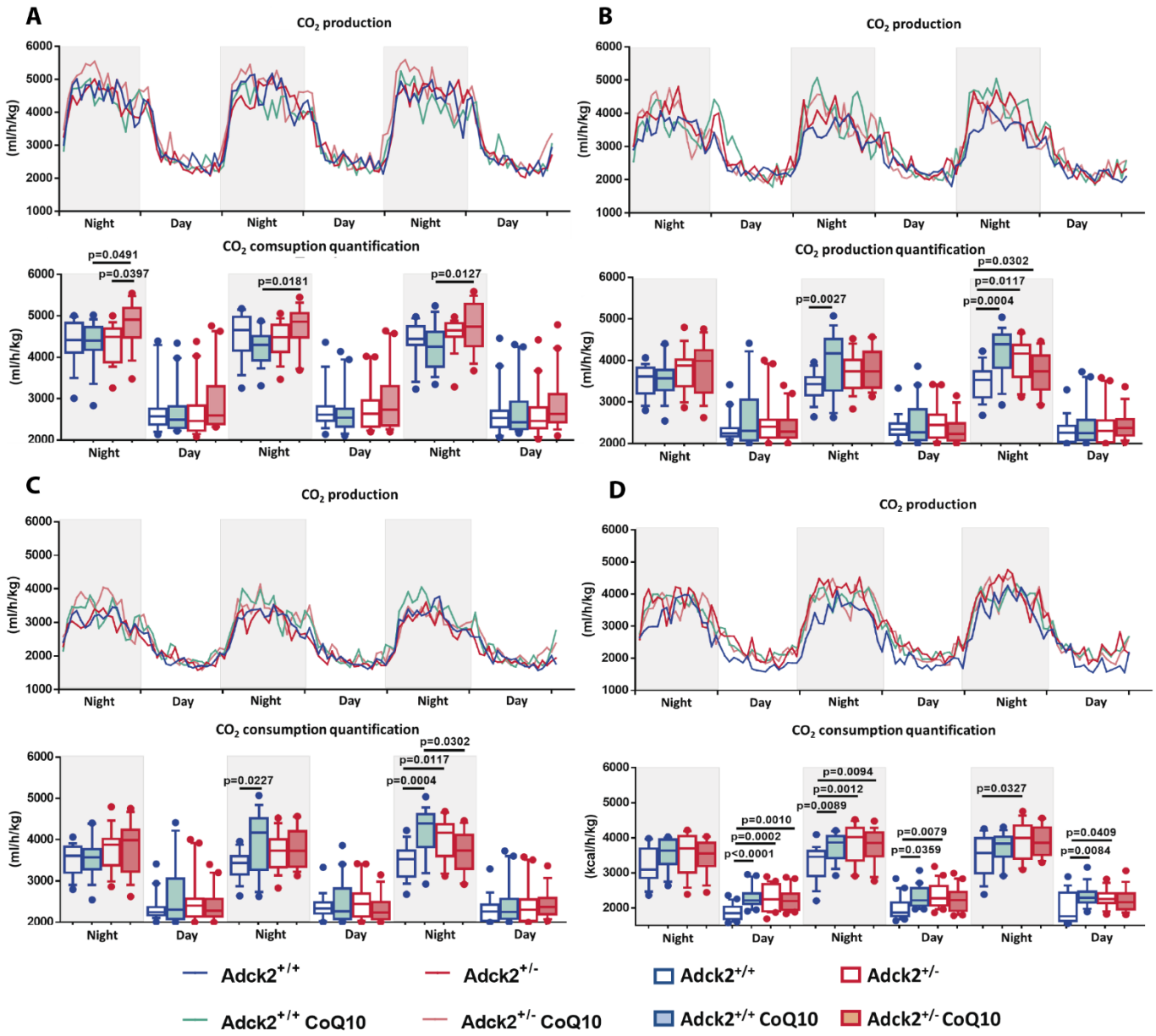

Figure 60 CO2 production through the ageing process

CO2 production measured with the automated home cage phenotyping system is shown for a three-night/day period. Young (A), adult (B), old-adult (C) and old (D) mice were studied. CoQ_{10} was added to the water bottle of mice under CoQ_{10} administration conditions. The first 36 hours from every experiment were considered the acclimatization period and were not used for the analysis. Data represent the mean +/- SD (N=5-8). A one-way ANOVA test was applied. P-values <0.05 were considered statistically significant.

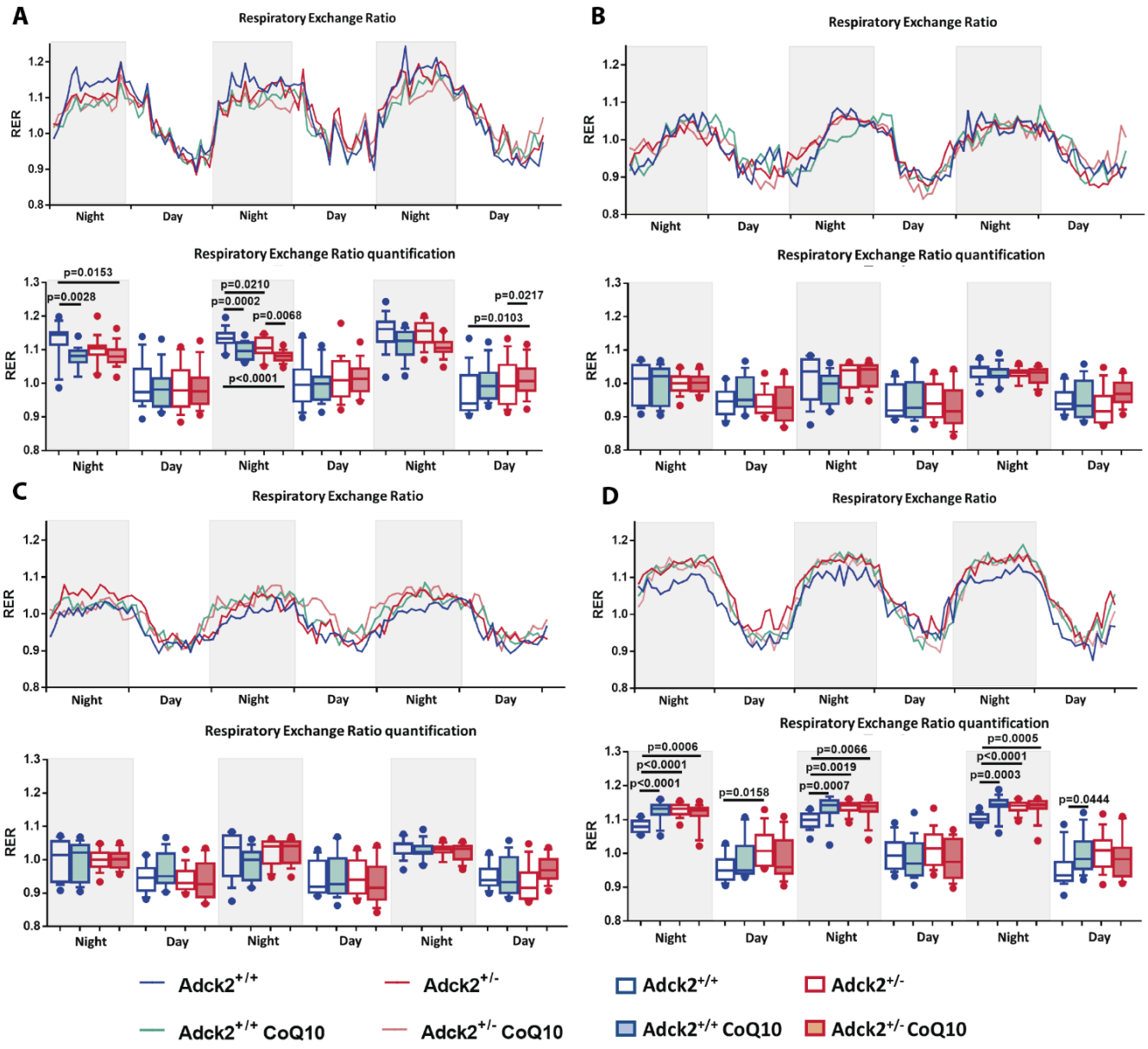

Figure 61 Respiratory Exchange Ratio through the ageing process

Respiratory Exchange Ratio (RER) measured with the automated home cage phenotyping system is shown for a three-night/day period. Young (A), adult (B), old-adult (C) and old (D) mice were studied. CoQ_{10} was added to the water bottle of mice under CoQ_{10} administration conditions. The first 36 hours from every experiment were considered the acclimatization periods and were not used for the analysis. Data represent the mean +/- SD (N=5-8). A one-way ANOVA test was applied. P-values <0.05 were considered statistically significant.

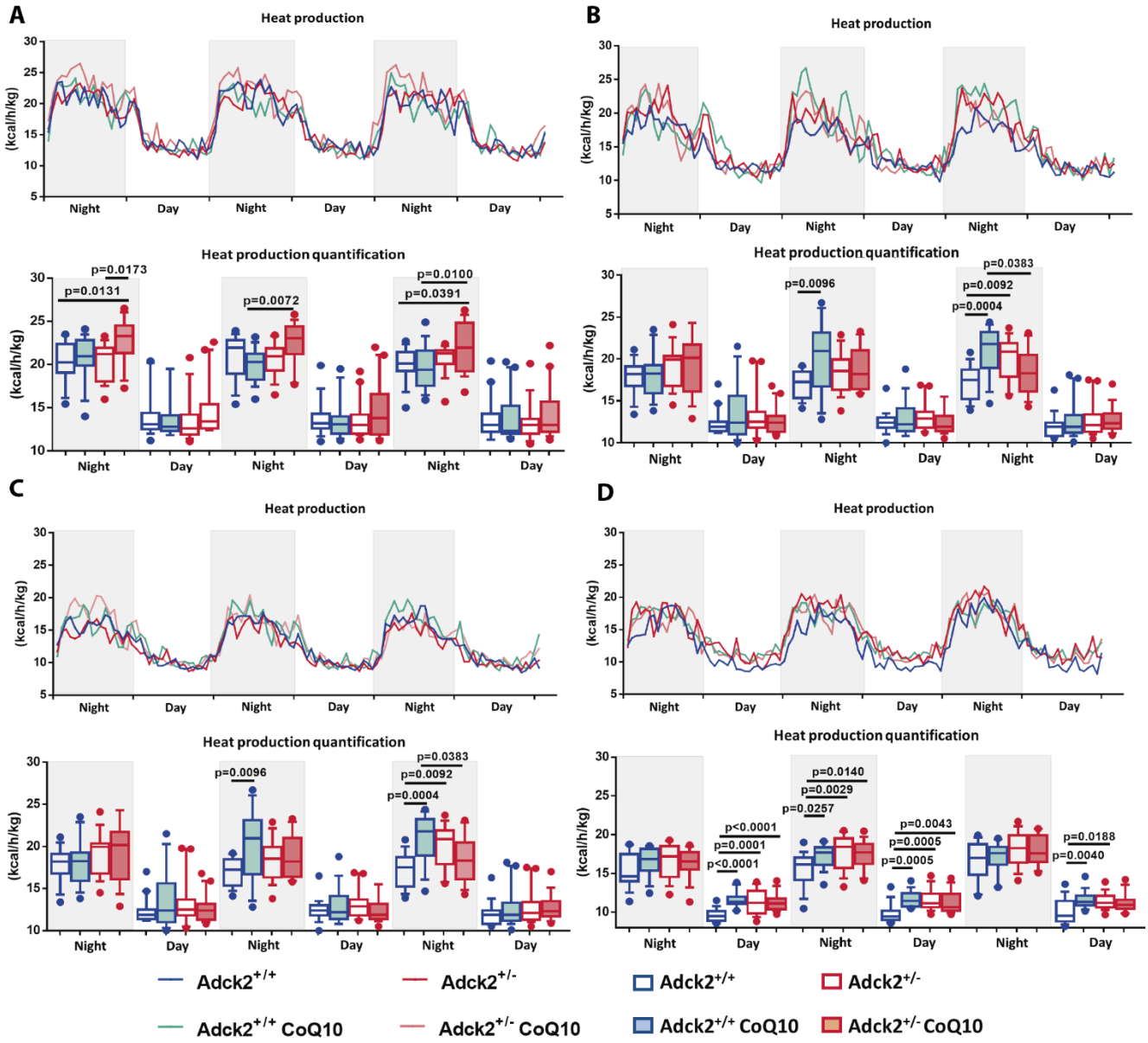

Figure 62 Heat production through the ageing process

Heat production measured with the automated home cage phenotyping system is shown for a three-night/day period. Young (A), adult (B), old-adult (C) and old (D) mice were studied. CoQ_{10} was added to the water bottle of mice under CoQ_{10} administration conditions. The first 36 hours from every experiment were considered the acclimatization periods and were not used for the analysis. Data represent the mean +/- SD (N=5-8). A one-way ANOVA test was applied. P-values <0.05 were considered statistically significant.

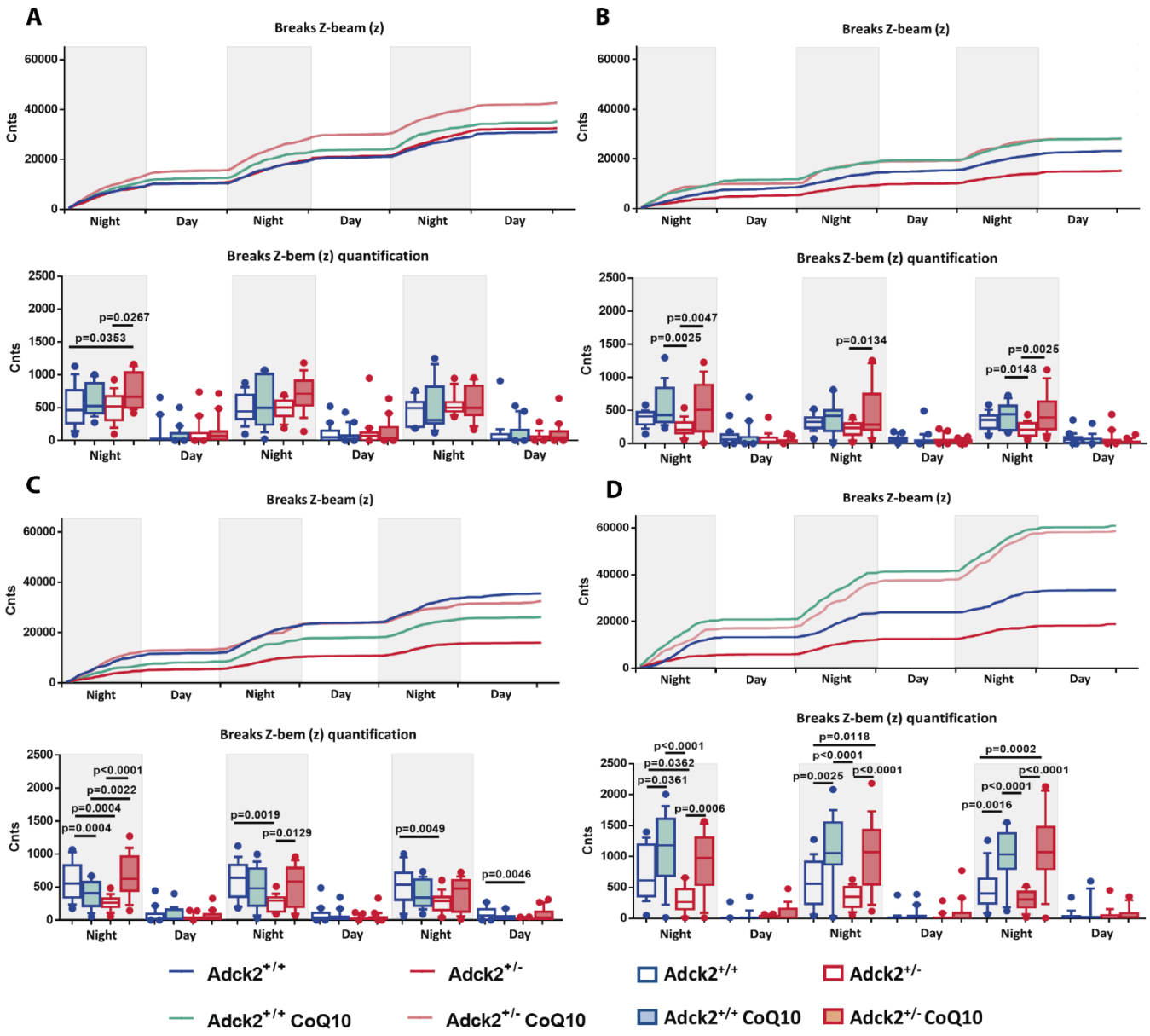

Figure 63 Breaks Z-beam through the ageing process

Breaks of Z-beam measured with the automated home cage phenotyping system are shown for a three-night/day period. Young (A), adult (B), old-adult (C) and old (D) mice were studied. CoQ_{10} was added to the water bottle of mice under CoQ_{10} administration conditions. The first 36 hours from every experiment were considered the acclimatization periods and were not used for the analysis. Data represent the mean +/- SD (N=5-8). A one-way ANOVA test was applied. P-values <0.05 were considered statistically significant.

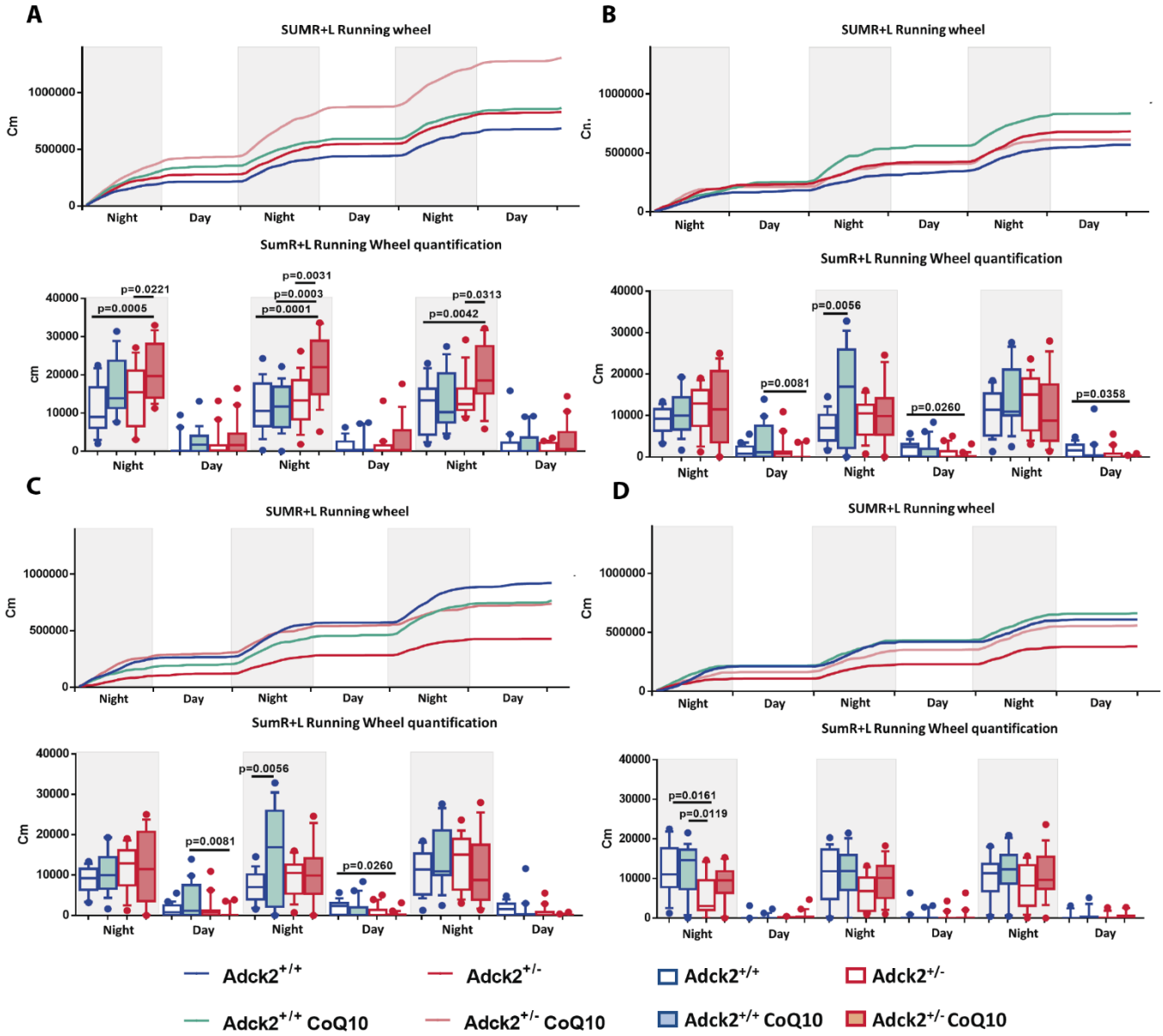

Figure 64 Voluntary wheel-running activity through the ageing process

Voluntary wheel running activity consumption measured with the automated home cage phenotyping system is shown for a three-night/day period. Young (A), adult (B), old-adult (C) and old (D) mice were studied. CoQ_{10} was added to the water bottle of mice under CoQ_{10} administration conditions. The first 36 hours from every experiment were considered the acclimatization periods and were not used for the analysis. Data represent the mean +/- SD (N=5-8). A one-way ANOVA test was applied. P-values <0.05 were considered statistically significant.

Mitochondrial respiration analysis reveals a bioenergetic defect.

We have demonstrated that the decrease in strength associated with ageing was higher in old mutant mice and the damages that present skeletal muscle structure and physiology. Consequently, all the results obtained led us to investigate mitochondrial function in old mice to explain the defect found in skeletal muscle function and metabolism associated with ageing. For that purpose, we developed an updated and detailed protocol to study respiration in mitochondria isolated from skeletal muscle to evaluate ETC and OXPHOS function (158). We decided to analyse the mitochondrial respiration in a mitochondrial enriched fraction freshly isolated from the skeletal muscle of young and old mice. To do that, we homogenized the skeletal muscle and isolated the mitochondria fraction with progressive centrifugations, maintaining the intracellular osmosis level during the whole process to preserve mitochondrial viability, using solutions that contain sucrose, mannitol and BSA as we previously described (158). The pH of these solutions was meticulously adjusted to avoid changes that could affect mitochondrial function.

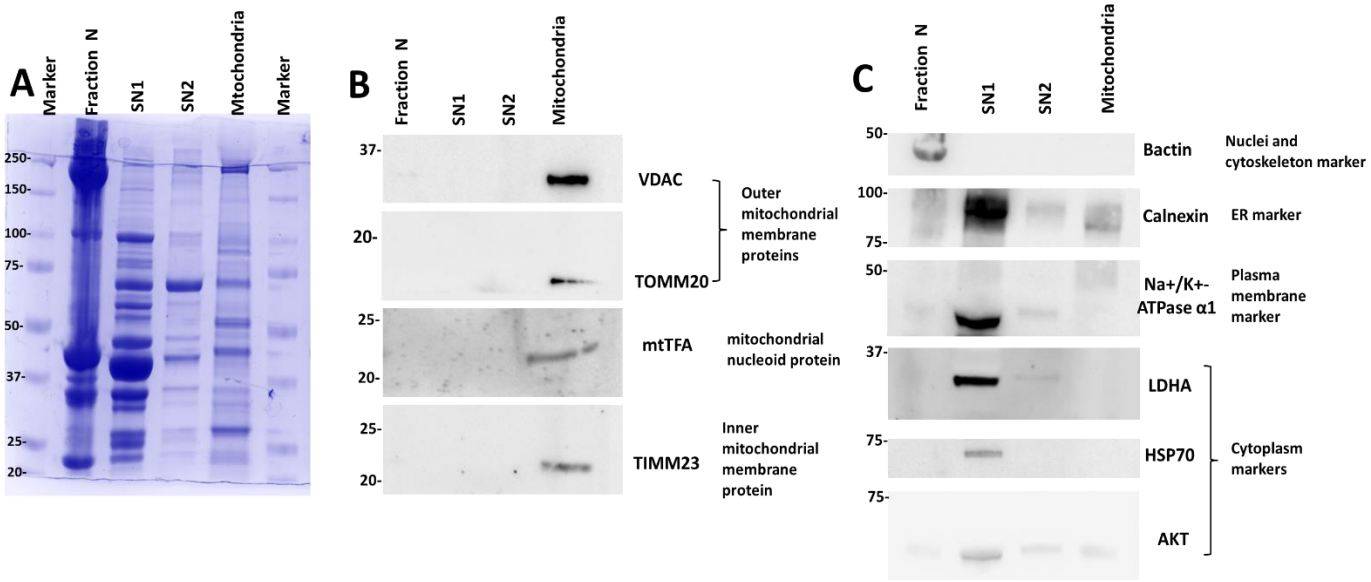

Figure 65 Mitochondrial purity during skeletal muscle mitochondria isolation process
(A). General protein profile stained with Comassie. (B). Mitochondrial protein purity profile including VDAC, TOMM20, mtTFA and TIMM23. (C). Non-mitochondrial markers include β-actin, Calnexin, Na+/K+ ATPase α1, LDHA, HSP70 and AKT. The different fractions obtained during mitochondria isolation were loaded and incubated with antibodies against different proteins located in specific subcellular fractions. fraction N= non-homogenized tissue and nuclei; SN1 = supernatant number 1: cytoplasm + organelles; SN2 = supernatant number 2: cytoplasm + organelles; VDAC = voltage-dependent anion channel; TOMM20 = translocase of outer mitochondrial membrane 20; mtTFA = mitochondrial transcription factor A; TIMM23 = translocase of inner mitochondrial membrane 23; LDHA = lactate dehydrogenase A; HSP70 = heat shock protein 70; ER = endoplasmic reticulum

We checked the purity of the mitochondrial fraction isolated for respiratory analysis, also determined the contamination of other organelles or cell components in our mitochondrial fraction. Figure 65A show the general protein profile of the different fractions isolated where it was clear that every fraction displayed a specific protein profile indicating a different composition. Figure 65B showed the mitochondrial purity with proteins from the outer and the inner mitochondrial membrane and the mitochondrial nucleoid protein indicating that our mitochondrial fractions contained the whole mitochondria. Figure 65C show the location of different cellular components from the nuclei, the ER, the plasma membrane and the cytoplasm. Where only little contamination of ER was detected in our mitochondrial fraction. In balance, these results indicated that our fragmentation process was an adequate method for mitochondrial isolation.

First, we analysed the mitochondrial respiration using isolated mitochondrial from skeletal muscle of young mice. We used pyruvate plus malate as substrates in the coupling assay to stimulate ETC fuelled by the Krebs cycle (Figure 66A), and palmitoyl-L-carnitine plus malate in the β-oxidation to activate the ETC function associated with β-oxidation (Figure 66B). Mitochondria from mutant mice showed lower respiration in both assays supporting the idea that mutant mice have a compromised mitochondrial function. All parameters analysed were highly affected in mutant mitochondria, like the basal respiration, the different states of mitochondrial respiration (states III and IV), the respiratory control ratio and the spare capacity. In contrast, when we tested mitochondria from mutant mice supplemented with CoQ_{10}, we did not find a decrease in any parameter compared with mitochondria from wild type mice, indicating the effectiveness of CoQ_{10} administration. Moreover, we did not find changes in the general protein profile of the mitochondrial fraction (Figure 66C), suggesting the idea that there were no structural changes in mitochondria proteins.

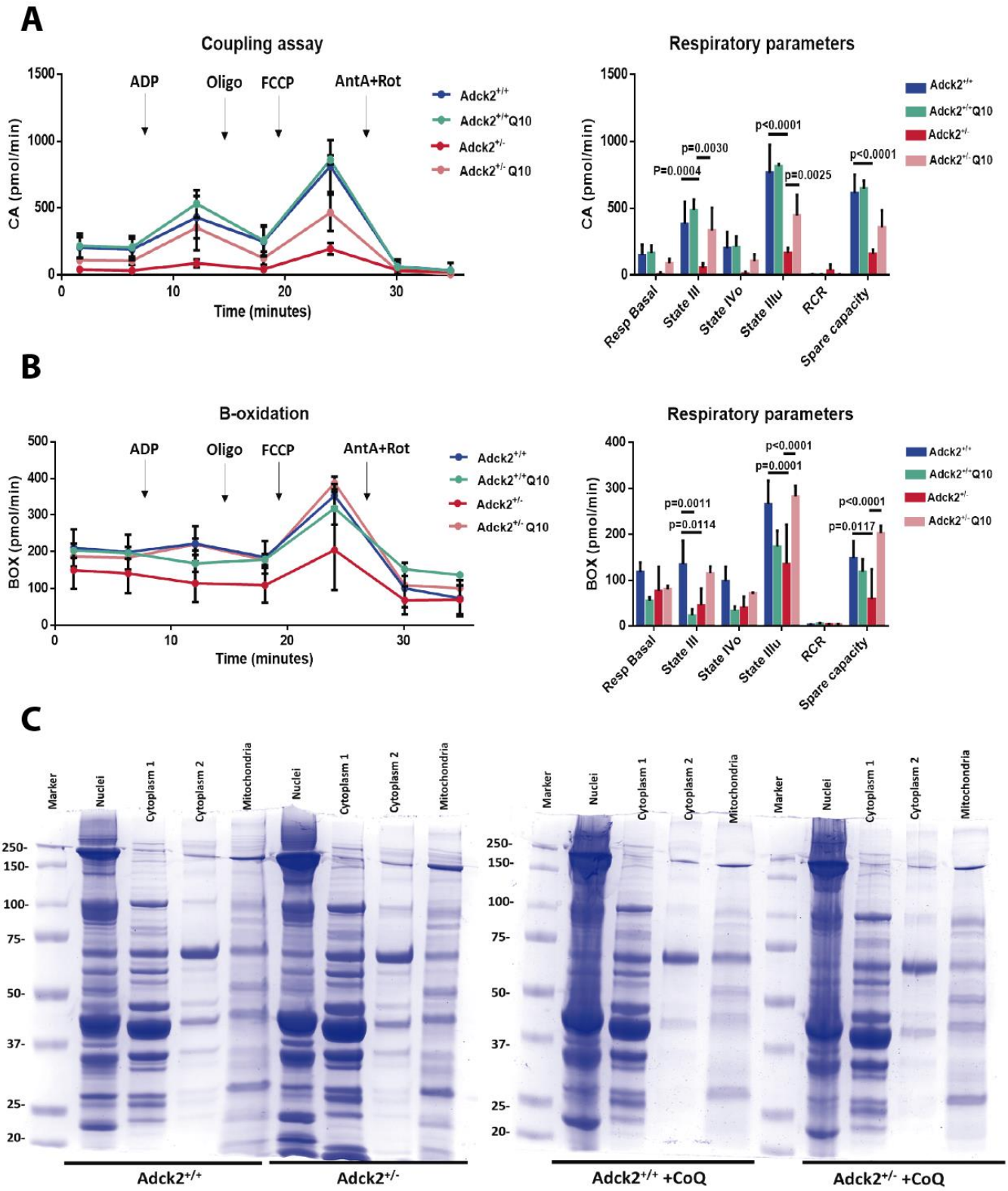

Figure 66. Respiratory analysis on isolated mitochondria from skeletal muscle of young muscle.
(A). Coupling Assay in mitochondria from young mice. (B). Fatty-acids β-oxidation in mitochondria from young mice. (C). General protein profile from the different fractions obtained during the isolation process. The figure above shows an analysis of mitochondrial respiration using isolated mitochondria from skeletal muscle of young mice. We used pyruvate plus malate as substrates in the coupling assay to stimulate ETC fuelled by the Krebs cycle, but we used palmitoyl-L-carnitine plus malate in the β-oxidation assay to activate the ETC function associated with β-oxidation. One representative experiment of three independent experiments is shown. Data represent the mean +/- SD (N=4-5). One-way or two-way ANOVA tests were applied. P-values <0.05 were considered statistically significant. Electron transport chain (ETC).

Also, mitochondria from old mutant mice exhibited lower respiration in both assays (Figure 67A and 67B) supporting the idea that mutant mice have a compromised mitochondrial function. In contrast, when we analysed mitochondria from mutant mice supplemented with CoQ_{10}, not only we did no find alteration in respiration, but some parameters were increased in mitochondria from mutant mice supplemented with CoQ_{10}, suggesting the idea that old mutant mice could overpass to old wild type mice, as we found previously on strength. Furthermore, old mice displayed changes in the protein profile of the mitochondria fraction supporting the idea that mitochondrial protein composition could be different between the groups studied.

Finally, we performed an *in vitro* assay to quantify the activity of respiratory complexes assembly in these mitochondrial fractions. To do that digitonin-solubilized mitochondria were examined in a Blue Native Gel electrophoresis, both in-gel activity (Figure 68A) and western blot with specific antibodies (Figure 68B). We did not find any differences between wild type and mutant mice, but CoQ_{10} administration could increase the levels of isolate complex such as complex I or even the assembly between different complexes including complexes $I+III_2+II_n$, suggesting that longitudinal CoQ_{10} administration could modulate complexes assembly at the ETC. These results could be associated with improvements in mitochondrial respiration.

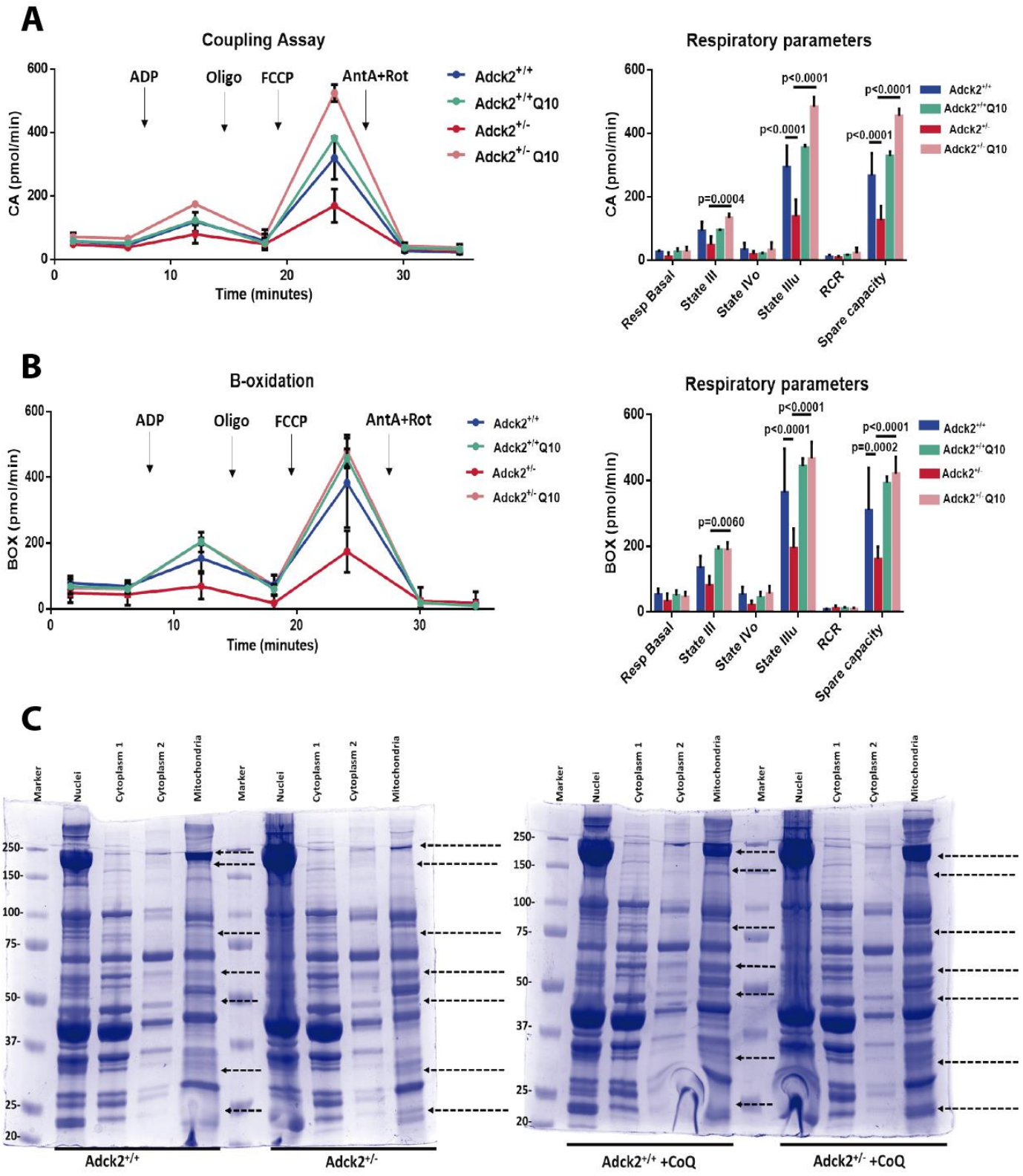

Figure 67. Respiratory analysis on isolated mitochondria from skeletal muscle in old mice.

(A). Coupling Assay in mitochondria isolated from old mice. (B). Fatty acids β-oxidation in mitochondria isolated from old mice. (C). General protein profile from the different fractions obtained during the isolation process. Arrows indicate proteins from the mitochondrial fractions that could change among groups. The figure above shows an analysis of mitochondrial respiration using isolated mitochondrial from skeletal muscle of old mice. We used pyruvate plus malate as substrates in the coupling assay to stimulate ETC fuelled by the Krebs cycle, but we use palmitoyl-L-carnitine plus malate in the β-oxidation assay to activate the ETC function associated with β-oxidation. One representative experiment of three independent experiments is shown. Data represent the mean +/- SD (N=4-5). One-way or two-way ANOVA tests were applied. P-values <0.05 were considered statistically significant. Electron transport chain (ETC).

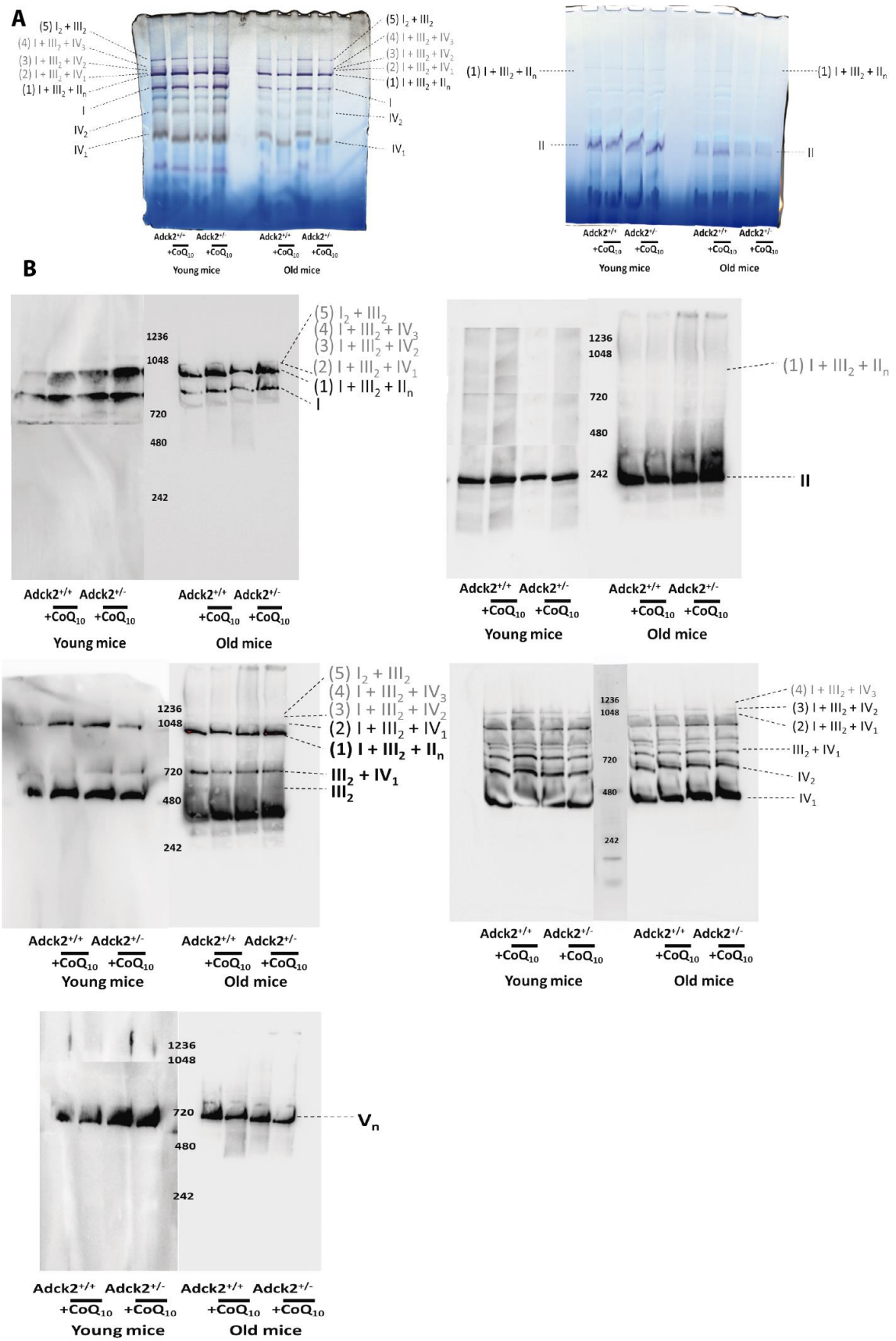

Figure 68. BNGE showing mitochondria complexes and supercomplexes assembly at the ETC

Mitochondria isolated from skeletal muscle of young and old mice and 100 µg of solution enriched in mitochondria were loaded per sample. (A). Gel activity assay of complexes and supercomplexes I, II and IV in isolated mitochondria from skeletal muscle of young and old mice (B). Detection of the respiratory complexes and potential supercomplexes after BNGE by immunoblotting to define bands for complexes and supercomplexes. Specific antibodies against complexes I, II, III, IV and V were used. Independent blots are shown. Blue native gel electrophoresis (BNGE).

Also, we measured the CoQ_9 and CoQ_{10} levels in these mitochondrial fractions (Figure 69). We found that young and old mutant mice exhibit a decrease in both isoforms of CoQ levels related to the mitochondrial defect displayed by mutant mice. However, prenatal CoQ_{10} administration induces an increase in mitochondrial CoQ_{10} levels in mutant mice, but also on CoQ_9, showing that CoQ_{10} could also promote an increase in CoQ_9 biosynthesis. The increase of CoQ could be associated with the improvement in mitochondrial function and working machinery obtained in mutant mice under CoQ_{10} administration.

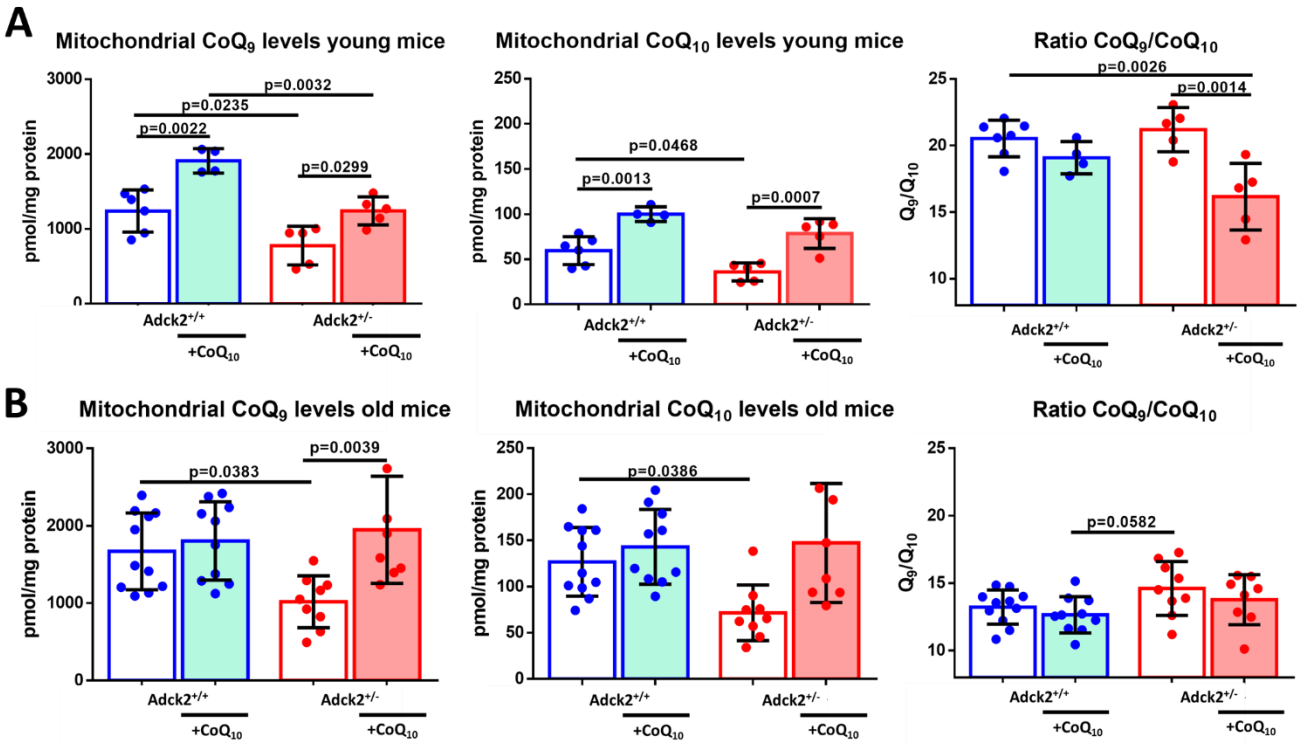

Figure 69 Analysis of CoQ levels in mitochondria from skeletal muscle through ageing

(A) Determination of CoQ_9 and CoQ_{10} levels in mitochondria isolated from gastrocnemius muscle in young mice. Ratio CoQ_9/CoQ_{10}. (B) Determination of CoQ_9 and CoQ_{10} levels in mitochondria isolated from gastrocnemius muscle in old mice. Ratio CoQ_9/CoQ_{10}. Mitochondria were isolated by skeletal muscle homogenization and serial centrifugations, after lipids extraction, CoQ levels were determined by HPLC as described in the materials and methods section. CoQ_{10} in nanoparticles was dissolved in the water bottle, mean CoQ_{10} intake was estimated at 1-1.5 mg/day (33.33-50 mg/kg/day). Data represent the mean +/- SD (N=4-8). A one-way ANOVA test was applied. P-values <0.05 were considered statistically significant.

4.3.2 Discussion of chapter 3:

The main objective of this chapter was to examine how the ageing process affects our mutant mice and if CoQ_{10} administration could have any effect on ageing, focusing our study on the mitochondria of skeletal muscle tissue. Ageing could be defined as the gradual loss of physiological unity, resulting in impaired function and a rising vulnerability to death (140). Ageing leads to a decrease in respiratory chain efficiency, rising electron leakage and decreasing ATP production (190). Particularly, mitochondrial dysfunction associated with ageing in skeletal muscle of mice has been shown to promote impaired mitochondrial respiration and sarcopenia (191). Besides, mutations and deletions of mtDNA lead to a gradual dysfunction of the respiratory chain and an accelerated ageing phenotype (192). Nonetheless, due to the high impact of mitochondrial in accelerating the ageing process, interventions that improve mitochondrial function could modulate ageing and lifespan (140).

About skeletal muscle, ageing declines the regenerative capacity of adult SCs, resulting in an incomplete regeneration process. The stem cell decline could be associated with multiple types of damage, such as changes in the niche of stem cells that decrease the performance of their regenerative capacity, which leads to a deterioration of the muscle and a loss of its regenerative capacity, and an increase in fibrosis that impedes a complete SCs activation and specification and an adequate myogenic proliferation and cell differentiation (193). Moreover, the specific age-related changes associated with the niche that contribute to the decline in the stem cell functions are still unknown, but potentially affect the stem cell cycle and decrease their self-renewing capacity, resulting in SCs depletion and loss of muscular regenerative capacity (194). Undoubtedly, reducing the stem cell and niche ageing could repercuss on tissue regenerative capacity so that an opportunity to improve tissue repair in the old organisms could be provide slowing down the ageing process through different interventions to rejuvenate old niche of SCs such as young medium, heterochronic parabiosis and defined factors (193). This reflection on the rejuvenation of old SCs niche allows us to propose longitudinal CoQ_{10} administration to promote the rejuvenation of adult muscle stem cells.

Particularly, the most important decline associated with ageing in skeletal muscle is sarcopenia, which includes the diminish of skeletal muscle mass and function that contributes to immobility, frailty and mortality in the old organisms. Sarcopenia is characterized by three different aspects: reduced muscle strength, a decrease in muscle mass and reduced physical performance (195). Sarcopenia has been associated with mitochondrial dysfunction that contributes to its pathogenesis, including mitochondrial fragmentation and an alteration of their morphology and mass (196). To counteract sarcopenia, a group of natural compounds, such as polyphenols, have

been shown to alleviate sarcopenia and reverse skeletal muscle decline associated with ageing modulating mitochondria metabolism (196). These compounds are found in fruit, nuts or berries and could improve exercise capacity and muscle function in models of age-related decline through mitochondrial respiratory capacity and preventing mitochondrial dysfunction (197). Even, oligonol (lychee polyphenol) stimulates mitochondrial biogenesis, fusion/fission and mitochondrial quality that leads to an increase in skeletal muscle mass, cross-sectional area and grip strength in 32 week-old senescence mice (198).

We have shown that haploinsufficiency of the *ADCK2* gene in humans produces slow and gradual muscle weakness and myalgia at muscular exertion and rest conditioning the muscular capacity of the patient (77). Several muscles were deeply affected presenting mitochondrial myopathy and lipids droplets. And what is more significant, the skeletal muscle defect showed a slowly progressive decline that gradually produced a progressive muscle weakness and incapacity through ageing, reducing the walking capacity, incapacity to stand and the requirement of a wheelchair and finally a die prematurely at 57 years old associated with dysfunction of torso muscles (77).

In this chapter, we showed that *ADCK2* mutation is associated with a progressive decline of skeletal muscle mass and mitochondrial dysfunction. Initially, the visual aspect of the mice did not show differences between groups in young mice, but old mutant mice presented a more compromised aspect compared with wild type, presenting bald spots over the body and irregular hair colour, while old mutant mice on CoQ_{10} supplementation present a better general aspect.

As the main tissue affected in our mutant mice was the skeletal muscle and because the oxidative/glycolytic myofibers are essential for muscle function, we studied myofiber composition in the TA muscle to determine the proportion of oxidative (type IIA), glycolytic (type IIB) and hybrid myofibers (type IIX). Young mutant mice tend to exhibit an increase in glycolytic type IIB myofibers, whereas old mutant mice displayed a lower proportion of oxidative type IIA and an increase in type IIX hybrid compared with wild type mice. Old mutant mice supplemented with CoQ_{10} did not suffer a reduction in type IIA myofibers and exhibited a profile similar to the wild type. Given the coordinate regulation of myofiber type and the mitochondrial function that associates mitochondrial oxidative metabolism to shift in myofiber composition in slow-twitch muscles (199) (200), the decrease in oxidative myofibers with ageing could be related to mitochondrial dysfunction that suffers our mutant mice. Additionally, we can propose that longitudinal CoQ_{10} administration counteracted the shift in myofiber typing promoting a more oxidative myofiber typing composition in the TA muscle of our old mutant mice.

Also, we analysed the size of myofibers, including their cross-sectional area, ferret diameter and their perimeter. We did not find differences between mutant and wild type in young mice in terms of myofiber dimensions, neither CoQ_{10} administration was able to modify myofiber size. However, old mutant mice showed a decrease in myofiber size compared with wild type mice, particularly in ferret diameter. This result allows establishing a potential defect in skeletal muscle structure in old mutant mice associated with ageing, including skeletal muscle loss and atrophy. Furthermore, when we analysed skeletal muscle from old mutant mice supplemented with CoQ_{10}, we discovered an increase in myofibers dimensions compared with old mutant mice under standard conditions, especially on ferret diameter. Consequently, we can propose that CoQ_{10} supplementation could be alleviating the decrease in myofiber size in old mutant mice. Our results are in agreement with previous studies that showed that compounds with bioenergetic properties that modulate mitochondria could reverse or decreased skeletal muscle sarcopenia associated with ageing including reduced myofiber size (197) (198). Based on these results, skeletal muscle function seems to be affected in our mutant mice and the ageing process is presented as a modulating factor, as it has been described with the creatine-kinase knockout mouse model, where ageing was postulated to affect the physical capacity in a dependent manner (201).

The exercise tests designed to evaluate muscle performance (grip strength test and the weights test) showed no differences between mutant and wild type young mice, but an ageing decline in strength in all tests performed was found, which was higher in mutant mice, suggesting that these mice could suffer a deterioration in skeletal muscle function associated to ageing. The results are in agreement with previous data that suggest that mitochondrial dysfunction could be responsible for premature ageing and deregulated bioenergetic metabolism (201). In contrast, mutant mice longitudinally supplemented with CoQ_{10} did not suffer this loss of skeletal muscle strength associated with ageing, suggesting that CoQ_{10} supplementation could be ameliorating skeletal muscle function through ageing. Our results corroborate previous data where CoQ_{10} administration preserved muscle mass and grip strength (202).

Additionally, we also studied our mice through ageing in the PhenoMaster that allows an automatic analysis of different parameters. Firstly, we examined oxygen consumption normalized by body weight in young mice, adult mice, old adult mice and old mice. There was no difference between wild type and mutant in young mice, but interestingly when mice get older, we found an increase in oxygen consumption in mutant mice in comparison with wild type mice which could mean deregulation in oxygen consumption in mutant mice associated with ageing. In parallel, CO_2 production was also studied at different stages of ageing. There was no

difference between young wild type and mutant mice. But, when mice get older, mutant mice present a higher CO_2 production compared with wild type mice, but no effect was found in mice supplemented with CoQ_{10}. Finally, respiratory exchange ratio (RER) was also examined obtaining no difference in young mice. However, old mutant mice exhibited a higher RER compared with wild type mice potentially indicating that mutant mice suffer metabolic deregulation associated with ageing.

We also analysed parameters associated with physical capacity. We studied the breaks Z beam that quantifies the number of times that the mice break the infrared line from the top of the cage by standing on two limbs in the different ageing stages. We did not find much difference in the stages analysed, but interestingly mutant old mice showed a lower breaks Z-beam than old wild type mice, possibly related to a lower skeletal muscle capacity to stand over two limbs. However, both groups of mice on CoQ_{10} administration showed a higher number of breaks Z-beam than old mutant mice. Furthermore, voluntary running capacity in the wheel was quantified, we did not observe differences in young and adult mice. But old-adult and old mutant mice presented a lower running capacity compared with old adult and old wild type mice showing the physical incapacity of mutant mice could be associated with ageing. CoQ_{10} administration could potentially improve the voluntary wild running in old mutant mice.

On the other hand, bioenergetic mitochondrial analysis on isolated mitochondria from skeletal muscle demonstrated that young mutant mice presented impaired mitochondrial respiration compared to wild type, indicating that young mutant mice suffer mitochondrial dysfunction. Mitochondria from heterozygous *Adck2* knockout mice supplemented with CoQ_{10} showed an increase in respiration in both assays demonstrating that CoQ_{10} administration could recover mitochondrial function *in vivo*, but young mutant mice did not reach wild type mice levels. Nonetheless, when we performed these analyses in old mice, mutant mice displayed impaired mitochondrial respiration in both assays compared with wild type mice and CoQ_{10} supplementation recovered mitochondrial respiration in both assays reaching wild type levels. Consequently, we found that mitochondrial respiration is deteriorated in mutant mice since youthfulness and probably the impaired mitochondrial function over time could result in the damages found in the skeletal muscle of old mice. More significantly, longitudinal CoQ_{10} administration recovered mitochondrial respiration in young and old mice, particularly in old mice reached wild type levels, suggesting that CoQ_{10} administration could reduce the impaired mitochondrial bioenergetic and it could be associated with the improvements found in skeletal muscle structure and composition found in old heterozygous *Adck2* knockout mice supplemented with CoQ_{10}. Importantly, we should mention that mitochondria enriched fraction

from TA muscle of old mutant mice presented a different protein profile to the rest, indicating that mitochondrial structure could be affected in two years old mutant mice. Also, the CoQ content in these mitochondrial fractions was lower in mutant mice, both in young and old. We measured CoQ_9 and CoQ_{10} levels, mutant mice presented lower levels of both isoforms. The protein profile of aged mutant mice supplemented with CoQ_{10} was similar to that of the old wild type mice.

In agreement with that, CoQ_{10} administration increased the amount of isolated complex I and the assembly of complex I with the rest of the mitochondrial complexes, supporting the idea that CoQ_{10} could be improving the mitochondrial architecture. Also, mitochondria of mutant mice supplemented with CoQ_{10} showed similar CoQ content to wild type mice, both in young and old mice.

These results indicated that mutant mice begin to be affected from youth since compromised mitochondrial function progressively resulted in ageing-associated skeletal muscle deterioration. However, the mutant mice supplemented with CoQ_{10} showed an increase in both isoforms, both in the juvenile and the elderly stages, and an improved mitochondrial function that could counteract the damage to skeletal muscle associated with the ageing process.

In summary, we demonstrated in this chapter that our heterozygous *Adck2* knockout mice presented a decline in skeletal muscle associated with ageing and that damage could be related to an impaired mitochondrial function. In contrast, we discovered that prolonged administration of CoQ_{10} could reverse alteration in aged skeletal muscle and maintain an adequate mitochondrial function.

Chapter 4

4.4 CHAPTER 4: Caloric restriction approach to stimulate muscle metabolism in *Adck2* mouse model.

4.4.1 Introduction

Metabolism could be defined as the group of biochemical reactions and physicochemical processes that occur at the cellular level of an organism. Mitochondrial diseases present important deregulation of the metabolism that is directly connected with the phenotype observed and the damages associated with these syndromes. On the other hand, CR is a potent metabolism modulator that can induce adaptations at cellular levels regarding energetic supply, specifically switching on from glucose to fatty acids and amino acids. CR promotes healthspan and longevity and reducing the incidence of diseases associated with ageing (203). In consequence, CR can modulate metabolism affecting directly mitochondrial activity, reporting a huge number of beneficial adaptions to promote a more efficient metabolism and even increasing healthspan.

The object of the present chapter was to examine the effect of CR on heterozygous *Adck2* knockout mice because CR could promote mitochondrial adaptations to modulate their deregulated metabolism. For this purpose, adult mice (6 month-old) were submitted to CR for 7 months. After that period, mice were sacrificed by cervical dislocation to analyse CR long term adaptations. CR mice have access to the 60% of their normal food intake, so food intake was reduced by 40%.

Initially, glucose and insulin homeostasis were analysed because these parameters are normally modulated by CR and are considered markers of CR adaptations (204). Exercise tests were also performed under CR because we previously described a reduced physical capacity in *Adck2* mutant mice and additionally CR has been reported to promote adaptation in terms of physical capacity (205) (206). Moreover, as CR has been shown to modulate skeletal metabolism, we performed immunohistochemical studies on the transversal TA skeletal muscle cuts to study myofiber composition due to CR has been shown to modulate myofiber typing in mice (205). Moreover, analysis of respiration on isolated mitochondria was also determined to check if CR could modulate mitochondrial physiology *in vivo*. Finally, we decided to develop an *in vitro* model of CR specifically for skeletal muscle. For this purpose, we collected serum from our mutant and wild type mice on *ad libitum* and on CR to culture adult muscle stem cells in presence of this serum, to check if a CR microenvironment could modulate stem cell differentiation and reproduce *in vitro* the adaptations that have been described *in vivo* (204) (205) (206).

On balance, all the experiments performed in the present chapter were focused on evaluating the mitochondrial metabolism of heterozygous *Adck2* knockout mice or cells under CR and to evaluate if adaptations modulated by CR in wild type mice were also reproduced in mutant mice.

Caloric restriction adaptation on weight, force production and muscle performance.

Six-month-old male wild type and mutant mice were on CR for seven months to induce long-term caloric restriction adaptations, the weight of the animals was recorded weekly. The food intake of CR mice was reduced to 60% of the mean baseline food intake. As control groups, age-matched wild type and mutant mice were on *ad libitum* condition.

On the *ad libitum* diet, mutant mice showed a higher weight gain compared with *ad libitum* wild type mice(Figure 70), while on CR only a small tendency by which mutant mice on CR seem to lose lower weight (Figure 70B). The higher increase in the bodyweight of mutant mice and a lower weight lost on CR could indicate a defect in metabolism.

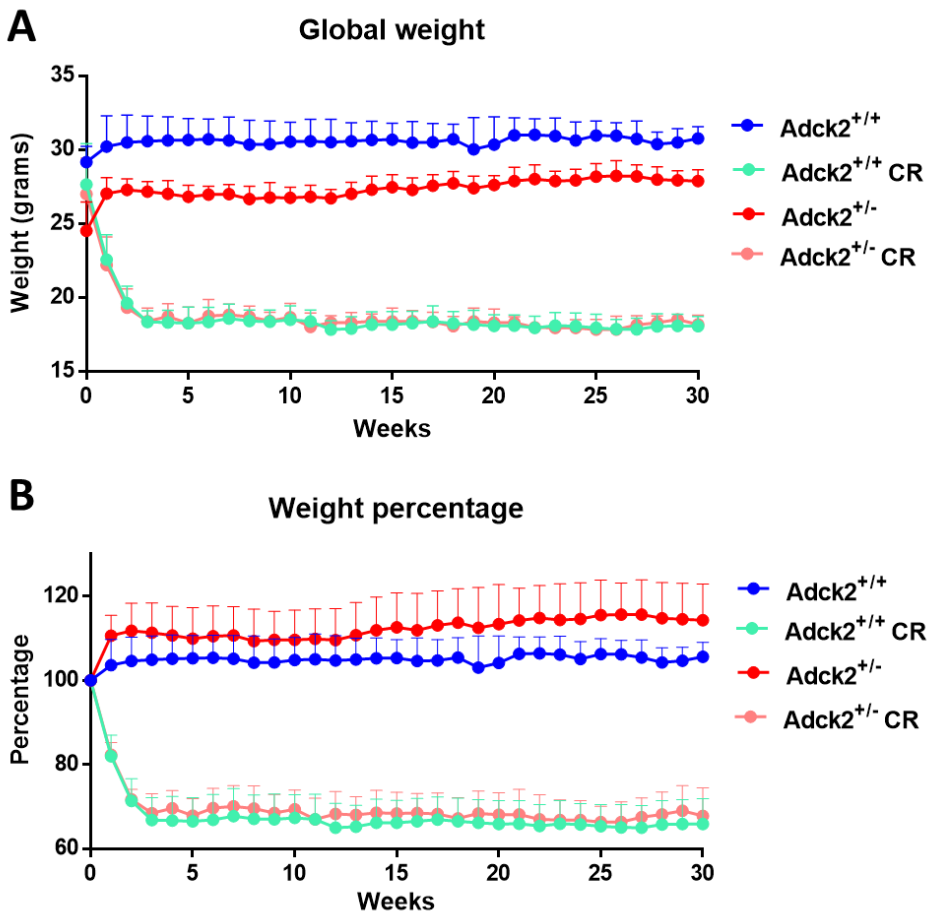

Figure 70. Characterization of caloric restriction adaptation on weight management.
(A). Weight analysis of wild type mice and *Adck2*$^{+/-}$ on ad libitum and CR diet along 30 weeks in grams. (B). Weight changes wild type mice and *Adck2*$^{+/-}$ on ad libitum and CR diet along 30 weeks on percentage. Mice were weighed every week on Tuesday first hour in the morning (09:00 am). (N=7-15).

In vivo force, production was assessed with different tests before CR intervention to determine the basal situation and at the end of the studied period to evaluate CR adaptations on skeletal muscle performance. Grip strength test and weights test were used to evaluate strength under basal conditions obtaining that mutant mice present lower strength for two (Figure 71A) and four limbs (Figure 71B) which could be indicative of a defect in mitochondrial skeletal muscle function. Interestingly CR increased strength on wild type and heterozygous *Adck2* knockout heterozygous *Adck2* knockout mice on both tests (Figure 71A, B and C), skeletal muscle on CR could be more efficient in force production.

Aerobic capacity was also analysed with a treadmill specifically designed to promote oxidative metabolism (Figure 71D), mice firstly run for a long period at low speed and after that speed was gradually increased at a low rate over time. Initially, mice run at a low speed (10 m/min) for 20 minutes and after that speed is increased gradually by 1m/min every 4 minutes for 60 minutes to promote the oxidative metabolism experienced during long-distance races at low speed. The time that mice were able to run, the maximum speed reached, and the total distance travelled were quantified. The results before CR suggested that mutant mice presented lower aerobic capacity on the treadmill again indicating a defect in oxidative pathways, whereas at the end of the CR period mutant mice on CR presented higher values than mutant mice on *ad libitum* similar to wild type mice. The increase observed in mutant mice on the treadmill test could mean that CR could be improving oxidative metabolism, particularly the use of energetic substrates such as fatty acids used during physical activities at a low intensity and long duration.

We also found that CR decreases heat production (Figure 72A) which could be associated which the adaptation of metabolism produced by CR. We found that mice on CR have a higher performance in the voluntary running wheel for three days, while mutant mice on *ad libitum* run a lower distance than wild type mice on *ad libitum* (Figure 72B). On balance, adaptations promoted by CR on wild type animals were also reproduced in heterozygous *Adck2* knockout mice on CR.

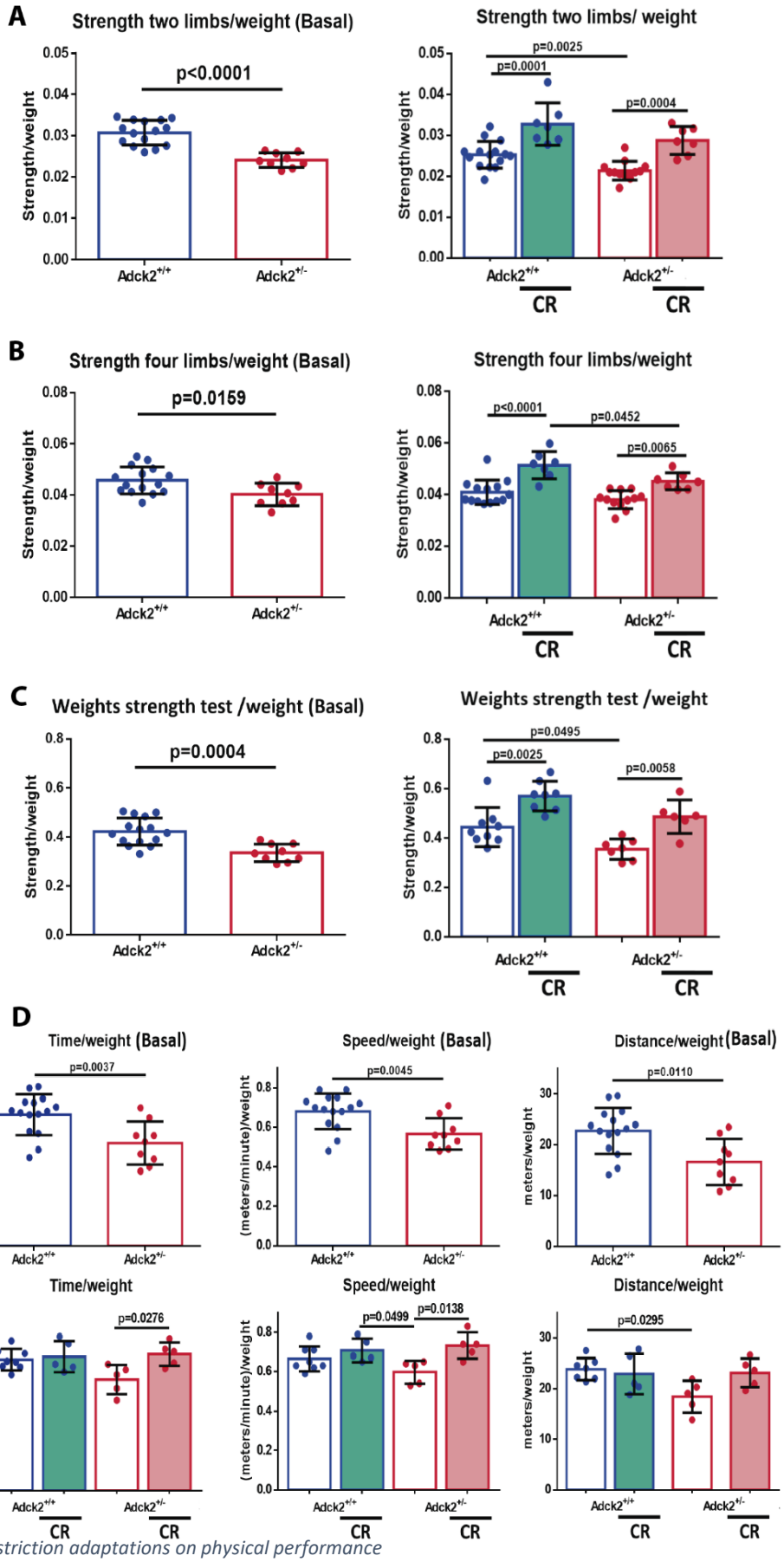

Figure 71 Caloric restriction adaptations on physical performance

Results for the two and four limbs grip strength tests, and the weight-lifting and aerobic treadmill tests are shown on basal conditions before starting diet period and at end of the diet period (A, B, C and D). All experiments were performed at the same time of the day to reduce variability associated with circadian rhythms. Mice were introduced into the experimental room 30 minutes before starting any behavioural test for acclimation. Data represent the mean +/- SD (N=5-15). Unpaired two-tailed t-test or one-way ANOVA tests were applied. P-values <0.05 were considered statistically significant.

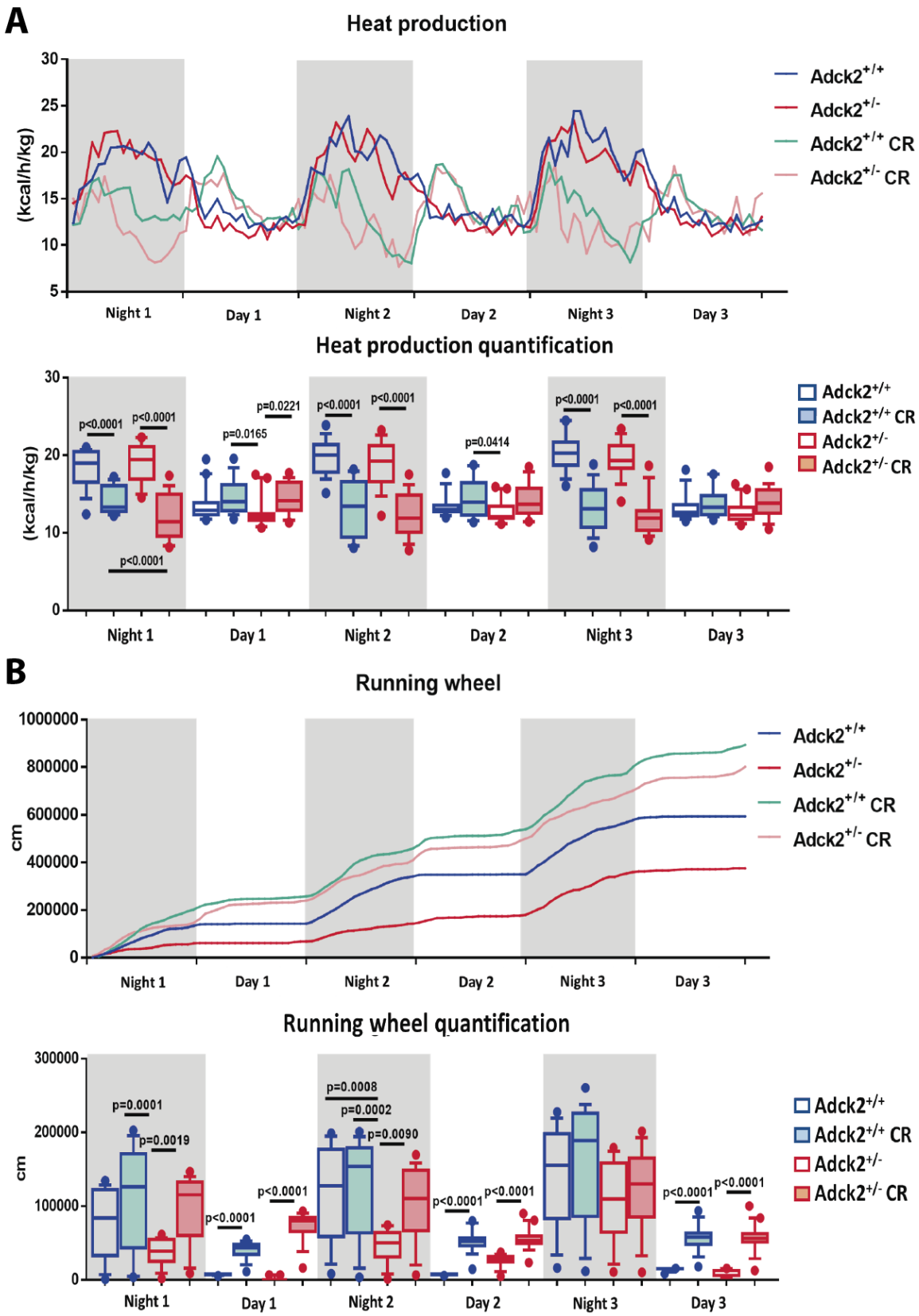

Figure 72 Heat production and running wheel activity on caloric restriction conditions.

Heat production and running wheel voluntary activity measured with the automated home cage phenotyping system is shown for a three night/day period. (A) Heat production is normalized by body weight (BW). (B). Voluntary wheel running on caloric restriction condition expressed as distanced travelled. The phenotyping system allows to record of in vivo parameters during the day and night periods including indirectly calorimetry analysis. The first 36 hours from every experiment were considered the acclimatization periods and were not used for the analysis. Data represent the mean +/- SD (N=5-8). A one-way ANOVA test was applied. P-values <0.05 were considered statistically significant.

Metabolic adaptations are promoted by the caloric restriction on glucose and insulin homeostasis.

Due to the implications of CR in glucose and insulin metabolism, we analysed glucose and insulin in fasting conditions (Figure 73A). Fasting glucose levels were higher in mutant mice on an *ad libitum* diet while both groups of animals on CR experienced a significant reduction in glucose levels. Fasting insulin levels were also increased in mutant mice on *ad libitum* condition and again, CR produced an important reduction in insulin levels in wild type and mutant mice. Furthermore, the HOMA index, which is a marker of insulin resistance and is calculated from glucose and insulin values, was higher in mutant mice on *ad libitum* condition. Particularly, CR produced an important decrease in the HOMA index in both groups. In balance, the three analyses reveal that mutant mice on *ad libitum* diet could be insulin resistant whereas mutant mice on CR experienced an improvement in insulin sensibility and glucose homeostasis.

Next, glucose and insulin homeostasis and metabolism were examined *in vivo* after introducing a stimulus. Initially, glucose homeostasis was examined with the glucose tolerance test (Figure 73B). In this regard, fasted animals were injected intraperitoneally with glucose and plasma glucose levels were monitored every 15 minutes for 60 minutes and after that every 30 minutes for 60 minutes post-injection. Mutant mice tended to have higher levels compared with wild type mice on *ad libitum* and a gradual and maintained glucose decrease. On the other hand, wild type and mutant mice on CR experienced a higher initial peak but a quicker decrease in glucose level, we quantified the area under the curve finding that CR mice have a lower area under the curve, probably indicating a faster glucose metabolism. CR stimulated a more efficient response increasing the speed of plasma glucose uptake by the different tissues, this response could be checked in the glucose tolerance test of our mutant mice on CR.

Insulin homeostasis was also checked with the insulin tolerance test (Figure 73C); therefore, mice were injected intraperitoneally with insulin after a short fasting period and glucose was controlled for 60 minutes after injection every 15 minutes. At first, mutant mice on *ad libitum* presented a more maintained glucose decrease during the test compared with wild type. The interpretation could be that intracellular fatty acids accumulation could be reducing Glut4 transport to the cell membrane (207) in response to the increment in insulin and, as consequence, glucose input to the cell could be delayed. In contrast, both groups on CR presented a more pronounced decrease in plasma glucose in response to insulin injection, indicating a more efficient transport of Glut4 to the cell membrane.

Besides, the generation of glucose in a fasted state from non-carbohydrate carbon substrates through hepatic gluconeogenesis was examined with the pyruvate test where fasted mice are injected with pyruvate and plasma glucose is controlled over 120 minutes (Figure 73D). At first, mutant mice on *ad libitum* present a lower glucose level compared with wild type mice on *ad libitum* indicating less efficient gluconeogenesis. Mice on CR presented a more maintained profile over the test. When the area under the curve was quantified, mutant mice on *ad libitum* presented a smaller value compared with wild type mice on *ad libitum*, but mutant mice on CR presented an increase in the area under the curve obtaining a mean value similar to the wild type.

Finally, insulin production after glucose injection was examined to understand if defects in glucose and insulin homeostasis could be associated with insulin production or could be related to the own metabolism of glucose and insulin. Insulin levels were measured on basal conditions and after 20- and 40-minutes post glucose injection (Figure 73E). We found a tendency by which mutant mice on *ad libitum* and CR presented higher levels of insulin production, but it is not significant suggesting the idea that the differences observed in the other tests could be associated with glucose and insulin metabolization and not with the production of insulin.

In summary, mutant mice on *ad libitum* presented a glucose and insulin deregulation that promoted an insulin resistance status compared with wild type mice, whereas mutant mice in CR present an improvement in insulin and glucose sensitivity similar to wild type condition.

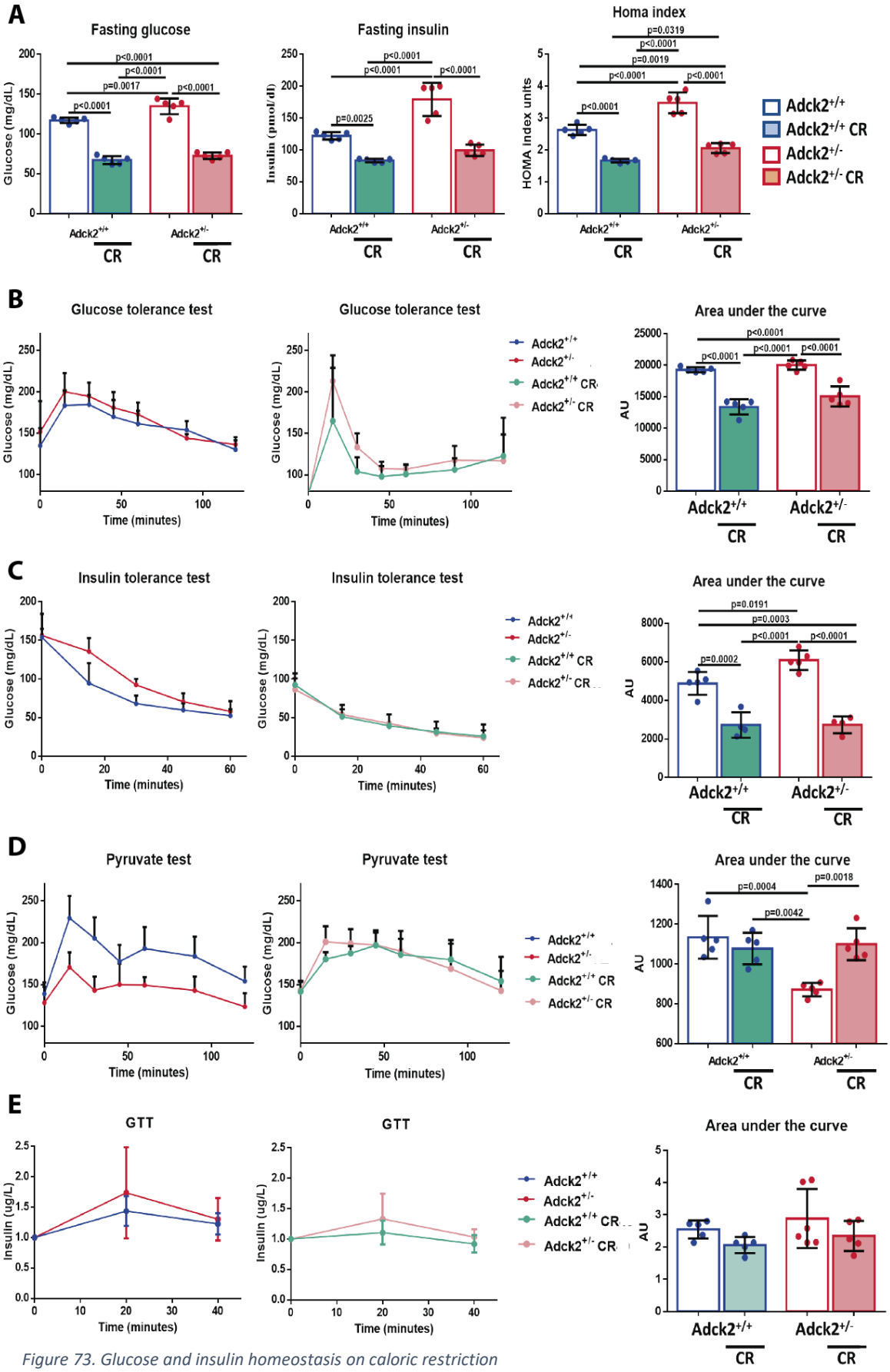

Figure 73. Glucose and insulin homeostasis on caloric restriction

(A) Fasting glucose and insulin, HOMA index. (B). Glucose tolerance test (GTT), glucose concentration in the blood after glucose load and area under the curve (AUC). (C). Insulin tolerance test (ITT), plasma levels of glucose after insulin injection and AUC quantification. (D). Pyruvate tolerance test (PTT). Glucose levels in the blood after pyruvate injection and AUC quantification. (E) Plasma insulin after glucose intraperitoneal (IP) injection. Data represent the mean +/- SD (N=4-5). A one-way ANOVA test was applied. P-values <0.05 were considered statistically significant.

Mitochondrial adaptations to caloric restriction

Next, we performed a bioenergetic characterization to determine the effect of CR on mitochondria metabolism. For this purpose, we isolated mitochondria from the skeletal muscle to quantify CoQ levels by HPLC (Figure 74A). Mutant mice on *ad libitum* presented a decrease in CoQ_9 and CoQ_{10} compared with wild type mice on *ad libitum*, as we have previously reported on this project. CR increased CoQ_9 and CoQ_{10} levels on mitochondria isolated from skeletal muscle while wild type on CR did not show any increase in CoQ_9 or CoQ_{10}. Probably, the explanation could be in the endogenous level of CoQ that the mitochondria can contain, which is at a maximum level in the wild type mitochondria and a lower level in mutant mitochondria, consequently, the effect of CR on CoQ biosynthesis stimulation was more pronounced in mutant mice. Furthermore, CoQ_9 and CoQ_{10} ratio was also calculated to check if any of the two isoforms was predominant over the other in any of the groups analysed in that case, but no significant changes were found indicating that the increase was reported in mutant mice on CR was in the biosynthesis of both isoforms. In all cases, CoQ_9 content was 13 times higher than CoQ_{10} in purified mitochondria, being CoQ_9 93% of the total ubiquinone pool and CoQ_{10} only the remaining 7%.

RER reflect the energetic substrate used *in vivo* by the mice. An RER close to 1.0 reflects a higher use of carbohydrates as energy while an RER value close to 0.7 indicates a higher use of fatty acids as energy substrate. When we analysed our mice in *ad libitum*, we observed that mutant animals have higher RER values indicating a higher use of glycolytic pathways for energy production (Figure 74B). When we analysed mice on CR, we found a total reorganization of RER metabolism and circadian rhythm potentially associated with the CR model used where mice re-feed the first hour in the morning. Mice on CR show an opposite profile to mice on *ad libitum* indicating that when mice on *ad libitum* are using carbohydrate substrates mice on CR are using fatty acids and vice versa. This reorganization could be associated with the metabolic changes that we previously found on mice on CR. However, it would be important to highlight that both groups of mice on CR showed higher extreme points indicating that mice on CR are more efficient to use carbohydrates or fatty acids.

Moreover, ketone bodies production was examined in plasma, we found a decrease in the levels of β-hydroxybutyrate in mutant mice on *ad libitum* compared with wild type, reflecting a defect on fatty acids β-oxidation (Figure 74C). Mutant mice on CR tend to present higher β-hydroxybutyrate levels than mutant mice on *ad libitum*.

Free fatty acids levels were also determined, observing a reduction in mice with CR, which could be probably stimulated by an increase in fatty acids transport inside of mitochondria on the tissues associated with CR (Figure 74B).

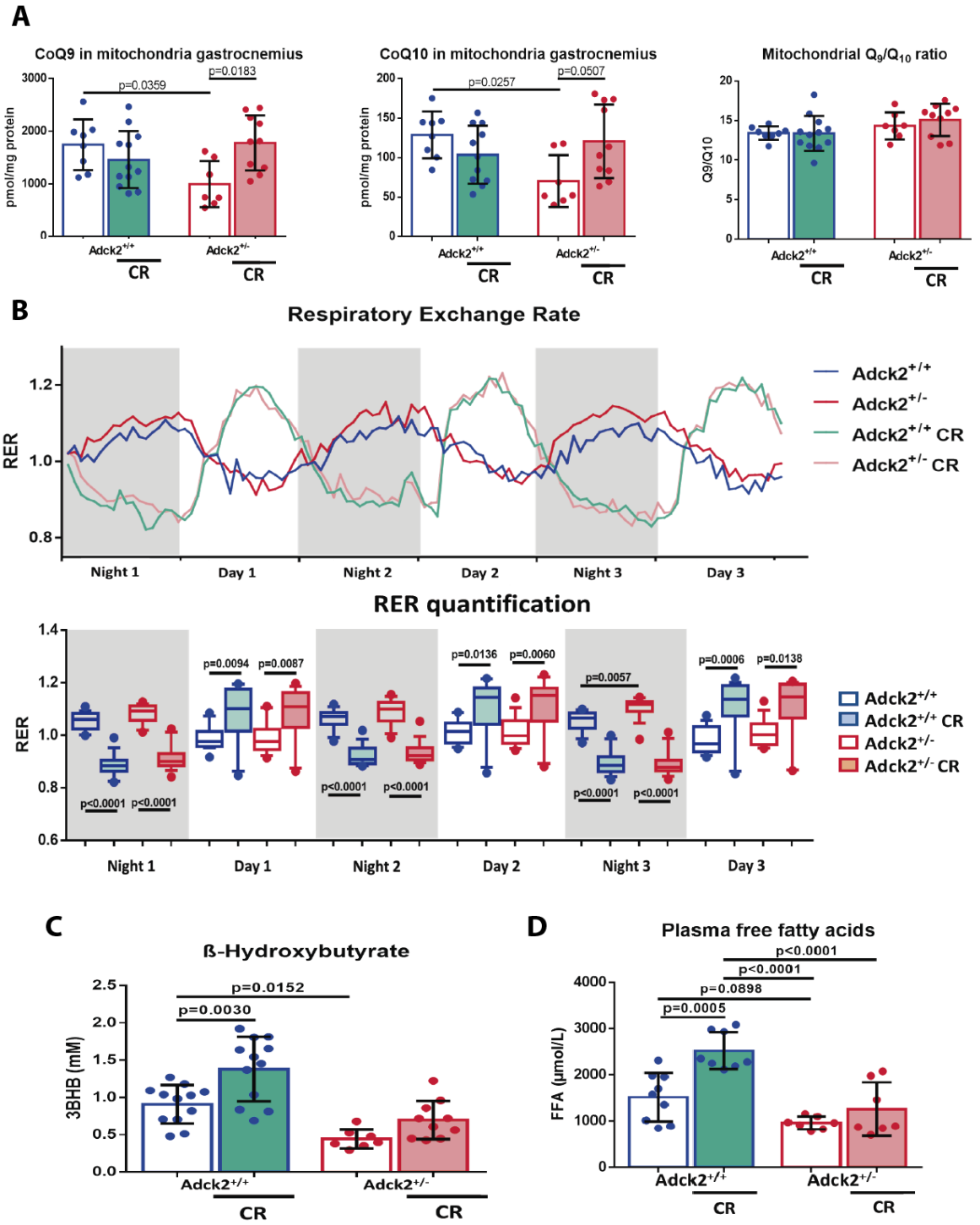

Figure 74 Bioenergetic and metabolic analysis on caloric restriction

(A). CoQ_9 and CoQ_{10} levels on mitochondria isolated from gastrocnemius muscle. Ratio CoQ_9/CoQ_{10} (N=7-12). Skeletal muscle was homogenized with a cell dissociator, mitochondria were isolated by serial centrifugations and after lipids extraction, CoQ_9 and CoQ_{10} were quantified by HPLC (B). Respiratory Exchange Ratio (RER) measured with the automated home cage phenotyping system is shown for a three night/day period. (N=5-8). (C) β-hydroxybutyrate levels and free fatty acids in plasma after mice were fasted for 12 hours (N=7-12). One representative experiment of three independent experiments is shown. Data represent the mean +/- SD. One-way or two ways ANOVA test were applied. P-values <0.05 were considered statistically significant.

Finally, we performed respiration analyses on isolated mitochondria to study *in vivo* mitochondrial metabolism in wild type and heterozygous *Adck2* knockout mice under *ad libitum* and CR conditions maintaining mitochondria alive and functional outside of the skeletal muscle and we perform respiration analysis using different energetic substrates such as pyruvate plus malate or palmitoyl-L-carnitine plus malate (Figure 75). We use different substrates in the assays to stimulate different energetic pathways, pyruvate plus malate was used in the coupling assay to stimulate the Krebs cycle plus ETC machinery whereas palmitoyl-L-carnitine plus malate were used to stimulate fatty acids β-oxidation plus ETC machinery. Mitochondria isolated from heterozygous *Adck2* knockout mice *ad libitum* present lower respiration in the Coupling Assay compared with mitochondria from wild type *ad libitum* (Figure 75A). Particularly State IIIu and Spare capacity were affected. More importantly, mitochondria isolated from mice on CR of both genotypes presented higher respiration levels than the same genotype on an *ad libitum* diet, indicating that CR could improve mitochondrial respiration. Particularly, mitochondria isolated from mutant mice on CR displayed a huge increase compared with mitochondria isolated from mutant mice on *ad libitum*. We also found a decrease in respiration in mitochondria isolated from mutant mice compared with wild type mitochondria on β-oxidation assay (Figure 75B). Even, we found differences in more parameters such as basal respiration, State III, State IIIu and Spare capacity, showing that mitochondria isolated from mutant mice could have a defect in fatty acids β-oxidation and CR improved the β-oxidation on all respiratory parameters analysed.

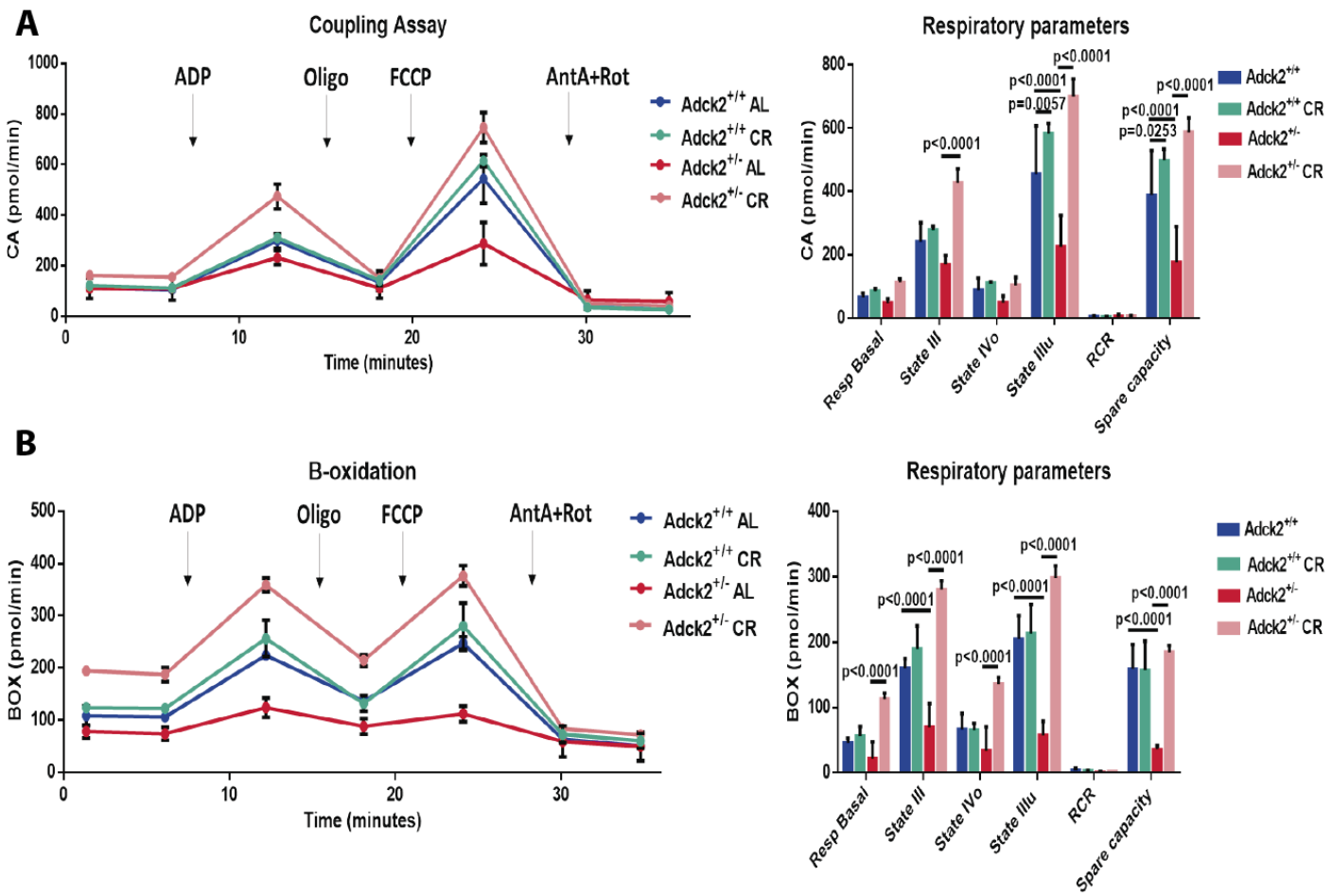

Figure 75 Respiration analysis on mitochondria isolated from skeletal muscle under caloric restriction
(A). Coupling assay on mitochondrial isolated from skeletal muscle on caloric restriction. (B) Fatty acids β-oxidation on mitochondria isolated from skeletal muscle(N=5). One representative experiment of three independent experiments is shown. Data represent the mean +/- SD. One-way or two ways ANOVA test were applied. P-values <0.05 were considered statistically significant.

These results indicated that mutant mice presented an alteration in mitochondrial function. So, we decided to examine mitochondrial complexes' activity and assembly to determine if the defects found in mutant mitochondria could be associated with an ETC disposition. Firstly, we studied the maximum activity of each complex in total homogenate from skeletal muscle. CR stimulated an increase in citrate synthase (Figure 76A) which was a marker of mitochondrial mass suggesting that CR increased mitochondria mass on skeletal muscle in both genotypes. The enzymatic activity of the different complexes was determined using specific substrates, resulting in CR that could enhance the activity of complexes I and II in both genotypes. Next, we studied the gel-activity of complexes for complex I and complex IV running a Blue Native electrophoresis where we did not find differences in the activity of complex I nor complex IV (Figure 76B). Finally, we performed immunoblotting with specific antibodies for complex I and IV and we found an increase in the isolated complex I isoform in mutant mice on CR and the association of

complexes I+III_2+II_n in both groups of mice on CR (Figure 76C). These results are in agreement with the enzymatic activity assays performed suggesting that CR stimulates complex I and complex I potential associations, probably could be associated with higher activation of mitochondria pathways resulting in a higher electron flow through ETC.

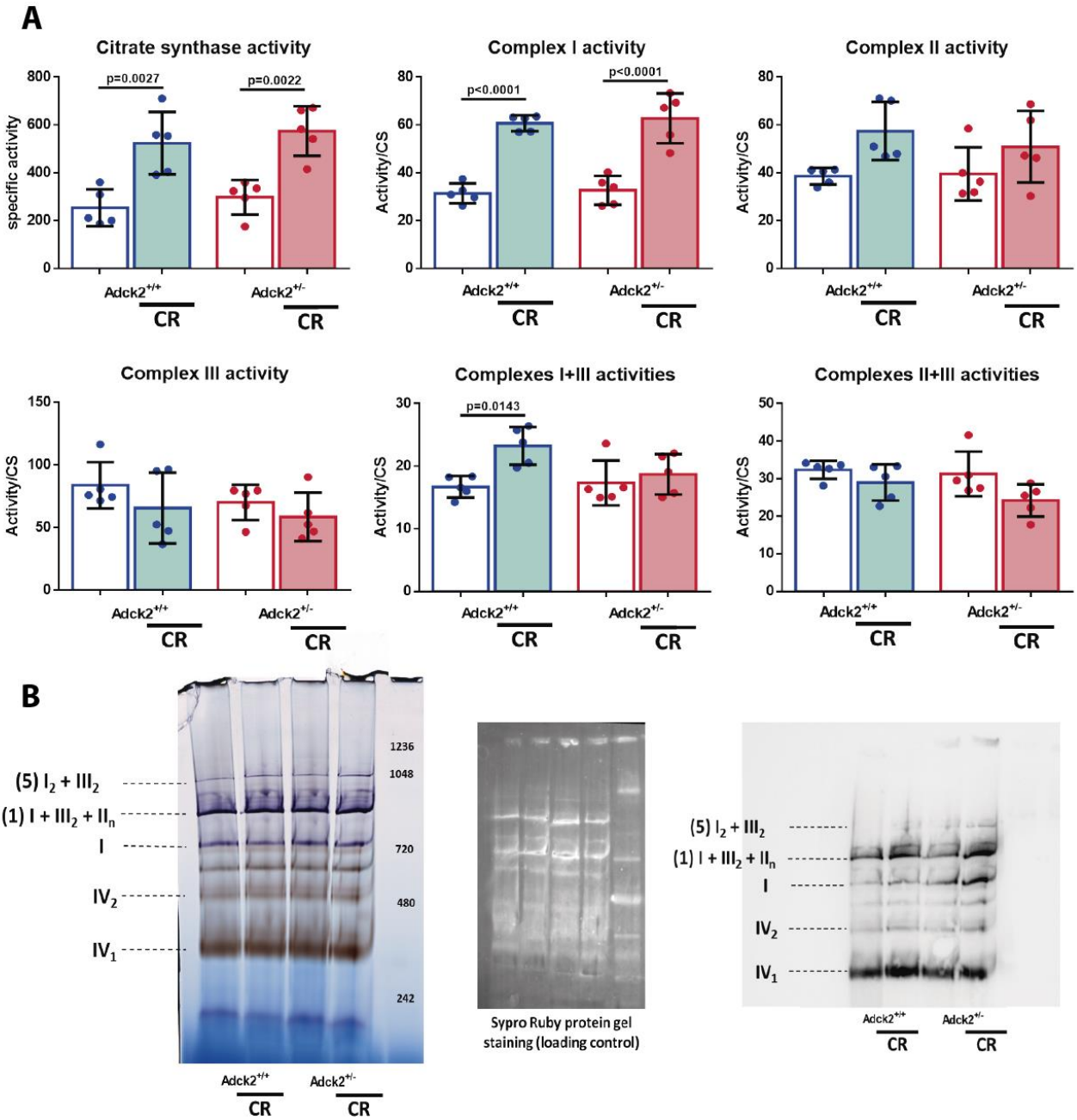

Figure 76 Analysis of the complexes of the ETC under caloric restriction condition

(A). Spectrophotometric activity of complexes and citrate synthase activity on gastrocnemius muscle. Data represent the mean +/- SD. A one-way ANOVA test was applied. P-values <0.05 were considered statistically significant. (B). Mitochondria isolated from skeletal muscle were used, and 100 µg of solution enriched in mitochondria were loaded per sample. Gel activity assay of complexes I and IV. Detection of the respiratory complexes and potential supercomplexes after BNGE by immunoblotting to define bands for complexes and supercomplexes. Specific antibodies against complexes I and V were used. Blue-native gel electrophoresis (BNGE).

On balance, mitochondria from mutant mice on *ad libitum* present a mitochondrial dysfunction characterized by lower mitochondrial CoQ_9 and CoQ_{10} levels and also by lower mitochondrial respiration using pyruvate or palmitoyl-L-carnitine as substrates, which could be improved by CR. We also found that CR could be increasing complex I activity and complex $I+III_2+II_n$ assembly which could contribute to an improvement in ETC performance.

Metabolic profile modulation by caloric restriction in different tissues

Mutant mice showed a mitochondrial dysfunction characterized by lower mitochondrial respiration with either pyruvate or fatty acids as substrates and lower CoQ_9 and CoQ_{10} levels. To understand its implication in the general metabolism of the mice we studied the metabolomic profile in muscle, liver and plasma from wild type and heterozygous mutant animals on CR and an *ad libitum* diet. The results indicate that CR depicts a specific tissue effect about the damage associated with the mutation in the *ADCK2* gene (Figure 77A). CR modulates liver metabolism similarly in wild type and mutant mice on CR compared with *ad libitum* mice. The liver of CR mice is adapted to use energy from peripheral tissues for subsequently gluconeogenesis, including increased levels of fatty acids and amino acids (essential, gluconeogenic and ketogenic amino acids), and an elevation of metabolites of different energetic pathways (TCA cycle, urea cycle and purines). Metabolic profile in plasma showed an elevation of TCA cycle metabolites and amino acids in wild type animals under CR compared with *ad libitum* showing an adaptation to fulfil energy demands for the different tissues. However, heterozygous *Adck2* mutant mice on CR did not exhibit the same increase in amino acids in plasma that was observed in CR wild type mice. Muscle metabolites profile determination reveals that CR in wild type mice induce an elevation in fatty acids, amino acids and TCA cycle metabolites in comparison with *ad libitum* CR promoted the use of fatty acids and amino acids as energy substrate instead of glucose from glycolysis.

Particularly, the metabolic profile in the liver shows that CR promoted the release of fatty acids (FA) from adipose tissue, because of the levels of myristate, stearic acid, laureate, 2-monopalmitic acid, adipic acid and cholesterol were increased (Figure 77B). Also, we found a breakdown of proteins from skeletal muscle about an increase in levels of a wide range of amino acids, including ketogenic (Phe, Tyr, Ileu) and glucogenic (Gly, Thr, Asp, Met), branched-chain (BCAAs, Val, Ileu y Leu) and essential amino acids (e.g., Val, Ileu, Leu, Met, Phe, Thr, Pro, Ala, Met). Other metabolites elevated were glutamine, glutamate, 3-hydroxybutyrate (a ketone body) and intermediaries of the TCA cycle such as citrate and isocitrate, which together with the

increment of ornithine agreed with activation of both the urea cycle and the TCA cycle to metabolize proteins. These data supported the idea that CR led to the mobilization of peripheral energy deposits that the liver can subsequently be utilized for gluconeogenesis. Purines elevation in CR were associated with ATP degradation suggesting a more efficient energy metabolization. Liver from heterozygous *Adck2* knockout mice on CR showed a partial adaptation to reproduce the changes observed in wild type mice on CR increasing amino acids levels, urea cycle intermediaries and purines.

Our results suggested that mitochondria from the liver on CR function mainly in catabolic mode (Figure 77B), with fatty acid β-oxidation driving the TCA cycle. Additionally, a profile consistent with anaplerotic replenishment via amino acids (both ketogenic and gluconeogenic) and the urea cycle activation was observed in wild type and mutant mice on CR. Under these circumstances, the anaplerotic filling of the TCA cycle together with the energetic fatty acids fuelling of mitochondria rendered a metabolism relying less on glucose. The apparent decrease of intermediaries of the glycolytic pathway and the increase in insulin sensitivity (e.g., significantly lower HOMA-IR index, fasting insulin and glucose in plasma) exhibited by the CR-treated mice support this notion. In response to CR, the liver's metabolites profile from wild type and mutant mice showed an enhancement in fatty acids use as a fuel to provide energy to the rest of energy-dependent tissues, suggesting a shift in hepatic substrate utilization toward gluconeogenesis instead of glycolysis.

Metabolites profile in plasma of mice on CR suggested induction of catabolism by a breakdown of proteins from skeletal muscle and an accumulation of metabolites for the TCA cycle in plasma (Figure 77C). We found an accumulation of several amino acids in plasma, ketogenic (e.g. Ileu) and gluconeogenic (e.g. Gly), including branched-chain (BCAAs, Val, Ileu, Leu) and essential (e.g., Phe and Trp) amino acids on CR wild type mice. However, these amino acids accumulation was not so clear in *Adck2* knockout mice on CR, suggesting the idea of the breakdown of skeletal muscle proteins was not happening properly, TCA cycle metabolites were also elevated in the plasma of mutant mice on CR, suggesting a mobilization of peripheral energy deposits that the liver could use for gluconeogenesis. As a consequence of the catabolic metabolism adapted in the liver of mice on CR, the TCA cycle metabolites were increased in plasma to feed the different tissues of the organism of the mice on CR. Additionally, CR induced activation of metabolites from purines and the urea cycle.

Metabolic profiles from skeletal muscle reveals that CR induced a series of adaptations that correspond with metabolic changes associated with energy deprivation (Figure 77D). CR wild

type mice exhibited an increase in fatty acids levels and TCA metabolites, and a decrease in amino acids. In contrast, mutant mice on CR a higher elevation of fatty acids in the muscle in comparison with mutant mice on *ad libitum*. Probably, the increase of fatty acids in the muscle was related to fatty acids β-oxidation promoted by energy deprivation, indicating a metabolic switch from glucose to the use of fatty acids as energy substrate.

In summary, a metabolomic study reveals that CR had a tissue-specific effect, affecting every tissue in a specific way (Figure 77A). CR mice showed a metabolic switch to use fatty acids instead of glucose as energy substrate.

Later, we validated the changes of some metabolites that were modulated by CR. We observed that CR promoted similar adaptations in the liver in both mutant and wild type animals (78). However, the changes promoted by CR on plasma (Figure 79B) and on skeletal muscle (Figure 79A) only occurred in some specific metabolites suggesting the idea that adaptation stimulated by CR did not completely occur. Principal Component Analysis (PCA) on the metabolomic analysis revealed that CR animals were displaced from mice on *ad libitum* in the three tissues studied, indicating that CR could produce an important metabolic reorganization in the same direction in both groups of mice (Figure 80).

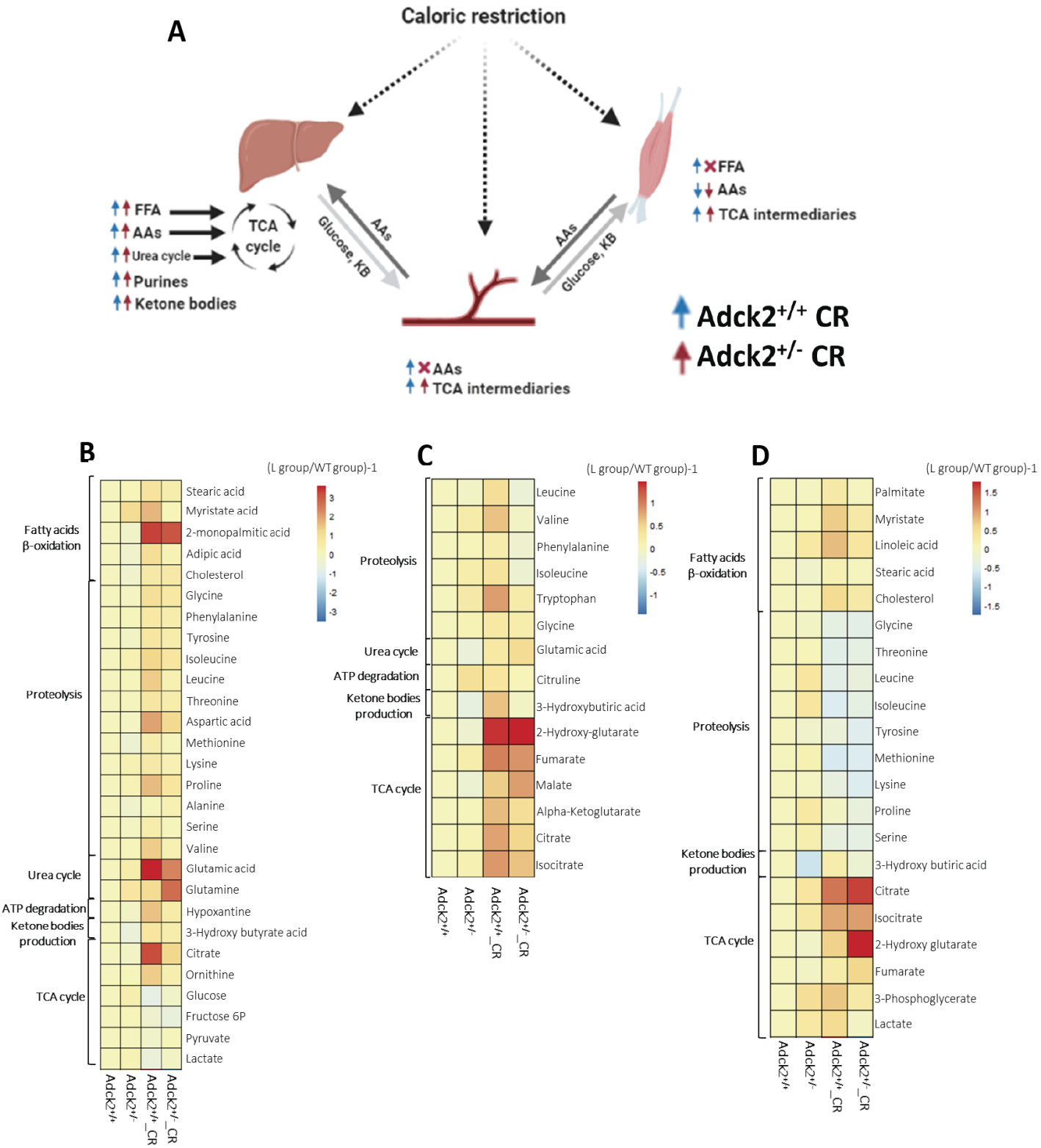

Figure 77. Metabolic profile in plasma, liver and muscle on calorie restriction conditions

(A). Summary of effects of caloric restriction on metabolomics (B). Metabolic profile in the liver (N=3-5). (C). Metabolic profile in plasma (N=3-5). (D). Metabolic profile in muscle (N=3-5). FFA free fatty acids. AAs aminoacids. TCA tricarboxylic cycle.

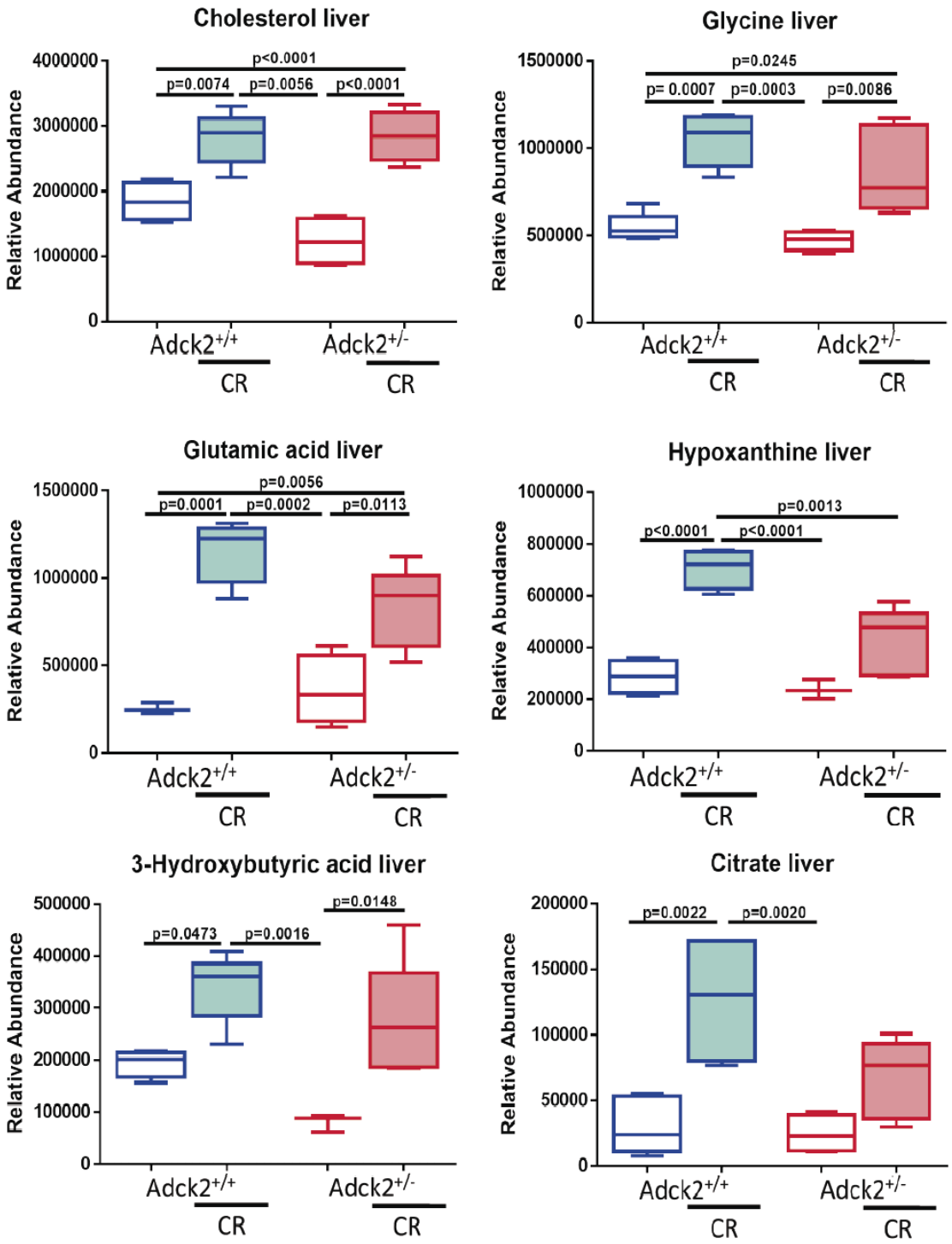

Figure 78 Functional validation and representation of metabolomics in liver

Metabolic profile in liver tissue (N=3-5). Data represent the mean +/- SD. A one-way ANOVA test was applied. P-values <0.05 were considered statistically significant.

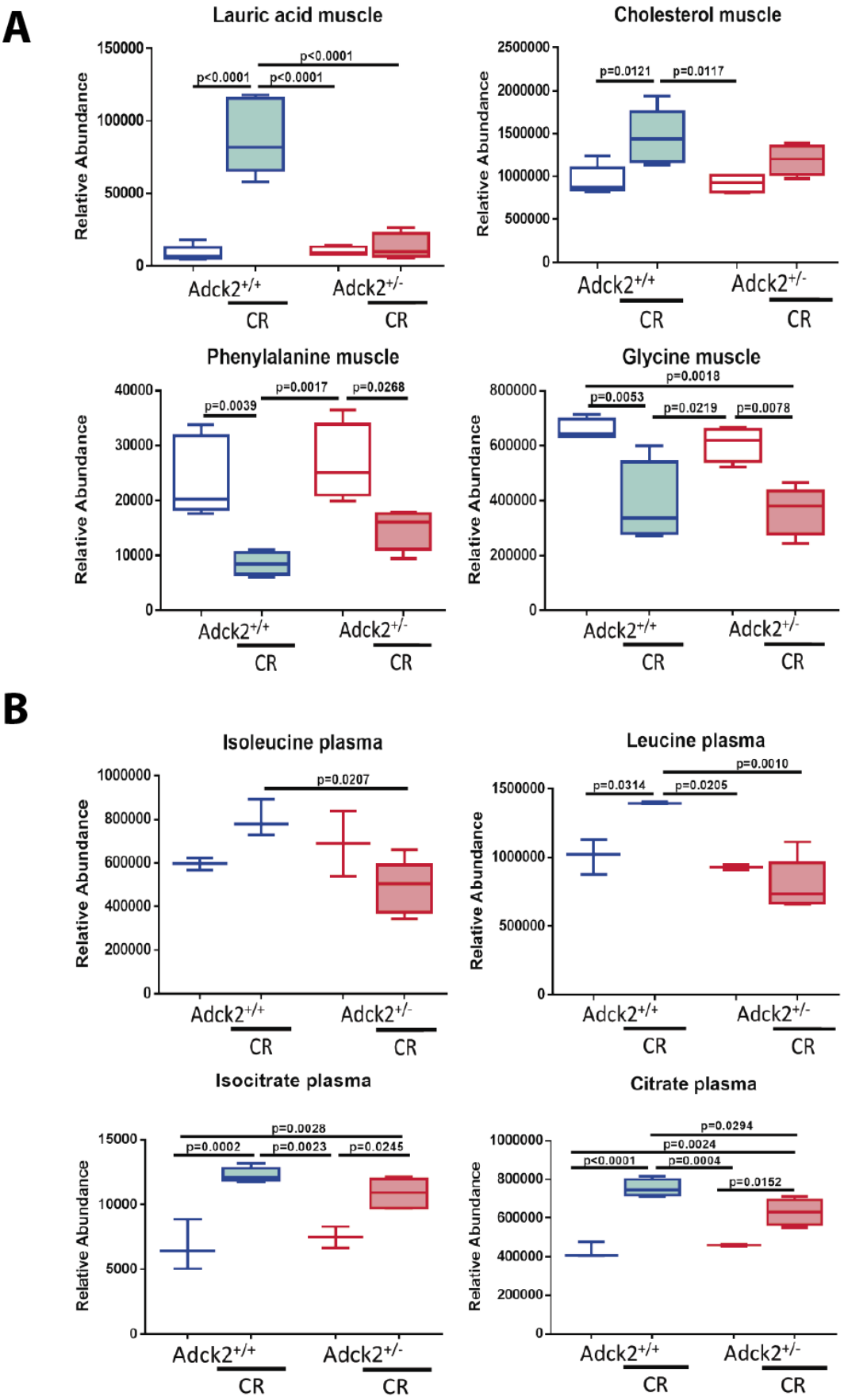

Figure 79 Functional validation and representation of metabolomics in muscle and plasma

(A). Metabolic profile in muscle (N=3-5). (C). Metabolic profile in plasma (N=3-5). Data represent the mean +/- SD. A one-way ANOVA test was applied. P-values <0.05 were considered statistically significant.

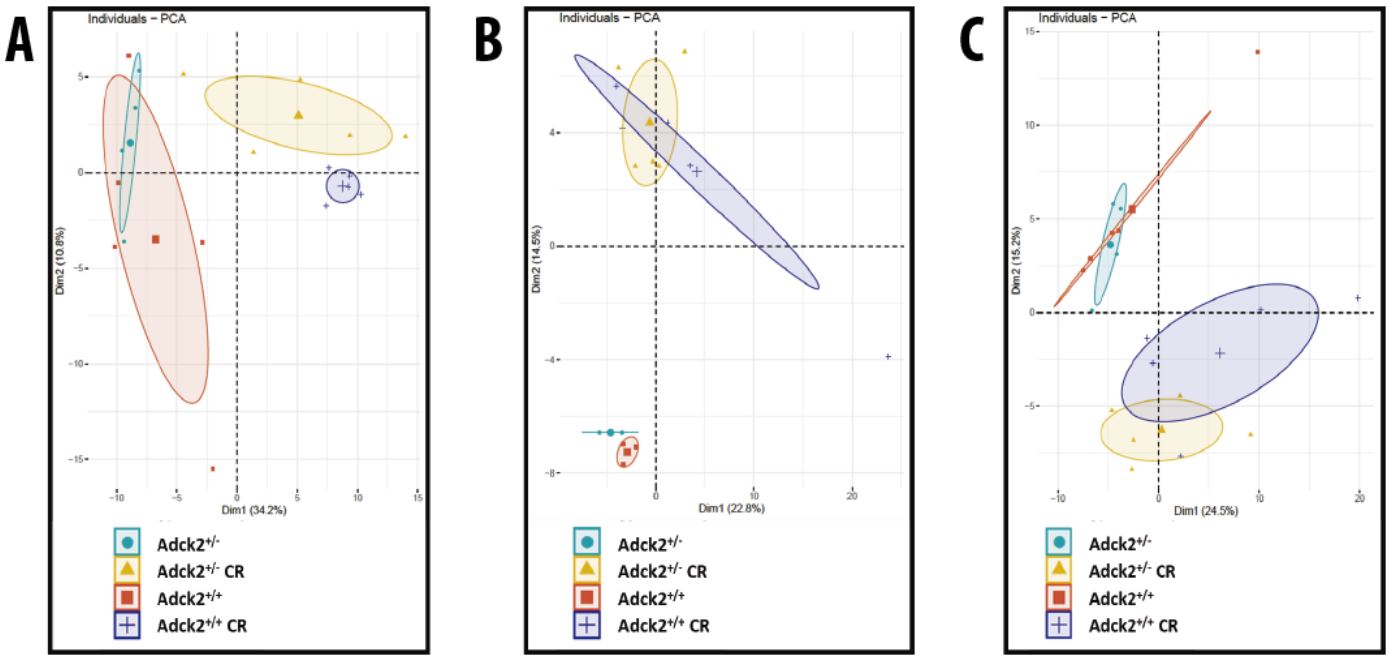

Figure 80 Principal Components Analysis of metabolomics.
PCA analysis on liver (A), plasma (B) and muscle (C). (N=3-5).

Myofiber typing modulation by caloric restriction

CR induces a metabolic switch to use oxidative pathways and fatty acids as energetic substrates instead of glycolytic pathways and glucose, together with an induction of protein catabolism. To examine if CR could lead to more oxidative metabolism in skeletal muscle, we studied the myofiber composition on TA muscle in heterozygous *Adck2* knockout and wild type mice under CR conditions (Figure 81). This staining identifies myofibers type IIA, myofibers type IIX and myofibers type IIB. Almost all myofibers in TA are type II myofibers, type IIA are more oxidative myofibers while type IIB myofibers are more glycolytic myofibers. Myofibers type IIX are hybrid myofibers that present a crossed metabolism.

Mutant mice on an *ad libitum* diet presented a lower proportion of oxidative myofibers type IIA compared with wild type mice, while mutant mice had a higher proportion of hybrid myofibers suggesting that mutant myofibers displayed a less oxidative profile (Figure 82). However, CR changed myofiber typing to a more oxidative profile in both genotypes increasing the proportion of myofibers type IIA to the detriment of the glycolytic type IIB myofibers. Particularly, heterozygous *Adck2* knockout mice on CR presented a profile similar to the wild type on CR and increased the proportion of myofibers type IIA compared with the mutant mice on *ad libitum* (Figure 82).

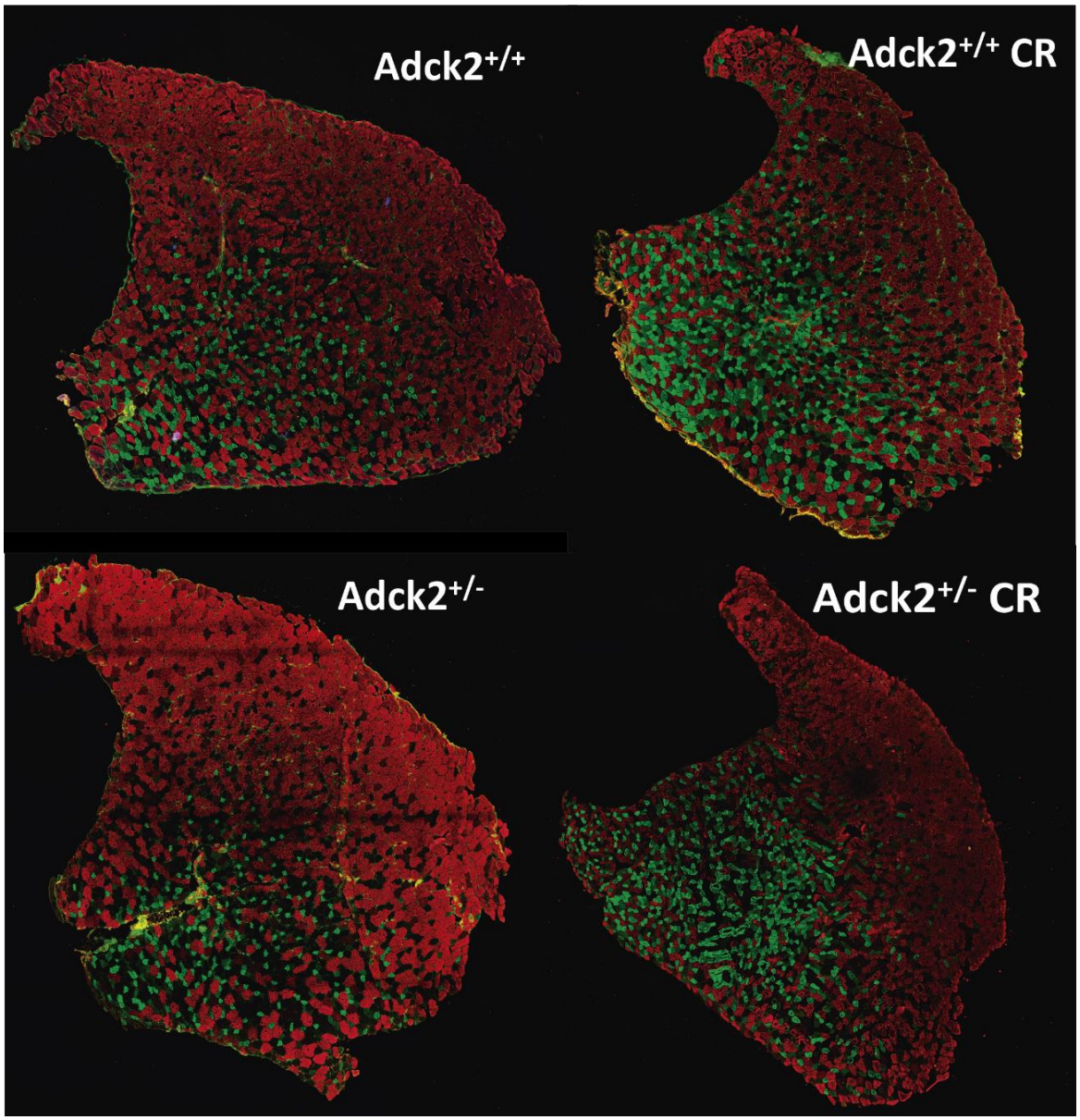

Figure 81 Representative images of myofiber composition on tibialis anterior (TA) muscle of mice under caloric restriction

Immunostaining analysis to determine myofiber composition in transversal sections from tibialis anterior (TA) muscle from adult mice (thirteen month-old). Myofibers type IIA, IIB and IIX appear in green, red and black. Cryosections of TA muscle (12 µm) were used for the immunostaining.

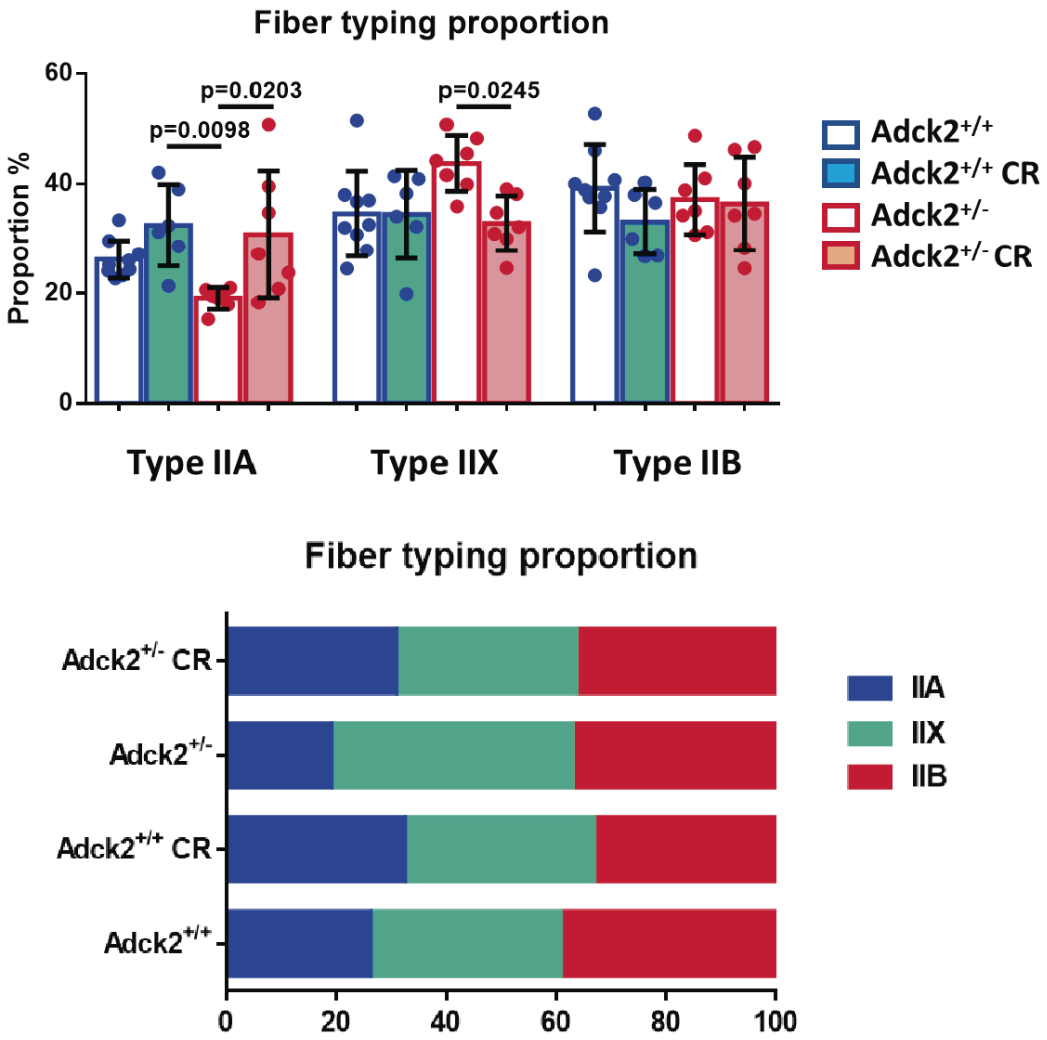

Figure 82 Myofiber composition in TA muscle from mice on caloric restriction

Myofiber composition was analysed in TA muscle from thirteen month-old mice. Type IIA, IIB and IIX appear in green, red and black. Data represent the mean +/- SD (N=6-8). A one-way ANOVA test was applied. P-values <0.05 were considered statistically significant.

Modulation of metabolic markers by caloric restriction

Gastrocnemius muscles were homogenized by sonication in RIPA buffer, after that protein concentration was quantified. Finally, protein solutions were mixed with LB5X and DDT and heated for 5 minutes at 95 ºC to perform western blot analyses.

Although, protein levels of mitochondrial mass marker were not different between wild type and Adck2$^{+/-}$ mice on ad libitum diet, we found an upregulation in both groups of mice on CR conditions for PGC1α (Figure 83A). Moreover, Sirt1 protein levels were upregulated in mice on CR, indicating an adequate adaptation to fasting. Sirt3 protein, the main mitochondrial deacetylase, was also increased in CR mutant mice (Figure 83A). AKT protein levels were increased on samples of mice submitted to CR indicating a higher sensibility to insulin (Figure

84), AMPKα and Foxo1 belong to a pathway activated during fasting, were upregulated in mice on CR. The response observed in ERK levels on animals from CR groups could indicate an activation of apoptosis. CR intervention induced lower levels of Foxo4 in skeletal muscle, which leads to the observed effect on glucose homeostasis. The increase on ACAA2 levels on mice on CR evidenced a higher fatty acids β-oxidation. These changes showed acclimatization to reduced energy intake and fasting in skeletal muscle under CR (Figure 84).

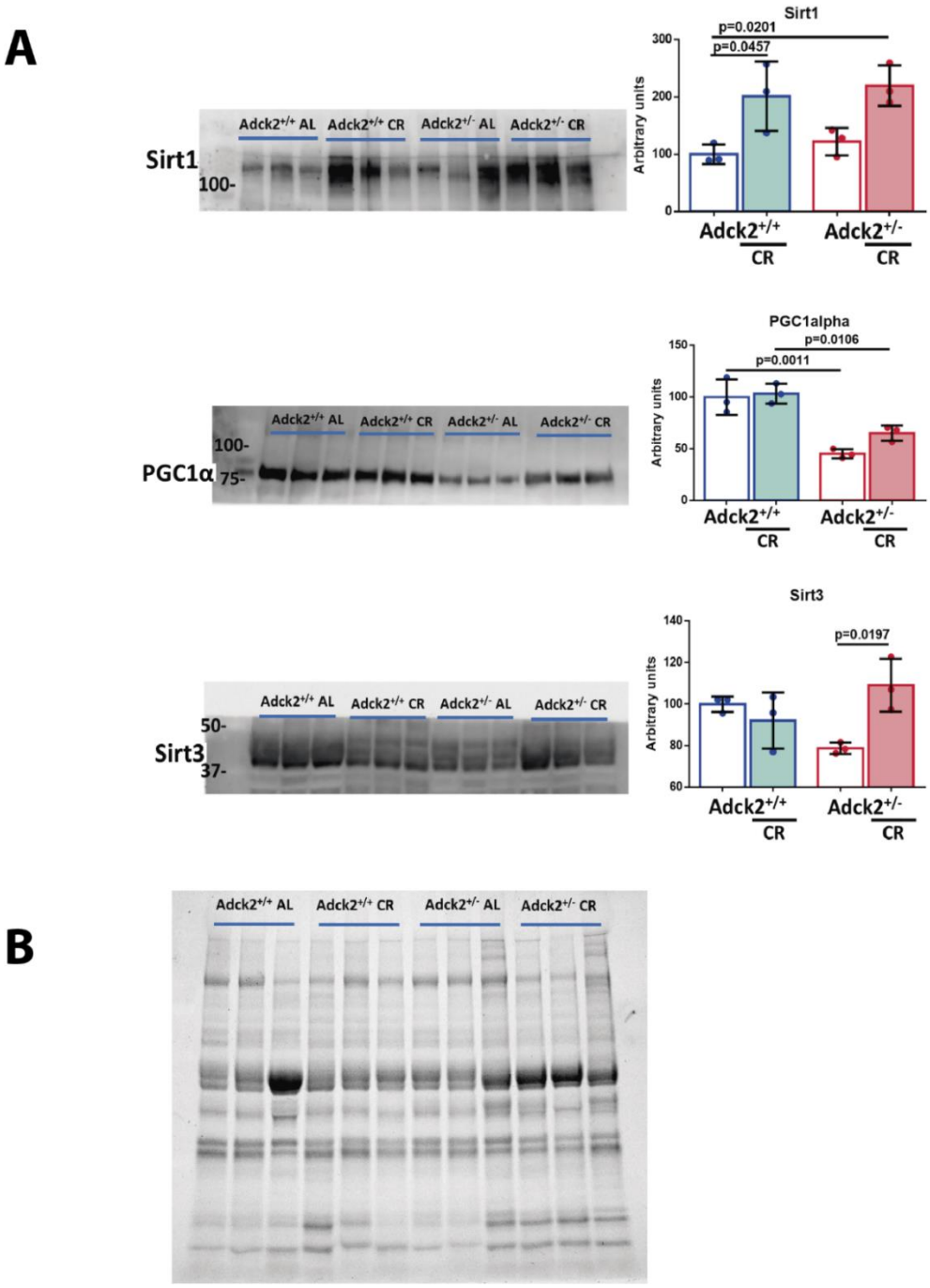

Figure 83 Modulation of metabolic markers associated with mitochondria.
(A). Protein levels of mitochondrial metabolic markers from gastrocnemius muscle homogenate. (B). Stain-free image used as control for protein load. Data represent the mean +/- SD (N=3). A one-way ANOVA test was applied. P-values <0.05 were considered statistically significant. Image Lab software was used for quantification analysing volume intensity parameters.

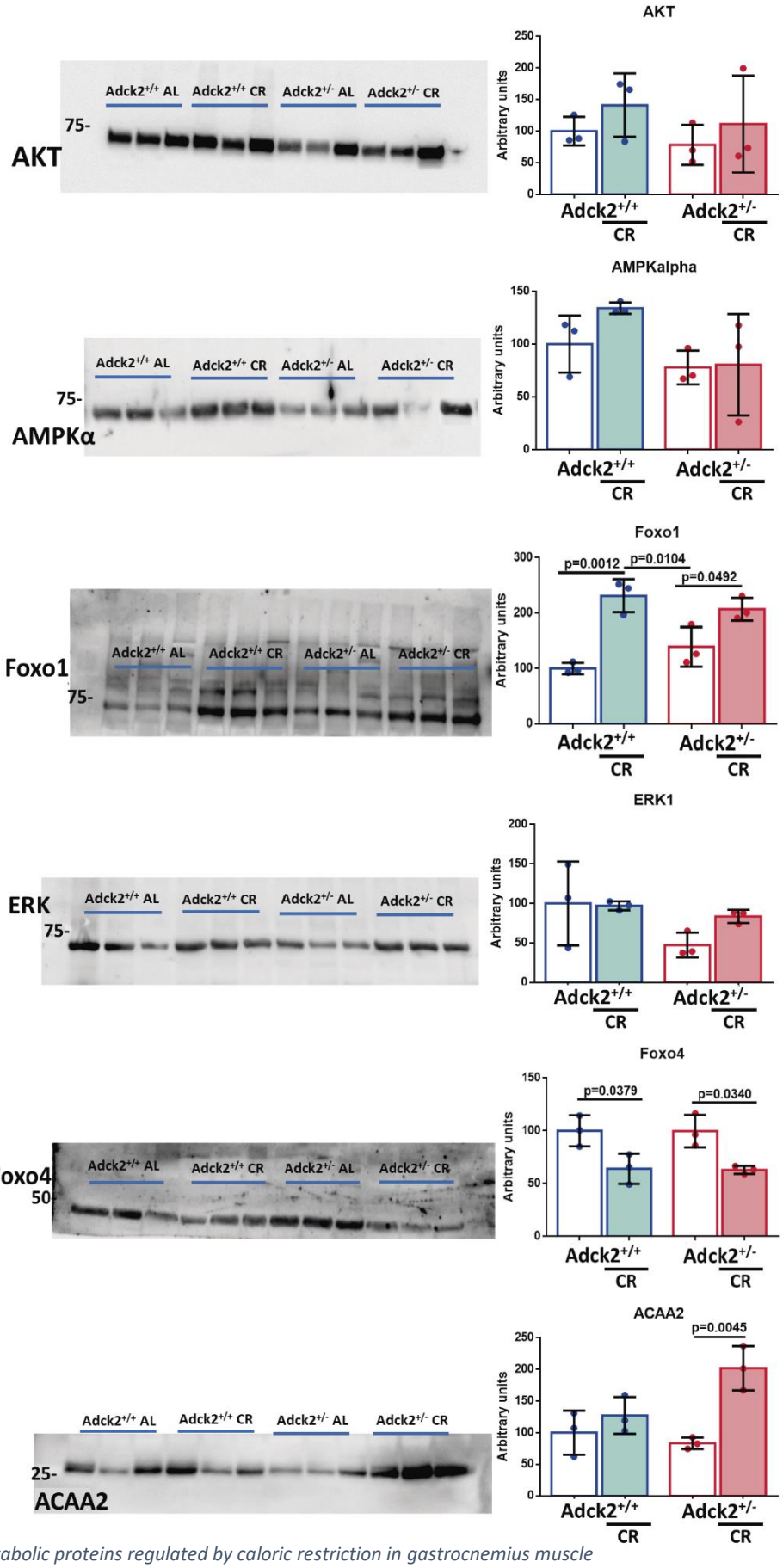

Figure 84 Metabolic proteins regulated by caloric restriction in gastrocnemius muscle

Data represent the mean +/- SD (N=3). A one-way ANOVA test was applied. P-values <0.05 were considered statistically significant. Image Lab software was used for quantification analysing volume intensity parameters.

Caloric restriction environment induces satellite cells differentiation

We have shown that CR was able to induce changes in myofiber composition and mitochondrial metabolism towards a more oxidative metabolism. Previously in chapter 2, we described that the differentiation process of SCs is affected in *Adck2* mutant mice possibly associated with a metabolic problem derived from a defect to carry out oxidative metabolism during differentiation. Based on these results, we decided to develop an *in vitro* approach to examine post-natal myogenesis under CR conditions to assess the potential effects of CR on SCs differentiation. However, SCs isolated from mice on CR would not reproduce CR *in vivo* adaptation because since almost 20 years ago it had been described that primary cell culture from mice on CR would lose CR adaptations 72 hours after seeding (208), and consequently using primary cells culture from mice on CR we would not be able to reproduce CR adaptation *in vitro*.

To reproduce CR *in vivo* adaptation, blood obtained from mice under CR and *ad libitum* conditions was collected and after that serum was isolated from blood. Later differentiation of SCs was induced with a differentiation medium that contains the serum from wild type and mutant mice on *ad libitum* and CR. We decided to use serum from mice instead of commercial serum and medium options due to we already identified on metabolomics analyses that there are differences in plasma nutrients composition between wild type and heterozygous *Adck2* knockout mice, and more significantly CR produce important changes in serum composition thus reproducing completely *in vivo* adaptations we thought that serum from mice was the most reliable option.

Group	Satellite cells isolated from	The serum used for the culture experiment
1	Wild type mice on *ad libitum*	Wild type on *ad libitum*
2	Wild type mice on *ad libitum*	Wild type on CR
3	Mutant mice on *ad libitum*	Mutant on *ad libitum*
4	Mutant mice on *ad libitum*	Mutant on CR

Initially, we studied differentiation by the measure of myotubes growth MyHC area and myotubes length for 72 hours (Figure 85). We found that myotubes from mutant mice cultivated with serum from mutant mice on *ad libitum* grew less than myotubes from wild type mice cultivated with serum from wild type mice on an *ad libitum* diet (Figure 86A). Furthermore, myotubes from wild type and mutant mice that have been cultivated with serum from their

respective CR mice present an increase in growth, suggesting the idea that CR serum composition could be accelerating SCs differentiation and myotubes growth (Figure 86A).

We also determined the differentiation index (Figure 86A), to discriminate between differentiated cells and non-differentiated cells. We found that myotubes from mutant mice incubated with serum from mutant mice on *ad libitum* present a lower proportion of differentiated cells compared with wild type myotubes cultivated with wild type *ad libitum* serum at 72 hours meaning that differentiation could be delayed (Figure 86A). In contrast, mutant myotubes with serum from CR mutant mice present an increase in differentiation, indicating that serum composition could be important in myogenic differentiation. We also calculated the ramification that the myotubes experienced during the differentiation process (Figure 86B), statistical analysis is shown in Table 19. We obtained that mutant myotubes incubated with the serum of mutant mice on *ad libitum* conditions present a lower proportion of branched myotubes compared to wild type myotubes plus serum from wild type mice on *ad libitum*. In addition, myotubes cultivated with serum from CR mice present a higher proportion of branched myotubes pointing out that serum from CR mice increases the branching capacity of the myotubes and could accelerate their differentiation process.

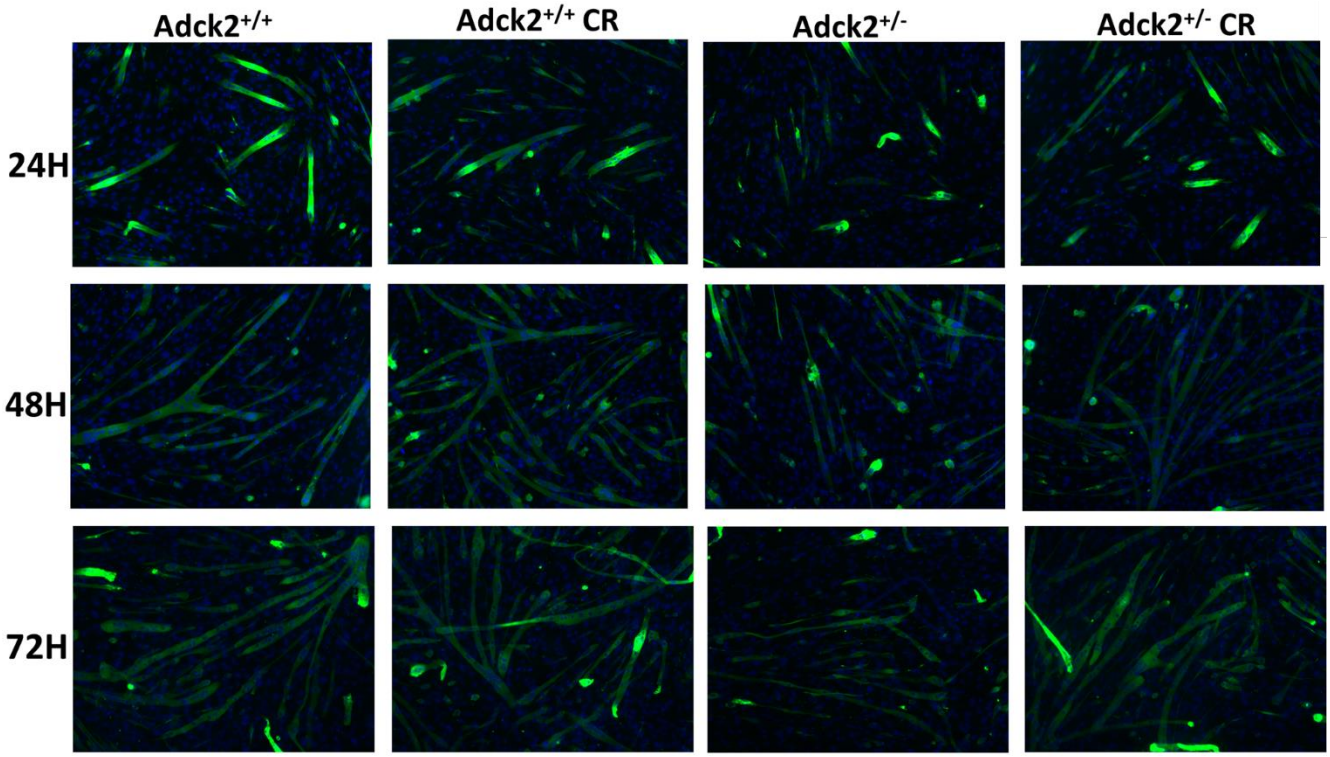

Figure 85. Representative images of the differentiation process of satellite cells cultivated with serum from mice
Representative images of satellite cells differentiate into myotubes, differentiation to myotubes was induced by a reduction in serum concentration. Fresh medium was replaced in each well every 48 hours to avoid nutrient depletion. DAPI was used to stain in blue the nuclei of the myotubes, while differentiated myotubes were stained in green with a MyHC antibody. The differentiation process was determined by following the increase of the MyHC area in myotubes. (A). Differentiation at 24 hours. (B). Differentiation at 48 hours. (C) Differentiation at 72 hours.

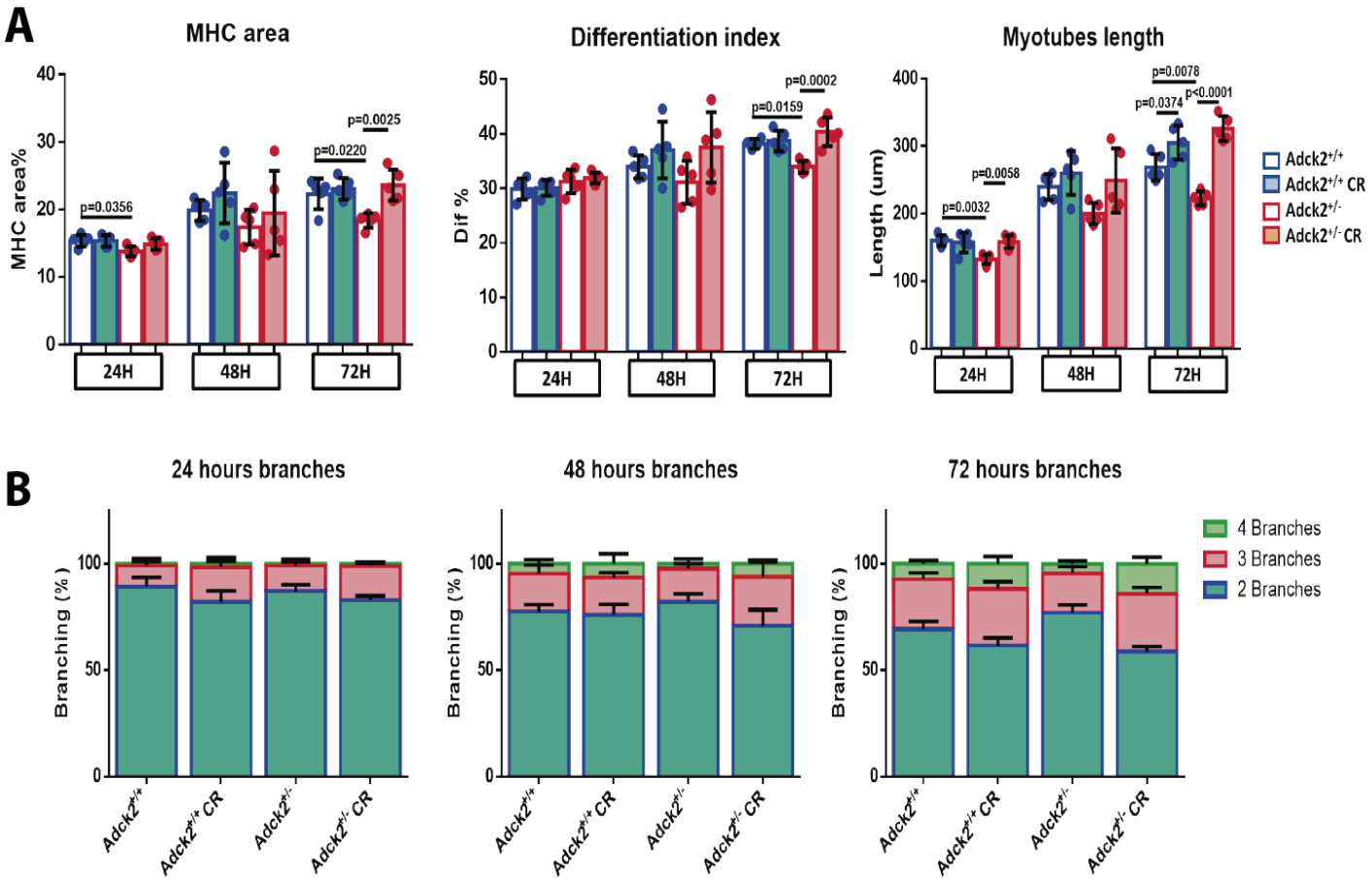

Figure 86. Differentiation process of satellite cells cultivated with serum from mice on ad libitum or CR diets.
Satellite cells were isolated and differentiated to myotubes for 72 hours. DAPI was used to stain in blue the nuclei of the myotubes, while differentiated myotubes were stained in green with Myosin heavy chain (MyHC) antibody. The differentiation process was determined by following the increase of MyHC expression by immunostaining. Differentiation of satellite cells to myotubes is induced by a reduction in serum concentration. (A). MyHC area, differentiation index and myotubes length analysis in myotubes differentiated from satellite cells. (B). Branching capacity analysis in myotubes differentiated from satellite cells. Data represent the mean +/- SD. A one-way ANOVA test was applied. P-values <0.05 were considered statistically significant.

Table 19 Statistic analysis of branchin capacity of myotubes under CR condition

Time point 24 hours					
Branches 2		**Branches 3**		**Branches 4**	
Comparison	**Significance**	**Comparison**	**Significance**	**Comparison**	**Significance**
$Adck2^{+/+}$ vs $Adck2^{+/+}$ CR	p=0.0398	$Adck2^{+/+}$ vs $Adck2^{+/+}$ CR	p=0.0281	$Adck2^{+/+}$ vs $Adck2^{+/+}$ CR	ns
$Adck2^{+/+}$ vs $Adck2^{+/-}$	ns	$Adck2^{+/+}$ vs $Adck2^{+/-}$	ns	$Adck2^{+/+}$ vs $Adck2^{+/-}$	ns
$Adck2^{+/+}$ vs $Adck2^{+/-}$ CR	ns	$Adck2^{+/+}$ vs $Adck2^{+/-}$ CR	p=0.0415	$Adck2^{+/+}$ vs $Adck2^{+/-}$ CR	ns
$Adck2^{+/+}$ CR vs $Adck2^{+/-}$	ns	$Adck2^{+/+}$ CR vs $Adck2^{+/-}$	ns	$Adck2^{+/+}$ CR vs $Adck2^{+/-}$	ns
$Adck2^{+/+}$ CR vs $Adck2^{+/-}$ CR	ns	$Adck2^{+/+}$ CR vs $Adck2^{+/-}$ CR	ns	$Adck2^{+/+}$ CR vs $Adck2^{+/-}$ CR	ns
$Adck2^{+/-}$ vs $Adck2^{+/-}$ CR	ns	$Adck2^{+/-}$ vs $Adck2^{+/-}$ CR	ns	$Adck2^{+/-}$ vs $Adck2^{+/-}$ CR	ns
Time point 48 hours					
Branches 2		**Branches 3**		**Branches 4**	
Comparison	**Significance**	**Comparison**	**Significance**	**Comparison**	**Significance**

Adck2$^{+/+}$ vs Adck2$^{+/+}$ CR	ns	Adck2$^{+/+}$ vs Adck2$^{+/+}$ CR	ns	Adck2$^{+/+}$ vs Adck2$^{+/+}$ CR	ns
Adck2$^{+/+}$ vs Adck2$^{+/-}$	ns	Adck2$^{+/+}$ vs Adck2$^{+/-}$	ns	Adck2$^{+/+}$ vs Adck2$^{+/-}$	ns
Adck2$^{+/+}$ vs Adck2$^{+/-}$ CR	ns	Adck2$^{+/+}$ vs Adck2$^{+/-}$ CR	ns	Adck2$^{+/+}$ vs Adck2$^{+/-}$ CR	ns
Adck2$^{+/+}$ CR vs Adck2$^{+/-}$	ns	Adck2$^{+/+}$ CR vs Adck2$^{+/-}$	ns	Adck2$^{+/+}$ CR vs Adck2$^{+/-}$	ns
Adck2$^{+/+}$ CR vs Adck2$^{+/-}$ CR	ns	Adck2$^{+/+}$ CR vs Adck2$^{+/-}$ CR	ns	Adck2$^{+/+}$ CR vs Adck2$^{+/-}$ CR	ns
Adck2$^{+/-}$ vs Adck2$^{+/-}$ CR	p=0.0145	Adck2$^{+/-}$ vs Adck2$^{+/-}$ CR	ns	Adck2$^{+/-}$ vs Adck2$^{+/-}$ CR	ns
Time point 72 hours					
Branches 2		**Branches 3**		**Branches 4**	
Comparison	**Significance**	**Comparison**	**Significance**	**Comparison**	**Significance**
Adck2$^{+/+}$ vs Adck2$^{+/+}$ CR	p=0.0118	Adck2$^{+/+}$ vs Adck2$^{+/+}$ CR	ns	Adck2$^{+/+}$ vs Adck2$^{+/+}$ CR	p=0.0488
Adck2$^{+/+}$ vs Adck2$^{+/-}$	p=0.0122	Adck2$^{+/+}$ vs Adck2$^{+/-}$	ns	Adck2$^{+/+}$ vs Adck2$^{+/-}$	ns
Adck2$^{+/+}$ vs Adck2$^{+/-}$ CR	p=0.0008	Adck2$^{+/+}$ vs Adck2$^{+/-}$ CR	ns	Adck2$^{+/+}$ vs Adck2$^{+/-}$ CR	p=0.0028
Adck2$^{+/+}$ CR vs Adck2$^{+/-}$	p<0.0001	Adck2$^{+/+}$ CR vs Adck2$^{+/-}$	p=0.0036	Adck2$^{+/+}$ CR vs Adck2$^{+/-}$	p=0.0014
Adck2$^{+/+}$ CR vs Adck2$^{+/-}$ CR	ns	Adck2$^{+/+}$ CR vs Adck2$^{+/-}$ CR	ns	Adck2$^{+/+}$ CR vs Adck2$^{+/-}$ CR	ns
Adck2$^{+/-}$ vs Adck2$^{+/-}$ CR	p<0.0001	Adck2$^{+/-}$ vs Adck2$^{+/-}$ CR	p=0.0019	Adck2$^{+/-}$ vs Adck2$^{+/-}$ CR	p<0.0001

Later quantify the velocity of differentiation of each SCs according to each serum by correlating each of these parameters along time to calculate the slope of the line (Table 20). Mutant myotubes cultivated on *ad libitum* presented a 50% slower growth and differentiation in the MyHC area and a differentiation index 3-times lower than wild type myotubes on *ad libitum*, whereas the myotube length was compromised by only 20%. On the other hand, mutant myotubes on CR serum showed an increase in all the differentiation parameters analysed, being the velocity of differentiation of these myotubes was even faster than wild type on CR.

Table 20 Differentiation analysis in myotubes on CR conditions

Parameter: MyHC area		
Group	The slope of the line	R squared on the graph
Adck2$^{+/+}$ *ad libitum* serum	0.1444x	$R^2 = 0.764$
Adck2$^{+/+}$ CR serum	0.16x	$R^2 = 0.5363$
Adck2$^{+/-}$ *ad libitum* serum	0.096x	$R^2 = 0.5793$
Adck2$^{+/-}$ CR serum	0.1814x	$R^2 = 0.5098$
Parameter: Differentiation Index		
Group	Slope of the line	R squared on the graph
Adck2$^{+/+}$ *ad libitum* serum	0.146x	$R^2 = 0.6411$
Adck2$^{+/+}$ CR serum	0.1801x	$R^2 = 0.5497$
Adck2$^{+/-}$ *ad libitum* serum	0.0564x	$R^2 = 0.1649$
Adck2$^{+/-}$ CR serum	0.1767x	$R^2 = 0.4671$
Parameter: Myotubes length		
Group	The slope of the line	R squared on the graph
Adck2$^{+/+}$ *ad libitum* serum	2.2595x	$R^2 = 0.8441$
Adck2$^{+/+}$ CR serum	3.0836x	$R^2 = 0.8406$
Adck2$^{+/-}$ *ad libitum* serum	1.8805x	$R^2 = 0.86$
Adck2$^{+/-}$ CR serum	3.4944x	$R^2 = 0.8647$
Parameter: Ramificated myotubes		
Group	The slope of the line	R squared on the graph
Adck2$^{+/+}$ ad libitum serum	0.4157x	$R^2 = 0.8473$
Adck2$^{+/+}$ CR serum	0.4289x	$R^2 = 0.7696$
Adck2$^{+/-}$ *ad libitum* serum	0.2099x	$R^2 = 0.6369$
Adck2$^{+/-}$ CR serum	0.5057x	$R^2 = 0.8452$

Finally, we studied the metabolism of the myotubes during differentiation to elucidate the reason for these differences. Therefore, we analysed the mitochondrial respiration of the myotubes, SCs were plated on the Seahorse plate, differentiation was induced directly in the wells of the plate by adding its corresponding serum. Next, respiration was determined by adding either two different energy substrates: glucose plus pyruvate and glutamine to determine OCR (Figure 87A), or palmitoyl-L-carnitine to quantify fatty acids β-oxidation (Figure 87B). Mutant myotubes incubated with serum from mutant mice on *ad libitum* showed a lower oxygen consumption rate when glucose was in the medium than myotubes from wild type mice cultivated with serum from *ad libitum* wild type mice, the bigger difference was found in maximum respiration. We found the same result in myotubes when palmitoyl-L-carnitine was used as a substrate during the assay. Myotubes from mutant mice incubated with serum from mutant mice on *ad libitum* presented a decrease in fatty acids β-oxidation compared with wild type myotubes cultivated with serum from wild type mice on *ad libitum*, proposing the idea that the defect observed in differentiation could be associated with alteration in fatty acids β-oxidation. Serum from CR mice increased β-oxidation and OCR in myotubes in both genotypes.

These results proposed the idea that the increase found in differentiation markers could be associated with an improvement in mitochondrial respiration, fatty acids β-oxidation rate and the capacity to use fatty acids as energetic substrates.

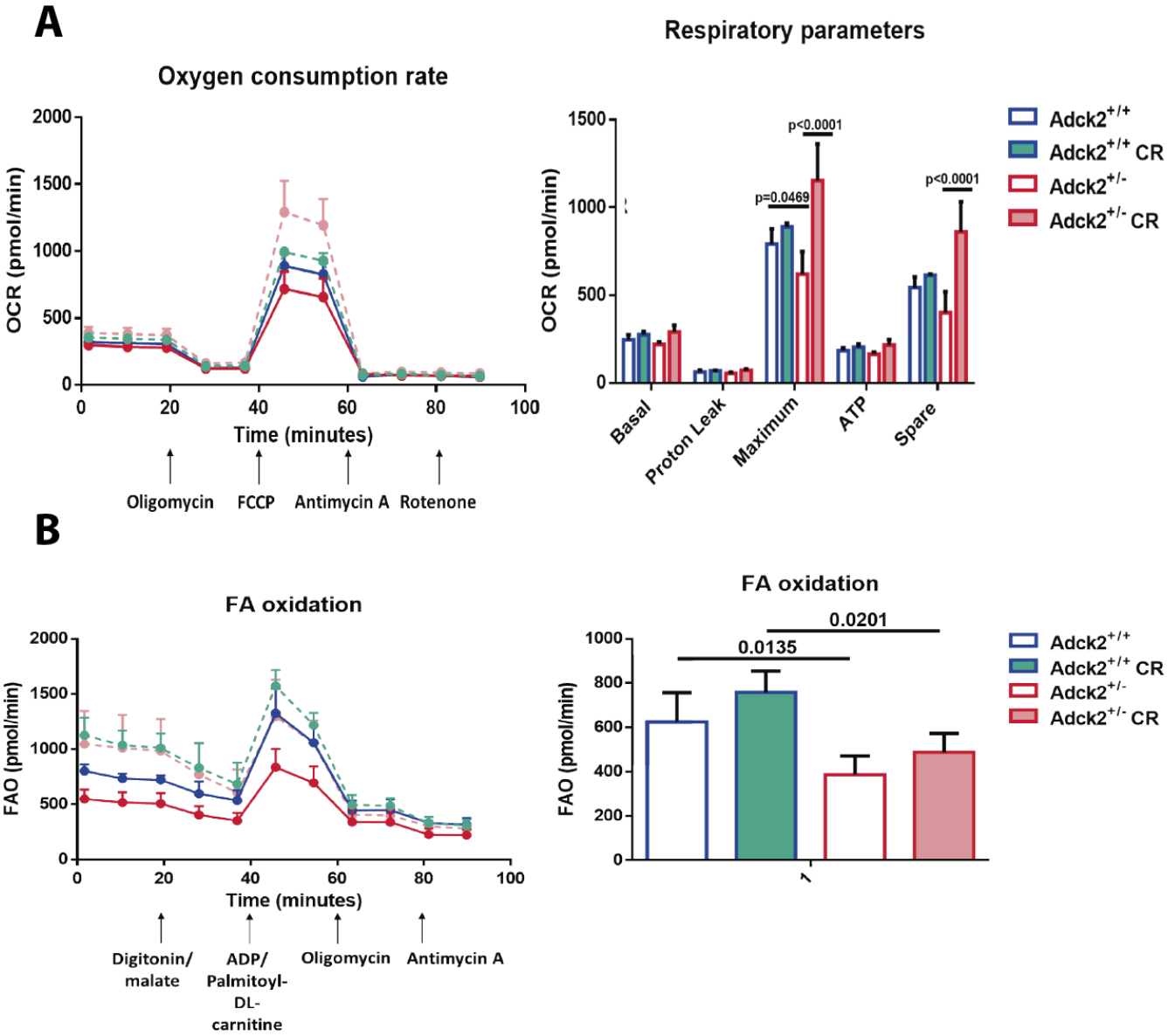

Figure 87 Respiration of satellite cells under calorie restriction conditions.
(A). Oxygen consumption rate in myotubes differentiated from satellite cells. (B) Fatty acids β-oxidation rate in myotubes differentiated from satellite cells. One representative experiment of two independent experiments is shown for each assay. FA, fatty acids; FAO, fatty acids oxidation; OCR, oxygen consumption rate; FCCP, Carbonyl cyanide-p-trifluoromethoxyphenylhydrazone; CR, calorie restriction. Data represent the mean +/- SD (N=4-5). One-way or two-way ANOVA tests were applied. P-values <0.05 were considered statistically significant.

On balance, we have developed an *in vitro* model using adult muscle stem cells, which can reproduce CR adaptations that we have previously observed *in vivo*. Additionally, this model allowed us to study skeletal muscle differentiation in a CR niche. We identified alterations in the metabolism of myotubes that could be recovered with the addition of serum from CR animals, suggesting the importance of the serum composition in skeletal muscle differentiation and metabolism.

4.4.2 Discussion of chapter 4:

The main objective of the present chapter was to examine the effect of a metabolic stress inducer as a beneficial modulator of mitochondrial disease. For this purpose, we studied our heterozygous *Adck2* knockout mice under CR conditions. Adult mice (six-month-old) were submitted to CR for seven months, after that mice (thirteen month-old) were sacrificed by cervical dislocation. Initially, we did not find differences in weight loss between wild type mice and mutant mice on CR, although both groups lost weight compared with their respective controls on an *ad libitum* diet, demonstrating that the CR approach was properly working. Besides, when we examined data of mice on *ad libitum*, mutant mice tend to gain weight compared with wild type mice, suggesting a defect in energy metabolism.

We performed two exercise tests focused on skeletal muscle strength, the grip strength and the weights lifting test, to evaluate the skeletal muscle function. On basal condition (before CR period), mutant mice presented a decrease in skeletal muscle production in both tests, indicating that probably mutant mice suffer a dysfunction in skeletal muscle. At the end of the CR period, when long term CR adaptations would have occurred, mutant mice on *ad libitum* presented a lower force production than wild type mice in both tests indicating that the defect in skeletal muscle function continued. Nevertheless, both wild type and mutant mice on CR presented an increase in force production in both tests showing an improvement in strength associated with CR. Previously, it has been reported that CR could attenuate strength loss associated with ageing and sarcopenia in mice using the grip strength test as an indicator of force production, suggesting that temporal restriction of food in CR could be helpful to maintain muscle function with ageing (205). In agreement, an improvement in the grip strength test on mice on CR has been reported demonstrating the influence of CR on physical capacity (209). Here, we could propose that CR could be promoting a more efficient skeletal muscle function and a higher performance on the test to evaluate strength, being CR even useful to prevent loss of strength associated with myopathy.

Furthermore, we developed a treadmill protocol to study aerobic metabolism *in vivo* where mice are forced to run until exhaustion using a mild electric shock on a 10º uphill open treadmill. In basal conditions, mutant mice showed a lower performance compared with wild type mice, as well they did after the diet period on *ad libitum* condition, while mutant mice on CR displayed an improvement in aerobic capacity. Additionally, the voluntary wheel running over three periods day/night period was determined, finding that both groups at CR presented a higher performance than *ad libitum* animals. Previously, the improvement in aerobic capacity in mice on CR has been associated with an improvement on slow muscle myofibers capacity (205) and

with higher efficiency in nutrients mobilization for physical activity (209). Our results were in line with the previous benefits of CR over aerobic performance, but, CR improved aerobic metabolism in our mutant mice, which presented a mitochondrial dysfunction, promoting a more efficient mitochondrial metabolism.

On the other hand, it is well known the effect of CR on glucose and insulin tolerance (210). For that reason, we checked the effect of CR on glucose and insulin homeostasis in our mutant mice to examine if CR would promote more efficient energy metabolism. Initially, we found higher levels of glucose and insulin in fasting conditions in *Adck2* heterozygous mice, suggesting that mutant mice on an *ad libitum* diet could present a potential insulin resistance while CR decreases levels of glucose and insulin similarly in both groups, CR could improve glucose and insulin sensitivity. Mutant mice on *ad libitum* presented a higher HOMA index that was also reduced in both groups of mice on CR. Moreover, we decided to study glucose and insulin *in vivo* after the induction with a series of stimuli, such as glucose, insulin or pyruvate. The glucose tolerance test was used to examine glucose plasma elevation after glucose injection, mice on *ad libitum* displayed a slower reduction in glucose curve compared with wild type mice indicating inadequate glucose management. Mice on CR exhibited a quicker reduction in glucose levels during the test, indicating that CR induces more efficient glucose homeostasis. The insulin tolerance test is used to study glucose plasma levels after insulin injection. Mutant mice on *ad libitum* presented a more moderate glucose level decrease compared with wild type mice, denoting again a lower glucose sensitivity and the inefficient entrance of plasma glucose into the cell. Besides, both groups of mice on CR presented a quicker reduction in glucose levels post insulin injection, demonstrating a more effective response to insulin. Hepatic gluconeogenesis was also evaluated with the pyruvate tolerance test as can be observed in Figure 73 when pyruvate was injected, and glucose levels were monitored to determine the generation of glucose from non-carbohydrate carbon substrates such as pyruvate. Mutant mice on *ad libitum* showed a lower glucose production post-injection compared with wild type mice on *ad libitum*, suggesting a defect in glucose homeostasis. CR produced an increase in glucose production in mutant mice, indicating more effective glucose homeostasis.

CR is a modulator of glucose and insulin homeostasis (204), post-prandial glucose rise stimulates insulin production in the pancreas to promote the uptake of plasma glucose by the different tissues. Our results on wild type mice under CR corroborate previous studies where CR was postulated to enhance glucose and insulin homeostasis (205), but what is more significant in our study was that CR was able to improve the deregulate glucose and insulin homeostasis and revert the altered profile, showing the potential effect of CR over glucose and insulin sensitivity.

The results from metabolomics studies in the different tissues analysed (skeletal muscle, plasma and liver) (Figure 77) suggested that the organism was adapted to food deprivation mobilizing substrates from peripheral tissues to produce de novo energy to support essential processes to fulfil energy demands. Particularly, the liver analysis reports the release of fatty acids and proteins that could be used to produce energy under food deprivation relying less on glycolytic substrates. Metabolomics data from the liver agree with the metabolomics found in plasma, that evidenced an increase of metabolites in plasma from peripheral energy deposits. Skeletal muscle displayed an increase on amino acids indicating a breakdown of muscle proteins to produce energy substrates and higher levels of fatty acids demonstrating a switch from glucose to fatty acids metabolism as it has been previously described on CR conditions (211). As expected, CR modulated metabolites on the three tissues examined leading to adaptation to fasting and reduced food intake enhancing metabolic flexibility and energy homeostasis, thus CR reproduces metabolic hallmarks in the metabolomics in wild type mice (212). However, the important point here is that CR promoted similar adaptations in Adck2 heterozygous mice showing that CR could modulate the metabolic dysfunction experienced in mutant mice.

We also performed a bioenergetic analysis of CR focusing on mitochondria where we analysed the CoQ levels on CR. Initially, mutant mice under *ad libitum* conditions presented a lower mitochondrial CoQ_9 and CoQ_{10} levels than wild type in line with the previous study that links the *ADCK2* gene to the maintenance of CoQ levels (178) (77). More significantly, CoQ_9 and CoQ_{10} levels were increased in our mutant mice on CR to almost reach wild type levels, suggesting that CR could stimulate the endogenous biosynthesis of CoQ. In contrast, we did not find an increase in CoQ levels in mitochondria of wild type mice on CR, probably because mitochondria from wild type mice are already full of CoQ and at their maximum capacity. However, mitochondria from mutant mice presented lower levels, then, we can detect the increase of CoQ stimulated by CR. A previous study examined CoQ levels in skeletal muscle on CR reporting an increase in both CoQ_9 and CoQ_{10} in skeletal muscle homogenate, and modulation of genes involved in CoQ biosynthesis (143). Consequently, we could propose that CR could be upregulating CoQ biosynthesis.

We analysed RER finding mutant mice on *ad libitum* conditions presented higher RER in the day/night period suggesting an inadequate fatty acids metabolism compared with wild type mice in *ad libitum*. However, mice on CR despite a complete opposite RER profile to mice on *ad libitum* conditions, and what is more important, in both phases (day and night) CR mice showed more extreme values, supporting the idea that mice on CR are more efficient on using different energetic substrates, as it has been previously suggested (205).

Furthermore, we performed an *in vivo* analysis of the bioenergetic metabolism in isolated mitochondria from skeletal muscle. In the coupling assay, pyruvate plus malate were in the medium, mitochondria from mutant mice on *ad libitum* displayed lower respiration capacity, a lower State IIIu and a lower spare capacity, whereas mitochondria from mutant mice on CR displayed an increase in respiration, suggesting an improvement on respiration and mitochondrial machinery. Additionally, in the β-oxidation assay, where the substrates were palmitoyl-L-carnitine plus malate, mitochondria from mutant mice on *ad libitum* presented lower respiration levels than mitochondria from wild type mice, supporting previous data that indicate that mutant mice present a defective fatty acids βoxidation. More importantly, mutant mice on CR presented an increase in respiration suggesting that CR could improve the oxidative metabolism in mutant mice. To our knowledge, this is the first study that studies the effect of CR on *in vivo* mitochondrial respiration, additionally, we found that CR was able to reprogramme the deregulated mitochondrial metabolism from heterozygous *Adck2* knockout mice.

The results suggest that CR could be regulating mitochondrial metabolism and skeletal muscle function, thus we decided to study myofibers typing on TA muscle to check if CR could be also modulating myofiber composition. Mutant mice on *ad libitum* presented a lower proportion of oxidative myofibers type IIA and a higher proportion of hybrid myofibers type IIX compared with wild type mice. CR produced an oxidative shift in myofiber composition inducing a higher proportion of myofibers type IIA in both wild type and heterozygous *Adck2* knockout mice. This result suggested that CR could be inducing a more oxidate metabolism in skeletal muscle. Additionally, metabolic protein markers activated during food deprivation were modulated in skeletal muscle of mice on CR suggesting an upregulation of AMPKα pathway that could be associated with the change of myofiber typing pattern found, an increase in oxidative pathway and evidenced an acclimatization to fasting.

Our results led us to develop a CR *in vitro* model to study the effect of CR on the skeletal muscle stem cell differentiation process. It has been described that CR improved skeletal muscle regeneration (145), although its effects on SCs remain to be discovered. Furthermore, SCs presented important metabolic flexibility to accommodate different metabolic substrates where secondary metabolites could have important outcomes over SCs control (182). These facts drive us to analyse the modification of SCs microenvironment by CR and its effects on their function.

Consequently, we decided to induce SCs differentiation in a microenvironment using freshly isolated SCs that were plated in a differentiation medium containing serum isolated from the different groups of mice studied. We periodically collected the serum of wild type and mutant

mice on both *ad libitum* and on CR, to create a microenvironment that reflects the blood composition of our mice, including the differences found in different metabolites and molecules in the metabolomics profile. SCs exhibit metabolic flexibility during activation, specification, proliferation and differentiation, displaying different metabolic shifts from several energetic substrates during these stages (177). More significantly, we induced metabolic reprogramming by adding the serum that would be specific to the genotype and the diet of mice.

The culture of cells with serum from caloric restricted rodents already reported improvement in oxidative stress response and mitochondrial function in astrocytes (213) and increased tolerance to stress by heat shock in murine melanoma cells (214) and primary hepatocytes culture (208). Additionally, the incubation of myotubes with serum from young or old individuals could modulate the myotubes diameter (215), showing that the composition of serum is crucial in the myotubes differentiation process. Moreover, the effect of CR serum on the culture of SCs has been never analysed. Besides, all previous studies mentioned, serum from wild type rats on CR was used while in our study we have used the serum of wild type or mutant mice on *ad libitum* or CR, thus every serum has the real composition of wild type and mutant mice on *ad libitum* or CR conditions mimicking the real status of mice, even we can distinguish between genotypes.

As can be visualized in Figure 86, myotubes differentiated from mutant SCs cultured in serum from mutant mice on *ad libitum* presented a lower MyHC area, but also a lower myotubes length and reduced branching capacity associated with a ramification defect. Therefore, these data could support the idea that myotubes from mutant mice cultured with the serum of *ad libitum* mutant presented a morphological defect that resulted in hypotrophic myotubes. Nevertheless, when we studied myotubes from mutant mice cultivated with serum from mutant CR mice we found an increase in the different parameters studied, proposing the idea that CR serum could decrease the hypotrophic phenotype.

SCs experienced a metabolic shift during differentiation becoming more dependent on OXPHOS and fatty acids β-oxidation than in glycolysis (177), exhibiting metabolic flexibility to accommodate energetic needs. Additionally, secondary metabolites that modulate reprogramming and alterations of the SCs environment could result in metabolic alterations (177). Based on that, we thought that the different serums could be creating different microenvironments for cell culture and particularly, serum from caloric restricted mice could force the utilization of the metabolic pathways that are active during myotubes differentiation (OXPHOS and fatty acids oxidation). For that reason, we performed mitochondria bioenergetic assays to evaluate oxidative phosphorylation and fatty acids β-oxidation. Mutant myotubes

cultivated with the serum of *ad libitum* mutant mice showed a decrease in oxygen consumption when the glucose was used as substrate compared with wild type myotubes cultivated with serum from wild type mice on *ad libitum*. More importantly, mutant myotubes cultivated with serum from mutant mice on CR showed an increase in respiration levels, especially on maximum respiration, indicating that serum from mice on CR could force the OXPHOS system from mutant myotubes to work better. Nonetheless, we also quantified the fatty acids β-oxidation using palmitoyl-L-carnitine as substrate, finding that mutant myotubes cultivated with serum from mutant mice on *ad libitum* showed a decrease in palmitoyl oxidation whereas mutant myotubes cultivated with the serum of mutant mice on CR increased fatty acids β-oxidation, suggesting that the microenvironment supplemented with the serum of mutant mice on CR could be efficiently improving the oxidative metabolism.

On balance, we developed an *in vitro* model of CR using adult muscle stem cells to describe a defect in differentiation that leads to a hypotrophic phenotype and smaller myotubes, defects that can potentially be related to the metabolic defects associated with *ADCK2*.

Conclusions

5 CONCLUSIONS

Chapter 1

- Damages in mutant *Adck2* knockout mice start during embryonic development.
- The alterations found during embryonic development are tissue-specific.
- A prenatal CoQ_{10} administration palliates the damages associated with the *ADCK2* gene during embryonic development.
- CoQ_{10} administration could recover some defects associated with the *ADCK2* gene, but also could activate or repress new genes or pathways.

Chapter 2

- Satellite cells differentiation is affected in our mutant mouse model, myotubes derived from mutant satellite cells present a defective myogenic differentiation.
- Differentiation defects could be associated with an incapacity of the mutant myotubes to use oxidative metabolic pathways during the differentiation process.
- Satellite cells derived from mice supplemented with CoQ_{10} present an improvement in the differentiation process associated with better oxidative metabolism.
- Damages found in mutant satellite cells are more severe in satellite cells from old mice.

Chapter 3

- Mutant mice present a skeletal muscle decline associated with ageing resulting in a change in the myofiber typing composition, myofiber size and a physical incapacity through the ageing process.
- CoQ_{10} longitudinal administration could delay the damages found in the skeletal muscle associated with ageing
- Mutant mice present a defective *in vivo* mitochondrial respiration while CoQ_{10} could recover the defect in mitochondrial respiration.

Chapter 4

- Mutant mice present a deregulated glucose and insulin homeostasis, caloric restriction enhances glucose and insulin sensitivity in mutant mice.
- The caloric restriction could improve mitochondrial physiology on mutant mice, ameliorating CoQ decrease and *in vivo* mitochondrial respiration.
- Caloric restriction produces almost the same metabolic adaptations in different tissues on wild type and mutant mice.

- Caloric restriction microenvironment on cell culture could enhance satellite cells differentiation forcing different oxidative pathways.

CONCLUSIONES

Capítulo 1

- Los daños del ratón Adck2 knockout empiezan durante el desarrollo embrionario.
- Las alteraciones encontradas durante el desarrollo embrionario son tejido-específicas.
- La administración prenatal de CoQ10 palía los daños asociados con el gen ADCK2 durante el desarrollo embrionario.
- La administración de CoQ10 puede recuperar defectos asociados con el gen ADCK2, pero también podría activar o reprimir otros genes o rutas.

Capítulo 2

- La diferenciación de células satélites esta afecta en el ratón mutante, los miotubos derivados de células mutantes presentan un defecto en la diferenciación miogénica.
- Los defectos en la diferenciación podrían estar asociados con la incapacidad de los miotubos mutantes para usar rutas metabólicas oxidativas durante el proceso de diferenciación.
- Las células satélites derivadas de ratones suplementados con CoQ10 presentan una mejora en el proceso de diferenciación asociado con un mejor metabolismo oxidativo.
- Los daños observados en las células satélites mutantes son más severos en células de ratones viejos.

Capítulo 3

- Los ratones mutantes presentan un decible en el músculo esquelético asociado con el envejecimiento que resulta en cambio en el tipo de fibras musculoesqueléticas, en el tamaño de la fibra y una incapacidad para la actividad física a lo largo del envejecimiento.
- La administración longitudinal de CoQ10 podría retrasar los daños encontrados en el músculo esqueléticos asociados al envejecimiento.
- Los ratones mutantes presentan un defecto en la respiración mitocondrial in vivo mientras la suplementación con CoQ10 podría recuperar el defecto de la respiración mitocondrial.

Capítulo 4

- Los ratones mutantes presentan una desregulada homeóstasis de la glucosa y la insulina, la restricción calórica podría mejorar la sensibilidad a la glucosa e insulina en ratones mutantes.
- La restricción calórica podría mejorar la fisiología mitocondrial en ratones mutantes, paliando el descenso de CoQ y mejorando la respiración mitocondrial in vivo.
- La restricción calórica produce casi las mismas adaptaciones metabólicas en los diferentes tejidos en ratones wild type y mutantes
- Un microambiente caracterizado por la restricción calórica en cultivo celular podría mejorar la diferenciación de las células satélites a través de diferentes rutas oxidativas.

References

6 REFERENCES

1. Lynn Margulis. Origin of Eukaryotic Cells. Evidence and Research Implications for a Theory of the Origin and Evolution of Microbial, Plant, and Animal Cells on the Precambrian Earth. Yale University Press; 1970.

2. Bruce Alberts, A. J., Julian Lewis, David Morgan, Martin Raff, Keith Roberts PW. Molecular Biology of the Cell. 6th ed. New York, NY : Garland Science T and FG, editor. 2015.

3. Schmidt O, Pfanner N, Meisinger C. Mitochondrial protein import: From proteomics to functional mechanisms. Vol. 11, Nature Reviews Molecular Cell Biology. 2010. p. 655–67.

4. MW H. Cancer a redox disease: Cancer cells are universally disturbed in their electronic energy balance, an understanding that potentially revolutionises cancer therapy and prevention. Journal of the Australasian College of Nutritional and Environmental Medicine. 2013. p. 32:12-18.

5. Montecinos-Franjola F, Ramachandran R. Imaging dynamin-related protein 1 (DRP1)-mediated mitochondrial fission in living cells. Methods Mol Biol. 2020;2159:205–17.

6. Mitchell P. Protonmotive redox mechanism of the cytochrome b-c1 complex in the respiratory chain: Protonmotive ubiquinone cycle. Vol. 56, FEBS Letters. 1975. p. 1–6.

7. Signes Marrahi A. Identification and characterisation of new factors and mechanisms regulating human cytochrome c oxidase biogenesis. (Doctoral thesis) University of Cambridge. 2019.

8. Herrmann JM, Riemer J. The intermembrane space of mitochondria. Vol. 13, Antioxidants and Redox Signaling. 2010. p. 1341–58.

9. Tilokani L, Nagashima S, Paupe V, Prudent J. Mitochondrial dynamics: Overview of molecular mechanisms. Vol. 62, Essays in Biochemistry. 2018. p. 341–60.

10. Kunji ERS, Robinson AJ. Coupling of proton and substrate translocation in the transport cycle of mitochondrial carriers. Vol. 20, Current Opinion in Structural Biology. 2010. p. 440–7.

11. Hirst J, Roessler MM. Energy conversion, redox catalysis and generation of reactive oxygen species by respiratory complex i. Biochim Biophys Acta - Bioenerg. 2016;1857:872–83.

12. Van Vranken JG, Na U, Winge DR, Rutter J. Protein-mediated assembly of succinate dehydrogenase and its cofactors. Vol. 50, Critical Reviews in Biochemistry and Molecular Biology. 2015. p. 168–80.

13. Cramer WA, Hasan SS, Yamashita E. The Q cycle of cytochrome bc complexes: A structure perspective. Vol. 1807, Biochimica et Biophysica Acta - Bioenergetics. 2011. p. 788–802.

14. Walker JE. The ATP synthase: The understood, the uncertain and the unknown. Biochem Soc Trans. 2013;41(1):1–16.

15. Acín-Pérez R, Fernández-Silva P, Peleato ML, Pérez-Martos A, Enriquez JA. Respiratory

Active Mitochondrial Supercomplexes. Mol Cell. 2008 Nov 21;32(4):529–39.

16. Gu J, Wu M, Guo R, Yan K, Lei J, Gao N, et al. The architecture of the mammalian respirasome. Nature. 2016;537(7622):639–43.

17. Hernansanz-Agustín P, Enríquez JA. Functional segmentation of CoQ and cyt c pools by respiratory complex superassembly. Free Radic Biol Med. 2021 May 1;167:232–42.

18. Paupe V, Prudent J. New insights into the role of mitochondrial calcium homeostasis in cell migration. Biochem Biophys Res Commun. 2018;500(1):75–86.

19. Russell OM, Gorman GS, Lightowlers RN, Turnbull DM. Mitochondrial Diseases: Hope for the Future. Vol. 181, Cell. 2020. p. 168–88.

20. Gorman GS, Chinnery PF, DiMauro S, Hirano M, Koga Y, McFarland R, et al. Mitochondrial diseases. Nat Rev Dis Prim. 2016;2:16080.

21. Festenstein GN, Heaton FW, Lowe JS, Morton RA. A constituent of the unsaponifiable portion of animal tissue lipids. Biochem J. 1955;59(4):558–66.

22. Crane FL, Hatefi Y, Lester RL, Widmer C. Isolation of a quinone from beef heart mitochondria. Biochim Biophys Acta. 1957 Jan 1;25(C):220–1.

23. Hernández-Camacho JD, Bernier M, López-Lluch G, Navas P. Coenzyme Q10 supplementation in aging and disease. Vol. 9, Frontiers in Physiology. Frontiers Media S.A.; 2018. p. 44.

24. Turunen M, Olsson J, Dallner G. Metabolism and function of coenzyme Q. Biochim Biophys Acta - Biomembr. 2004 Jan 28;1660(1–2):171–99.

25. Forsmark-AndrÉe P, Dallner G, Ernster L. Endogenous ubiquinol prevents protein modification accompanying lipid peroxidation in beef heart submitochondrial particles. Free Radic Biol Med. 1995 Dec 1;19(6):749–57.

26. Godic A, Poljšak B, Adamic M, Dahmane R. The Role of Antioxidants in Skin Cancer Prevention and Treatment. Oxid Med Cell Longev. 2014;2014.

27. Maroz A, Anderson R, Smith R, Murphy M. Reactivity of ubiquinone and ubiquinol with superoxide and the hydroperoxyl radical: implications for in vivo antioxidant activity. Free Radic Biol Med. 2009;46(1):105–9.

28. Bentinger M, Brismar K, Dallner G. The antioxidant role of coenzyme Q. Mitochondrion. 2007 Jun 1;7(SUPPL.):S41–50.

29. Kagan VE, Arroyo A, Tyurin VA, Tyurina YY, Villalba JM, Navas P. Plasma membrane NADH-coenzyme Q0 reductase generates semiquinone radicals and recycles vitamin E homologue in a superoxide-dependent reaction. FEBS Lett. 1998 May 22;428(1–2):43–6.

30. Navas P, Villalba JM, Lenaz G. Coenzyme Q-dependent functions of plasma membrane in the aging process. Vol. 27, Age. 2005. p. 139–46.

31. Tocilescu MA, Zickermann V, Zwicker K, Brandt U. Quinone binding and reduction by respiratory complex I. Vol. 1797, Biochimica et Biophysica Acta - Bioenergetics. 2010. p.

1883–90.

32. Bartoschek S, Johansson M, Geierstanger BH, Okun JG, Lancaster CRD, Humpfer E, et al. Three Molecules of Ubiquinone Bind Specifically to Mitochondrial Cytochrome bc1 Complex. J Biol Chem. 2001;276(38):35231–4.

33. Guarás A, Perales-Clemente E, Calvo E, Acín-Pérez R, Loureiro-Lopez M, Pujol C, et al. The CoQH2/CoQ Ratio Serves as a Sensor of Respiratory Chain Efficiency. Cell Rep. 2016;15:197–209.

34. Arroyo A, Navarro F, Gómez-Díaz C, Crane FL, Alcaín FJ, Navas P, et al. Interactions between ascorbyl free radical and coenzyme Q at the plasma membrane. J Bioenerg Biomembr. 2000;32(2):199–210.

35. Ross D, Siegel D. Functions of NQO1 in cellular protection and CoQ10 metabolism and its potential role as a redox sensitive molecular switch. Vol. 8, Frontiers in Physiology. 2017.

36. Fernández-Ayala DJM, Jiménez-Gancedo S, Guerra I, Navas P. Invertebrate Models for Coenzyme Q 10 Deficiency Overview of Coenzyme Q Function and Biosynthesis. Mol Syndr. 2014;5:170–9.

37. Bentinger M, Tekle M, Dallner G. Coenzyme Q - Biosynthesis and functions. Biochem Biophys Res Commun. 2010 May 21;396(1):74–9.

38. Fernández-Ayala DJM, Brea-Calvo G, López-Lluch G, Navas P. Coenzyme Q distribution in HL-60 human cells depends on the endomembrane system. Biochim Biophys Acta - Biomembr. 2005;1713:129–37.

39. Alcázar-Fabra M, Trevisson E, Brea-Calvo G. Clinical syndromes associated with Coenzyme Q10 deficiency. Vol. 62, Essays in Biochemistry. Portland Press Ltd; 2018. p. 377–98.

40. Stefely JA, Pagliarini DJ. Biochemistry of Mitochondrial Coenzyme Q Biosynthesis. Vol. 42, Trends in Biochemical Sciences. 2017. p. 824–43.

41. Eisenberg-Bord M, Tsui HS, Antunes D, Fernández-Del-Río L, Bradley MC, Dunn CD, et al. The Endoplasmic Reticulum-Mitochondria Encounter Structure Complex Coordinates Coenzyme Q Biosynthesis. Contact (Thousand Oaks). 2019;2:2515256418825409.

42. Alcázar-Fabra M, Navas P, Brea-Calvo G. Coenzyme Q biosynthesis and its role in the respiratory chain structure. Biochim Biophys Acta - Bioenerg. 2016 Aug 1;1857(8):1073–8.

43. Ozeir M, Mühlenhoff U, Webert H, Lill R, Fontecave M, Pierrel F. Coenzyme Q biosynthesis: Coq6 is required for the C5-hydroxylation reaction and substrate analogs rescue Coq6 deficiency. Chem Biol. 2011 Sep 23;18(9):1134–42.

44. Jonassen T, Clarke CF. Isolation and functional expression of human COQ3, a gene encoding a methyltransferase required for ubiquinone biosynthesis. J Biol Chem. 2000 Apr 28;275(17):12381–7.

45. Poon WW, Barkovich RJ, Hsu AY, Frankel A, Lee PT, Shepherd JN, et al. Yeast and rat Coq3

and Escherichia coli UbiG polypeptides catalyze both O-methyltransferase steps in coenzyme Q biosynthesis. J Biol Chem. 1999 Jul 30;274(31):21665–72.

46. Nguyen TPT, Casarin A, Desbats MA, Doimo M, Trevisson E, Santos-Ocaña C, et al. Molecular characterization of the human COQ5 C-methyltransferase in coenzyme Q10 biosynthesis. Biochim Biophys Acta - Mol Cell Biol Lipids. 2014 Nov 1;1841(11):1628–38.

47. Marbois BN, Clarke CF. The COQ7 gene encodes a protein in Saccharomyces cerevisiae necessary for ubiquinone biosynthesis. J Biol Chem. 1996 Feb 9;271(6):2995–3004.

48. Tauche A, Krause-Buchholz U, Rödel G. Ubiquinone biosynthesis in Saccharomyces cerevisiae : the molecular organization of O -methylase Coq3p depends on Abc1p/Coq8p. FEMS Yeast Res. 2008;8(8):1263–75.

49. Xie LX, Hsieh EJ, Watanabe S, Allan CM, Chen JY, Tran UC, et al. Expression of the human atypical kinase ADCK3 rescues coenzyme Q biosynthesis and phosphorylation of Coq polypeptides in yeast coq8 mutants. Biochim Biophys Acta - Mol Cell Biol Lipids. 2011 May 1;1811(5):348–60.

50. Stefely JA, Reidenbach AG, Ulbrich A, Oruganty K, Floyd BJ, Jochem A, et al. Mitochondrial ADCK3 employs an atypical protein kinase-like fold to enable coenzyme Q Biosynthesis. Mol Cell. 2015 Jan 8;57(1):83–94.

51. Marbois B, Gin P, Gulmezian M, Clarke CF. The yeast Coq4 polypeptide organizes a mitochondrial protein complex essential for coenzyme Q biosynthesis. Biochim Biophys Acta - Mol Cell Biol Lipids. 2009 Jan 1;1791(1):69–75.

52. Hsieh EJ, Gin P, Gulmezian M, Tran UPC, Saiki R, Marbois BN, et al. Saccharomyces cerevisiae Coq9 polypeptide is a subunit of the mitochondrial coenzyme Q biosynthetic complex. Arch Biochem Biophys. 2007 Jul 1;463(1):19–26.

53. Lohman DC, Forouhar F, Beebe ET, Stefely MS, Minogue CE, Ulbrich A, et al. Mitochondrial COQ9 is a lipid-binding protein that associates with COQ7 to enable coenzyme Q biosynthesis. Proc Natl Acad Sci U S A. 2014 Nov 4;111(44):4697–705.

54. Cui T-Z, Kawamukai M. Coq10, a mitochondrial coenzyme Q binding protein, is required for proper respiration in Schizosaccharomyces pombe. FEBS J. 2009;276(3):748–59.

55. Awad AM, Bradley MC, Fernández-del-Río L, Nag A, Tsui HS, Clarke CF. Coenzyme Q10 deficiencies: Pathways in yeast and humans. Vol. 62, Essays in Biochemistry. 2018. p. 361–76.

56. Hernández-Camacho JD, García-Corzo L, Moreno Fernández-Ayala DJ, Navas P, López-Lluch G, Pizzimenti S, et al. Coenzyme Q at the Hinge of Health and Metabolic Diseases. Antioxidants. 2021;10(11):1785.

57. Laredj LN, Licitra F, Puccio HM. The molecular genetics of coenzyme Q biosynthesis in health and disease. Vol. 100, Biochimie. Elsevier; 2014. p. 78–87.

58. Desbats MA, Lunardi G, Doimo M, Trevisson E, Salviati L. Genetic bases and clinical manifestations of coenzyme Q10 (CoQ10) deficiency. J Inherit Metab Dis.

2014;38(1):145–56.

59. Yubero D, Montero R, Santos-Ocaña C, Salviati L, Navas P, Artuch R. Molecular diagnosis of coenzyme Q 10 deficiency: an update. Expert Rev Mol Diagn. 2018;18(6):491–8.

60. Yubero D, Allen G, Artuch R, Montero R. The Value of Coenzyme Q10 Determination in Mitochondrial Patients. J Clin Med. 2017;6(4):37.

61. Yubero D, O'Callaghan M, Montero R, Ormazabal A, Armstrong J, Espinos C, et al. Association between coenzyme Q10 and glucose transporter (GLUT1) deficiency. BMC Pediatr. 2014;14(1).

62. Balreira A, Boczonadi V, Barca E, Pyle A, Bansagi B, Appleton M, et al. ANO10 mutations cause ataxia and coenzyme Q10 deficiency. J Neurol. 2014;261(11):2192–8.

63. Gempel K, Topaloglu H, Talim B, Schneiderat P, Schoser BGH, Hans VH, et al. The myopathic form of coenzyme Q10 deficiency is caused by mutations in the electron-transferring-flavoprotein dehydrogenase (ETFDH) gene. Brain. 2007;130:2037–44.

64. Sacconi S, Trevisson E, Salviati L, Aymé S, Rigal O, Garcia Redondo A, et al. Coenzyme Q10 is frequently reduced in muscle of patients with mitochondrial myopathy. Neuromuscul Disord. 2010;20(1):44–8.

65. Doimo M, Desbats MA, Cerqua C, Cassina M, Trevisson E, Salviati L. Genetics of coenzyme Q10 deficiency. Mol Syndromol. 2014;5(3–4):156–62.

66. Quinzii CM, Kattah AG, Naini A, Akman HO, Mootha VK, DiMauro S, et al. Coenzyme Q deficiency and cerebellar ataxia associated with an aprataxin mutation. Neurology. 2005;64(3):539–41.

67. Yubero D, Montero R, Martín MA, Montoya J, Ribes A, Grazina M, et al. Secondary coenzyme Q10 deficiencies in oxidative phosphorylation (OXPHOS) and non-OXPHOS disorders. Mitochondrion. 2016;30:51–8.

68. Montini G, Malaventura C, Salviati L. Early coenzyme Q10 supplementation in primary coenzyme Q10 deficiency. Vol. 358, New England Journal of Medicine. 2008. p. 2849–50.

69. Rawat V, Browne M, Bellringer M, Greer N, Kolandai-Matchett K, Rockloff M, et al. A tale of two countries: comparing disability weights for gambling problems in New Zealand and Australia. Qual Life Res. 2018;27(9):2361–71.

70. Saiki R, Lunceford AL, Shi Y, Marbois B, King R, Pachuski J, et al. Coenzyme Q10 supplementation rescues renal disease in Pdss2 kd/kd mice with mutations in prenyl diphosphate synthase subunit 2. Am J Physiol - Ren Physiol. 2008;295(5).

71. López-Lluch G, del Pozo-Cruz J, Sánchez-Cuesta A, Cortés-Rodríguez AB, Navas P. Bioavailability of coenzyme Q10 supplements depends on carrier lipids and solubilization. Nutrition. 2019;57:133–40.

72. Miles M V., Patterson BJ, Schapiro MB, Hickey FJ, Chalfonte-Evans M, Horn PS, et al. Coenzyme Q10 Absorption and Tolerance in Children With Down Syndrome: A Dose-Ranging Trial. Pediatr Neurol. 2006;35(1):30–7.

73. Trevisson E, Dimauro S, Navas P, Salviati L. Coenzyme Q deficiency in muscle. Vol. 24, Current Opinion in Neurology. 2011. p. 449–56.

74. Garone C, Gurgel-Giannetti J, Sanna-Cherchi S, Krishna S, Naini A, Quinzii CM, et al. A novel SUCLA2 mutation presenting as a complex childhood movement disorder. J Child Neurol. 2017;32:246–50.

75. van Dijkman SC, de Jager NCB, Rauwé WM, Danhof M PO. Effect of Age-Related Factors on the Pharmacokinetics of Lamotrigine and Potential Implications for Maintenance Dose Optimisation in Future Clinical Trials. Clin Pharmacokinet. 2018;57(8):1039–53.

76. Aeby A, Sznajer Y, Cavé H, Rebuffat E, Coster R Van, Rigal O, et al. Cardiofaciocutaneous (CFC) syndrome associated with muscular coenzyme Q10 deficiency. J Inherit Metab Dis. 2007;30(5):827–827.

77. Vázquez-Fonseca, Schaefer, Navas-Enamorado, Santos-Ocaña, Hernández-Camacho, Guerra, et al. ADCK2 Haploinsufficiency Reduces Mitochondrial Lipid Oxidation and Causes Myopathy Associated with CoQ Deficiency. J Clin Med. 2019;8(9):1374.

78. Smith KM, Matson S, Matson WR, Cormier K, Del Signore SJ, Hagerty SW, Stack EC, Ryu H FR. Dose ranging and efficacy study of high-dose coenzyme Q10 formulations in Huntington's disease mice. Biochim Biophys Acta. 2006;1762(6):616–26.

79. Yang X, Yang Y, Li G, Wang J YE. Coenzyme Q10 attenuates beta-amyloid pathology in the aged transgenic mice with Alzheimer presenilin 1 mutation. J Mol Neurosci. 2008;34(2):165–71.

80. Wadsworth JTL, Bishop JA, Pappu AS, Woltjer RL QJ. Evaluation of coenzyme Q as an antioxidant strategy for Alzheimer's disease. J Alzheimers Dis. 2008;14(2):225–34.

81. Gairola CG, Howatt DA DA. Dietary coenzyme Q10 does not protect against cigarette smoke-augmented atherosclerosis in apoE-deficient mice. Free Radic Biol Med. 2010;48(11):1535–9.

82. Schmelzer C, Kubo H, Mori M, Sawashita J, Kitano M, Hosoe K, et al. Supplementation with the reduced form of Coenzyme Q10 decelerates phenotypic characteristics of senescence and induces a peroxisome proliferator-activated receptor-α gene expression signature in SAMP1 mice. Mol Nutr Food Res. 2010 Jun 1;54(6):805–15.

83. Shetty RA, Forster MJ SN. Coenzyme Q(10) supplementation reverses age-related impairments in spatial learning and lowers protein oxidation. Age (Dordr). 2013;35(5):1821–34.

84. Sourris KC, Harcourt BE, Tang PH, Morley AL, Huynh K, Penfold SA, Coughlan ME, Cooper ME, Nguyen TV, Ritchie RH FJ. Ubiquinone (coenzyme Q10) prevents renal mitochondrial dysfunction in an experimental model of type 2 diabetes. Free Radic Biol Med. 2012;52(3):716–23.

85. Yan J, Fujii K, Yao J, Kishida H, Hosoe K, Sawashita J, Takeda T, Mori M HK. Reduced coenzyme Q10 supplementation decelerates senescence in SAMP1 mice. Exp Gerontol. 2006;41(2):130–40.

86. Shi TJS, Zhang MD, Zeberg H, Nilsson J, Grünler J, Liu SX, Xiang Q, Persson J, Fried KJ, Catrina SB, Watanabe M, Arhem P, Brismar K HT. Coenzyme Q10 prevents peripheral neuropathy and attenuates neuron loss in the db-/db- mouse, a type 2 diabetes model. Proc Natl Acad Sci U S A. 2013;110(2):690–5.

87. Stefely JA, Licitra F, Laredj L, Reidenbach AG, Kemmerer ZA, Grangeray A, et al. Cerebellar Ataxia and Coenzyme Q Deficiency through Loss of Unorthodox Kinase Activity. Mol Cell. 2016 Aug 18;63(4):608–20.

88. Blumkin L, Leshinsky-Silver E, Zerem A, Yosovich K, Lerman-Sagie T, Lev D. Heterozygous mutations in the ADCK3 gene in siblings with cerebellar atrophy and extreme phenotypic variability. In: JIMD Reports. Springer; 2014. p. 103–7.

89. Mollet J, Delahodde A, Serre V, Chretien D, Schlemmer D, Lombes A, et al. CABC1 Gene Mutations Cause Ubiquinone Deficiency with Cerebellar Ataxia and Seizures. Am J Hum Genet. 2008 Mar 3;82(3):623–30.

90. Ashraf S, Gee HY, Woerner S, Xie LX, Vega-Warner V, Lovric S, et al. ADCK4 mutations promote steroid-Resistant nephrotic syndrome through CoQ10 biosynthesis disruption. J Clin Invest. 2013 Dec 2;123(12):5179–89.

91. Kemmerer ZA, Robinson KP, Schmitz JM, Paulson BR, Jochem A, Hutchins PD, et al. UbiB proteins regulate cellular CoQ distribution. bioRxiv. 2020. p. 2020.12.09.418202.

92. González-García P, Barriocanal-Casado E, Díaz-Casado ME, López-Herrador S, Hidalgo-Gutiérrez A, López LC. Animal Models of Coenzyme Q Deficiency: Mechanistic and Translational Learnings. Antioxidants 2021, Vol 10, Page 1687. 2021;10(11):1687.

93. Casuso RA, Huertas JR. The emerging role of skeletal muscle mitochondrial dynamics in exercise and ageing. Vol. 58, Ageing Research Reviews. Elsevier Ireland Ltd; 2020. p. 101025.

94. Marzetti E, Hwang JCY, Lees HA, Wohlgemuth SE, Dupont-Versteegden EE, Carter CS, et al. Mitochondrial death effectors: Relevance to sarcopenia and disuse muscle atrophy. Vol. 1800, Biochimica et Biophysica Acta - General Subjects. Elsevier; 2010. p. 235–44.

95. Calvani R, Joseph AM, Adhihetty PJ, Miccheli A, Bossola M, Leeuwenburgh C, et al. Mitochondrial pathways in sarcopenia of aging and disuse muscle atrophy. Vol. 394, Biological Chemistry. NIH Public Access; 2013. p. 393–414.

96. Min K, Smuder AJ, Kwon OS, Kavazis AN, Szeto HH, Powers SK. Mitochondrial-targeted antioxidants protect skeletal muscle against immobilization-induced muscle atrophy. J Appl Physiol. 2011 Nov;111(5):1459–66.

97. Palmer JW, Tandler B, Hoppel CL. Biochemical properties of subsarcolemmal and interfibrillar mitochondria isolated from rat cardiac muscle. J Biol Chem. 1977;252(23):8731–9.

98. Riva A, Tandler B, Lesnefsky EJ, Conti G, Loffredo F, Vazquez E, et al. Structure of cristae in cardiac mitochondria of aged rat.

99. Mukund K, Subramaniam S. Skeletal muscle: A review of molecular structure and function, in health and disease. Vol. 12, Wiley Interdisciplinary Reviews: Systems Biology and Medicine. Wiley-Blackwell; 2020. p. e1462.

100. Csapo R, Gumpenberger M, Wessner B. Skeletal Muscle Extracellular Matrix – What Do We Know About Its Composition, Regulation, and Physiological Roles? A Narrative Review. Vol. 11, Frontiers in Physiology. 2020. p. 253.

101. Morgan J, Partridge T. Skeletal muscle in health and disease. Vol. 13, DMM Disease Models and Mechanisms. Company of Biologists Ltd; 2020. p. dmm042192.

102. Rossi G, Bonfanti C, Antonini S, Bastoni M, Monteverde S, Innocenzi A, et al. Silencing Nfix rescues muscular dystrophy by delaying muscle regeneration. Nat Commun. 2017 Dec 1;8(1):1–12.

103. Mercuri E, Muntoni F. Muscular dystrophies. Vol. 381, The Lancet. Lancet Publishing Group; 2013. p. 845–60.

104. Emery AEH. The muscular dystrophies. In: Lancet. Elsevier Limited; 2002. p. 687–95.

105. Bogdanovich S, Krag TOB, Barton ER, Morris LD, Whittemore LA, Ahima RS, et al. Functional improvement of dystrophic muscle by myostatin blockade. Nature. 2002 Nov 28;420(6914):418–21.

106. Schertzer JD, Gehrig SM, Ryall JG, Lynch GS. Modulation of Insulin-like Growth Factor (IGF)-I and IGF-binding protein interactions enhances skeletal muscle regeneration and ameliorates the dystrophic pathology in mdx mice. Am J Pathol. 2007 Oct 1;171(4):1180–8.

107. Mercuri E, Bönnemann CG, Muntoni F. Muscular dystrophies. Vol. 394, The Lancet. Lancet Publishing Group; 2019. p. 2025–38.

108. Ricotti V, Mandy WPL, Scoto M, Pane M, Deconinck N, Messina S, et al. Neurodevelopmental, emotional, and behavioural problems in Duchenne muscular dystrophy in relation to underlying dystrophin gene mutations. Dev Med Child Neurol. 2016;58(1):77–84.

109. Stitzel ML, Seydoux G. Regulation of the oocyte-to-zygote transition. Vol. 316, Science. American Association for the Advancement of Science; 2007. p. 407–8.

110. Lu X, Gao Z, Qin D, Li L. A Maternal Functional Module in the Mammalian Oocyte-To-Embryo Transition. Vol. 23, Trends in Molecular Medicine. Elsevier Ltd; 2017. p. 1014–23.

111. Tajbakhsh S, Cossu G. Establishing myogenic identity during somitogenesis. Curr Opin Genet Dev. 1997 Oct 1;7(5):634–41.

112. Fragouli E, Munne S, Wells D. The cytogenetic constitution of human blastocysts: insights from comprehensive chromosome screening strategies. Hum Reprod Update. 2019;25:15–33.

113. Arnold SJ, Robertson EJ. Making a commitment: Cell lineage allocation and axis

patterning in the early mouse embryo. Vol. 10, Nature Reviews Molecular Cell Biology. Nature Publishing Group; 2009. p. 91–103.

114. Buckingham M, Rigby PWJ. Gene Regulatory Networks and Transcriptional Mechanisms that Control Myogenesis. Vol. 28, Developmental Cell. Elsevier; 2014. p. 225–38.

115. Denetclaw WF, Christ B, Ordahl CP. Location and growth of epaxial myotome precursor cells. Development. 1997;124(8):1601–10.

116. Bajanca F, Luz M, Duxson MJ, Thorsteinsdóttir S. Integrins in the mouse myotome: Developmental changes and differences between the epaxial and hypaxial lineage. Dev Dyn. 2004;231(2):402–15.

117. Bajanca F, Luz M, Raymond K, Martins GG, Sonnenberg A, Tajbakhsh S, et al. Integrin α6β1-laminin interactions regulate early myotome formation in the mouse embryo. Development. 2006;133(9):1635–44.

118. Moreno-Garcia MA, Rosenblatt DS, Jerome-Majewska LA. The methylmalonic aciduria related genes, Mmaa, Mmab, and Mut, are broadly expressed in placental and embryonic tissues during mouse organogenesis. Mol Genet Metab. 2012 Nov 1;107(3):368–74.

119. von Maltzahn J, Chang NC, Bentzinger CF, Rudnicki MA. Wnt signaling in myogenesis. Vol. 22, Trends in Cell Biology. NIH Public Access; 2012. p. 602–9.

120. Pownall ME, Gustafsson MK, Emerson CP. Myogenic Regulatory Factors and the Specification of Muscle Progenitors in Vertebrate Embryos. Annu Rev Cell Dev Biol. 2002 Nov 28;18(1):747–83.

121. Buas MF, Kadesch T. Regulation of skeletal myogenesis by Notch. Vol. 316, Experimental Cell Research. Academic Press Inc.; 2010. p. 3028–33.

122. Hernández-Hernández JM, García-González EG, Brun CE, Rudnicki MA. The myogenic regulatory factors, determinants of muscle development, cell identity and regeneration. Vol. 72, Seminars in Cell and Developmental Biology. 2017. p. 10–8.

123. Moncaut N, Rigby PWJ, Carvajal JJ. Dial M(RF) for myogenesis. Vol. 280, FEBS Journal. FEBS J; 2013. p. 3980–90.

124. Birchmeier C, Brohmann H. Genes that control the development of migrating muscle precursor cells. Vol. 12, Current Opinion in Cell Biology. Elsevier Ltd; 2000. p. 725–30.

125. Lee ASJ, Harris J, Bate M, Vijayraghavan K, Fisher L, Tajbakhsh S, et al. Initiation of primary myogenesis in amniote limb muscles. Dev Dyn. 2013;242(9):1043–55.

126. Lepper C, Fan CM. Inducible lineage tracing of Pax7-descendant cells reveals embryonic origin of adult satellite cells. Genesis. 2010;48(7):424–36.

127. Gamage DG, Leikina E, Quinn ME, Ratinov A, Chernomordik L V., Millay DP. Insights into the localization and function of myomaker during myoblast fusion. J Biol Chem. 2017 Oct 20;292(42):17272–89.

128. Millay DP, O'Rourke JR, Sutherland LB, Bezprozvannaya S, Shelton JM, Bassel-Duby R, et

al. Myomaker is a membrane activator of myoblast fusion and muscle formation. Nature. 2013 Jul 17;499(7458):301–5.

129. Millay DP, Sutherland LB, Bassel-Duby R, Olson EN. Myomaker is essential for muscle regeneration. Genes Dev. 2014 Aug 1;28(15):1641–6.

130. Sato T. Induction of Skeletal Muscle Progenitors and Stem Cells from human induced Pluripotent Stem Cells. J Neuromuscul Dis. 2020 Jan 1;7(4):395–405.

131. Crist CG, Montarras D, Buckingham M. Muscle satellite cells are primed for myogenesis but maintain quiescence with sequestration of Myf5 mRNA targeted by microRNA-31 in mRNP granules. Cell Stem Cell. 2012 Jul 6;11(1):118–26.

132. Zammit PS, Golding JP, Nagata Y, Hudon V, Partridge TA, Beauchamp JR. Muscle satellite cells adopt divergent fates: A mechanism for self-renewal? J Cell Biol. 2004 Aug 2;166(3):347–57.

133. Bröhl D, Vasyutina E, Czajkowski MT, Griger J, Rassek C, Rahn HP, et al. Colonization of the Satellite Cell Niche by Skeletal Muscle Progenitor Cells Depends on Notch Signals. Dev Cell. 2012 Sep 11;23(3):469–81.

134. Almeida CF, Martins PCM, Vainzof M. Comparative transcriptome analysis of muscular dystrophy models Largemyd, DMDmdx /Largemyd and DMDmdx: What makes them different? Eur J Hum Genet. 2016 Aug 1;24(9):1301–9.

135. Dalle S, Poffé C, Hiroux C, Suhr F, Deldicque L, Koppo K. Ibuprofen does not Impair Skeletal Muscle Regeneration Upon Cardiotoxin-Induced Injury. Physiol Res. 2020;69:847–59.

136. Kang X, Yang MY, Shi YX, Xie MM, Zhu M, Zheng XL, et al. Interleukin-15 facilitates muscle regeneration through modulation of fibro/adipogenic progenitors. Cell Commun Signal. 2018;16(1):42.

137. Garry GA, Antony ML GD. Cardiotoxin Induced Injury and Skeletal Muscle Regeneration. Methods Mol Biol. 2016;1460:61–71.

138. Tajbakhsh S. Skeletal muscle stem cells in developmental versus regenerative myogenesis. J Intern Med. 2009;266(4):372–89.

139. Mattison JA, Roth GS, Mark Beasley T, Tilmont EM, Handy AM, Herbert RL, et al. Impact of caloric restriction on health and survival in rhesus monkeys from the NIA study. Nature. 2012;489(7415):318–21.

140. López-Otín C, Blasco MA, Partridge L, Serrano M, Kroemer G. The hallmarks of aging. Vol. 153, Cell. 2013. p. 1194.

141. Chung KW, Kim DH, Park MH, Choi YJ, Kim ND, Lee J, et al. Recent advances in calorie restriction research on aging. Vol. 48, Experimental Gerontology. Exp Gerontol; 2013. p. 1049–53.

142. Fontana L, Partridge L, Longo VD. Extending healthy life span-from yeast to humans. Vol. 328, Science. 2010. p. 321–6.

143. Parrado-Fernández C, López-Lluch G, Rodríguez-Bies E, Santa-Cruz S, Navas P, Ramsey JJ, et al. Calorie restriction modifies ubiquinone and COQ transcript levels in mouse tissues. Free Radic Biol Med. 2011;50(12):1728–36.

144. Kamzalov S, Sohal RS. Effect of age and caloric restriction on coenzyme Q and α-tocopherol levels in the rat. Exp Gerontol. 2004;39(8):1199–205.

145. Cerletti M, Jang YC, Finley LWS, Haigis MC, Wagers AJ. Short-term calorie restriction enhances skeletal muscle stem cell function. Cell Stem Cell. 2012 May;10(5):515–9.

146. Boldrin L, Ross JA, Whitmore C, Doreste B, Beaver C, Eddaoudi A, et al. The effect of calorie restriction on mouse skeletal muscle is sex, strain and time-dependent. Sci Rep. 2017;7(1):5160.

147. Carvajal JJ, Cox D, Summerbell D, Rigby PWJ. A BAC transgenic analysis of the Mrf4/Myf5 locus reveals interdigitated elements that control activation and maintenance of gene expression during muscle development. Development. 2001;128(10):1857–68.

148. Theiin A, Schedin S DG. Half-life of ubiquinone-9 in rat tissues. FEBS J. 1992;313(2):118–20.

149. Aartsma-Rus A, van Putten M. Assessing functional performance in the Mdx mouse model. J Vis Exp. 2014 Mar 27;(85):51303.

150. Deacon RMJ. Measuring the strength of mice. J Vis Exp. 2013;(76):e2609.

151. Rocchi A, He C. Activating autophagy by aerobic exercise in mice. J Vis Exp. 2017;2017(120):55099.

152. Dougherty JP, Springer DA, Gershengorn MC. The treadmill fatigue test: A simple, high-throughput assay of fatigue-like behavior for the mouse. J Vis Exp. 2016;(111):54052.

153. van Putten M, Raymackers J-M, Rüegg Biozentrum M, Grange Virginia Tech RW. Use of treadmill and wheel exercise for impact on mdx mice phenotype SOP (ID) Number. 2008.

154. Richardson A, Fischer KE, Speakman JR, De Cabo R, Mitchell SJ, Peterson CA, et al. Measures of Healthspan as Indices of Aging in Mice-A Recommendation. J Gerontol A Biol Sci Med Sci. 2016;71(4):427–30.

155. Fernández-Calleja JMS, Konstanti P, Swarts HJM, Bouwman LMS, Garcia-Campayo V, Billecke N, et al. Non-invasive continuous real-time in vivo analysis of microbial hydrogen production shows adaptation to fermentable carbohydrates in mice. Sci Rep. 2018;8:1–16.

156. Morton AB, Norton CE, Jacobsen NL, Fernando CA, Cornelison DDW, Segal SS. Barium chloride injures myofibers through calcium-induced proteolysis with fragmentation of motor nerves and microvessels. Skelet Muscle. 2019;9(1):27.

157. Hardy D, Besnard A, Latil M, Jouvion G, Briand D, Thépenier C, et al. Comparative study of injury models for studying muscle regeneration in mice. PLoS One. 2016;11(1):e0147198.

158. Hernández-Camacho JD, Vicente-García C, Sánchez-Cuesta A, Fernandez-Ayala DJM, Carvajal JJ, Navas P. Isolation of Mitochondria from Mouse Skeletal Muscle for Respirometric Assays. J Vis Exp. 2022;(180).

159. Rodríguez-Aguilera J, Cortés A, Fernández-Ayala D, Navas P. Biochemical Assessment of Coenzyme Q10 Deficiency. J Clin Med. 2017;6(3):27.

160. Jha P, Wang X AJ. Analysis of Mitochondrial Respiratory Chain Supercomplexes Using Blue Native Polyacrylamide Gel Electrophoresis (BN-PAGE). Curr Protoc Mouse Biol. 2016;6(1):1–14.

161. Nijtmans LGJ, Henderson NS HI. Blue Native electrophoresis to study mitochondrial and other protein complexes. Methods. 2002;26(4):327–34.

162. H S. Native electrophoresis for isolation of mitochondrial oxidative phosphorylation protein complexes. Methods Enzymol. 1995;260:190–202.

163. Fernandez-Ayala DJM, Guerra I, Jiménez-Gancedo S, Cascajo M V., GaviÍn A, DiMauro S, et al. Survival transcriptome in the coenzyme Q10 deficiency syndrome is acquired by epigenetic modifications: A modelling study for human coenzyme Q10 deficiencies. BMJ Open. 2013 Jan 1;3(3):e002524.

164. Moyle LA, Zammit PS. Isolation, culture and immunostaining of skeletal muscle fibres to study myogenic progression in satellite cells. Methods Mol Biol. 2014;1210:63–78.

165. Li R, Steyn FJ, Stout MB, Lee K, Cully TR, Calderón JC, et al. Development of a high-throughput method for real-time assessment of cellular metabolism in intact long skeletal muscle fibre bundles. J Physiol. 2016;594(24):7197–213.

166. Ortuste Quiroga HP, Goto K, Zammit PS. Isolation, cryosection and immunostaining of skeletal muscle. In: Methods in Molecular Biology. 2016. p. 85–100.

167. Banerji CRS, Panamarova M, Pruller J, Figeac N, Hebaishi H, Fidanis E, et al. Dynamic transcriptomic analysis reveals suppression of PGC1α/ERRα drives perturbed myogenesis in facioscapulohumeral muscular dystrophy. Hum Mol Genet. 2019;28(8):1244–59.

168. Pala F, Di Girolamo D, Mella S, Yennek S, Chatre L, Ricchetti M, et al. Distinct metabolic states govern skeletal muscle stem cell fates during prenatal and postnatal myogenesis. J Cell Sci. 2018 Jul 1;131(14):jcs212977.

169. Levavasseur FF, Miyadera H, Sirois J, Tremblay ML, Kita K, Shoubridge E HS. Ubiquinone is necessary for mouse embryonic development but is not essential for mitochondrial respiration. J Biol Chem. 2001;276(49):46160–4.

170. Lu S, Lu LY, Liu MF, Yuan QJ, Sham MH, Guan XY HJ. Cerebellar defects in Pdss2 conditional knockout mice during embryonic development and in adulthood. Neurobiol Dis. 2012;45(1):219–33.

171. Skinner MK. Endocrine disruptor induction of epigenetic transgenerational inheritance of disease. Vol. 398, Molecular and Cellular Endocrinology. 2014. p. 4–12.

172. Donkin I, Versteyhe S, Ingerslev LR, Qian K, Mechta M, Nordkap L, et al. Obesity and

bariatric surgery drive epigenetic variation of spermatozoa in humans. Cell Metab. 2016;23(2):369–78.

173. Ferguson-Smith AC, Patti ME. You are what your dad ate. Vol. 13, Cell Metabolism. 2011. p. 115–7.

174. Alcázar-Fabra M, Rodríguez-Sánchez F, Trevisson E B-CG. Primary Coenzyme Q deficiencies: A literature review and online platform of clinical features to uncover genotype-phenotype correlations. Free Radic Biol Med. 2021;167:141–80.

175. Kozawa TS, Ueda R, Urayama K, Sagawa F, Endo S, Shiizaki K, Kurosu H, de Almeida GM, Hasan SM, Nakazato K, Ozaki S, Yamashita Y, Kuro-O M ST. The Body-wide Transcriptome Landscape of Disease Models. iScience. 2018;2:238–68.

176. Fomin M, Nomokonova N, Arnold HH. Identification of a critical control element directing expression of the muscle-specific transcription factor MRF4 in the mouse embryo. Dev Biol. 2004 Aug 15;272(2):498–509.

177. F. Relaix, M. Bencze, M. J. Borok, A. Der Vartanian, F. Gattazzo, D. Mademtzoglou, S. Perez-Diaz, A. Prola, P. C. Reyes-Fernandez AR& T V. Perspectives on skeletal muscle stem cells. Nat Commun. 2021;12(1):692–703.

178. Kemmerer ZA, Robinson KP, Schmitz JM, Manicki M, Paulson BR, Jochem A, Hutchins PD, Coon JJ PD. UbiB proteins regulate cellular CoQ distribution in Saccharomyces cerevisiae. Nat Commun. 2021;12(1):4769.

179. Rehman J. Empowering self-renewal and differentiation: the role of mitochondria in stem cells. J Mol Med 2010 8810. 2010;88(10):981–6.

180. Bhattacharya D, Scimè A. Mitochondrial Function in Muscle Stem Cell Fates. Front Cell Dev Biol. 2020 Jun 16;8:480.

181. Ryall JG, Dell'Orso S, Derfoul A, Juan A, Zare H, Feng X, Clermont D, Koulnis M, Gutierrez-Cruz G, Fulco M S V. The NAD(+)-dependent SIRT1 deacetylase translates a metabolic switch into regulatory epigenetics in skeletal muscle stem cells. Cell Stem Cell. 2015;16(2):171–83.

182. L'honoré A, Commère P-H, Negroni E, Pallafacchina G, Friguet B, Drouin J, et al. The role of Pitx2 and Pitx3 in muscle stem cells gives new insights into P38α MAP kinase and redox regulation of muscle regeneration. Elife. 2018;7:e32991.

183. Theret M, Gsaier L, Schaffer B, Juban G, Larbi SB, Weiss-Gayet M, Bultot L, Collodet C, Foretz M, Desplanches D, Sanz P, Zang Z MR. AMPKα1-LDH pathway regulates muscle stem cell self-renewal by controlling metabolic homeostasis. EMBO J. 2017;36(13):1946–62.

184. Cairns G, Thumiah-Mootoo M, Burelle Y, Khacho M. Mitophagy: A New Player in Stem Cell Biology. Biology (Basel). 2020;9(12):1–24.

185. Banerjee R, Purhonen J KJ. The mitochondrial coenzyme Q junction and complex III: biochemistry and pathophysiology. FEBS J. 2021;Online ahe.

186. Tanaka Y, Kita S, Nishizawa H, Fukuda S, Fujishima Y, Obata Y, et al. Adiponectin promotes muscle regeneration through binding to T-cadherin. Sci Rep. 2019;9(1):16.

187. Brunetti D, Bottani E, Segala A, Marchet S, Rossi F, Orlando F, et al. Targeting Multiple Mitochondrial Processes by a Metabolic Modulator Prevents Sarcopenia and Cognitive Decline in SAMP8 Mice. Front Pharmacol. 2020 Jul 31;11:1171.

188. Bloemberg D, Quadrilatero J. Rapid determination of myosin heavy chain expression in rat, mouse, and human skeletal muscle using multicolor immunofluorescence analysis. PLoS One. 2012 Apr 18;7(4):e35273.

189. Schiaffino S. Fibre types in skeletal muscle: a personal account. Acta Physiol. 2010;199(4):451–63.

190. Green DR, Galluzzi L KG. Mitochondria and the autophagy-inflammation-cell death axis in organismal aging. Science. 2011;333:1109–12.

191. Hiona A, Sanz A, Kujoth G, Pamplona R, Seo AY, Hofer T, Someya S, Miyakawa T, Nakayama C, Samhan-Arias AK, Servais S, Barger JL, Portero-Otín M, Tanokura M, Prolla TA LC. Mitochondrial DNA mutations induce mitochondrial dysfunction, apoptosis and sarcopenia in skeletal muscle of mitochondrial DNA mutator mice. PLoS One. 2010;5(7):e11468.

192. Edgar D, Shabalina I, Camara Y, Wredenberg A, Calvaruso MA, Nijtmans L, et al. Random Point Mutations with Major Effects on Protein-Coding Genes Are the Driving Force behind Premature Aging in mtDNA Mutator Mice. Cell Metab. 2009;10(2):131–8.

193. Conboy IM, Rando TA. Heterochronic parabiosis for the study of the effects of aging on stem cells and their niches. Cell Cycle. 2012;11(12):2260.

194. Chakkalakal JV, Jones KM, Basson MA BA. The aged niche disrupts muscle stem cell quiescence. Nature. 2012;490(7420):355–60.

195. Pan L, Xie W, Fu X, Lu W, Jin H, Lai J, et al. Inflammation and sarcopenia: A focus on circulating inflammatory cytokines. Exp Gerontol. 2021;154:111544.

196. Christian CJ, Benian GM. Animal models of sarcopenia. Aging Cell. 2020;19(10):e13223.

197. Ryu D, Mouchiroud L, Andreux PA, Katsyuba E, Moullan N, Nicolet-dit-Félix AA, et al. Urolithin A induces mitophagy and prolongs lifespan in C. elegans and increases muscle function in rodents. Nat Med 2016 228. 2016;22(8):879–88.

198. Chang YC, Chen YT, Liu HW, Chan YC, Liu MY, Hu SH, Tseng WT, Wu HL, Wang MF CS. Oligonol Alleviates Sarcopenia by Regulation of Signaling Pathways Involved in Protein Turnover and Mitochondrial Quality. Mol Nutr Food Res. 2019;63(10):e1801102.

199. Liu J, Liang X, Zhou D, Lai L, Xiao L, Liu L, et al. Coupling of mitochondrial function and skeletal muscle fiber type by a miR-499/Fnip1/AMPK circuit. EMBO Mol Med. 2016;(10):1212–28.

200. Handschin C, Chin S, Li P, Liu F, Maratos-Flier E, LeBrasseur NK, et al. Skeletal Muscle Fiber-type Switching, Exercise Intolerance, and Myopathy in PGC-1 Muscle-specific

Knock-out Animals. J Biol Chem. 2007;282:30014–21.

201. Niel R, Le Moyec L, Launay T, Mille-Hamard L, Triba MN, Maciejak O, Billat VL MI. Physical performance level in sarcomeric mitochondria creatine kinase knockout mouse model throughout ageing. Exp Gerontol. 2021;146:111246.

202. Rossetti ML, Dunlap KR, Salazar G, Hickner RC, Kim JS, Chase BP, Miller BF GB. Systemic delivery of a mitochondria targeted antioxidant partially preserves limb muscle mass and grip strength in response to androgen deprivation. Mol Cell Endocrinol. 2021;535:111391.

203. De Cabo Rafael, Carmona-Gutierrez Didac, Bernier Michel, Hall Michael N, Frank M. The Search for Antiaging Interventions: From Elixirs to Fasting Regimens. Cell. 2014;157(7):1515–26.

204. Duregon E, Pomatto-Watson LCDD, Bernier M, Price NL de CR. Intermittent fasting: from calories to time restriction. GeroScience. 2021;43(3):1083–92.

205. Ham DJ, Börsch A, Chojnowska K, Lin S, Leuchtmann AB, Ham AS, et al. Distinct and additive effects of calorie restriction and rapamycin in aging skeletal muscle. bioRxiv. 2021;446097.

206. Pons V, Riera J, Capó X, Martorell M, Sureda A, Tur JA, Drobnic F PA. Calorie restriction regime enhances physical performance of trained athletes. J Int Soc Sports Nutr. 2018;15(1):12.

207. Furuzono S, Kubota T, Taura J, Konishi M, Naito A, Tsutsui M, et al. A xanthene derivative, DS20060511, attenuates glucose intolerance by inducing skeletal muscle-specific GLUT4 translocation in mice. Commun Biol 2021 41. 2021;4:1–13.

208. De Cabo R, Fürer-Galbán S, Anson RM, Gilman C, Gorospe M, Lane MA. An in vitro model of caloric restriction. Exp Gerontol. 2003;38(6):631–9.

209. Rodríguez-Bies E, Calvo SS-C, Fontán-Lozano Á, Amaro JP, Rosa FJB de la, Carrión ÁM, et al. Muscle Physiology Changes Induced by Every Other Day Feeding and Endurance Exercise in Mice: Effects on Physical Performance. PLoS One. 2010;5(11):13900.

210. Almendáriz-Palacios C, Mousseau DD, Eskiw CH GZ. Still Living Better through Chemistry: An Update on Caloric Restriction and Caloric Restriction Mimetics as Tools to Promote Health and Lifespan. Int J Mol Sci. 2020;21(23):1–41.

211. Collet TH, Sonoyama T, Henning E, Keogh JM, Ingram B, Kelway S, et al. A Metabolomic Signature of Acute Caloric Restriction. J Clin Endocrinol Metab. 2017;102(12):4486–95.

212. Mitchell SJ, Madrigal-Matute J, Scheibye-Knudsen M, Fang E, Aon M, González-Reyes JA, et al. Effects of Sex, Strain, and Energy Intake on Hallmarks of Aging in Mice. Cell Metab. 2016;23(6):1093–112.

213. García-Matas S, Paul RK, Molina-Martínez P, Palacios H, Gutierrez VM, Corpas R, et al. In vitro caloric restriction induces protective genes and functional rejuvenation in senescent SAMP8 astrocytes. Aging Cell. 2015;14(3):334–44.

214. Novelle MG, Davis A, Price NL, Ali A, Fürer-Galvan S, Zhang Y, Becker K, Bernier M de CR. Caloric restriction induces heat shock response and inhibits B16F10 cell tumorigenesis both in vitro and in vivo. Aging (Albany NY). 2015;7(4):233–40.

215. Allen SL, Marshall RN, Edwards SJ, Lord JM, Lavery GG, Breen L. The effect of young and old ex vivo human serum on cellular protein synthesis and growth in an in vitro model of aging. Am J Physiol Cell Physiol. 2021;321(1):26–37.